POLISH ACADEMY OF SCIENCES
INSTITUTE OF FUNDAMENTAL TECHNOLOGICAL RESEARCH
COMMITTEE ON ACOUSTICS • POLISH ACOUSTICAL SOCIETY

ARCHIVES of ACOUSTICS

QUARTERLY, Vol. 38, No. 3, 2013

Technical Notes

Letter to the Editors

Chronicle

Editorial Board Office:
Pawińskiego 5B, 02-106 Warszawa (Poland)
fax (48-22) 826 98 15, phone (48-22) 826 12 81 ext. 206
e-mail: akustyka@ippt.pan.pl http://acoustics.ippt.pan.pl

PRINTED IN POLAND

Indexed and abstracted in Science Citation Index Expanded (also known as SciSearch®)
and Journal Citation Reports/Science Edition
Abstracted in Acoustics Abstracts, in Applied Mechanics Reviews
and indexed in Journal of the Acoustical Society of America
Recognised by the International Institute of Acoustics and Vibration, I IAV

Edition co-sponsored by Ministry of Science and Higher Education

Arkuszy wydawniczych 24 Arkuszy drukarskich 19,5
Skład i łamanie w systemie TEX: Dział Wydawnictw IPPT PAN

PAN
ARCHIVES OF ACOUSTICS
Vol. **38**, No. 3, pp. 297–301 (2013)

DOI: 10.2478/aoa-2013-0036

Investigation of Ultrasonic Emulsifying Processes of a Linseed Oil and Water Mixture

Andrzej SKUMIEL[(1)], Arkadiusz JÓZEFCZAK[(1)], Krzysztof HELLER[(2)], Tomasz HORNOWSKI[(1)], Katarzyna WIELGUSZ[(2)]

[(1)] *Institute of Acoustics, Faculty of Physics, Adam Mickiewicz University*
Umultowska 85, 61-614 Poznań, Poland; e-mail: skumiel@amu.edu.pl

[(2)] *Institute of Natural Fibres and Medicinal Plants*
Wojska Polskiego 71b, 60-630 Poznań, Poland

(*received October 2, 2012; accepted January 31, 2013*)

Ultrasonic emulsifying processes of immiscible liquids can be used to obtain stable emulsions. The authors used an ultrasonic sandwich head with an energy concentrator to obtain a suitable value of the energy density necessary for the emerge of ultrasonic cavitation. Two piezoelectric ring ($D_{\text{ext}} = 50$ mm) transducers of Pz-26 type produced by FERROPERM were used to design the ultrasonic sandwich head. The frequency of the ultrasonic wave was 18.4 kHz and the excitation time of the ultrasonic transducer exiting 5 minutes. Visible bubbles during the generation of ultrasonic waves appeared in the mixture after exceeding the cavitation threshold. The authors determined also the cavitation threshold by measuring the electrical voltage conducted to the transducers. To receive long-lasting emulsion, the electrical voltage attained 300 V_{peak}. The dispersion dependence on the emulsifying time was determined. The emulsion of linseed oil and water was stable through some months without surfactants.

Keywords: ultrasonic cavitation, ultrasonic emulsifying processes, emulsion, cavitation threshold.

1. Introduction

Emulsified vegetable oils are used as active ingredients (a.i.) of adjuvants increasing pesticides efficacy in agriculture. Such mixtures used as sprays for plants protection allow a better moistening of the surface of leaves and stems and thanks to that to improve the procedure efficiency and simultaneously to ensure their economical application.

The preparation of the emulsion is based on dispersion of one non-miscible liquid into the other one. In addition to the traditional mechanical method of preparation of oil and water emulsions, ultrasonic waves of lower frequency and large intensities ($\sim$10 W·cm^{-2}) can also be used for these purposes (Śliwiński, 2001; Jagodziński, 1997; Elpiner, 1968). Then, the emulgation processes are closely connected with ultrasonic cavitation. In the ultrasonic emulgation process, the dispersed-phase particles can achieve a large degree of size reduction (0.1÷0.5 μm) and the system shows an unquestionable homogeneity. Ultrasonic waves have a considerable influence on the coagulation and coalescence of emulgated particles. The oil-water emulsion is a dispersed system of two liquids: a polar and a nonpolar one and shows therefore a limited thermodynamic stability.

The use of an emulgator during emulgation increases the kinetic durability which is connected with the reduction of work required to prepare the emulsion (Elpiner, 1968; Lee, 1999). When the sonicated fluid contains additionally a gas phase in form of tiny (air or water stem) bubbles, it is easier to form an emulsion. Generally, the amount of the oil-water emulsion increases with the growth of the ultrasonic waves intensity. In turn, a considerable increase of temperature of the mixture during ultrasonic emulgation reduces the emulsion forming rate which is explained by the cavitation decrease. However, in the case of weak heating (30–40°C), the formation of the dispersed phase is slightly easier because of a viscosity and surface tension decrease of both components of the emulgating system. Moreover, the nature of the ultrasonic field has an influence on the intensification of the emulgation processes.

The coagulation of dispersed particles appears in the standing wave field. In aqueous systems, it proceeds in an antinode or in a node, depending on the density of the dispersed phase in comparison with that of the dispersed phase. If the density of the dispersion medium is higher than that of dispersed phase, the coagulation of disperse particles proceeds in the antinodes.

In the experiments carried out by the authors, a linseed oil and water were used in a wide range of concentrations. The linseed oil is produced by cold pressing of the *Linum usitatissimum* L. seeds cultivated in countries of dry, warm and moderate climate.

2. Experimental setup and methods

The measurement setup presented in Fig. 1 consists of a signal generator connected to a high frequency power amplifier model AL-300-HF-A ($P = 300$ W) which drives through a transformer two piezoceramic rings (Pz-26 type produced by Ferroperm). These rings are mechanically pressed with help of a steel bolt to back (steel) and front (aluminum) vibrating masses. Front acoustic mass vibrates with an aluminum concentrator of length corresponding to the half ultrasonic wave ($\lambda/2 \cong 125$ mm) (Gudra, 2000; Gudra, Ciszewski, 1979). The tip of the concentrator is immersed in the liquid medium ($V = 20$ ml), where a thermocouple temperature sensor of the thermoelectric thermometer is also placed. It makes possible the recording the temperature values during emulsification. During the propagation of the ultrasonic wave in a medium with an amplitude absorption coefficient α the release of the thermal energy – which volume density P_V is determined by the following expression (Nowicki, 1998):

$$P_V = I \cdot 2\alpha, \tag{1}$$

where I is the intensity of the ultrasounds – is occured. In the appendix, the authors presented a derivation of this formula.

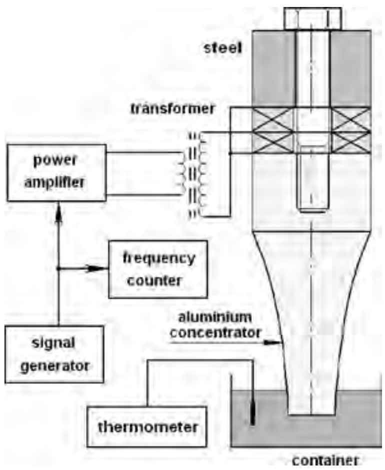

Fig. 1. Experimental setup for the investigation of the emulsifying processes in the mixture of linseed oil with water by the ultrasonic head of "sandwich" type with an acoustic wave concentrator.

The ultrasonic wave frequency at which the tip displacement has the maximum value was 18.4 kHz. The excitation time of the ultrasonic transducer was 5 minutes.

The linseed oil contained over 60% of linolenic acid (omega-3), 15% of linoleic acid (omega-6), 15% of oleic acid (omega-9) and a small amount of saturated fatty acids. The oil-water mixture poured into the container was 20 ml in volume.

3. Results

In the experiments, the authors used some values of concentration of the linseed oil in water (c_o = 5%, 30%, 50% and 70%). For each concentration, the time changes in temperature at selected values of the electric voltages over the cavitation threshold were recorded (Fig. 2).

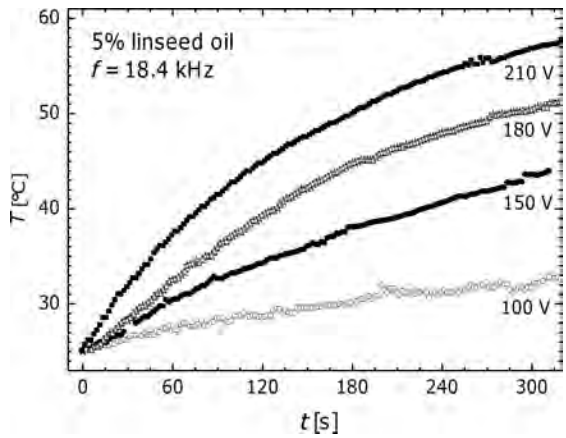

Fig. 2. Time changes in temperature in the container with a mixture of 5% linseed oil with water during the propagation of the ultrasonic wave for some selected voltage amplitudes fed to the piezoceramic rings.

All the records were taken with a start temperature of 25°C. Before switching on electrical voltage on the ultrasonic transducers, two liquids were mixed up and each phase looked transparent. An non-transparent white emulsion was created in the container when the electrical voltage was switched on. The increase in the temperature was the result of heat energy losses caused by the propagation of a high intensity ultrasonic wave in the real dissipative medium.

4. Discussion

There is a determined limit of the emulsion concentration increase, which can be explained by a state of equilibrium of formation between two opposite processes, which take place between the emulgation and coagulation. The defined emulsion concentration corresponds to a given ultrasonic wave intensity. The time changes in temperature presented in Fig. 2 have different values of the temperature slope at the initial time ($t \geq 0$). Taking into account the experimental values of $(\mathrm{d}T/\mathrm{d}t)_{t\geq 0}$ for different voltages, we obtained for example dependences shown in Figs. 3. A very good agreement between the experimental data and the fitted funcation was obtained using the following expression:

$$\left(\frac{\mathrm{d}T}{\mathrm{d}t}\right)_{t=0} = a \cdot \left(\frac{U}{U_0}\right)^n, \tag{2}$$

where a, U_0 and n are parameter values from the fit procedure. In Table 1, the a, n and U_0 parameter values from the fit procedure are listed.

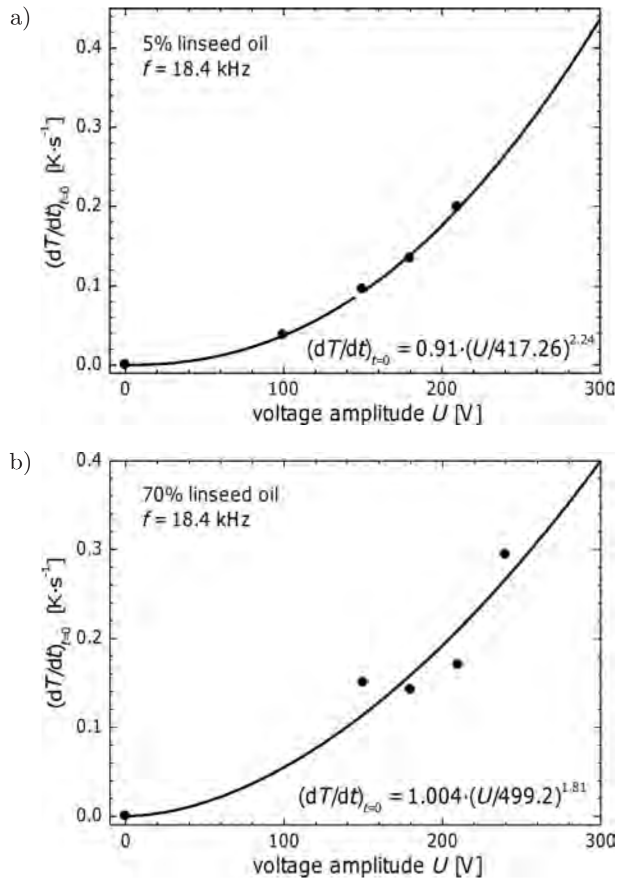

Fig. 3. The temperature rate $(\mathrm{d}T/\mathrm{d}t)_{t=0}$ during propagation of the ultrasonic wave in the sample in the initial period since switching on the electrical voltage U for two concentrations of linseed oil in water: a) 5%, b) 70%.

Table 1. Parameter values of a, U_0 and n obtained from the fitting of function (2) to the experimental data of the temperature increase rate $(\mathrm{d}T/\mathrm{d}t)_{t=0}$.

Concentration of linseed oil in water c_o [%]	a [K·s^{-1}]	U_0 [V]	n [–]
5	0.9139	417.3	2.238
30	1.018	486.1	1.639
50	1.087	465.3	1.918
70	1.004	499.2	1.806

According to calorimetric law, the heat losses power of density released in the sample is equal to:

$$P_v = \rho_{\mathrm{em}} \cdot C_{\mathrm{Pem}} \cdot \left(\frac{\mathrm{d}T}{\mathrm{d}t}\right)_{t=0} \left[\frac{\mathrm{W}}{\mathrm{cm}^3}\right], \tag{3}$$

where ρ_{em} [g·cm^{-3}] is the emulsion density and C_{Pem} [J·g·K^{-1}] is the specific heat capacity of the emulsion. Taking into account Eq. (3), we made the graphic presentation of the heat power density as shown in Fig. 4. The solid lines are functions which were made with the help of Eqs. (2) and (3).

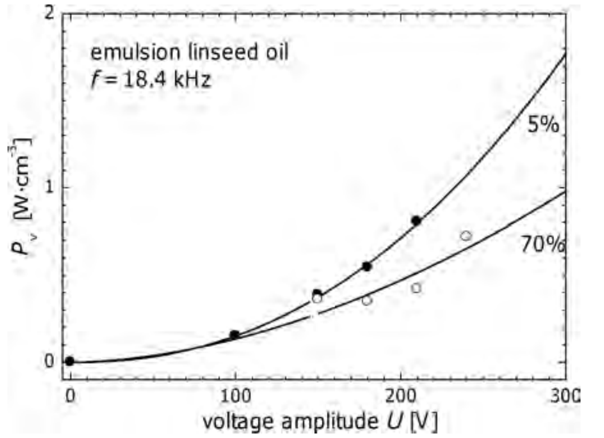

Fig. 4. The dependencies between the heat losses power density released in the sample during propagation of the ultrasonic wave and the electrical voltage amplitude (fed to piezoceramic rings) for two selected concentrations of linseed oil in water.

In turn, Fig. 5 presents the dependence of the heat losses power density P_V and the linseed oil concentration c_o in water for selected electrical voltage amplitudes ($U = 300$ V$_p$). In this case the authors applied

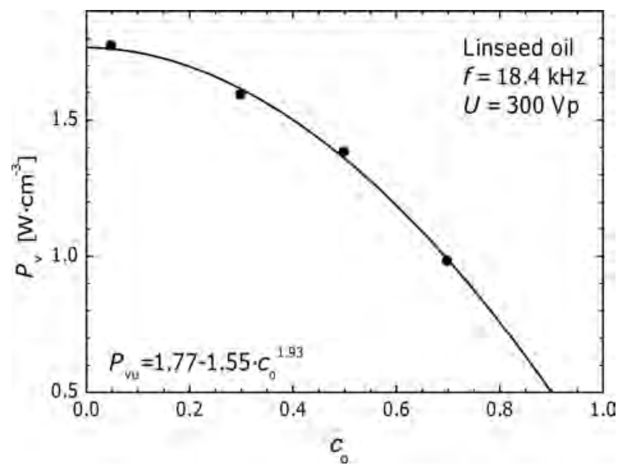

Fig. 5. The dependence of the heat losses power density released in the sample during the propagation of ultrasonic wave on the concentration of linseed oil in water for a selected electrical voltage amplitude.

Table 2. Values of heat losses power density P_V, absorption of ultrasonic wave coefficient α and ultrasonic wave intensity I for some concentrations of linseed oil in water.

Concentration of linseed oil in water c_o	ρ_{em} (Niesteruk, 1996)	C_{Pem} (Niesteruk, 1996)	P_V at $U = 300$ V	α at 18.4 kHz	$I = P_V/(2 \cdot \alpha)$ at 18.4 kHz
%	g·cm^{-3}	J·g^{-1}·K^{-1}	W·cm^{-3}	cm^{-1}	W·cm^{-2}
5	0.997	4.071	1.77	0.0164	54.02
30	0.979	3.513	1.59	0.0911	8.73
50	0.966	3.052	1.38	0.1341	5.14
70	0.952	2.578	0.98	0.1622	3.02

the following expression as the fitting function to experimental data:

$$P_v = b - k \cdot c_o^N \quad \left[\frac{\mathrm{W}}{\mathrm{cm}^3}\right], \tag{4}$$

where b, k and N are parameters obtained from the fitting procedure. For the electrical voltage amplitude $U = 300\ \mathrm{V}_p$, the values of those parameters are: $b = 1.766$, $k = 1.55$ and $N = 1.927$.

Table 2 contains values of the heat losses power density P_V, the absorption of ultrasonic wave coefficient α and the ultrasonic wave intensity I for some concentrations of linseed oil in water. In the literature (Basaran *et al.*, 1998), we found for oil-in-water emulsions the absorption coefficient values measured at frequency $f_1 = 5$ MHz. Because our experiments were carried out at a considerably smaller frequency ($f = 18.4$ kHz), we can use the following equation (Nowicki, 1998; Jaroszyk, 1993):

$$\alpha = \alpha_1 \left(\frac{f}{f_1}\right)^p, \tag{5}$$

where $p \cong 2$.

5. Conclusions

The decreasing of the ultrasonic wave amplitude propagating through the emulsion is caused by absorption, scattering and divergence of the ultrasounds. To exceed a cavitation threshold, a voltage amplitude over 100 V on the converters is required.

The emulgation process is accompanied by a heat released in the emulgated medium.

The oil-water emulsions are much more stable than water-oil emulsions obtained without any emulgator.

Appendix. Derivation of the dependence of the heat losses power density on the ultrasonic wave intensity

Imagine that a flat ultrasonic wave propagates in a liquid lossy medium.

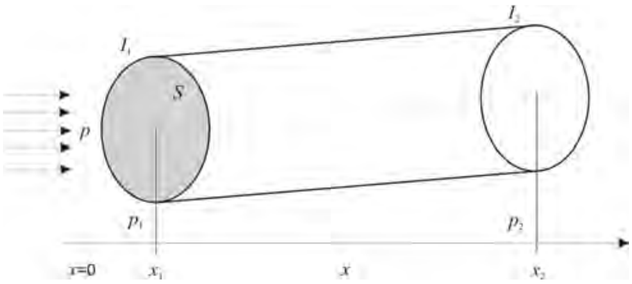

Fig. 6. Ultrasonic wave in a lossy medium.

In position x_1 the pressure amplitude is p_1, and in position x_2 it is p_2

$$p(x) = p_1 \cdot e^{-\alpha(x-x_1)}, \quad p_2 = p_1 \cdot e^{-\alpha(x_2-x_1)}, \tag{6}$$

where α is the amplitude absorption coefficient of this medium, $x_2 - x_1 = l$.

Since the amplitude of the ultrasonic wave intensity is proportional to the second power of the amplitude ultrasonic pressure

$$I \propto p^2, \tag{7}$$

we can write:

$$I(x) = I_1 \cdot e^{-2\alpha(x-x_1)}, \quad I_2 = I_1 \cdot e^{-2\alpha(x_2-x_1)}. \tag{8}$$

There is a following difference between I_1 and I_2:

$$\Delta I = I_2 - I_1 = I_1 \cdot e^{-2\alpha(x_2-x_1)} - I_1 \tag{9}$$

$$= I_1 \cdot \left(1 - e^{-2\alpha \cdot l}\right). \tag{10}$$

Taking into account that the difference in the ultrasonic wave intensities ΔI on the length l is caused by the heat power losses P, we can write:

$$P = I_1 \cdot \left(1 - e^{-2\alpha \cdot l}\right) \cdot S, \tag{11}$$

where S is the cross-section of ultrasonic wave beam.

The volume between the points $x_2 - x_1$ is $V = S \cdot l$, thus the heat losses power density P^* is equal:

$$P^* = \frac{P}{V} = \frac{I_1 \cdot \left(1 - e^{-2\alpha \cdot l}\right) \cdot S}{l \cdot S} = \frac{I_1}{l} \cdot \left(1 - e^{-2\alpha \cdot l}\right). \tag{12}$$

Replacing $e^{-2\alpha l} \cong 1 - 2\alpha l$, we obtained finally:

$$P^* = \frac{I_1}{l} \cdot (1 - 1 + 2\alpha \cdot l) = 2 \cdot \alpha \cdot I_1 \qquad \left[\frac{\mathrm{W}}{\mathrm{m}^3}\right], \qquad (13)$$

where P^* is the heat losses power density and I_1 is the ultrasonic wave intensity.

References

1. Basaran T.K., Demetriades K., McClements D.J. (1998), *Ultrasonic imaging of gravitational separation in emulsions*, Colloids and Surfaces, A: Physicochemical and Engineering Aspects, **136**, 1–2, 169–181.
2. Elpiner I.E. (1968), *Ultrasounds – physical, chemical and biological effects* [in Polish: *Ultradźwięki – działanie fizykochemiczne i biologiczne*], PWN, Warszawa.
3. Gudra T. (2000), *Analysis of a resonator with a directional ultrasonic vibration converter of R-L type using the finite elements method*, Archives of Acoustics, **25**, 2, 157–174.
4. Gudra T., Ciszewski T. (1979), Patent Description No. 101987, *Layered electro-acoustic transducer and method for producing layered electroacoustic transducer* [in Polish: *Warstwowy przetwornik elektro-akustyczny i sposób wytwarzania warstwowego przetwornika elektroakustycznego*], The Patent Office PRL.
5. Jagodziński Z. (1997), *Ultrasonic transducers* [in Polish: *Przetworniki ultradźwiękowe*], WKŁ, Warszawa.
6. Jaroszyk F. [Ed.] (1993), *Medical Biophysics*, [in Polish: *Biofizyka medyczna*], Wydawnictwo Uczelniane Akademii Medycznej im. Karola Marcinkowskiego, Poznań.
7. Lee R.F. (1999), *Agents Which Promote and Stabilize Water-in-Oil Emulsions,* Spill Science & Technology Bulletin, **5**, 2, 117–126.
8. Niesteruk R. (1996), *Thermophysical properties of food* [in Polish: *Właściwości termofizyczne żywności*], Rozprawy Naukowe Nr 33, Wydawnictwa Politechniki Białostockiej, Białystok.
9. Nowicki A. (1998), *Basics of Ultrasonography* [in Polish: *Podstawy ultrasonografii*], PWN, Warszawa.
10. Śliwiński A. (2001), *Ultrasounds and its applications* [in Polish: *Ultradźwięki i ich zastosowania*], WNT, Warszawa.

ARCHIVES OF ACOUSTICS
Vol. **38**, No. 3, pp. 303–310 (2013)

DOI: 10.2478/aoa-2013-0037

Discrimination of Acoustic Emission Signals for Damage Assessment in a Reinforced Concrete Slab Subjected to Seismic Simulations

Francisco A. SAGASTA, Juan L. TORNÉ, Antonio SÁNCHEZ-PAREJO, Antolino GALLEGO

Department of Applied Physics, Building Engineering School, University of Granada
18071 Granada, Spain; e-mail: antolino@ugr.es

(*received October 30, 2012; accepted February 7, 2013*)

The purpose of this work is to distinguish between Acoustic Emission (AE) signals coming from mechanical friction and AE signals coming from concrete cracking, recorded during fourteen seismic simulations conducted with the shaking table of the University of Granada on a reinforced concrete slab supported on four steel columns. To this end, a particular criterion is established based on the Root Mean Square of the AE waveforms calculated in two different temporal windows. This criterion includes a parameter calculated by optimizing the correlation between the mechanical energy dissipated by the specimen (calculated by means of measurements with accelerometers and displacement transducers) and the energy obtained from the AE signals recorded by low-frequency piezoelectric sensors located on the specimen. The final goal of this project, initiated four years ago, is to provide a reliable evaluation of the level of damage of Reinforced Concrete specimens by means of AE signals to be used in future Structural Health Monitoring strategies involving RC structures.

Keywords: acoustic emission, structural health monitoring, reinforced concrete structures, signal processing.

1. Introduction

Reinforced concrete (RC) structures located in earthquake-prone areas are susceptible to suffering damage caused by the cyclic loading induced by ground acceleration during seismic events. It is well known that moderate tremors, which may occur several times during the lifetime of a structure, produce damage of the concrete due to cracking.

Structural Health Monitoring (SHM) strategies and techniques can play an important role in this context in the future. The measurement, recording, and analysis of acoustic emission (AE) signals generated during a seismic event could prove very effective as a health monitoring technique when dealing with remote or inaccessible parts of a structure difficult to evaluate by means of other methods. To date, the AE technique has been applied to RC elements at the level of material (concrete) or individual elements (beams, columns) (Yuyama *et al.*, 1999; 2001), though little research has focused on assemblages of several structural elements (Carpinteri *et al.*, 2007); in the latter case, research involved the AE generated by relatively simple loadings such as vibrations induced by traffic. In this overall context, papers published by our research group in past years address damage assessment of RC structures subjected to low-cycle fatigue loads (Benavent-Climent *et al.*, 2009; 2010), and more recently, to complex dynamic loadings such as those induced by earthquakes (Benavent-Climent *et al.*, 2011; Gallego *et al.*, 2011). More information about the application of the AE technique to other fields can be found in (Guzik *et al.*, 2006; Wozniak *et al.*, 2006; Jasieński *et al.*, 2012).

However, the set of AE signals recorded during seismic events can be complicated, as it may be highly contaminated by sources of noise, mainly due to friction between different parts of the specimen or internal friction in the macrofractures and microfractures already opened inside the concrete. More details about internal cracks in concrete, including some interesting images in stereo optical and electron scanning microscopes, and the application of the AE technique for damage assessment, can be found in (Ranachowski *et al.*, 2012). For this reason, unveiling their relation with the damage accumulated on the structure requires considerable post-processing work on the set of AE signals recorded.

A simple procedure for discriminating between the AE signals coming from friction – *Type (ii)* – and those from concrete cracking – *Type (i)* – was already proposed in (Gallego, 2011). This algorithm is based on the definition of appropriate temporal windows in the AE waveforms, calculation of the RMS (Root Mean Square) in these windows, and establishment of a final comparison criterion of the RMS to decide if a particular AE signal is *Type (i)* or *Type (ii)*. Once the signals have been discriminated, the AE energy of the signals identified as *Type (i)*, from the concrete cracking, is calculated as a tentative index to evaluate the damage of the specimen (Gallego *et al.*, 2011).

In (Gallego *et al.*, 2011), a fixed criterion was put forth regarding the RMS in each window: a signal is *Type (i)* if the relationship $\mathrm{RMS}_1 \geq Q \cdot \mathrm{RMS}_2$ holds, RMS_1 and RMS_2 being the RMSs calculated in each temporal window. Some physical considerations were used to define the temporal width of the two windows, but not to acquire the criterion parameter Q. Moreover, the same Q value was assumed for all the seismic events, even though this assumption obviously reduces the effectiveness of the signal discrimination procedure, because the level and number of friction AE signals – *Type (i)* – can be strongly dependent upon the severity of the seismic event.

This paper proposes a further improvement of the procedure described in (Gallego, 2011) by considering that parameter Q depends on the severity of the seismic event. Namely, an algorithm is proposed to automatically estimate Q in each seismic simulation; it is based on an optimization of the correlation between the mechanical energy dissipated by the specimen and the AE energy.

This optimized algorithm allows for a better classification of *Type (i)* and *Type (ii)* signals, and thus a closer correlation between mechanical and acoustic energies, providing a more accurate evaluation of the level of damage in the specimen.

Results of application with the optimized procedure are presented for a RC concrete slab supported on four steel columns subjected to seismic events of different severity, tested with the $3{\times}3$ m^2 MTS shaking table at the University of Granada.

2. Test model, experimental set-up, and instrumentation

A one-story (2.8 m height) and one-bay (4.8 m length) prototype structure consisting of a RC slab supported on four box-type steel columns was designed following current Spanish codes NCSE-02 (Ministry of Construction of Spain, 2002) and EHE-08 (Ministry of Construction of Spain, 2008). From the prototype structure, the corresponding test model was derived by applying the similarity laws described in (Benavent-Climent *et al.*, 2011). The depth of the slab was 125 mm. It was reinforced with steel meshes, one on the top made with 6 mm diameter bars spaced 100 mm, and another on the bottom consisting of 10 mm diameter bars spaced 75 mm. The average yield stress of the reinforcing steel was 467 MPa, and the average concrete strength was 23.5 MPa. The concrete was obtained by mixing together Portland cement, fine aggregate, coarse aggregate (maximum size 12.5 mm), superplasticizer additive CONPLAST SP-337, with the water-cement ratio 0.54. Concrete was vibrated for a few seconds and the specimen was cured at the room temperature of the laboratory for 28 days. The specimen was finally subjected to seismic loads after 15 additional days for its optimal instrumentation.

The model was tested with the uniaxial MTS $3{\times}3$ m^2 shaking table of the University of Granada (Spain) shown in Fig. 1. The bottom ends of the columns were fixed to the table by bolts. Similitude requirements between prototype and test model and the dead and live gravity loads were satisfied by attaching

a)

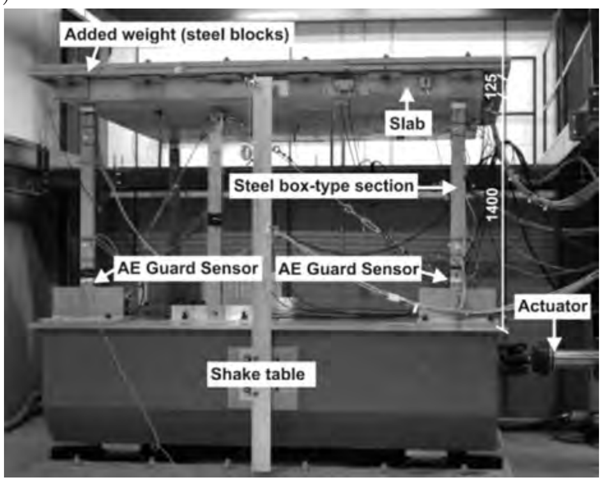

b)

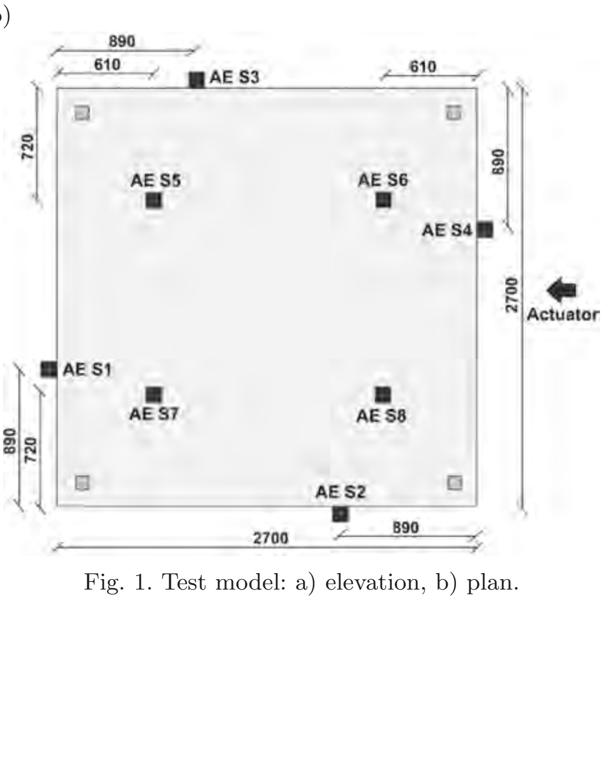

Fig. 1. Test model: a) elevation, b) plan.

additional steel blocks on the top of the RC slab. The total mass of the slab including the added steel blocks was $m = 7390$ kg. The acceleration record used for the shaking table tests reproduced the NS component of the 1980 Campano-Lucano earthquake recorded at Calitri (Italy). Two series of seismic simulations were applied to the test model. The same accelerogram was used in all simulations, the scaling factor of the peak accelerations (PA) being the only difference. The third column of Table 1 shows the PA applied in each simulation. The first series consisted of eight simulations with PA increasing progressively from $0.08g$ to $0.58g$ (where g is the acceleration of gravity). The second series consisted of six simulations with PA increasing from $0.19g$ to $0.95g$, this series starting with values of PA smaller than the maximum obtained in the first series. That is, in several simulations of the second series, the test model was subjected to load levels smaller than the ones previously undergone, so that the simulations reproduced two types of situations on the structure: (i) the AE energy and plastic strain energy were dominated by the new damage associated with the opening and extension of cracks; and (ii) the AE energy and hysteretic energy were dominated by friction generated from the existing damage. Both situations are realistic scenarios that a structure may experience over its lifetime.

Table 1. Seismic Simulations (name and Peak Acceleration (PA)).

Test series		PA (g)
1	2	
Simulation (in order of application)		
A1		0.08
B1		0.10
C1		0.12
D1		0.19
E1		0.29
F1		0.38
G1		0.44
H1		0.58
	A2	0.19
	B2	0.38
	C2	0.58
	D2	0.66
	E2	0.74
	F2	0.95

Displacements, strains, and accelerations were acquired simultaneously during each seismic simulation. The relative horizontal displacement between the shaking table and the slab was measured by LVDT (Linear Variable Differential Transformer) displacement transducers. Accelerometers were fixed to the shaking table and to the slab, to measure the absolute acceleration of the table and the absolute response acceleration of the slab in the direction of shaking, respectively. The parameter called the mechanical energy dissipated by concrete was obtained for all data. See (Benavent-Climent *et al.*, 2011) for details.

A Vallen System ASMY-5 was used to measure the AE signals during testing. Eight VS30 AE flat low-frequency sensors were placed on the specimen at the eight positions indicated in Fig. 1. These sensors were set in the range 20–80 kHz, using the 25–180 kHz frequency band during signal acquisition with a sample period of 1.6 μs and 1024 data for recording waveforms (200 of them, before the arrival time). Thus, the entire duration of the record window was $t_{\max} = 1318$ μs.

Before testing, the electric noise in the laboratory was measured and a calibration test was carried out by breaking pencil leads (Hsu-Nielsen source) along the specimen. Thus, it was established that using 45 dB as the threshold of detection, pencil leads broken at any place on the specimen could be recorded by all the sensors. Moreover, in an attempt to prevent or reduce friction noise generated between the different metallic elements located in the specimen (added steel blocks, screws, fixing systems of sensors, accelerometers, LVDTs, etc.), rubbers and teflon films were inserted between any two contacting surfaces susceptible of generating noise.

3. AE signal discrimination procedure

Firstly, detailed observation of the AE waveforms recorded in all sensors was made. From it, two patterns of signals were found to be qualitatively different:

Type (i): short-duration signals, whose energy was concentrated mainly at the beginning of the signal, and whose duration was not excessively great;

Type (ii): long-duration signals, whose energy was not concentrated at the beginning of the signal but distributed along the whole signal.

It was observed that both types of signals had largely varying durations and amplitudes, a feature that complicates their separation by traditional filters based only on the classic parameters of AE signals (amplitude, duration, rise-time, etc.). Therefore, developing a post-processing means of identifying and discriminating these signals was mandatory.

The discrimination procedure departs from the premise, based on bibliographical documentation and our own experience with this type of material, that the short-duration signals referred to above as *Type (i)* can correspond to concrete cracking, whereas the long-duration signals designated as *Type (ii)* can be statistically associated with various spurious sources (mainly friction).

As the *first step* of the discrimination process, the following temporal windows were defined in all the AE waveforms (see Fig. 2):

W_1 **(window 1):** 0–450 μs. Samples from $N = 0$ to $N = N_1$, with $N_1 = 281$;

W_2 **(window 2):** 450–1300 μs. Samples from $N = N_1 + 1$ to $N = N_2$, with $N_2 = 824$.

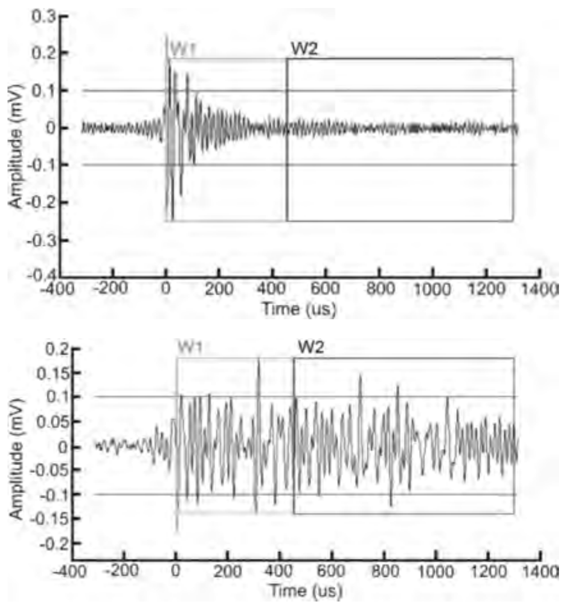

Fig. 2. Some AE Signals corresponding to simulation D1. Top: *Type (i)*; Bottom: *Type (ii)*. Windows W_1 and W_2 are marked on the signals.

The length of W_1 was established in view of the following physical criteria. The propagation speed of longitudinal waves in a bar of this kind of concrete was measured, yielding 3200 m/s. Thus, as the maximum distance between the center of the structure and the sensors was 1.44 m, the maximum arrival time was 450 μs, the time used for W_1. The second window duration (W_2) was from the end point W_1 (450 μs) to the end of the wave (1300 μs).

As the *second step*, the RMS in both windows was calculated. It is defined as

$$\mathrm{RMS}_1 = \sqrt{\frac{1}{N_1}\sum_{N=0}^{N_1} x_i^2}, \tag{1}$$

$$\mathrm{RMS}_2 = \sqrt{\frac{1}{N_2 - N_1}\sum_{N=N_1+1}^{N_2} x_i^2}, \tag{2}$$

where x_i is the discretized AE signal.

As the *third step*, the following criterion was established to discriminate between *Type (i)* and *Type (ii)* signals:

$$\text{If } \mathrm{RMS}_1 \geq Q \cdot \mathrm{RMS}_2 \rightarrow \textit{Type (i)}, \tag{3}$$

$$\text{If } \mathrm{RMS}_1 < Q \cdot \mathrm{RMS}_2 \rightarrow \textit{Type (ii)}, \tag{4}$$

where the parameter Q needs to be previously determined as explained in the Section below.

4. Optimization procedure for obtaining parameter Q

A range of values of Q was previously set to carry out the search during the optimization process. Thus, for each particular value $Q_i \in [Q_1,\ Q_2]$, two physical variables were calculated:

- The acoustic energy MARSE (Measured Area under Rectified Signal Envelope) for all the AE waveforms meeting the condition given in Eq. (3), i.e. for signals of *Type (i)*. The accumulated value of this energy over a particular seismic event, normalized by its value at the end of this seismic event, was calculated for each value of Q_i. It was denoted $E_i^{\mathrm{AE}}(t)$, where t is the time along the seismic event normalized to its maximum value (this normalized time named pseudotime, from $t = 0$ to $t = 1$). Note that $E_i^{\mathrm{AE}}(t)$ depends strongly on the value of Q_i, because it is calculated only for *Type (i)* signals, and the set of these signals depends on the criterion used for discriminating (Eqs. (3) and (4)).
- The mechanical energy dissipated by the specimen in the course of the seismic event, $W_p(t)$, normalized by its value at the end the seismic event (see (Benavent-Climent, 2011) for details to calculate this energy). Obviously, this energy is totally independent on the value of Q_i, because it is not based on acoustic emission measurements.

After calculating both energies, the following quantity was calculated in order to make a comparison and minimize the differences between them:

$$D_{Q_i} = \sqrt{\int_0^1 \left|(E_i^{\mathrm{AE}})^2 - (W_p^2)\right| \,\mathrm{d}t}. \tag{5}$$

Finally, the optimum value of Q, denoted O_{opt}, was established as the one that locally minimizes D defined in Eq. (5) in the range of values $Q_i \in [Q_1,\ Q_2]$, i.e.

$$Q_{\mathrm{opt}} = \min_{Q_i \in [Q_1, Q_2]} \{D_{Q_i}\}. \tag{6}$$

5. Results

The optimization procedure to discriminate the signals was applied to the fourteen seismic simulations conducted with a shaking table, using the range of values $Q_i \in [Q_1,\ Q_2] = [0.6,\ 2]$, beyond which the results proved to be inconsistent. A step of 0.05 was used for Q_i in this range. Table 2 shows the optimum value obtained for Q in all the seismic events, while Fig. 4 shows a superimposed comparison of the accumulated mechanical and acoustic energies, $W_p(t)$ and $E_i^{AE}(t)$,

Table 2. Q_{opt} values obtained for each seismic simulation.

Test	PA (g)	Q_{opt}
A1	0.08	1.68
B1	0.10	1.23
C1	0.12	1.06
D1	0.19	1.94
E1	0.29	0.60
F1	0.38	0.60
G1	0.44	0.60
H1	0.58	0.60
A2	0.19	1.53
B2	0.38	1.08
C2	0.58	1.44
D2	0.66	1.99
E2	0.74	1.68
F2	0.95	1.99

in all the seismic events. It can be clearly seen that, in general and as intended, there is a reasonably good correlation between them, indicating the effectiveness of the discrimination algorithm proposed. Moreover, comparison of these correlations and those previously published in (Gallego, 2011) reveals a clear improvement, supporting the optimization procedure proposed here.

As an example, Fig. 3 shows 6 signals classified as *Type (i)* (three on the left side) and *Type (ii)* (three on the right side), respectively. Simple visual inspection confirms that all were correctly classified.

Finally, Fig. 5 plots both the acoustic energy and the mechanical energy dissipated by the specimen, accumulated over all the seismic events. Both energies are normalized to their values at the end of event F1, the point at which plastification of the steel began to occur (as corroborated by strain gages attached on the steel in the columns and the reinforcements (Benavent-Climent, 2011)). It is evident that

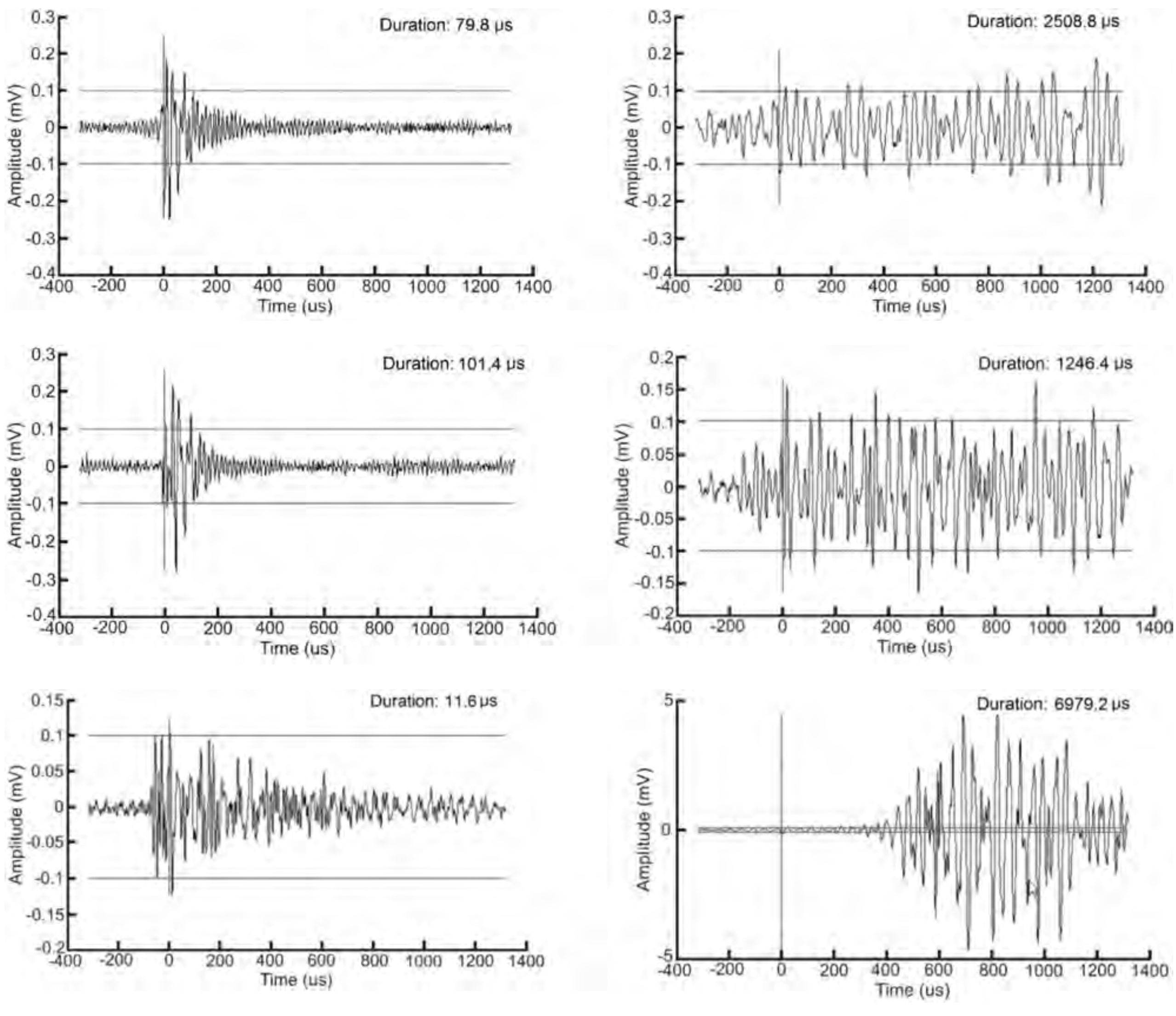

Fig. 3. Some AE Signals corresponding to simulation D1. Left column: *Type* (*i*); Right column: *Type (ii)*.

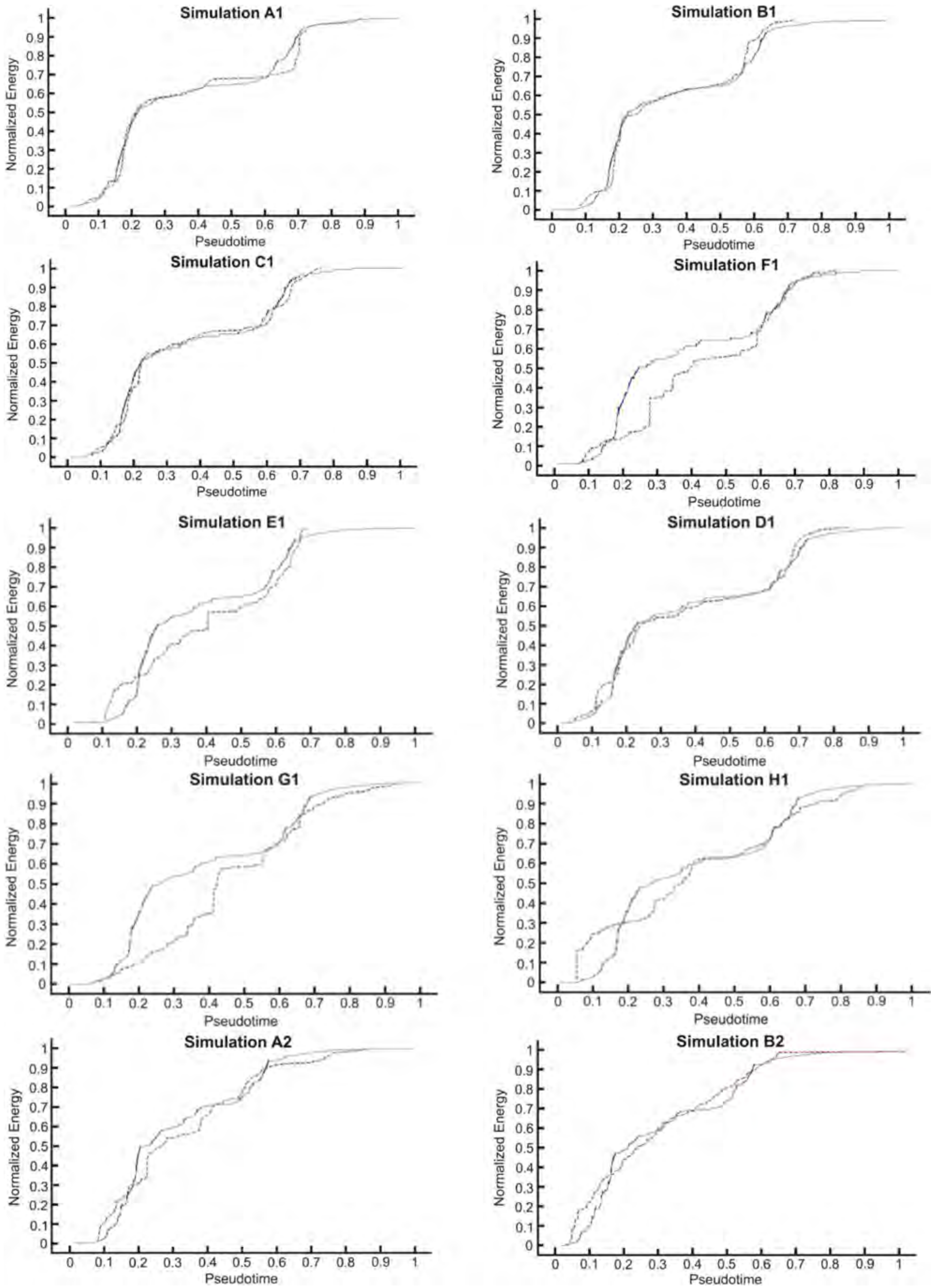
Simulation A1
Simulation B1
Simulation C1
Simulation F1
Simulation E1
Simulation D1
Simulation G1
Simulation H1
Simulation A2
Simulation B2
Normalized Energy
Pseudotime
0
0.1
0.2
0.3
0.4
0.5
0.6
0.7
0.8
0.9
1

[Fig. 4]

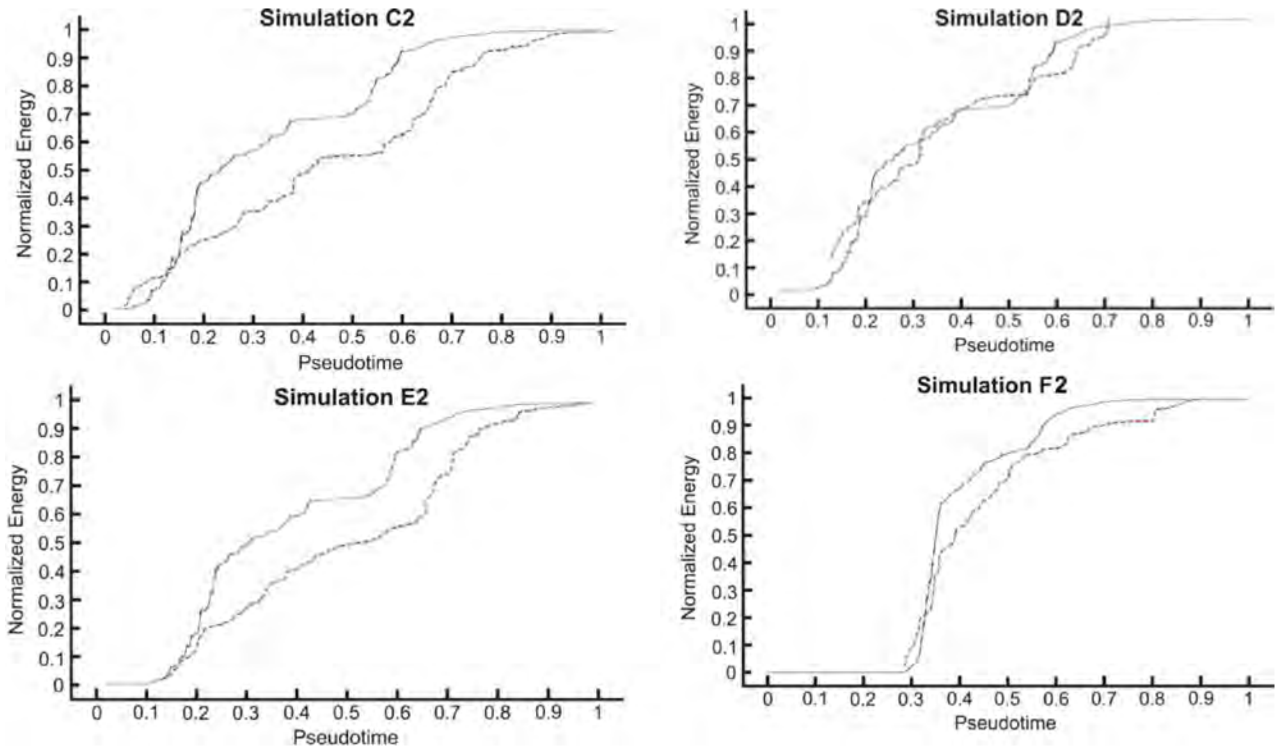

Fig. 4. Normalized E^{AE} (red dotted line) and W_p (blue solid line) for each seismic simulation.

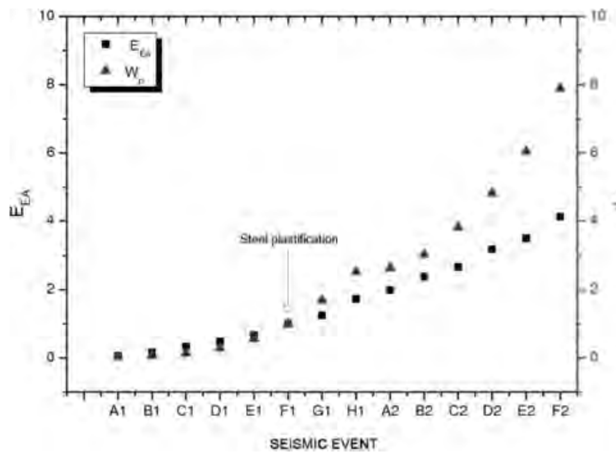

Fig. 5. W_p and E^{AE} energies accumulated along the whole load history, normalized by their respective values at the end of simulation F1.

before this point (F1), there is an excellent correlation between the two energies, thus demonstrating that the AE energy is an adequate indicator for cracking level evaluation in the RC structure. However, from this point on, there is a clear separation between the two energies (always $E^{\mathrm{AE}} < W_p$) because the AE produced by the plastification of the steel cannot be recorded with the AE instrumentation used and the high threshold set for detection (45 dB). It is very well known that steel plastification usually produces AE amplitudes lower than 30 dB. For this reason, it is physically justified that when steel plastification occurs, the E^{AE} remains consistently lower than W_p (see (Benavent-Climent, 2011) for details).

6. Conclusions

An improvement of the algorithm proposed in (Gallego, 2011) to discriminate AE signals mainly coming from friction and signals from concrete cracking was presented. It was improved by introducing an optimization process for the difference between the AE energy and the mechanical energy dissipated by the specimen. The proposal provides a better match between these two energies and for all the seismic events carried out on the test specimen. The plastic strain energy W_p is commonly accepted as an appropriate parameter for characterizing low-cycle fatigue damage in RC components, and it is used in well-established RC damage indexes. The finding that there is a good correlation between W_p and AE energy, calculated by means of AE signals filtered through the procedure proposed, suggests that AE energy can be used as a parameter to quantitatively assess the level of damage in an RC structure subjected to seismic loading. Ongoing research aims to develop new damage indexes for RC structures subjected to seismic loadings expressed merely in terms of AE energy.

Acknowledgments

This research received the financial support of the local government of Spain, Consejería de Innovación, Ciencia y Tecnología, Project P07-TEP-02610. The work also received support from the European Union (Fonds Européen de Dévelopment Régional) and the Scholarship of Initiation to the Investigation of the University of Granada Research Plan (Beca de Iniciación a la Investigación del Plan Propio de la Universidad de Granada). The authors thank Prof. Benavent-Climent for his scientific contributions.

References

1. Benavent-Climent A., Castro E., Gallego A. (2009), *AE Monitoring for Damage Assessment of RC Exterior Beam-Column Subassemblages Subjected to Cyclic Loading*, Structural Health Monitoring, **8**, 175–189.
2. Benavent-Climent A., Castro E., Gallego A. (2010), *Evaluation of low cycle fatigue damage in RC exterior beam-column subassemblages by acoustic emission*, Construction and Building Materials, **24**, 1830–1842.
3. Benavent-Climent A., Gallego A., Vico J.M. (2011), *An acoustic emission energy index for damage evaluation of reinforced concrete slabs under seismic loads*, Structural Health Monitoring, **11**, 1, 69–81.
4. Carpinteri A., Lacidogna G., Pugno N. (2007), *Structural damage diagnosis and life-time assessment by acoustic emission monitoring*, *Engineering Fracture* Mechanics, **74**, 1–2, 273–289.
5. Gallego A., Benavent-Climent A., Cristóbal I. (2011), *Health monitoring of reinforced concrete slabs subjected to earthquake-type dynamic loading via measurement and analysis of acoustic emission signals*, Smart Structures and Systems, **8**, 4, 385–398.
6. Guzik J., Wojtyniak M., Olszowski S., Marczak M., Ranachowski Z. (2006), *Investigation of acoustic emission signal generated in the friction pair lubricated with oils containing various lubricity additives*, Engineering Transactions, **54**, 2, 159–166.
7. Jasieński Z., Pawelek A., Piatkowski A., Ranachowski Z. (2009), *Twinning and shear band formation in channel-die compressed silver single crystals identified by Acoustic Emission method*, Archives of Metallurgy and Materials, **54**, 1, 29–33.
8. Ministry of Construction of Spain (2002), *Spanish Seismic Code NCSE-02*, Madrid.
9. Ministry of Construction of Spain (2008), *Spanish Concrete Code EHE-08*, Madrid.
10. Ranachowski Z., Jóźwiak-Niedźwiecka D., Brandt A.M., Dębowski T. (2012), *Application of the acoustic emission technique to determine critical stress in fiber reinforced mortar beams*, Archives of Acoustics, **37**, 3, 261–268.
11. Wozniak T.Z., Ranachowski Z. (2006), *Acoustic Emission during austenite decomposition into lower bainite with midrib*, Archives of Acoustics, **31**, 3, 319–334.
12. Yuyama S., Li ZW., Ito Y., Arazoe M. (1999), *Quantitative analysis of fracture process in RC column foundation by moment tensor analysis of acoustic emission*, Construction and Building Materials, **13**, 1–2, 87–97.
13. Yuyama S., Li ZW., Yoshizawa M., Tomokiyo T., Uomoto T. (2001), *Evaluation of fatigue damage in reinforced concrete slab by acoustic emission*, NDT&E International, **34**, 6, 381–387.

PAN
ARCHIVES OF ACOUSTICS
Vol. **38**, No. 3, pp. 311–319 (2013)

DOI: 10.2478/aoa-2013-0038

Source Width of Frontal Phantom Sources: Perception, Measurement, and Modeling

Matthias FRANK

Institute of Electronic Music and Acoustics, University of Music and Performing Arts Graz
Inffeldgasse 10/3, 8010 Graz, Austria; e-mail: frank@iem.at

(*received July 4, 2012; accepted February 8, 2013*)

Phantom sources are known to be perceived similar to real sound sources but with some differences. One of the differences is an increase of the perceived source width. This article discusses the perception, measurement, and modeling of source width for frontal phantom sources with different symmetrical arrangements of up to three active loudspeakers. The perceived source width is evaluated on the basis of a listening test. The test results are compared to technical measures that are applied in room acoustics: the inter-aural cross correlation coefficient (IACC) and the lateral energy fraction (LF). Adaptation of the latter measure makes it possible to predict the results by considering simultaneous sound incidence. Finally, a simple model is presented for the prediction of the perceived source width that does not require acoustic measurements as it is solely based on the loudspeaker directions and gains.

Keywords: source width, phantom source, stereophony, IACC, LF, energy vector.

1. Introduction

It is known from concert hall acoustics that reflections from walls and the ceiling influence the perceived spatial extent of instruments. This perceived size of a sound source is often called *auditory* or *apparent source width* (ASW). There are technical measures that correlate with the perception of ASW (Schroeder *et al.*, 1974; Barron, Marshall, 1981; Blauert, Lindemann, 1986a; Hidaka *et al.*, 1995; Morimoto, Iida, 2005). The two most common measures are the inter-aural cross correlation coefficient (IACC) using a dummy head and the lateral energy fraction (LF) using a combination of an omni-directional and a figure-of-eight microphone.

A *phantom source* is an auditory event that is perceived at a location where there is no real source present (Wendt, 1963), i.e. a location between loudspeakers. The simplest method to create a phantom source with two loudspeakers is *stereophony* (Blumlein, 1958) which uses level and/or time-delay differences between the loudspeakers to control the location of the phantom source. Other methods, such as *multiple-direction amplitude panning* (Pulkki, 1999) or *Ambisonics* (Daniel, 2001), use more than two loudspeakers for the creation of a single phantom source. It is known that phantom sources differ from real sources with respect to the perceived source width. Different terms have been used to describe this difference: image focus (Martin *et al.*, 1999), locatedness (Simon *et al.*, 2009), or spatial spread (Pulkki, 1999).

Studies show that the loudspeaker spacing influences the perceived source width (Frank *et al.*, 2011; Kin, Plaskota, 2011). However, there is no systematic study about how the number of loudspeakers and their directions and gains are related to the width of phantom sources. To start discussion about this relationship, this article presents a study with loudspeaker arrangements of various width in a listening setup with dominant direct sound. The loudspeaker arrangements are symmetrical to the 0° axis and use one, two, or three loudspeakers that play the same signal.

The second section of this paper describes a listening test that evaluates the perceived source width. The impulse responses of the loudspeakers in the listening test setup were also measured with a dummy head and a microphone array. From these measurements, section three derives the IACC and LF measures. These measures are compared to the results of the listening test. The third section also presents an adaptation of LF to make it a valid predictor for the experimental data. Section four introduces a simple model for the perceived source width that predicts the data without acoustic measurement, just based on the gains and directions of the loudspeakers and assuming no dependency on room reflections.

In this paper, the directions of L loudspeakers are vectors of unit length $\boldsymbol{\theta}_l = [\cos(\phi_l),\ \sin(\phi_l)]^{\mathrm{T}}$ that depend on their azimuth angle ϕ_l in the horizontal plane, see Fig. 1. For each loudspeaker $l \in \{1, \ldots, \mathrm{L}\}$, the scalar weight g_l denotes its adjustable gain. Impulse responses are represented by $h(t)$.

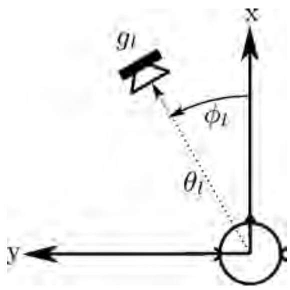

Fig. 1. Reference system used in this paper.

2. Perceptual evaluation

This section describes the method and results of the perceptual evaluation of phantom source width by a listening test. The goal of the measurements and modeling presented later is to find valid technical estimators for the data of the time consuming listening test.

2.1. Method

The evaluation studied perception of source width for one, two, and three active loudspeakers playing the same signal and different spacings between them. Figure 2 shows the test setup with 17 Genelec 8020 loudspeakers: loudspeaker 0 at 0°, and loudspeaker pairs $1 \ldots 8$ at $\pm 5° \ldots \pm 40°$. The setup was built in the center of a 11 m × 11 m × 5 m room with a reverberation time within the limits of ITU-R BS.1116-1 (ITU, 1997). The distance to the central listening position was 2.5 m for each loudspeaker, which lies within the effective critical distance. The height of the loudspeakers (referred to halfway between woofer and tweeter) was adjusted to 1.2 m, which was also the ear height of the subjects. The control of the entire listening test, as well as the creation of the loudspeaker signals used the open source software pure data (freely available on http://puredata.info/downloads) on a PC with an RME HDSPe MADI and RME M-16 DA D/A converters. All measurements in the remainder of this paper were using the same setup and conditions.

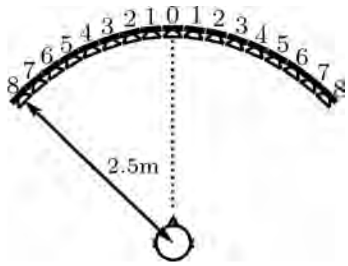

Fig. 2. Loudspeaker setup used for the perceptual evaluation and measurements.

Table 1 shows the angles and gains of the loudspeakers for each of the 16 conditions. Empty entries in the table mean that the corresponding loudspeakers

Table 1. Conditions in the listening test: loudspeaker indices, directions ϕ_l, and gains g_l (gains of zero are not shown).

loudspeaker(s)	0	1	2	3	4	5	6	7	8
angle(s) ϕ_l in °	0	±5	±10	±15	±20	±25	±30	±35	±40
0	1								
10		$1/\sqrt{2}$							
20			$1/\sqrt{2}$						
30				$1/\sqrt{2}$					
40					$1/\sqrt{2}$				
50						$1/\sqrt{2}$			
60							$1/\sqrt{2}$		
70								$1/\sqrt{2}$	
80									$1/\sqrt{2}$
$C10$	$1/\sqrt{3}$	$1/\sqrt{3}$							
$C20$	$1/\sqrt{3}$		$1/\sqrt{3}$						
$C30$	$1/\sqrt{3}$			$1/\sqrt{3}$					
$C40$	$1/\sqrt{3}$				$1/\sqrt{3}$				
$C50$	$1/\sqrt{3}$					$1/\sqrt{3}$			
$C70$	$1/\sqrt{3}$							$1/\sqrt{3}$	
$C80$	$1/\sqrt{3}$								$1/\sqrt{3}$

are not active. Condition 0 is a single loudspeaker playing from 0° in front of the listener. Conditions $10\ldots80$ correspond to 2-channel stereophony on frontally centered pairs of loudspeakers with the same amplitude gain and aperture angles ranging from 10° to 80°. In conditions $C10\ldots C80$ the central loudspeaker (loudspeaker 0 at 0°) is added with the same gain. These additional conditions aim at extending the applicability of the relationships obtained to arbitrary amplitude panning methods that use more than two loudspeakers, such as multiple-direction amplitude panning (Pulkki, 1999) or Ambisonics (Daniel, 2001). Note that condition $C60$ has not been tested due to an error in the playback software. The gains in all conditions were normalized to a constant overall energy which results in gains that depend on the number of active loudspeakers. Furthermore, the symmetrical arrangement aims at creating a phantom source direction of 0° for all conditions in order to exclude differences in the localization direction between the conditions.

Fourteen subjects participated in the listening test; their individual hearing loss was less than 12 dB between 250 Hz and 8 kHz. All of them were members of a trained expert listening panel (Sontacchi *et al.*, 2009; Frank *et al.*, 2010; Frank, Sontacchi, 2012) and had already participated in listening tests about source width (Frank *et al.*, 2011; Zotter *et al.*, 2011). Each of the 16 conditions was presented seven times for each subject in random order. The stimulus was 1.5 s of pink noise at a level of 65 dB(A). The subjects were allowed to repeat the stimulus at will by pressing a button on a keyboard. They were asked to measure the perceived source width in terms of an index and to write their answer in a questionnaire. The index expressed the perceived width in terms of numbers on the increasingly wide, nested loudspeaker pairs according to Fig. 2. It was also possible to use half indices to rate perceived widths that are between adjacent indices which results in a possible resolution of 5°. The subjects were told to face forward but there was no head fixation in order to allow small head movements. It has been shown that these movements are performed unconsciously (Blauert, 1983) but are important for localization (Mackensen, 2008) and assessment of spatial impression (Brookes *et al.*, 2007).

2.2. Results

The answers were averaged over all subjects and all repetitions. No subjects were excluded from the results. Figure 3 shows the resulting mean value and corresponding 95% confidence interval of the perceived source width for each condition. The results in the figure were arranged to ascending aperture angle between the two outmost active loudspeakers.

Within the 2-channel conditions $10\ldots80$, an increase of the aperture angle yields an increase of the perceived source width. An analysis of variance confirms the aperture angle as a highly significant factor ($p \ll 0.001$). This holds true for the conditions with the additional central loudspeaker $C10\ldots C80$. Comparing both groups with and without the central loudspeaker, the addition of the central loudspeaker yields a highly significant decrease of the perceived source width. This relation agrees with the findings in (Kin, Plaskota, 2011) and can be explained by the fact that the active central loudspeaker decreases the relative share of lateral sound. Note that in pairwise comparisons of the corresponding conditions with and without central loudspeaker, differences between the mean values of $C10/10$ and $C50/50$ are not significant ($p > 0.05$).

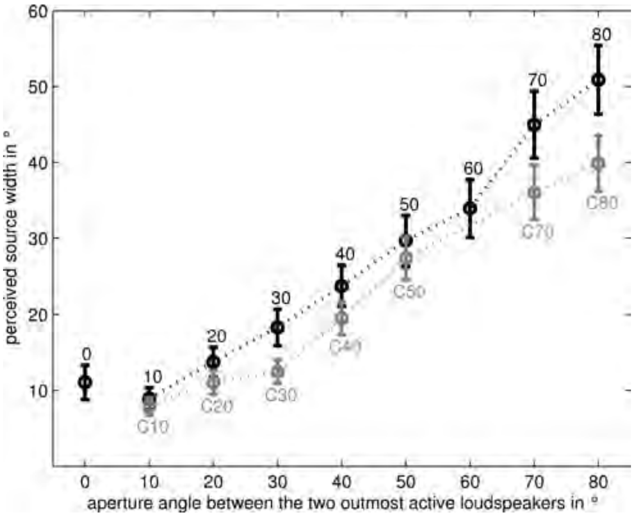

Fig. 3. Mean and 95% confidence interval of the perceived source width for each condition, arranged to ascending aperture angle between the two outmost active loudspeakers.

Interestingly, conditions $C10$, 10, and $C20$ yield smaller mean values for the perceived source width than the single central loudspeaker 0. However, the mean values are not significantly different. Hence, the lower bound for perception of source width is about 10° in our test setup. This bound is expected to be dependent on the acoustical properties of the room and may differ for other rooms.

3. Technical measures

This section presents technical measures obtained by acoustic measurements and their correlation to the listening test results above. As these measures are typically applied to reverberant concert halls, this section examines the suitability of the measures for the prediction of phantom source width. The measurements were performed on exactly the same experimental setup and environment as in the listening test.

3.1. Inter-Aural Cross Correlation Coefficient (IACC)

In order to calculate the inter-aural cross correlation coefficient (IACC), binaural impulse responses were measured for each loudspeaker using a B&K 4128C dummy head. For each condition, h_{left} and h_{right} are the impulse responses of the left and the right ear of the dummy head, respectively. They are calculated as the linear superposition of the binaural impulse responses for each loudspeaker $h_{l,\text{left}}$ and $h_{l,\text{right}}$ with the appropriate loudspeaker gains g_l according to Table 1

$$h_{\text{left}} = \sum_{l=1}^{L} h_{l,\text{left}}\, g_l \quad \text{and} \quad h_{\text{right}} = \sum_{l=1}^{L} h_{l,\text{right}}\, g_l. \tag{1}$$

The IACC is defined as the maximum of the interaural cross correlation function (IACF), cf. (ISO, 2009)

$$\text{IACF}(\tau) = \frac{\int_{t_1}^{t_2} h_{\text{left}}(t) h_{\text{right}}(t+\tau)\,\mathrm{d}t}{\sqrt{\left[\int_{t_1}^{t_2} h^2_{\text{left}}(t)\,\mathrm{d}t\right]\left[\int_{t_1}^{t_2} h^2_{\text{right}}(t)\,\mathrm{d}t\right]}}, \tag{2}$$

$$\text{IACC} = \max_{\tau\in[-1\text{ms};1\text{ms}]} |\text{IACF}(\tau)|, \tag{3}$$

Typically, the observation time is set to the first 80 ms of the impulse responses, i.e. $t_1 = 0$ ms and $t_2 = 80$ ms. As this version of the IACC considers only the early part of the impulse responses, it is called early IACC or IACC_{E}. Furthermore, the IACC is mostly not calculated for the broadband signals, but separately for three octave bands around 500 Hz, 1 kHz, and 2 kHz (Hidaka *et al.*, 1995). The three correlation coefficients are averaged. Here the early IACC is employed for the three octave bands, denoted as IACC_{E3}.

There are different values for the perceptually just noticeable difference (JND) of IACC_{E3} in the literature: 0.075 (ISO, 2009; Cox *et al.*, 1993), 0.05–0.08 (Okano, 2002), 0.038 (Blau, 2002).

Figure 4 draws the computed $1-\text{IACC}_{\text{E3}}$ measures of all conditions in relation to the mean of the perceived source width from the listening test. The IACC_{E3} values range from 0.8 to 0.95 and cover 2–4 JNDs which predicts a poor discriminability that is in contradiction to the results of the listening test results, cf. Fig. 3. The value of $\text{R}^2 = 0.65$ for the coefficient of determination reveals a fair correlation between the listening test results and the objective measure. Altogether, IACC_{E3} does not seem to be an optimal predictor of the perceived source width in case of simultaneous sound incidence. It obviously refers to a longer temporal structure of the impulse responses. In other cases, the IACC_{E3} is a better predictor if the temporal structure of the loudspeaker signals is manipulated, e.g., by decorrelation algorithms (Zotter *et al.*, 2011), which is not the case in the experimental conditions, here.

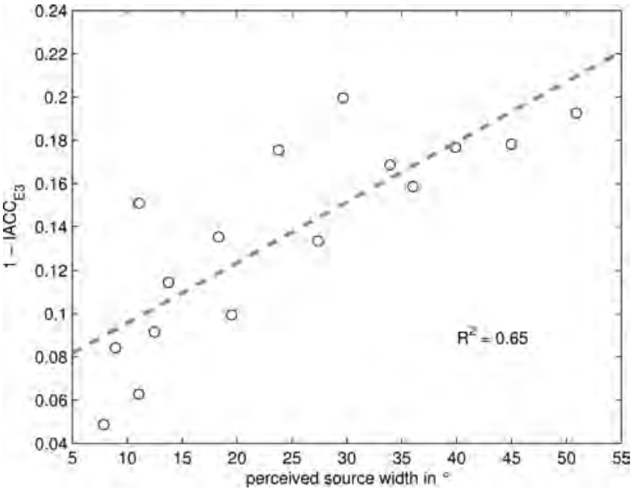

Fig. 4. Regression of $1-\text{IACC}_{\text{E3}}$ to the listening test results.

3.2. Lateral Energy Fraction (LF)

The lateral energy fraction (LF) is also used to describe width. It is derived from the impulse response measurements using an omni-directional microphone and a figure-of-eight microphone, yielding the responses $h_\circ$ and h_∞, respectively. For each condition, both responses are computed from the linear superposition of the individual impulse responses of each loudspeaker $h_{l,\circ}$ and $h_{l,\infty}$ with the appropriate loudspeaker gains g_l according to Table 1

$$h_\circ = \sum_{l=1}^{L} h_{l,\circ}\, g_l \qquad \text{and} \qquad h_\infty = \sum_{l=1}^{L} h_{l,\infty}\, g_l, \tag{4}$$

$$\text{LF} = \frac{\int_{t_0}^{80\,\text{ms}} h^2_\infty\,\mathrm{d}t}{\int_{0\,\text{ms}}^{80\,\text{ms}} h^2_\circ\,\mathrm{d}t}. \tag{5}$$

As the upper integration bound is normally set to 80 ms, the measure is sometimes also called early lateral energy fraction (Cox *et al.*, 1993). According to ISO3382 (ISO, 2009), the lower integration bound of the figure-of-eight signal is defined as $t_0 = 5$ ms. Although some authors calculate the LF in three octave bands around 500 Hz, 1 kHz, and 2 kHz, i.e. similar to the IACC_{E3}, the broadband version of the LF is used in this article.

Literature gives the following values for the JND of the LF: 0.048 (computed) and 0.058 (measured) (Cox *et al.*, 1993), 0.075 (ISO, 2009), and 0.045–0.07 (Blau, 2002).

The measurements used a Schoeps CCM 8 figure-of-eight microphone and an NTI MM2210 omnidirectional microphone. Figure 5 shows that the standard LF measure is not related ($R^2 = 0.19$) to the listening test results. Furthermore, the LF values range from 0.01 to 0.022 and lie within one JND only, which contradicts the listening test results. These LF values represent the effect of the early reflections exclusively that are perceptually independent of the condition. The exclusion of the direct part of the sound is caused by the lower integration bound of $t_0 = 5$ ms for the figure-of-eight signal.

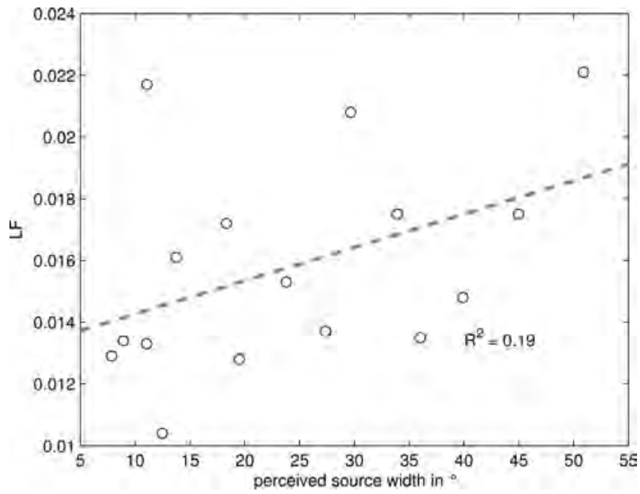

Fig. 5. Regression of the standard LF measures ($t_0 = 5$ ms) to the listening test results.

3.2.1. Reducing the lower integration bound t_0 for h_∞

In order to improve the suitability of the LF for direct sound, the lower integration bound t_0 of the figure-of-eight signal h_∞ is changed to $t_0 = 0$ ms.

Figure 6 shows the regression results of the improved LF measures ($t_0 = 0$ ms) to the listening test results. The value of $R^2 = 0.69$ verifies the improvement of the LF measures. The new measures range from 0.015 to 0.094 and cover 2–3 JNDs. Thus, the quality of the new LF measures is comparable to the $\mathrm{IACC}_{\mathrm{E3}}$ measures.

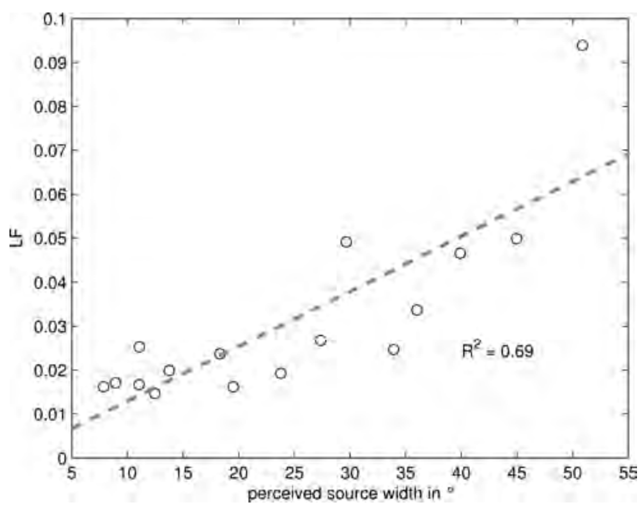

Fig. 6. Regression of the LF measures ($t_0 = 0$ ms) to the listening test results.

The limitation of the range is most likely caused by signal cancellation of the simultaneous sound incidence at the figure-of-eight microphone. The next paragraph presents an approach to overcome the poor prediction of the significant differences from the listening test by further improvement of the LF measurement.

3.2.2. Energetic superposition

If the impulse responses of the loudspeakers have been measured independently, their signals can be superimposed without interference. Formally, this is achieved by energetic superposition

$$
\begin{aligned}
h_\circ &= \sqrt{\sum_{l=1}^{\mathrm{L}} (h_{l,\circ}\, g_l)^2}, \\
h_\infty &= \sqrt{\sum_{l=1}^{\mathrm{L}} (h_{l,\infty}\, g_l)^2}.
\end{aligned} \tag{6}
$$

This was done for all conditions and the LF measures were calculated again. Figure 9 shows that the correlation between these values and the perceived source width is high ($R^2 = 0.95$). The LF values now range from 0.025 to 0.41 and cover 6–9 JNDs, which is comparable to the listening test results.

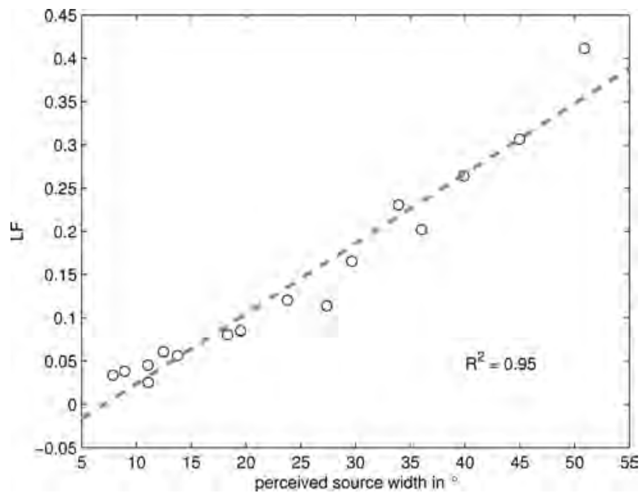

Fig. 7. Regression of the energetically superimposed LF measures ($t_0 = 0$ ms) to the listening test results.

Nevertheless, the energetically superimposed lateral energy fraction cannot be measured by a single measurement of simultaneously active loudspeakers, as the superposition in the sound field is linear. In order to avoid signal cancellation for the case of simultaneously active loudspeakers, an alternative definition of the LF has to be found.

3.2.3. Multiple measurement positions

Two equally loud coincident signals from the symmetric pair of loudspeakers cancel each other in the figure-of-eight microphone due to its pickup pattern. The cancellation is not entirely destructive when measuring at a position that is slightly off-center. This is because the pair of loudspeaker signals arrives with unequal time-delays, i.e., with a phase difference that linearly grows with frequency. Thus, cancellation can be reduced by measuring at N positions on a line that is shifted along the axis of the figure-of-eight microphone and averaging the LF_n values hereby obtained

$$\mathrm{LF} = \frac{1}{N}\sum_{n=1}^{N}\mathrm{LF}_n. \tag{7}$$

Each of the LF_n values results from a linear superposition of the loudspeaker signals as in Eq. (4). The displacement is only effective above a certain frequency $f_{\min}$ that is determined by the measurement aperture $d_{\max}$, i.e. the distance between the outmost measurement positions

$$f_{\min} = \frac{\mathrm{c}}{2d_{\max}} \tag{8}$$

with $\mathrm{c} = 343$ m/s in air at 20°C temperature.

A simulation was done in order to evaluate the quality of the approximation of the energetic superposition by averaging over multiple measurement positions with linear superposition of the loudspeaker signals. These measurement positions were simulated by appropriate delaying (rounded to integer samples at a sampling rate of 44.1 kHz) and level adjustment of the measured impulse responses from the central listening/measurement position. The simulation ignored the influence of the loudspeaker directivity which is negligible for the used range of $d_{\max}$. In the simulation, the number of measurement positions N and the size of the measurement aperture $d_{\max}$ was varied. The maximum error between the LF measures of the energetic superposition and the average linear superposition at multiple measurement positions was used as quality measure for the approximation. To ensure that there is no perceptible difference in the approximation, the error must be $\leq 1/2$ JND of the LF, which is approximately 0.03. In Fig. 8, the absolute value of the error is presented in gray scale. Whenever the error is below the value of 0.03, the area is white. Darker areas represent larger errors.

The number of measurement positions N has a weak influence on the maximum error. Only for small aperture sizes $d_{\max}$, a larger number N decreases the maximum error. For apertures $d_{\max} \geq 0.14$ m, the errors are smaller than 0.03, even when averaging over only $N = 2$ positions. Interestingly, this distance is

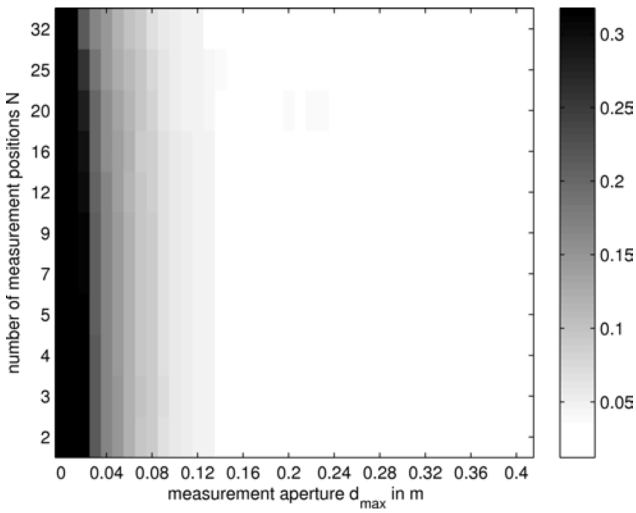

Fig. 8. Maximum error of the approximation of the energetic superposition by averaging over multiple linear superimposed measurement positions in dependence of the number of measurement positions N and the aperture $d_{\max}$.

similar to the head diameter. This distance results in a lower frequency bound for the avoidance of destructive interference of $f_{\min} = 1.2$ kHz. For phantom source width, higher frequency components seem to be important. This result agrees to the findings in (Blauert, Lindemann, 1986b; Morimoto, Maekawa, 1988) stating that higher frequency components also contribute to the perception of source width in concert halls.

Figure 9 shows the regression of the listening test results to the linearly superimposed LF measures that are averaged over $N = 2$ positions with $d_{\max} = 0.14$ m (±0.07 m apart from the center of the arrangement). The regression yields similar results compared to the energetically superimposed LF measures, cf. Fig. 7.

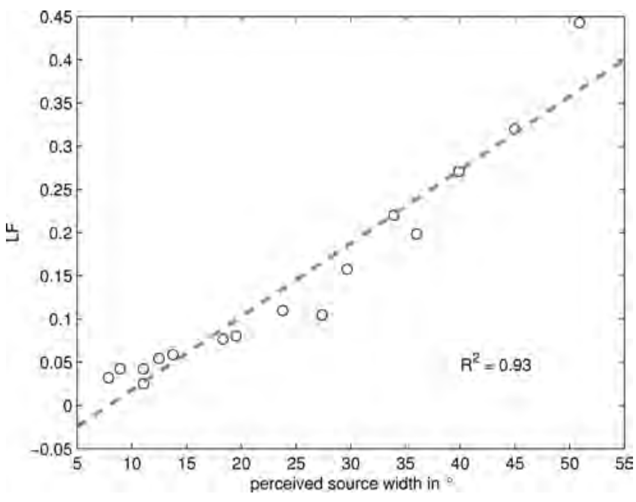

Fig. 9. Regression of the LF measure with linear superposition at 2 positions $d_{\max} = 0.14$ m ($t_0 = 0$ ms) to the listening test results.

Figure 10 compares the different LF measures. The standard LF measure (1 position, linear superposition, $t_0 = 5$ ms) yields small values and does not increase for conditions with larger loudspeaker spacing. Lowering of the integration bound for h_∞ to $t_0 = 0$ ms improves the quality of the LF measure. The largest value range and the best correlation to the listening test results is achieved by the energetic superposition or its approximation by two measurement positions with linear superposition. The advantage of multiple measurement positions can also be found in other fields of acoustics. In recording technique, spaced main microphone arrays are preferred over coincident arrays when capturing spatial impressions (Theile, 1991). The literature about room acoustics tells about large spatial fluctuation of room acoustic measures in concert halls that occur only in measurements, but not in perception (de Vries *et al.*, 2001; van Dorp Schuitman, 2011).

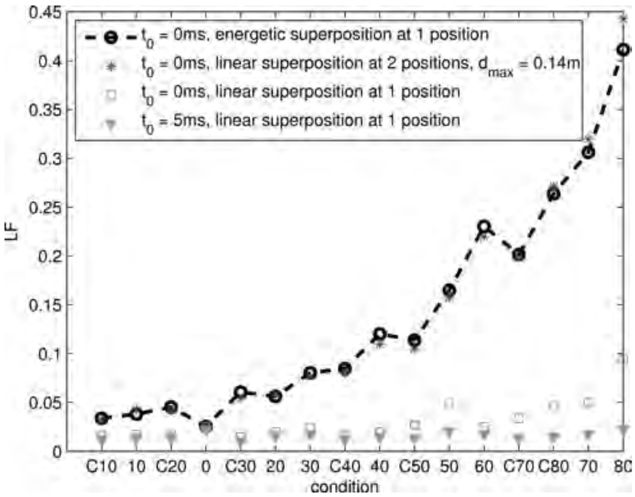

Fig. 10. Comparison of the different LF measures for each condition, arranged to ascending mean values of the listening test results.

Obviously, all presented LF measures yield nearly the same values for condition 0 (a single loudspeaker at 0°). The non-zero values for this condition are due to early reflections and define a lower bound for source width in the listening room. Nevertheless, the differences between the conditions are mainly caused by the differences in the direct sound of the loudspeakers.

The presented adaptations of the LF measure will not decrease their suitability for room acoustic measurements, where source width is mainly caused by early reflections. They will yield similar results as the standard LF measure when they are applied in reverberant rooms, as it is unlikely that there are reflections within the first 5 ms or multiple early reflections arriving at exactly the same time on opposite sides of the figure-of-eight microphone.

4. Simple prediction model

The previous section presented technical measures based on acoustic measurements. These measurements still require the efforts to set up the system under evaluation. This section presents a simple model that can predict the perceived source width without the need of a real setup. The model assumes that the direct sound is more prominent than the early reflections, resulting in a condition-independent contribution of the reflections to the source width. As shown in the section above, this assumption holds for our listening setup, as well as for setups according to the ITU recommendation (ITU, 1997) where the listener sits within the effective critical distance.

4.1. Energy vector ($\boldsymbol{r}_\mathrm{E}$)

The magnitude of the so-called *energy vector* $\boldsymbol{r}_\mathrm{E}$ (Gerzon, 1992) is proposed as predictor of the perceived source width. It is calculated from the direction vectors $\boldsymbol{\theta}_l$ and scalar gains g_l of each loudspeaker

$$\boldsymbol{r}_\mathrm{E} = \frac{\sum\limits_{l=1}^{\mathrm{L}} g_l^2 \boldsymbol{\theta}_l}{\sum\limits_{l=1}^{\mathrm{L}} g_l^2}. \tag{9}$$

In the tested conditions, all L active loudspeakers are driven by $g_l = 1/\sqrt{\mathrm{L}}$ and the overall energy is normalized $\sum\limits_{l=1}^{\mathrm{L}} g_l^2 = 1$. In this case, $\boldsymbol{r}_\mathrm{E}$ is the average of the direction vectors $1/\mathrm{L} \sum\limits_{l=1}^{\mathrm{L}} \boldsymbol{\theta}_l$. Its direction and magnitude relates to the direction and spread of the acoustic energy, respectively. A magnitude value of 1 indicates that only one loudspeaker is active, while one of 0 corresponds to energy distributed in all directions or in opposing directions. The energy vector was originally proposed as a predictor for the direction of phantom sources (Gerzon, 1992). Later works also use it to describe energy distribution (Daniel, 2001). For the tested, frontal conditions, the magnitude of the energy vector is strongly related to the lateral energy fraction under free-field conditions. Therefore, it is not surprising that first hints towards the correlation of the magnitude of the energy vector to the perceived width of phantom sources were discovered (Frank *et al.*, 2011).

Figure 11 shows an excellent correlation ($R^2 = 0.97$) between the listening test results and the magnitude of the energy vector. The regression coefficients yield a formula for the prediction of the perceived source width

$$\alpha = 186.4° \cdot (1 - |\boldsymbol{r}_\mathrm{E}|) + 10.7°. \tag{10}$$

The additive bias of 10.7° relates to the lower bound for the perception of source width that was

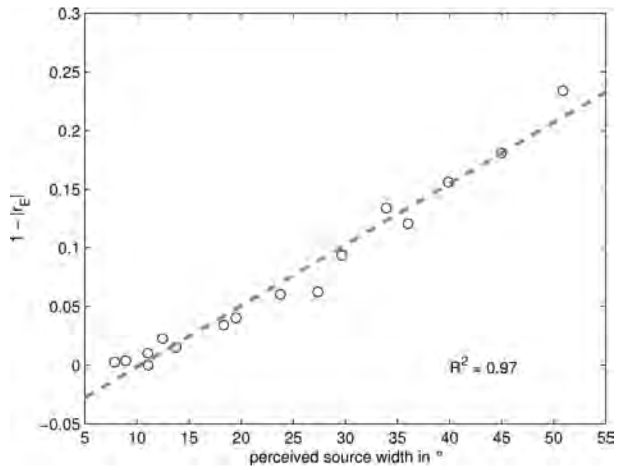

Fig. 11. Regression of $1 - |\boldsymbol{r}_{\mathrm{E}}|$ to the listening test results.

found in the listening test, cf. Fig. 3, and the amount of the LF measure that is caused by early reflections independently of the condition, cf. Fig. 10. Of course, the exact value of this bias is dependent on the room. Nevertheless, the linear relation between the length of the energy vector and the perceived source width is valid for other rooms, as long as the listener sits in the direct sound field of the loudspeakers.

5. Conclusion

This article studied the source width of frontal phantom sources created by two and three loudspeakers playing the same signal in a listening setup with dominant direct sound. For the two-channel conditions, a listening test revealed the relation between the physical width of the active loudspeaker pair and the perceived width of the phantom source. This relation was also demonstrated to work for the case of an additional central loudspeaker. Comparing both groups of stimuli, the addition of the central loudspeaker decreases the source width. This finding agrees with results from the literature (Kin, Plaskota, 2011).

The listening test results were compared to the early inter-aural cross correlation coefficient ($\mathrm{IACC_{E3}}$) and the lateral energy fraction (LF). The $\mathrm{IACC_{E3}}$ yields a fair correlation to the listening test results, whereas the correlation to the standard version of the LF is poor. That is because the standard LF measure excludes the direct sound and solely considers the early reflections whose amount was found to be condition-independent in our listening setup. Improvements were presented that adapt the LF measurement for simultaneous incidence of direct sound. By reducing the lower bound for the integration of the figure-of-eight microphone, a fair correlation could be established, which supports the importance of the direct sound. Further improvement could be achieved by avoiding signal cancellation at the figure-of-eight microphone. The optimal solution would be an energetic superposition of the loudspeaker signals at the microphone, which is not possible in practice for simultaneous playback using multiple loudspeakers. The more versatile way of measuring approximates this by measuring at multiple positions. Averaging of two positions at a distance of ±7 cm is sufficient. As this distance avoids signal cancellation only above 1.2 kHz, the importance of high frequency components for source width is obvious. Despite the improved prediction of source width under listening conditions with dominant direct sound, the adapted LF measures are still applicable for measurements in reverberant rooms.

Finally, a simple model was found that can predict the perceived source width from the listening test solely based on loudspeaker directions and gains. This energy vector model assumes typical studio conditions where the listener sits within the effective critical distance, i.e. the direct sound is more prominent than the reflections. The condition-independent lower bound for source width caused by reflections is incorporated in the model by adding a constant bias. The exact value of this bias depends on the listening setup. The model can be extended to surrounding sound incidence, frequency dependency, and three-dimensional loudspeaker arrangements. Further research is planned about the suitability of the energy vector for predicting phantom source localization.

Acknowledgments

The author is grateful to Franz Zotter for proofreading of the article and fruitful discussions, and the anonymous reviewers for comments that helped improving the paper. This research is partly supported by the project AAP, which is funded by Austrian ministries BMVIT, BMWFJ, the Styrian Business Promotion Agency (SFG), and the departments 3 and 14 of the Styrian Government. The Austrian Research Promotion Agency (FFG) conducted the funding under the Competence Centers for Excellent Technologies (COMET, K-Project), a program of the above-mentioned institutions.

References

1. Barron M., Marshall A.H. (1981), *Spatial impression due to early lateral reflections in concert halls: The derivation of a physical measure*, Journal of Sound and Vibration, **77**, 2, 211–232.
2. Blau M. (2002), *Difference limens for measures of apparent source width*, Forum Acusticum, Sevilla, Spain.
3. Blauert J., Lindemann W. (1986), *Spatial mapping of intracranial auditory events for various degrees of interaural coherence*, The Journal of the Acoustical Society of America, **79**, 3, 806–813.

4. Blauert J., Lindemann W. (1986), *Auditory spaciousness: Some further psychoacoustic analyses*, The Journal of the Acoustical Society of America, **80**, 2, 533–542.
5. Blauert J. (1983), *Spatial Hearing*, MIT Press.
6. Blumlein A.D. (1958), *British patent specification 394,325 (improvements in and relating to sound-transmission, sound-recording and sound-reproducing systems)*, J. Audio Eng. Soc., **6**, 2, 91–98.
7. Brookes T., Kim C., Mason R. (2007), *An investigation into head movements made when evaluating various attributes of sound*, Preprint 7031, 122nd Conv. Audio Eng. Soc., Vienna.
8. Cox T.J., Davies W.J., Lam Y.W. (1993), *The sensitivity of listeners to early sound field changes in auditoria*, Acta Acustica united with Acustica, **79**, 1, 27–41.
9. Daniel J. (2001), *Représentation de champs acoustiques, application à la transmission et à la reproduction de scénes sonores complexes dans un contexte multimédia*, Ph.D. Thesis, Université Paris 6.
10. de Vries D., Hulsebos E.M., Baan J. (2001), *Spatial fluctuations in measures for spaciousness*, The Journal of the Acoustical Society of America, **110**, 2, 947–954.
11. Frank M., Sontacchi A. (2012), *Performance review of an expert listening panel*, [in:] Fortschritte der Akustik, DAGA, Darmstadt.
12. Frank M., Sontacchi A., Höldrich R. (2010), *Training and guidance tool for listening panels*, [in:] Fortschritte der Akustik, DAGA, Berlin.
13. Frank M., Marentakis G., Sontacchi A. (2011), *A simple technical measure for the perceived source width*, [in:] Fortschritte der Akustik, DAGA, Düsseldorf.
14. Gerzon M.A. (1992), *General metatheory of auditory localisation*, [in:] Preprint 3306, 92nd Conv. Audio Eng. Soc., Vienna.
15. Hidaka T., Beranek L.L., Okano T. (1995), *Interaural cross-correlation, lateral fraction, and low- and high-frequency sound levels as measures of acoustical quality in concert halls*, The Journal of the Acoustical Society of America, **98**, 2, 988–1007.
16. ISO (2009), ISO 3382-1:2009: *Acoustics – measurement of room acoustic parameters – part 1: Performance spaces.*
17. ITU (1997), ITU-R BS.1116-1: *Methods for the subjective assessment of small impairments in audio systems including multichannel sound systems.*
18. Kin M.J., Plaskota P. (2011), *Comparison of sound attributes of multichannel and mixed-down stereo recordings*, Archives of Acoustics, **36**, 2, 333–345.
19. Mackensen P. (2008), *Auditive Localization & Head Movements*, Ph.D. Thesis, TU Berlin.
20. Martin G., Woszczyk W., Corey J., Quesnel R. (1999), *Controlling phantom image focus in a multichannel reproduction system*, [in:] Preprint 4996, 107th Conv. Audio Eng. Soc., New York.
21. Morimoto M., Iida K. (2005), *Appropriate frequency bandwidth in measuring interaural cross-correlation as a physical measure of auditory source width*, Acoustical Science and Technology, **26**, 2, 179–184.
22. Morimoto M., Maekawa Z. (1988), *Effects of low frequency components on auditory spaciousness*, Acta Acustica united with Acustica, **66**, 4, 190–196.
23. Okano T. (2002), *Judgments of noticeable differences in sound fields of concert halls caused by intensity variations in early reflections*, The Journal of the Acoustical Society of America, **111**, 1, 217–229.
24. Pulkki V. (1999), *Uniform spreading of amplitude panned virtual sources*, [in:] IEEE Workshop on Applications of Signal Processing to Audio and Acoustics, 187–190.
25. Schroeder M.R., Gottlob D., Siebrasse K.F. (1974), *Comparative study of european concert halls: correlation of subjective preference with geometric and acoustic parameters*, The Journal of the Acoustical Society of America, **56**, 4, 1195–1201.
26. Simon L.S.R., Mason R., Rumsey F. (2009), *Localization curves for a regularly-spaced octagon loudspeaker array*, [in:] Preprint 7915, 127th Conv. Audio Eng. Soc., New York.
27. Sontacchi A., Pomberger H., Höldrich R. (2009), *Recruiting and evaluation process of an expert listening panel*, [in:] NAG/DAGA International Conference on Acoustics, Rotterdam.
28. Theile G. (1991), *On the naturalness of two-channel stereo sound*, J. Audio Eng. Soc., **39**, 10, 761–767.
29. van Dorp Schuitman J. (2011), *Auditory modelling for assessing room acoustics*, Ph.D. Thesis, Technische Universiteit Delft.
30. Wendt K. (1963), *Das Richtungshören bei der Überlagerung zweier Schallfelder bei Intensitäts- und Laufzeitstereophonie*, Ph.D. Thesis, RWTH Aachen.
31. Zotter F., Frank M., Marentakis G., Sontacchi A. (2011), *Phantom source widening with deterministic frequency dependent time delays*, [in:] DAFx-11, Paris.

PAN ARCHIVES OF ACOUSTICS
Vol. **38**, No. 3, pp. 321–334 (2013)

DOI: 10.2478/aoa-2013-0039

Ultrasound Transmission Tomography Imaging of Structure of Breast Elastography Phantom Compared to US, CT and MRI

Krzysztof J. OPIELIŃSKI[(1)], Piotr PRUCHNICKI[(1)], Tadeusz GUDRA[(1)],
Przemysław PODGÓRSKI[(2)], Tomasz KRAŚNICKI[(2)], Jacek KURCZ[(2)], Marek SĄSIADEK[(2)]

[(1)] *Chair of Acoustics and Multimedia, Faculty of Electronics, Wrocław University of Technology*
Wybrzeże Wyspiańskiego 27, 50-370 Wrocław, Poland; e-mail: krzysztof.opielinski@pwr.wroc.pl

[(2)] *Department of Radiology, Wrocław Medical University*
Borowska 213, 50-556 Wrocław, Poland

(*received October 18, 2012; accepted February 18, 2013*)

The paper presents an analysis of the results of ultrasound transmission tomography (UTT) imaging of the internal structure of a breast elastography phantom used for biopsy training, and compares them with the results of CT, MRI and, conventional US imaging; the results of the phantom examination were the basis for the analysis of UTT method resolution. The obtained UTT, CT and MRI images of the CIRS Model 059 breast phantom structure show comparable (in the context of size and location) heterogeneities inside it. The UTT image of distribution of the ultrasound velocity clearly demonstrates continuous changes of density. The UTT image of derivative of attenuation coefficient in relation to frequency is better for visualising sharp edges, and the UTT image of the distribution of attenuation coefficient visualises continuous and stepped changes in an indirect way. The inclusions visualized by CT have sharply delineated edges but are hardly distinguishable from the phantom gel background even with increased image contrast. MRI images of the studied phantom relatively clearly show inclusions in the structure. Ultrasonography images do not show any diversification of the structure of the phantom. The obtained examination results indicate that, if the scanning process is accelerated, ultrasound transmission tomography method can be successfully used to detect and diagnose early breast malignant lesions. Ultrasonic transmission tomography imaging can be applied in medicine for diagnostic examination of women's breasts and similarly for X-ray computed tomography, while eliminating the need to expose patients to the harmful ionising radiation.

Keywords: ultrasound transmission tomography (UTT), ultrasonography (US), computed tomography (CT), magnetic resonance (MR) mammography, breast biopsy phantom.

1. Introduction

The unquestionable advantage of using ultrasound *in vivo* medical diagnostics is their harmless and non-invasive nature. Today, in the age of computerization, experts not only strive to perfect methods of ultrasonographic (reflection) imaging of tissue structure (Nowicki, 2010; Camacho *et al.*, 2012; Stotzka *et al.*, 2002), but also conduct intensive development of transmission methods (Opieliński, 2011), focusing especially on ultrasonic projection UP (analogous to roentgenography RTG) (Ermert *et al.*, 2000; Opieliński, 2011; 2012; Reguieg *et al.*, 2006) and ultrasound transmission tomography UTT (analogous to X-ray computed tomography CT) (Duric *et al.*, 2007; Opieliński, Gudra, 2010; Opieliński, 2011; Ruiter *et al.*, 2005).

The most common diagnostic tests used for early detection of breast malignant lesions include palpation, traditional X-ray mammography, ultrasound (US) imaging and MRI mammography (magnetic resonance imaging of women's breasts). Unfortunately, MRI cannot be performed in patients with cardiac pacemakers, neurostimulators, and ferromagnetic implants under any circumstances. Additionally, in patients with severe renal failure and/or allergy to contrast medium intravenous administration of contrast agents is contraindicated, which reduces the effectiveness of the examination. At a later stage cytological tests of biopsy-obtained material are performed.

There are also other diagnostic imaging modalities that can be implemented in prevention and diagnosis of breast cancer, such as (Opieliński, 2011): elastography (USE), thermography, electrical impedance tomography (EIT), single-photon emission computed tomography (SPECT), and positron emission tomography (PET). It became clear that ultrasound transmission tomography can also be used for imaging and early detection of breast malignant lesions (Duric *et al.*, 2007; Opieliński, 2011). Several research centres around the world (including the Chair of Acoustics and Multimedia of the Faculty of Electronics at Wroclaw University of Technology) are working to construct a prototype of UTT for women's breast examination (Duric *et al.*, 2007; Opieliński, Gudra, 2010; Opieliński, 2011; Ruiter *et al.*, 2005).

The following paper presents and analyses the results of ultrasound transmission tomography imaging of the internal structure of a CIRS Model 059 breast phantom used for ultrasonography (with elastography option) assisted biopsy training and compares them with the results of imaging by means of dual-energy CT method, MRI, and conventional US.

2. Materials and methods

A simplified block diagram of the research stand for UTT in divergent beam geometry with a constant angular distance, developed by the team at the Ultrasonic Technology Laboratory of Chair of Acoustics and Multimedia of the Faculty of Electronics at Wroclaw University of Technology is shown in Fig. 1 (Opieliński, 2011). The ultrasonic ring probe (Gudra, Opieliński, 2006) consists of 1024 of 0.5×18 mm piezoceramic sending-receiving transducers which are excited by short pulse signals with the frequency of 2 MHz and amplitude of 60 V_{pp} using a voltage amplifier and a demultiplexer system. Signals transmitted through the studied biological medium are received using a multiplexer and a receiving low noise amplifier. The received signals are registered by a computer using a digital oscilloscope card. The computer is then, by means of suitable software with acoustic parameter measurement algorithms, used to reconstruct images of a cross-section of the internal structure of the studied biological medium. One sending transducer and several hundred (usually 511) receiving transducers operate during one of the 1024 measurement cycles. The measurements are performed in distilled water that fills the ring probe tank, using a base, which allows precise vertical movement of the studied object.

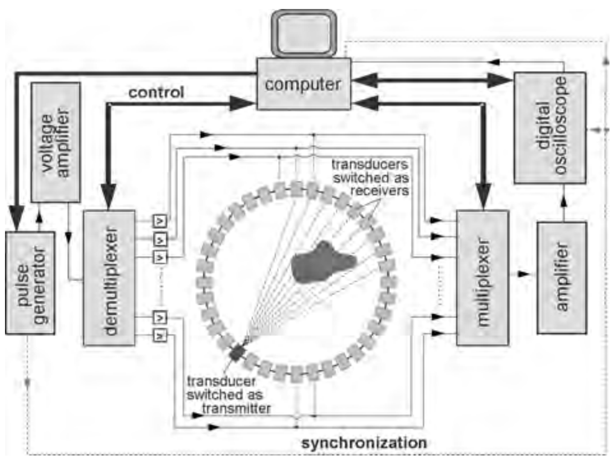

Fig. 1. Simplified block diagram of the measurement research stand for UTT with the ring probe.

A complete measurement of one cross-section, performed using the research stand, currently takes about 10 minutes. It will be reduced to a split of a second in the prototype by means of a parallel acquisition for each projection (the simultaneous recording of pulses from about 511 receiving transducers for each sending one), the FPGA based electronics, a faster transfer protocol, the parallel data processing, and the image reconstruction using CUDA^{TM} NVidia$^{®}$ graphic card with GPU's (graphics processing units). The reconstruction time using NVidia$^{®}$ is about few milliseconds for one cross-section image.

The CIRS Model 059 phantom mimics average values of acoustic parameters of tissues normal for the woman's breast for the purpose of elastography examination (Hoskins, 2010). The size (150:120:70 mm, volume: 600 cm^3) and shape of the phantom simulate female breast in the supine position. The phantom is made of Zerdine^{TM} gel, which imitates tissue and which contains 13 compact structure areas type inclusions that are about 3 times harder (rigid) than the surrounding gel. Those inclusions are positioned randomly inside the phantom. Inclusion size is in the range of about $2 \div 10$ mm. One of the advantages of the phantom in relation to its use for transmission examination in water, is its smooth surface, which minimizes loss of oblique incident ultrasonic wave. It should be noted that according to the manufacturer, the inclusions in the phantom structure are not visible in images obtained using conventional ultrasonographs. They are, however, visible in elastograms (Hoskins, 2010). Average velocity of ultrasound in water was $c \approx 1490.6$ m/s ($t \approx 22.8°$C, temperature fluctuation $\Delta t \approx \pm 0.2°$C), in gel it was $c \approx 1503 \div 1507$ m/s, and in inclusions it was $c \approx 1510 \div 1515$ m/s.

The manner in which UTT examination of the phantom was performed is shown in Fig. 2. UTT images composed of 457×457 pixels with the size of 0.4 mm. Individual longitudinal cross-sections of the phantom (in the coronal plane – the base was perpendicular to the surface of the transducers) were measured with a vertical step of 2 mm, as shown in Fig. 3. The fast filtered back projection algorithm with Hamming filter assuming straight-line propagation was used for the image reconstruction (Kak, Slaney, 1988).

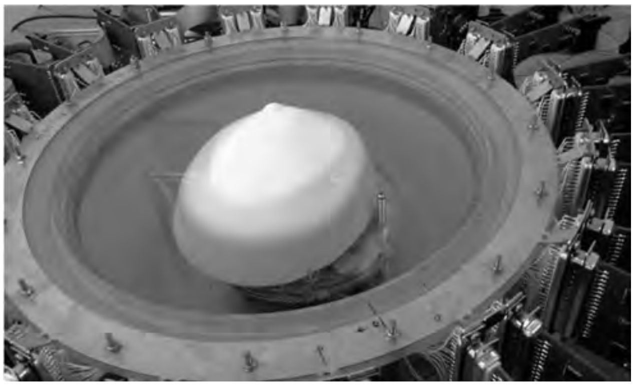

Fig. 2. Measurement UTT methodology.

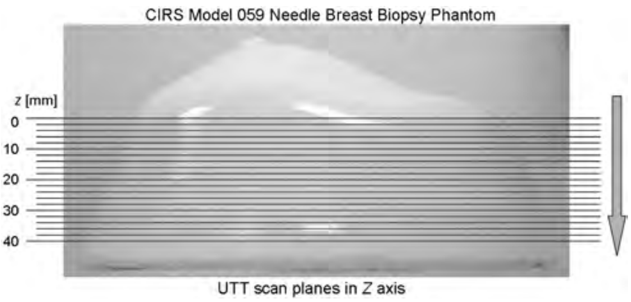

Fig. 3. Way of UTT measurements of individual longitudinal cross-sections of the phantom.

The manner in which conventional US examination of the phantom was performed is shown in Fig. 4. The transversal cross-sections of the phantom were imaged using a 3.5 MHz and 5 MHz linear probe (operating with a Picker LS2400 scanner), that was submerged in water and moved along the phantom on a special base with a horizontal step of 5 mm.

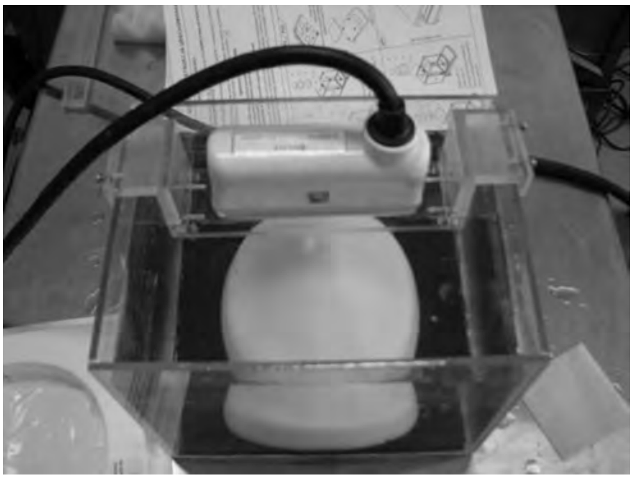

Fig. 4. US measurement methodology – a view of the tank.

CT and MRI examinations of the phantom were performed in the Department of General Radiology, Interventional Radiology and Neuroradiology of the Wroclaw Medical University Hospital, using Discovery CT 750HD GE Healthcare and Signa HDxt 1.5T, GE Healthcare devices respectively (Fig. 5). The CT examination was performed using a dual-energy protocol: 80 keV and 140 keV (Wang, Pelc, 2011). Next, secondary reconstructions of images for energy of 40 keV were obtained using dedicated software (GSI Viewer, GE Healthcare). The phantom was positioned so that its base was parallel to the surface of the gantry hole and perpendicular to the axis of the table surface (the coronal plane). The layer thickness was 0.625 mm and the resolution of the obtained image reconstructions was 512×512 pixels with the size of 0.52 mm. For the MRI examination the T2 FSE sequences were obtained using the following parameters: repetition time $T_r = 4940$ ms and echo time $T_e = 80.3$ ms. The phantom was examined using the 8-channel coil dedicated for breast imaging (8ch HD Breast Array). The phantom was positioned in a special breast grip, with the side surface parallel to the gantry hole. The layer thickness was 5 mm. The resulting array size was 512×512 pixels with the size of 0.38 mm.

a)

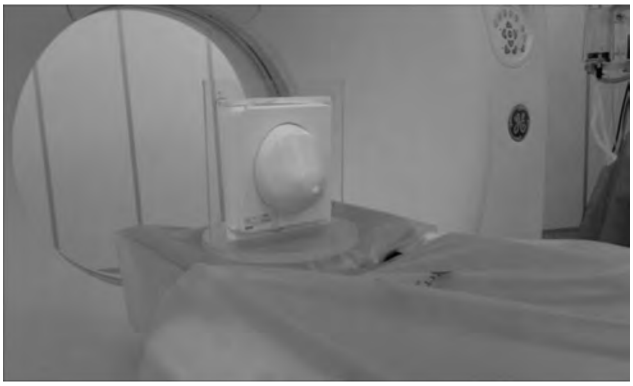

b)

Fig. 5. Way of the breast phantom CT (a) and MRI (b) measurements.

3. Imaging

The results of UTT examinations for the longitudinal cross-section of the CIRS Model 059 phan-

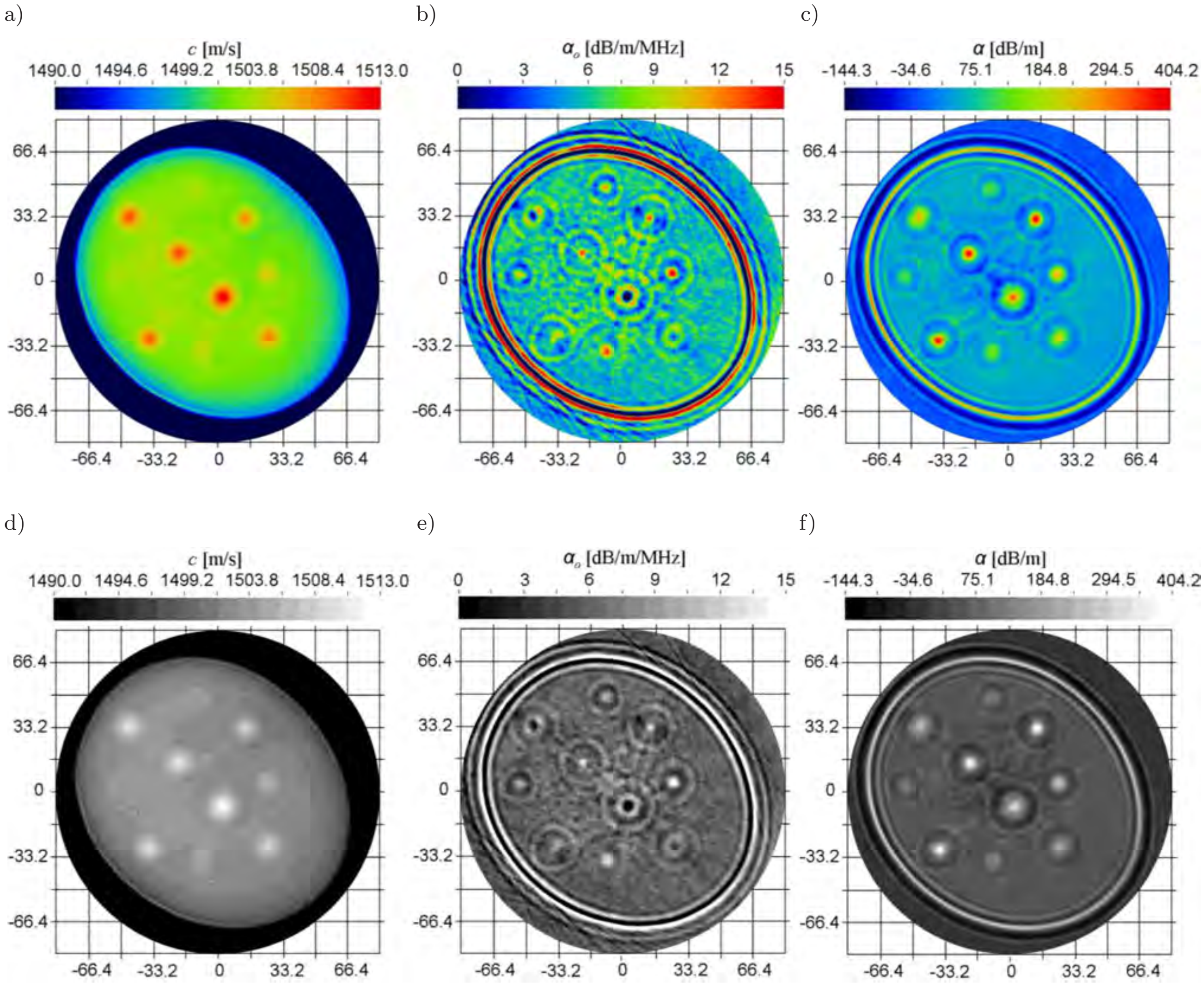

Fig. 6. UTT images of the CIRS Model 059 phantom longitudinal cross-section at the height of $z = 20$ mm (presented in rainbow colours and greyscale): a), d) ultrasound propagation velocity, b), e) derivative of the ultrasound attenuation coefficient in relation to frequency, c), f) the ultrasound attenuation coefficient.

tom (the coronal plane) for the selected height of $z = 20$ mm (see Fig. 3) are shown in Fig. 6. Three different UTT images in rainbow colours and greyscale from black to white (Fig. 6) were reconstructed from the determined values of ultrasonic pulse parameters recorded in the cross-section for divergent geometry (runtime, amplitude, frequency (Duric *et al.*, 2007; Opieliński, Gudra, 2010; Opieliński, 2011; 2012)). The images correspond in turn to distributions of local ultrasound velocity values, derivative of ultrasound attenuation coefficient in relation to the frequency and ultrasound attenuation coefficient (Opieliński, Gudra, 2010; Opieliński, 2011; 2012). Negative and inflated values of the attenuation coefficient (Fig. 6c,f) result from errors of attenuation reconstruction based on the pulse amplitude – it is additionally reduced by phenomena occurring during ultrasonic wave transmission (Opieliński, 2011). The most significant disturbances occur near the heterogeneity borders (signal loss and dropout). The images of the distribution of ultrasound attenuation derivative and ultrasound attenuation are significantly affected by multiple reflections with low amplitudes which cause so-called edge radiation (Opieliński, 2011) (Fig. 6b,c,e,f).

Examples of US images of transversal cross-sections of the CIRS Model 059 phantom (where inclusions expected) obtained using a 3.5 MHz linear probe are shown in Fig. 7. The US scanning with a 5 MHz linear probe was inconvenient because the probe length was shorter than the phantom width, but none of the US images of the examined phantom cross-sections made it possible to see the heterogeneity of its structure.

The CT image of the CIRS Model 059 phantom longitudinal cross-section (in the coronal plane) for the height of $z = 20$ mm is shown in Fig. 8.

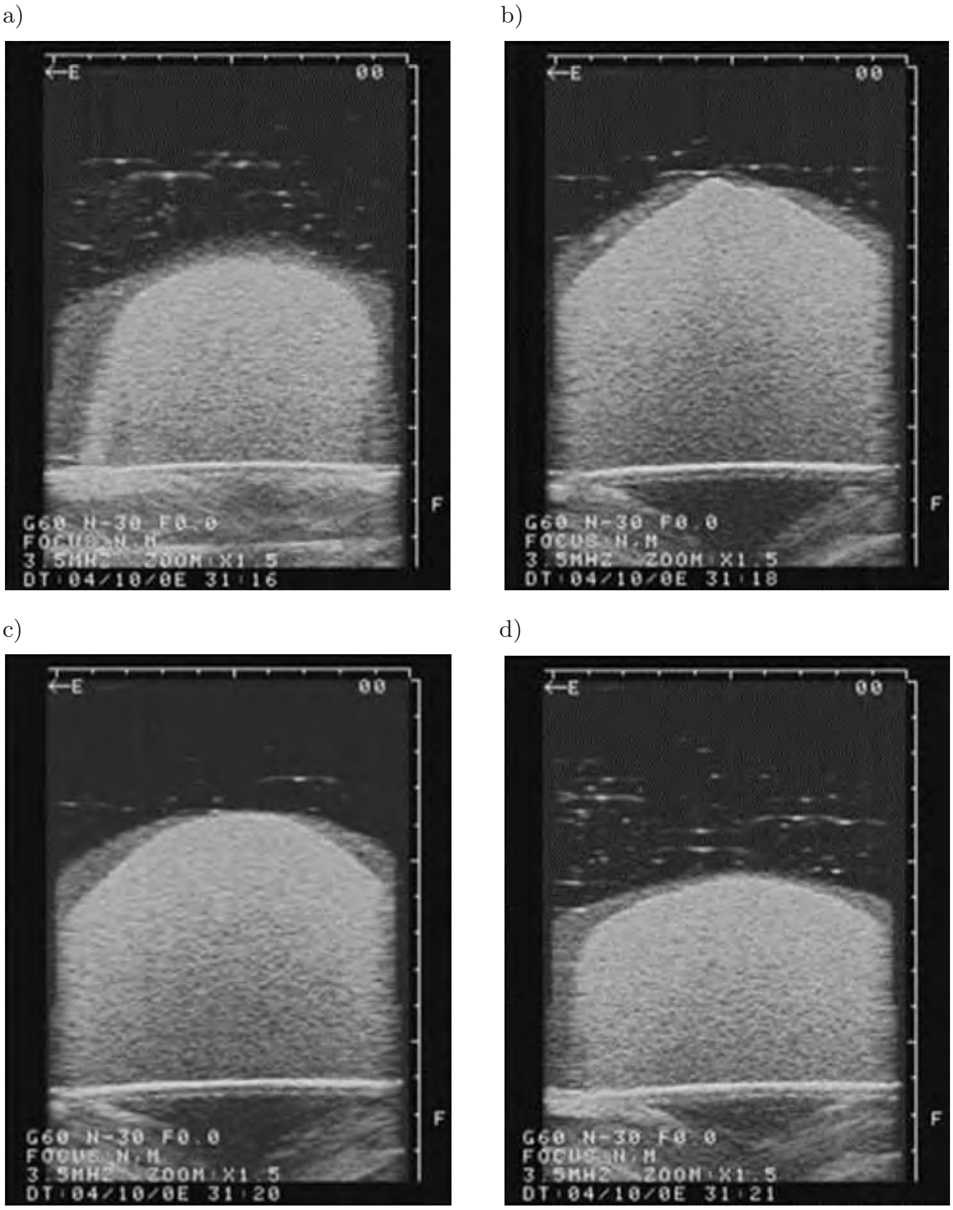

Fig. 7. Examples of US images of transverse cross-sections of the CIRS Model 059 phantom for the following distances of the linear probe axis from the edge of the tank (where inclusions expected): a) 2 cm, b) 5.5 cm, c) 7.5 cm, d) 11 cm.

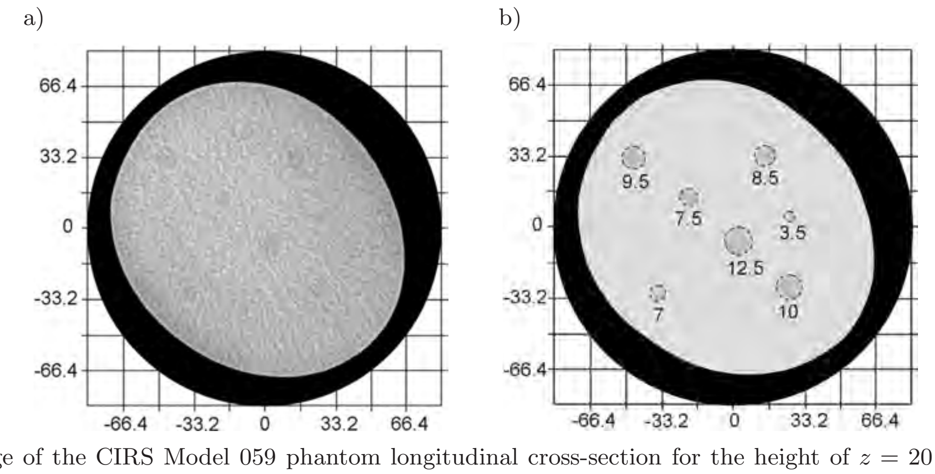

Fig. 8. CT image of the CIRS Model 059 phantom longitudinal cross-section for the height of $z = 20$ mm: a) increased contrast image, b) estimation of the size of distinguishable heterogeneous areas using an edge rendering image method.

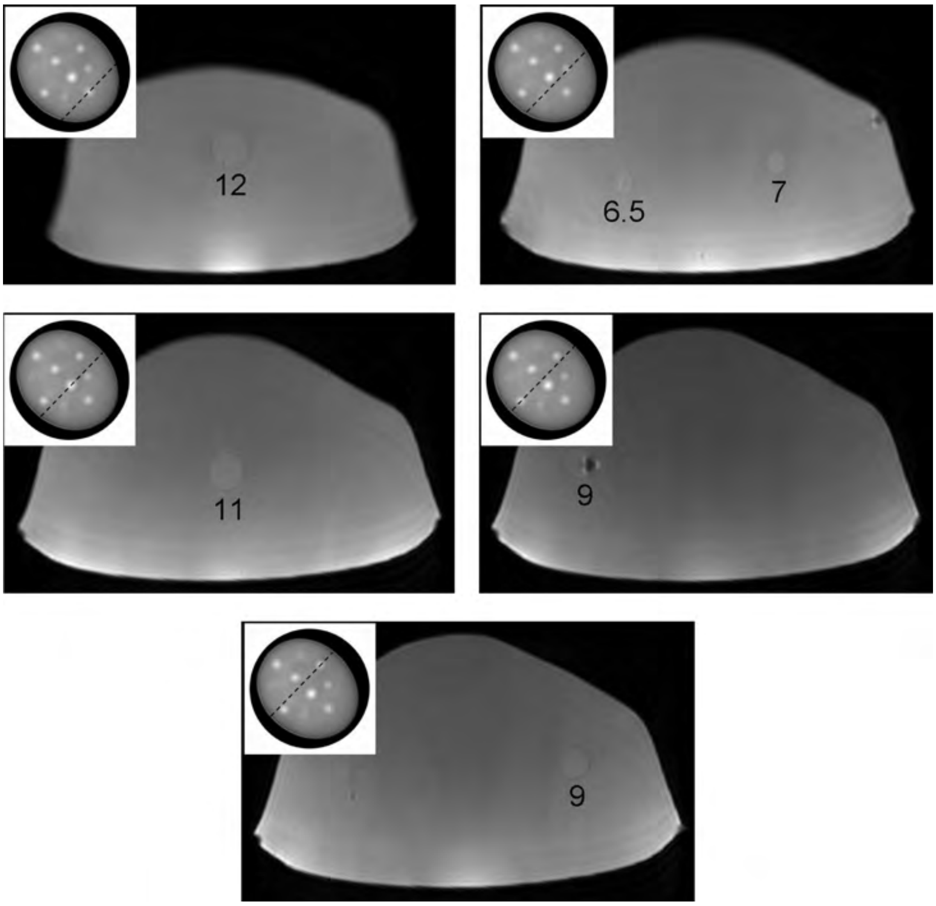

Fig. 9. MRI images of transverse cross-sections of the CIRS Model 059 phantom along selected heterogeneous areas which are presented on miniature UTT images (contrast was increased for better visibility of the inclusions).

Selected results of MRI examination of transversal cross-sections of the CIRS Model 059 phantom are shown in Fig. 9. For each MRI image the dashed line indicated the cross-section in relation to the UTT image of the ultrasound velocity distribution (Fig. 6d), and the size of the imaged heterogeneous areas was determined.

4. Image analysis

4.1. Computed Tomography

Breast tomosynthesis (3D mammography) is an adequate method for 3D breast imaging, however, in order to retain the shape and structure of the phantom used in this study, CT method was implemented. The CT method is not typically used in diagnostic management of the women's breast because of high kV values (usually 120 kV) used, which leads to a low diversity of tissue radiation attenuation. For the same reason, CT images of the CIRS Model 059 breast phantom structure reconstructed from direct measurements using energy of 80 keV or 140 keV, did not allow to recognize heterogeneous areas. However, inclusions in the phantom gel could be visualised on secondary reconstruction images obtained in dual-energy CT examination at the virtual energy level of 40 keV (Wang, Pelc, 2011). The visualised inclusions have sharply delineated edges but are hardly distinguishable from the phantom gel background (the contrast values between structures and the background contain in the maximum range $0 \div 6$ dB and the average value is about 3 dB, see Table 1) even with increased image contrast (Fig. 8a). In a standard CT examination, radiological density (the level of X-ray opacity) and Hounsfield scale (based on radiological density), which is a linear transformation of the original linear attenuation coefficient measurement for X-rays, are the differentiating parameters. The darker areas are called hypodense, whereas the brighter ones are hyperdense. Radiodensity of distilled water in standard temperature and pressure is defined as zero on Hounsfield scale, while air density in typical conditions is -1000 Hounsfield units (HU) (Pruszyński, 2000). Multi-energy imaging modality utilises evaluation based on the measurement of relative atomic number of the examined tissues. The value of beam's linear attenuation coefficient for two different energies is simultaneously tested in dual-energy CT imaging. The linear attenuation coefficient is dependent on two phenomena occurring during radiation-matter interaction: Compton scatter and photoelectric effect. These phenomena depend on the substances radiation interacts with. Therefore, it is possible to measure the distribution of the effective atomic number in the examined tissues. Next, based on the linear attenuation coefficient value one can calculate HU values of the tested material for specified energy.

The CT method is characterised by soft tissue contrast resolution of about 0.2%. Potential spatial resolutions achievable in CT systems are about 0.2÷0.3 mm (Pruszyński, 2000), which is why CT images of the structure of the examined phantom became the comparative standard and were the basis when calculating the size of the visualised heterogeneous areas (Fig. 8b).

4.2. Ultrasound Transmission Tomography

Figure 10a shows (in rainbow colours) an UTT image of the distribution of local values of propagation velocity of ultrasonic wave for the CIRS Model 059 phantom longitudinal cross-section for the height of $z = 20$ mm, with contours of the shape of the phantom longitudinal cross-section and inclusion edges rendered from a CT image for the same cross-section (Fig. 8b) by means of an edge detection algorithm using the Laplace image filter (Watkins *et al.*, 1993). In order to sharpen inclusion edges, Fig. 10b shows the same image in greyscale with suitably boosted contrast (50 → 80%) and reduced brightness (50 → 32%). Figure 10a and Fig. 10b also show lines of image pixels, the value distribution of which was drawn in Fig. 11 for 3 different UTT images (see Fig. 6). Analysis of the graphs of pixel values along the diameters of individual phantom inclusions demonstrates that the 3 visualised distributions of local values of acoustic parameters: the ultrasound velocity c, derivative of the ultrasound attenuation coefficient in relation to frequency $\alpha_o = \partial\alpha/\partial f$, and ultrasound attenuation coefficient α are perfectly complementary to each other.

The image of ultrasound velocity (Fig. 6a,d) is a quantitative image, which makes it possible to distinguish heterogeneous areas from the background that differ in ultrasound velocity by at least one [m/s]. It is also possible to visualise both continuous and stepped changes (Fig. 6a,d shows water penetrating the edges of the phantom gel). One disadvantage of this type of imaging is fuzzy edges, which results in errors in evaluation of the size of inclusions and distorted ultrasound velocity values in small heterogeneous areas caused by multipath effect during ultrasonic wave propagation in a heterogeneous structure (Crawford, Kak, 1982).

Quan and Huang (2007) determined on the basis of simulation calculations that due to the multipath effect, ultrasonic transmission tomography based on runtime measurements (image of the distribution of ultrasound velocity) allows precise reconstruction of the ultrasound velocity for structures larger than 5 wavelengths. For structures smaller than 2 wavelengths, reconstruction is more qualitative, as it only makes it possible to identify heterogeneous areas, but distort local ultrasound velocity values inside.

Based on earlier research conducted by Opieliński and Gudra (2006) it can be concluded that in the case of real objects with diversified structure, the ability to visualise heterogeneous areas: their shape and velocity values in their internal structure, depends additionally on the actual value of the difference between the ultrasound velocity in a heterogeneous area and around it, on the effect of refraction, as well as on the lateral and

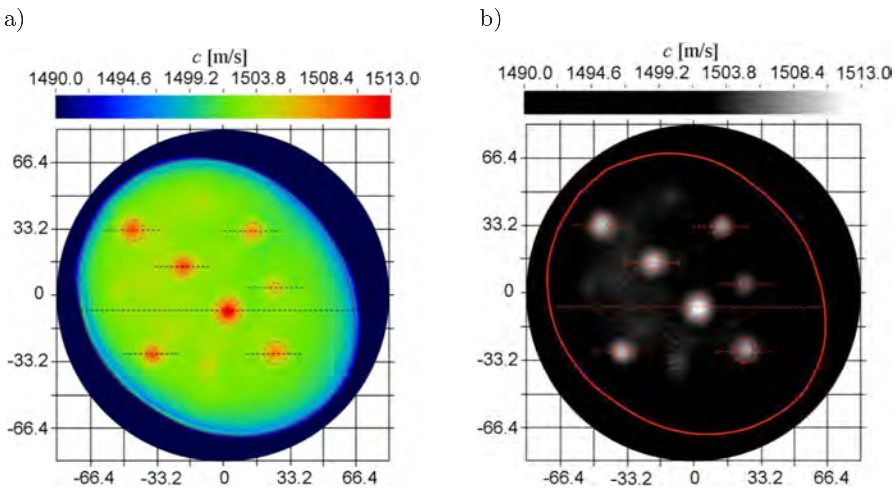

Fig. 10. UTT image of distribution of local values of ultrasound velocity for the CIRS Model 059 phantom longitudinal cross-section for the height of $z = 20$ mm, with contours of the shape of the cross-section and inclusion edges rendered from a CT image (Fig. 8b): a) rainbow colours image, b) greyscale image with boosted contrast (50 → 80%) and reduced brightness (50 → 32%).

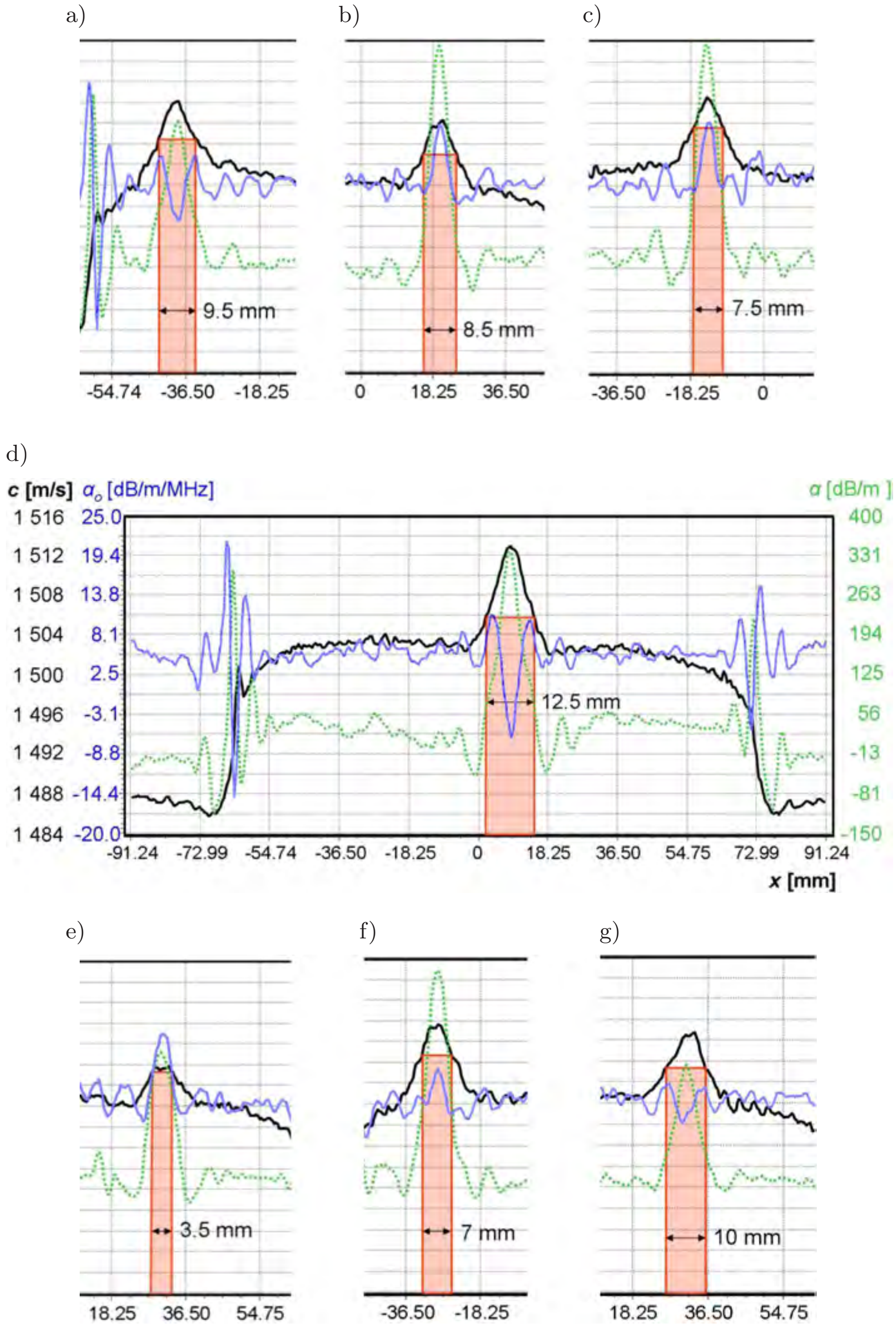

Fig. 11. Pixel value distributions for the lines indicated in Fig. 10, along the diameters of individual phantom inclusions, drawn in turn for 3 different UTT images (see Fig. 6), the ultrasound velocity – black colour, derivative of ultrasound attenuation coefficient in relation to frequency – blue colour, ultrasound attenuation coefficient – green colour: a) d_{inc1} = 9.5 mm, b) d_{inc2} = 8.5 mm, c) d_{inc3} = 7.5 mm, d) d_{inc4} = 12.5 mm, e) d_{inc5} = 3.5 mm, f) d_{inc6} = 7 mm, g) d_{inc7} = 10 mm.

longitudinal resolution. In the case of measurements of ultrasound velocity values by detection of the ultrasonic wave pulse runtime using digital methods, it is possible to determine the projection value of runtime with the precision of single nanoseconds. Therefore, projection value of the ultrasound velocity can be determined with the precision of about 0.01 m/s (when ignoring measurement uncertainty which can be much higher depending on the measurement setup and conditions, as well as noise and interference). This means that for the measured projection values of the ultrasound velocity it is possible to identify the influence of an inclusion for its size appropriately correlated with the difference between the local velocity value in the structure of this inclusion and the structure around it. If the existence of an inclusion alters projection values of the ultrasound velocity measured from multiple directions, it will be possible to identify the inclusion in an UTT image reconstructed based on such measurements. Calculations show that if the total precision of determining projection values of the ultrasound velocity is at 0.01 m/s, it will be possible to distinguish, in an UTT image, heterogeneous areas different from the surrounding tissue in the value of the ultrasound velocity: 1 m/s with the size > 2.3 mm, 2 m/s with the size > 1.2 mm, 5 m/s with the size > 460 μm, 10 m/s with the size > 240 μm, 15 m/s with the size > 160 μm, 20 m/s with the size of 120 μm (Fig. 12). For any precision of determining projection values of the ultrasound velocity, UTT contrast resolution can be determined from graphs presented in specific papers (Opieliński, Gudra, 2006; Opieliński, 2012).

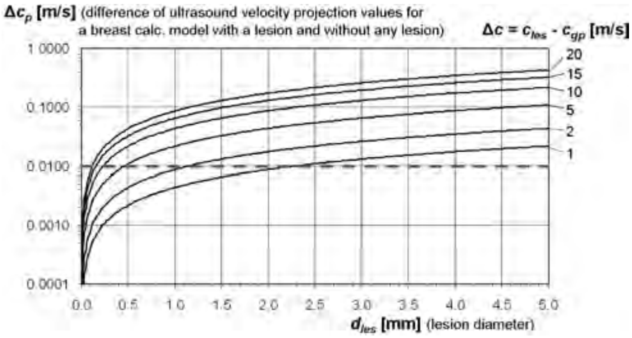

Fig. 12. Calculations of the difference of ultrasound velocity projection values for a breast calculation model with a lesion and without any lesion, depending on the lesion diameter, with the parameter $\Delta c = 1, 2, 5, 10, 15, 20$ m/s.

Moreover, a strict limitation is in effect related to longitudinal resolution dependent on wavelength and scanning pulse length. The calculated contrast resolution increases with decreasing relation between transmitter-receiver distance and inclusion size. Change of the ultrasound velocity in the coupling medium (water) surrounding the examined tissue has negligible influences (Opieliński, 2012). Heterogeneous areas are usually diversified in terms of shapes and sizes. In such cases, the heterogeneous areas will be visible in projection measurements for some projection planes and not visible for others. Existence of such discontinuities will be visualised in a tomographic UTT image, if the difference of ultrasound velocity values in a projection (caused by structure heterogeneity in relation to the surroundings) are detectable for at least a few projection directions.

The image of derivative of the ultrasound attenuation coefficient in relation to frequency (Fig. 6b,e) is better for visualising edges but bad for continuous changes, in general. It is rather a qualitative image because it distorts the reconstructed absolute values as a result of received pulses being overlapped by side and multiple reflections and interference, as well as assuming linear changes of ultrasound attenuation with frequency in the process of reconstruction (Opieliński, 2011). However, it allows precise determination of the size of heterogeneous areas > 9 mm, as visible in Fig. 11a,d,g (two boundary peaks inside), and a little less precise lesion areas in the size range 5÷9 mm (start and end of one peak inside), as visible in Fig. 11b,c,f. An evaluation of sizes is possible for inclusions' areas < 5 mm (Fig. 11e).

The image of the distribution of attenuation coefficient can be treated as a quantitatively qualitative one, an image that indirectly visualises continuous and stepped changes (Fig. 6c,f). This image is a perfect complement of the images of velocity and the derivative of ultrasound attenuation, as it makes it possible to anticipate which of the visible heterogeneous areas are located in the horizontal plane that cuts across the centre of the surface of the sending and receiving transducer and which are outside of it (Fig. 13). The radiating surface of elementary ultrasonic transducers of the ring probe have to be narrow and high, due to the required high effectiveness and sensitivity, as well as the ability of high scanning resolution. It also makes it possible to achieve a beam that is wide horizontally and narrow vertically. Unfortunately, considerable height of the transducers (several mm) causes the imaged tissue cross-section to be averaged to the transducer's height.

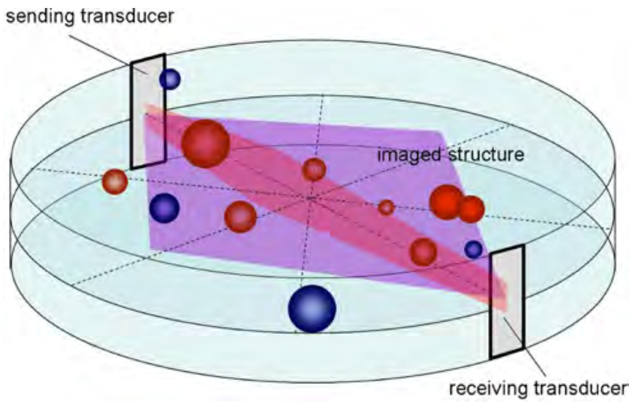

Fig. 13. Exemplary representation of the location of inclusions in the examined structure for the measurement space whose height is equal to the height of the elementary ultrasonic transducers of a ring probe (red inclusions are located in the horizontal plane of the transducer's axis).

As a result, the cross-section image shows structures that are slightly below and above the horizontal plane of the transducer's axis: there are 7 visible inclusions in the CT image (Fig. 8), and 10 in the UTT images (Fig. 6). As a result of a significant diversification of values of the attenuation coefficient inside inclusions, in comparison to the background (Fig. 11), the image of the distribution of local values of the ultrasound attenuation coefficient makes it possible, with increased contrast, to identify structures located only in the studied cross-section with a high likelihood (Fig. 14). However, in a real breast tissue examination, a lesion located in the imaging plan can give less attenuation that another lesion, not located within the plane but with a higher attenuation coefficient. In that case, a contrast boost method can eliminate the on-plane lesion, which should be found on images of other kinds (attenuation derivative and velocity image) or on another cross-section image (close to the contrasted one).

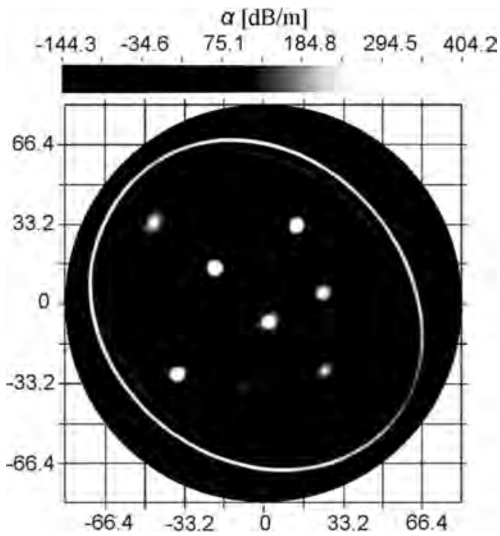

Fig. 14. UTT image of the distribution of local values of the ultrasound attenuation coefficient for the CIRS Model 059 phantom longitudinal cross-section for the height of $z = 20$ mm, with boosted contrast ($50 \rightarrow 90\%$) and reduced brightness ($50 \rightarrow 43\%$).

Lateral resolution of the UTT method (horizontal plane scanning density) primarily depends on ring probe's resolution (the number, width, and spacing of the elementary transducers), most of all. In the case of the 1024-element probe with 0.5 mm wide elementary transducers located 0.2 mm apart used in this study, the lateral resolution can be estimated to be in the range of 0.3÷0.4 mm, after transformation to the Cartesian coordinate system (1):

$$\Delta r_l = R_{\text{probe}} \cdot \sin\left(\frac{\pi}{N_{\text{probe}}}\right), \tag{1}$$

where Δr_l – lateral resolution, R_{probe} – inner radius of a ring ultrasonic probe, N_{probe} – number of elementary transducers in a ring probe. Lateral resolution should not be lower than longitudinal resolution.

In the ultrasonic echo method the longitudinal resolution (axial, along the path of the wave beam) is often optimistically assumed to be half of the wavelength (Duric *et al.*, 2007). In real measurements it should rather be assumed that this resolution is derived from the length (duration) of a received pulse, converted to distance in relation to the assumed ultrasound wave velocity in the measured structure (Nowicki, 2010). For the ultrasound frequency $f = 2$ MHz and single cycle length of pulse in a tissue, longitudinal resolution of the UTT method, determining sharpening in a tomographic image of the borders of the detected heterogeneous areas, can be estimated to be 0.77 mm. In reality it should be slightly better, as the structures that are smaller than the wavelength may be visible in an image as a result of diffraction – ultrasonic wave flows around a structure which, for example, means that the measured runtime is longer (Opieliński, Gudra, 2008). In such a case, however, information on the internal structure is distorted. Longitudinal and lateral resolution is additionally limited depending on the difference between the value of the acoustic parameter inside a heterogeneous structure and outside of it, as well as on the size of the structure. It is, therefore, possible to identify a heterogeneous area in an UTT image on condition that the average value of the acoustic parameter (measured on the path of ultrasonic wave beam from the transmitter to the receiver for directions around the heterogeneous area) is different from that value for the surrounding to a degree that can be measured. Additionally, the size of a heterogeneous area should not be lower than the scanning resolution and received pulse duration converted to distance. In other words, UTT contrast resolution affects spatial resolution and vice versa. It is also dependent on the examined structure. Longitudinal resolution can be improved by increasing ultrasonic wave frequency (although, attenuation inside a breast is a limiting factor) and by decreasing the Q-factor of the ultrasonic transducers (this leads to increased bandwidth and shortened pulse but also reduced effectiveness).

Vertical (elevation) resolution (in height) primarily depends on the vertical scanning density (layer thickness), with a limitation resulting from the transducer's height. If known simple equations are used (Nowicki, 2010), it is possible, for the 1024-element ring probe with 18 mm high elementary transducers, to estimate the vertical resolution to be around 5 mm for the distance of 60 mm from the transducer (2):

$$\Delta r_v = \lambda \frac{2r}{h_t}, \tag{2}$$

where Δr_v is the vertical resolution, λ is the wave length, r is the distance from the transducer of a probe, h_t is the height of the elementary transducer of a probe. This, however, is not a significant limitation for the UTT method because there are ways to focus the beam vertically and consequently to increase elevation resolution. One of the ways is to use a lens on the surface of the transducers of the ring probe in the form of a suitably shaped layer. Ultrasonic concave lenses are made of elastic materials, e.g. plexiglass ($c \approx 2700$ m/s) or epoxy resin ($c \approx 2750$ m/s), while convex lenses are made of silicone based materials, whose ultrasound velocity is below 1500 m/s. It is also possible to use transducers whose surface is shaped as a concave sphere. Another method is to make a horizontal incision (or a cut) in the radiated surfaces of elementary transducers and divide them into several lines (3 or 5) which make it possible to focus on using the electronic delay along their height (so called 1.5-D arrays) (Nowicki, 2010).

4.3. US

Ultrasonography (US) is one of the methods of diagnostic breast imaging that is routinely used as the first or complementary test in relation to roentgen mammography (Basset *et al.*, 2005). For example, the method allows to distinguish cysts from solid lesions, it is useful for precise determination of the location of a breast lesion, especially before a planned fine-needle biopsy and in young women, whose breast tissue is typically too dense for diagnostically reliable roentgen mammography. Ultrasonic probes with 5÷10, 5÷12 MHz range variable frequencies are mostly used in breast US diagnostics. Thus, US detects breast microcalcifications and, most importantly, makes it possible to assess lesion vascularity (abundance of blood vessels is typical of malignant and inflammatory lesions). However, it is a qualitative type of imaging which only allows visualisation of heterogeneity borders (Wronkowski, Zwierno, 2000). Reflections of ultrasonic wave pulses from microcalcifications allow for signals received by the US-scanner to be obtained. This, however, does not mean that such signals will always be distinguishable in an US image from many other signals received from the border of the adipose, fibrous, glandular tissue, and their heterogeneity (tissue noise) (Filipczyński, 1983). The use of US scanners with Doppler method allows for lesion vascularity to be assessed. However, this method does not make it possible to distinguish unequivocally malignant lesions from benign ones. Additionally, US imaging produces a limited viewing area, it is subjective (depends on the examining person's assessment) and generates results that are an effect of a compromise between the ultrasonic wave penetration depth and image resolution (a higher frequency of the ultrasonic wave increases resolution but also attenuation and, as a result, it decreases the penetration depth). Imaging fidelity of an US image is dramatically affected by the width and frequency of the ultrasonic beam and scanning pulse length. The probability of early breast cancer detection using US is estimated to be about 50% (Wronkowski, Zwierno, 2000).

None of the US images of the examined CIRS Model 059 phantom cross-sections revealed the heterogeneity of its structure. The differentiating parameter in ultrasonography is acoustic impedance, which means that the difference of its value between gel and inclusions structure is in this case too small and cannot be visualized.

4.4. Magnetic Resonance Imaging

MRI mammography (magnetic resonance imaging of women's breasts) is a method that makes it possible to detect even small areas in breasts that with high probability can be identified as early-stage neoplasm (Basset *et al.*, 2005; Pruszyński, 2000). However, it usually requires a contrast medium to be intravenously injected. If a patient receives a contrast agent, it is always possible that there could be an allergic reaction. This risk, however, is lower than in the case of contrast substances containing iodine that are typically used during roentgenography and computed tomography. No additional patient health hazards have been found in MRI. Since the examination exposes patient to a strong magnetic field, it is contraindicated for those patients that have (ferromagnetic) metal instruments or implants. Magnetic resonance imaging visualizes concentration of nuclei of hydrogen atoms (protons) (Pruszyński, 2000). The largest number of protons can be found in water molecules. Water is the basic component of tissues but proportions in relation to other chemical compounds varies. This results in observable changes of signals in resonance emission caused by hydrogen atoms present in water molecules in tissues. Magnetic resonance imaging allows chemical analysis of biological media showing differences in water contents in comparison to other chemical compounds. As a result, MRI is the best type of examination for detecting diseases which cause an increase in fluid amount in the areas of pathological lesions caused by tumours, infections, and inflammations.

The quality of MRI images is significantly affected by the specifications of the measurement equipment (value of the magnet's induction, force of the gradients, receiving system, the coil used, etc.) and selection of the parameters of the scanning sequence (Pruszyński, 2000). Seemingly unimportant changes in the basic imaging parameters can result in obtaining slightly different data which enable various diagnostic interpretations. MRI signal intensity depends on the used measurement sequence and, at the same time, on at least five tissue distinguishable factors: proton density ρ_p, longitudinal relaxation time (spin-lattice) T_1, transversal relaxation time (spin-spin) T_2, repetition time T_r, time of the echo T_e. By selecting specific T_e and T_r it is possible to emphasize the effect of individual tissue parameters in a signal; it is also possible to select such imaging parameters that the signal of a given substance will be muted (e.g. water, fat). If, for example, amplitude intensity of the nuclear magnetic resonance is primarily dependent on the density of protons, relaxation time effect will be reduced. Similarly, it is possible to create images dependent on times T_1 and T_2.

For short times T_e and T_r the image is dependent on time T_1 (water on the images is hypointense – black), and for long times T_e and T_r the image is dependent on time T_2 (water on the images is hyperintense – bright). Long times T_r and short times T_e make it possible to obtain an image dependent on the proton density. Water protons in malignant neoplasm tissue are usually characterised by longer relaxation times T_1 and T_2. In an image dependent on T_1, neoplasm tissue is darker, while in an image dependent on T_2 it is brighter that the surrounding area. The choice of T_r and T_e results from the need to achieve a maximum contrast between tissues. MRI images' resolution depends on the number of water protons, both free and as part of macromolecules, in a medium. The resolution of magnetic resonance imaging can be as high as about 0.4÷1 mm. However, MRI tomographs are very expensive. Significant costs are also associated with their installation and maintenance, as it is necessary to service and calibrate them periodically.

MRI images of the studied CIRS Model 059 phantom clearly show inclusions in the structure. The sizes of the same inclusions estimated based on MRI images (Fig. 9) are different from those estimated based on CT images but this is caused by the difference between the tested cross-sections, as well as possible differences (mismatch) between the sizes of inclusions for the horizontal (CT) and vertical cross-sections (MRI). Another problem was related to the examination method (same as in the case of *in vivo* breast examination): the phantom was positioned in a special breast grip, at an angle, with the side parallel to the gantry hole (Fig. 5b). As a result, it is difficult to match and compare cross-sections with other imaging types. Additionally, the resolution of scanning of cross-sections of the phantom was just 5 mm (thickness of the layer). On the other hand, the advantage of MRI images is additionally showing the diversification of the structures inside the inclusions (Fig. 9). The small black areas in the inclusion structure and phantom gel are air bubbles.

5. Conclusions

The comparison of resolutions of all imaging methods used in the paper is presented in Table 1. Additionally, the contrast values between an inclusion and the background in obtained images of the CIRS Model 059 breast phantom structure were evaluated, together with the average pixel value range variation in the background phantom gel (Table 1).

The obtained UTT, CT, and MRI images of the CIRS Model 059 breast phantom structure show comparable (in the context of size and location) heterogeneities inside it. On CT images they are hardly distinguished from the background, while on MRI images the distinction is fairly clear. The edges of inclusion in the phantom on CT and MRI images are sharp because of a high spatial resolution of those methods. US images are not suitable to identify any inclusions in any cross-section of that phantom.

Each of the 3 UTT images is characterised by slightly different features of the phantom's structure. The image of distribution of the ultrasound velocity clearly demonstrates continuous changes of density. The edges of small inclusions are fuzzy. It is a typical quantitative image, because of a high precision of digital determination of runtime. As a result, it is possible to identify the character of a breast lesion (benign or malignant (Opieliński, 2011)) based on pixel values in the lesion area in relation to the background. The image of the derivative of the attenuation coefficient in relation to frequency is good for visualising edges and

Table 1. Comparison of resolutions and evaluated contrast values between an inclusion and the background in the CIRS Model 059 breast phantom structure images obtained by CT, UTT, US, and MRI.

Methods	Parameters			
	Spatial resolution [mm]	Layer thickness resolution [mm]	Longitudinal resolution [mm]	Contrast between an inclusion and the background imaging
CT	0.52	0.625	N/A	3 dB (3 dB range variation in the background)
UTT (velocity)	0.4	5	0.77 (2 MHz)	30 dB (3 dB range variation in the background)
UTT (attenuation derivative)	0.4	5	0.77 (2 MHz)	40 dB (4 dB range variation in the background)
UTT (attenuation)	0.4	5	0.77 (2 MHz)	40 dB (0.5 dB range variation in the background)
US	≤ 2.0 ≤ 1.5	2.9 2.5	0.44 (3.5 MHz) 0.31 (5 MHz)	0 dB – inclusions invisible (10 dB range variation in the background)
MRI	0.38	5	N/A	1.5 dB (0.5 dB range variation in the background)

bad for continuous changes. Since it distorts absolute values of the image pixels, it can be treated as more qualitative. The image of the distribution of attenuation coefficient can be treated as quantitatively qualitative. It visualises continuous and stepped changes in an indirect way. All the images show slightly different features of the structure and in this manner complement one another, providing important diagnostic information.

The obtained results show that, after the scanning process is accelerated making it possible to perform *in vivo* examinations (duration time of data acquisition, processing, and image reconstruction for one cross-section will be no longer than one second), the developed UTT method can successfully be used to detect and diagnose focal lesions in women's breasts (3-D whole breast imaging will take about 1.5 minute). Lesions that cannot be visualised using conventional US method can be imaged thanks to the UTT method. It combines the advantages of ultrasonography (no X-rays and contrast used, as well as no contraindications in the case of ferromagnetic implants) with transmission technology used in CT, making it an innovative (and most importantly) unusually sensitive "hybrid" method. The further developed prototype of a multimode ultrasonotomograph for *in vivo* examination of women's breasts will, apart from various 2-D and 3-D UTT images of the breast structure, reconstruct amplitude and phase URT images (ultrasound reflection tomography) (Stotzka *et al.*, 2002), combined US 2-D and 3-D images (Camacho *et al.*, 2012) and conventional US images that make it possible to view any part of a horizontal breast section in real time using a selected sector of a ring probe positioned at a given height.

Acknowledgments

The authors would like to thank DRAMIŃSKI Polish Company for financing the research as part of a process of introducing an ultrasonic transmission tomograph for examining women's breasts to the market.

References

1. Basset L.W., Jackson V.P., Fu K.L., Fu Y.S. (2005), *Diagnosis of Diseases of the Breast*, Elsevier Saunders, Philadelphia.
2. Camacho J., Medina L., Cruza J.F., Moreno J.M., Fritsch C. (2012), *Multimodal Ultrasonic Imaging for Breast Cancer Detection*, Archives of Acoustics, **37**, 3, 253–260.
3. Crawford C.R., Kak A.C. (1982), *Multipath artifact corrections in ultrasonic transmission tomography*, Ultrasonic Imaging, **4**, 234–266.
4. Duric N., Littrup P., Poulo L., Babkin A., Pevzner R., Holsapple E., Rama O., Glide C. (2007), *Detection of breast cancer with ultrasound tomography: First results with the Computed Ultrasound Risk Evaluation (CURE) prototype*, Medical Physics, **34**, 2, 773–785.
5. Ermert H., Keitmann O., Oppelt R., Granz B., Pesavento A., Vester M., Tillig B., Sander V. (2000), *A New Concept for a Real-Time Ultrasound Transmission Camera*, IEEE Ultrasonics Symp. Proc., 1611–1614.
6. Filipczyński L. (1983), *Detectability of calcifications in breast tissues by the ultrasonic echo method*, Archives of Acoustics, **8**, 3, 205–222.
7. Gudra T., Opieliński K.J. (2006), *The ultrasonic probe for the investigating of internal object structure by ultrasound transmission tomography*, Ultrasonics, **44**, 1–4, e295–e302.
8. Hoskins P.R. (2010), *Elastography Physics and Equipment* [in:] *Diagnostic Ultrasonud Physics and Equimpment*, Hoskins P.R., Martin K., Thrush A. [Eds.], Cambridge University Press, Cambridge, 196–214.
9. Kak A.C., Slaney M. (1988), *Principles of Computerized Tomographic Imaging*, IEEE Press, New York.
10. Nowicki A. (2010), *Ultrasound in medicine – introduction to modern ultrasonography* [in Polish], Wydawnictwo IPPT PAN, Warszawa.
11. Opieliński K.J., Gudra T. (2006), *Multi-parameter ultrasound transmission tomography of biological media*, Ultrasonics, **44**, 1–4, e295–e302.
12. Opieliński K., Gudra T. (2008), *Nondestructive tests of cylindrical steel samples using the ultrasonic projection method and the ultrasound transmission tomography method*, Acoustics '08, Paris, 4919–4924.
13. Opieliński K.J., Gudra T. (2010), *Ultrasonic Transmission Tomography* [in:] *Industrial and Biological Tomography*, Sikora J., Wójtowicz S. [Eds.], pp. 263–338, Wydawnictwo Książkowe Instytutu Elektrotechniki, Warszawa.
14. Opieliński K.J. (2011), *Application of transmission waves for characterization and imaging of biological media structures* [in Polish], Oficyna Wydawnicza PWr., Wrocław.
15. Opieliński K.J. (2012), *Ultrasonic Projection* [in:] *Ultrasonic Waves*, Antunes Dos Santos Júnior [Ed.], pp. 29–58, INTECH, Rijeka.
16. Pruszyński B. (2000), *Radiology, RTG, CT, USG, MRI Image Diagnostics and Radioisotopes* [in Polish], PZWL, Warszawa.
17. Quan Y., Huang L. (2007), *Sound-speed tomography using first-arrival transmission ultrasound for a ring array*, Proceedings of SPIE, **6513**, 651306-1-9.
18. Reguieg D., Padilla F., Defontaine M., Patat F., Laugier P. (2006), *Ultrasonic Transmission Device*

Based on Crossed Beam Forming, IEEE Ultrasonic Symp. Proc., **2**, Vancouver, Canada, 2108–2111.

19. Ruiter N.V., Zapf M., Stotzka R., Müller T.O., Schlote–Holubek K., Göbel G., Gemmeke H. (2005), *First Images with a 3D–Prototype for Ultrasound Computer Tomography*, IEEE Ultrasonics Symp. Proc., **4**, Rotterdam, 2042–2045.

20. Stotzka R., Würfel J., Müller T.O., Gemmeke H. (2002), *Medical Imaging by Ultrasound-Computertomography*, Proc. SPIE, **4687**, 110–119.

21. Wang A.S., Pelc N.J. (2011), *Synthetic CT: Simulating low dose single and dual energy protocols from a dual energy scan*, Medical Physics, **38**, 10, 5551–5562.

22. Watkins Ch.D., Sadun A., Marenka S. (1993), *Modern Image Processing: Warping, Morphing and Classical Techniques*, Academic Press.

23. Wronkowski Z., Zwierno M. (2000), *Brest cancer – practical information – interview, diagnostics, classification of changes* [in Polish], Służba Zdrowia, **24–26**, 2917–2919.

PAN ARCHIVES OF ACOUSTICS
Vol. **38**, No. 3, pp. 335–350 (2013)

DOI: 10.2478/aoa-2013-0040

Analysis of Spectral Characteristics of Sound Waves Scattered from a Cracked Cylindrical Elastic Shell Filled with a Viscous Fluid

Olexa PIDDUBNIAK[(1)], Nadia PIDDUBNIAK[(2)]

[(1)] *Faculty of Process and Environmental Engineering, Lodz University of Technology*
Wółczańska 213, 90-924 Łódź, Poland

[(2)] *Lviv, Ukraine*
e-mail: piddub@wp.pl

(*received April 17, 2012; accepted April 3, 2013*)

The scattering of plane steady-state sound waves from a viscous fluid-filled thin cylindrical shell weakened by a long linear slit and submerged in an ideal fluid is studied. For the description of vibrations of elastic objects the Kirchhoff–Love shell-theory approximation is used. An exact solution of this problem is obtained in the form of series with cylindrical harmonics. The numerical analysis is carried out for a steel shell filled with oil and immersed in seawater. The modules and phases of the scattering amplitudes *versus* the dimensionless wavenumber of the incident sound wave as well as directivity patterns of the scattered field are investigated taking into consideration the orientation of the slit on the elastic shell surface. The plots obtained show a considerable influence of the slit and viscous fluid filler on the diffraction process.

Keywords: sound scattering, elastic shell, slit, scattering amplitude, pattern directivity, seawater, oil

1. Introduction

The acoustic diagnostics of pipelines with natural gas or oil is one of the important problems of the safety of transportation of these substances and of the preservation of the environment (Makino *et al.*, 2001). The methods of non-destructive testing of underwater pipelines are continuously developed (Mohamed *et al.*, 2011). One of these methods is the long distance acoustic identification of the defects in underwater pipeline shells.

The echo-signals reflected from the thin circular cylindrical with a long linear slit elastic shell empty inside were investigated by Goldsberry (1967), Piddubniak (1995), Piddubniak *et al.* (2009), Porokhovski, (2008), and for case of the air-filled shell are described in the article of Kerbrat *et al.* (2002).

On the other hand, the problem of sound scattering by cylindrical viscous fluid-filled shells was considered in many works. And so Kachaenko *et al.* (1990) had investigated the three-dimension problem of sound diffraction from orthotropic elastic cylindrical shells with a viscous fluid inside on the base of the Timoshenko thin elastic shell theory. The sound diffraction from the viscoelastic polymer hollow cylinders and spheres filled with viscous fluids was analyzed by Hasheminejad, Safari (2003). Kubenko *et al.* (1989) considered the diffraction of sound pulses from coaxial piezoceramic cylindrical shells also filled with a viscous fluid. The wave guided properties of elastic cylindrical shells containing the viscous fluids were investigated by Vollmann, Dual (1997).

The aim of our paper is the study of the spectral structure of sound waves reflected from a thin elastic cylindrical shell surrounded by an ideal compressible fluid (sea water) and filled with a compressible viscous fluid (oil) in case when the shell is weakened by an infinitely long linear slit. We show that the slit present in the shell causes three additional components in the scattering amplitude connected with tangential, angular and radial vibrations of the shell edges on the crack. On the basis of the conclusions from this analysis we make an attempt to estimate the possibility of hydroacoustic diagnostics of oil-pipelines of this type.

2. Formulation of the problem and basic relations

Let us consider in the acoustic medium a thin cylindrical elastic shell of thickness h and a radius a of the middle surface weakened along the $\theta = \theta_0$ line by an infinitely long slit. The plane harmonic sound wave incidents on the shell with the phase front parallel to the axis of the object (Fig. 1). The shell is filled with a viscous barotropic compressible fluid, in general moved in the axial direction.

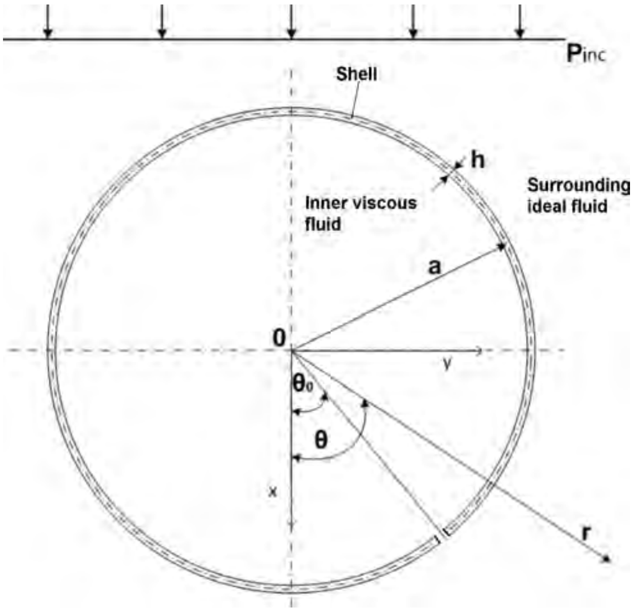

Fig. 1. Scheme of the interaction of sound wave and elastic shell filled with viscous fluid.

The sound waves reflected from the surface of the shell, as well as the waves re-radiated through the shell from the fluid filler, generate an acoustic scattered field. Therefore, it is necessary to study the spectral structure of the scattered sound waves, in particular, to investigate the influence of slit in shell and its orientation with respect to the direction of the incident wave, and also to take into consideration the presence of the viscous fluid filler.

For the description of the wave process we use the linear acoustic theories of ideal and viscous fluids and the linear Kirchhoff–Love theory of thin elastic shells.

From the first one, it is noted that the influence of the fluid motion in the tube must be neglected in the echo-signal because the front of the incident sound wave is parallel to the direction of this motion (Yeh, 1968).

The pressure in the reflected wave is described by the Helmholtz equation (Brekhovskikh, Godin, 1989)

$$(\Delta + k^2) p_{\mathrm{sc}}(r,\theta,\omega) = 0 \quad (r > a), \tag{1}$$

where k is the wave number of the ideal acoustical fluid, $k = \omega/c$, ω is the circular frequency, r and θ are the polar co-ordinates with an origin at the axis of the shell, c is the sound velocity in the outer fluid, Δ is the Laplace operator

$$\Delta \equiv \nabla \cdot \nabla = \frac{\partial^2}{\partial r^2} + \frac{1}{r}\frac{\partial}{\partial r} + \frac{1}{r^2}\frac{\partial^2}{\partial \theta^2} \tag{2}$$

$\nabla \equiv \mathrm{grad}$ is the Hamilton operator of gradient

$$\nabla \equiv \mathbf{i}_r \frac{\partial}{\partial r} + \mathbf{i}_\theta \frac{1}{r}\frac{\partial}{\partial \theta}, \tag{3}$$

$\mathbf{i}_r$ and $\mathbf{i}_\theta$ are the unit vectors in the polar system of coordinates. The harmonic factor $\exp(-i\omega t)$ is neglected in this paper, $i = \sqrt{-1}$.

The particles displacement vector $\mathbf{u}_{\mathrm{sc}}(r,\theta,\omega)$ in the outer acoustical medium is connected with the pressure $p_{\mathrm{sc}}(r,\theta,\omega)$ as follows (Brekhovskikh, Godin, 1989):

$$\mathbf{u}_{\mathrm{sc}}(r,\theta,\omega) = \frac{1}{\rho\omega^2}\nabla p_{\mathrm{sc}}(r,\theta,\omega) \quad (r > a), \tag{4}$$

where ρ is the density of the outer fluid.

In particular, for the radial component of the displacement vector we obtain

$$w_{\mathrm{sc}}(r,\theta,\omega) = \frac{1}{\rho\omega^2}\frac{\partial p_{\mathrm{sc}}(r,\theta,\omega)}{\partial r}. \tag{5}$$

The vibrations of the thin elastic cylindrical shell are described by the Kirchhoff-Love equations (Pidstryhach, Shvetz, 1978)

$$N_2(\theta,\omega) - \frac{\partial Q_2(\theta,\omega)}{\partial \theta} = \rho_s \omega^2 a h w(\theta,\omega) + a q_r(\theta,\omega), \tag{6}$$

$$\frac{\partial N_2(\theta,\omega)}{\partial \theta} + \frac{1}{a}\frac{\partial M_2(\theta,\omega)}{\partial \theta} = -\rho_s \omega^2 a h v(\theta,\omega) - a q_\theta(\theta,\omega), \tag{7}$$

where $N_2(\theta,\omega)$ is the outer normal stress resultant in the shell, $M_2(\theta,\omega)$ is the stress couple, $Q_2(\theta,\omega)$ is the resultant shear stress, $v(\theta,\omega)$ is the angular component of the displacement vector in the shell, $w(\theta,\omega)$ is the radial component of this vector, $q_r(\theta,\omega)$ and $q_\theta(\theta,\omega)$ are the radial and angular components of the outer force vector, respectively, ρ_s is the material density of shell.

For these characteristics, the following physical and geometrical relations are accomplished (Pidstryhach, Shvetz, 1978):

$$N_2(\theta,\omega) = \frac{D_1}{a}\left[\frac{\partial v(\theta,\omega)}{\partial \theta} + w(\theta,\omega)\right], \tag{8}$$

$$M_2(\theta,\omega) = -\frac{D_2}{a}\frac{\partial \vartheta(\theta,\omega)}{\partial \theta}, \tag{9}$$

$$Q_2(\theta,\omega) = \frac{1}{a}\frac{\partial M_2(\theta,\omega)}{\partial \theta}, \tag{10}$$

$$\vartheta(\theta,\omega) = \frac{1}{a}\left[\frac{\partial w(\theta,\omega)}{\partial \theta} - v(\theta,\omega)\right], \tag{11}$$

where D_1 and D_2 are the tension and bending stiffness of the shell material, respectively

$$D_1 = \frac{Eh}{1-\nu^2}, \qquad D_2 = \frac{Eh^3}{12(1-\nu^2)}, \tag{12}$$

E is the Young modulus, ν is the Poisson number, $\vartheta(\theta,\omega)$ is the angle of the shell middle surface rotation.

For the description of sound propagation in the viscous barotropic fluid, we use the Navier-Stokes equations, which formally (in the harmonic regime of vibrations) coincide with equations of the theory of elasticity, but with the Lamé constants λ_f and μ_f depending on the frequencies of vibrations (Landau, Lifsitz, 1987; Brekhovskikh, Godin, 1989):

$$\lambda_f(\omega) = \rho_f c_f^2 + i\omega\left(\frac{2}{3}\eta_f - \zeta_f\right), \qquad \mu_f(\omega) = -i\omega\eta_f, \tag{13}$$

where ρ_f is the density of the viscous fluid, c_f is the sound velocity for the adiabatic process, η_s is the first (shear) viscosity, ζ_f is the second (volume) viscosity.

Then the radial w_f and angular v_f components of the displacement vector in the viscous cylinder can be represented in the following form (Achenbach, 1973):

$$w_f(r,\theta,\omega) = \frac{\partial\Phi(r,\theta,\omega)}{\partial r} + \frac{1}{r}\frac{\partial\Psi(r,\theta,\omega)}{\partial\theta}, \tag{14}$$

$$v_f(r,\theta,\omega) = \frac{1}{r}\frac{\partial\Phi(r,\theta,\omega)}{\partial\theta} - \frac{\partial\Psi(r,\theta,\omega)}{\partial r}, \tag{15}$$

where $\Phi(r,\theta,\omega)$ and $\Psi(r,\theta,\omega)$ are longitudinal and shear elastic field potential functions, which satisfy the following wave equations:

$$(\Delta + k_{fL}^2)\Phi(r,\theta,\omega) = 0 \quad (0 < r < a), \tag{16}$$

$$(\Delta + k_{fT}^2)\Psi(r,\theta,\omega) = 0 \quad (0 < r < a). \tag{17}$$

Here $k_{fA} = \omega/c_{fA}$ $(A = L, T)$ are the wave numbers in the viscous fluid, c_{fL} is the longitudinal wave velocity and c_{fT} is the shear wave velocity, which are defined from the relations:

$$c_{fL} \equiv c_{fL}(\omega) = \sqrt{\frac{\lambda_f(\omega) + 2\mu_f(\omega)}{\rho_f}}, \qquad c_{fT} \equiv c_{fT}(\omega) = \sqrt{\frac{\mu_f(\omega)}{\rho_f}}. \tag{18}$$

Using the connections between the components of the stress tensor, the vector of displacement (Achenbach, 1973), and the formulas (14), (15), we obtain the following necessary relations (Pidstryhach, Piddubniak, 1986):

$$\sigma_{fr}(r,\theta,\omega) = 2\mu_f(\omega) \cdot \left(-L_1\Phi(r,\theta,\omega) + L_2\frac{\partial\Psi(r,\theta,\omega)}{\partial\theta}\right), \tag{19}$$

$$\tau_{fr\theta}(r,\theta,\omega) = 2\mu_f(\omega) \cdot \left(L_2\frac{\partial\Phi(r,\theta,\omega)}{\partial\theta} + L_1\Psi(r,\theta,\omega)\right), \tag{20}$$

where

$$L_1 \equiv \frac{1}{r}\left(\frac{\partial}{\partial r} + 2\frac{\partial^2}{\partial\theta^2}\right) + \frac{1}{2}k_{fT}^2, \qquad L_2 \equiv \frac{1}{r}\left(\frac{\partial}{\partial r} - \frac{1}{r}\right). \tag{21}$$

There, the following boundary conditions must be added to the Eqs. (1), (6), (7), (16), and (17):

$$q_r(\theta,\omega) = -[p_{\text{tot}}(a,\theta,\omega) + \sigma_{fr}(a,\theta,\omega)], \tag{22}$$

$$q_\theta(\theta,\omega) = -\tau_{fr}(a,\theta,\omega), \tag{23}$$

$$w(\theta,\omega) = w_{\text{tot}}(a,\theta,\omega) = w_f(a,\theta,\omega), \tag{24}$$

$$v(\theta,\omega) = v_f(a,\theta,\omega). \tag{25}$$

Here

$$p_{\text{tot}}(r,\theta,\omega) = p_{\text{inc}}(r,\theta,\omega) + p_{\text{sc}}(r,\theta,\omega), \qquad w_{\text{tot}}(r,\theta,\omega) = w_{\text{inc}}(r,\theta,\omega) + w_{\text{sc}}(r,\theta,\omega) \tag{26}$$

are the total sound fields, which contain the sum of incident and scattered waves.

Next, we also assume that the shell edges on the slit $\theta = \theta_0$ are free from loadings, i.e.

$$N_2(\theta_0 \pm 0,\omega) = 0, \qquad Q_2(\theta_0 \pm 0,\omega) = 0, \qquad M_2(\theta_0 \pm 0,\omega) = 0. \tag{27}$$

3. The method of solution of the problem

Suppose the plane wave of acoustical pressure incidents on the cylindrical elastic shell

$$p_{\text{inc}}(x,\omega) \equiv p_{\text{inc}}(r,\theta,\omega) = p_0 e^{ikx} = p_0 e^{ikr\cos\theta}, \tag{28}$$

where p_0 is the constant value of the dimension of pressure.

The expression (28) can be represented as the Fourier-Bessel complex series (Bateman, Erdélyi, 1953; Felsen, Markuvitz, 1973)

$$p_{\text{inc}}(r,\theta,\omega) = p_0 \sum_{m=-\infty}^{\infty} i^m J_m(kr) e^{-im\theta} \qquad (r \geq a,\ 0 \leq \theta \leq 2\pi) \tag{29}$$

and similarly from Eq. (5)

$$w_{\text{inc}}(r,\theta,\omega) = \frac{1}{\rho\omega^2}\frac{\partial p_{\text{inc}}(r,\theta,\omega)}{\partial r} = \frac{p_0}{\rho\omega^2}\sum_{m=-\infty}^{\infty} i^m J_m'(kr) e^{-im\theta} \qquad (r \geq a,\ 0 \leq \theta \leq 2\pi), \tag{30}$$

$J_m(kr)$ and $J'_m(kr)$ are the Bessel functions of m-th order and its derivative over argument, respectively.

The solution of the Eq. (1) for the sound waves scattered from the shell may be represented in the form

$$p_{\text{sc}}(r,\theta,\omega) = \sum_{m=-\infty}^{\infty} p_{sm} H_m^{(1)}(kr) e^{-im\theta} \qquad (r \geq a,\ 0 \leq \theta \leq 2\pi) \tag{31}$$

and the particle radial displacement in the scattered sound field is obtained from Eq. (5) as

$$w_{\text{sc}}(r,\theta,\omega) = \frac{1}{\rho\omega^2} \sum_{m=-\infty}^{\infty} p_{sm} H_m^{(1)'}(kr) e^{-im\theta} \qquad (r \geq a,\ 0 \leq \theta \leq 2\pi), \tag{32}$$

where $H_m^{(1)}(kr)$ and $H_m^{(1)'}(kr)$ are the Hankel functions of second kind and m-th order and its derivate over argument, respectively; p_{sm} are the unknown quantities.

Similarly, we obtain the solutions of Eqs. (16) and (17) for the inner fluid viscous cylinder

$$\Phi(r,\theta,\omega) = \sum_{m=-\infty}^{\infty} \Phi_m J_m(k_{fL} r) e^{-im\theta} \qquad (0 \leq r \leq a,\ 0 \leq \theta \leq 2\pi), \tag{33}$$

$$\Psi(r,\theta,\omega) = \sum_{m=-\infty}^{\infty} \Psi_m J_m(k_{fT} r) e^{-im\theta} \qquad (0 \leq r \leq a,\ 0 \leq \theta \leq 2\pi), \tag{34}$$

where Φ_m and Ψ_m are the unknown quantities.

Substituting the relations (33), (34) to the Eqs. (14), (15), and (23)–(25) we obtain (Pidstryhach, Piddubniak, 1986):

$$w_f(r,\theta,\omega) = \sum_{m=-\infty}^{\infty} \left[\Phi_m \chi_{1m}(k_{fL} r) + M\Psi_m \chi_{2m}(k_{fT} r)\right] e^{-im\theta}, \tag{35}$$

$$v_f(r,\theta,\omega) = -i \sum_{m=-\infty}^{\infty} m \left[\Phi_m \chi_{2m}(k_{fL} r) + \Psi_m \chi_{1m}(k_{fT} r)\right] e^{-im\theta}, \tag{36}$$

$$\sigma_{fr}(r,\theta,\omega) = 2\mu_f(\omega) \sum_{m=-\infty}^{\infty} \left[\Phi_m \chi_{3m}(k_{fL} r) + M\Psi_m \chi_{4m}(k_{fT} r)\right] e^{-im\theta}, \tag{37}$$

$$\tau_{fr\theta}(r,\theta,\omega) = -2\mu_f(\omega) i \sum_{m=-\infty}^{\infty} m \left[\Phi_m \chi_{4m}(k_{fL} r) + \Psi_m \chi_{3m}(k_{fT} r)\right] e^{-im\theta}, \tag{38}$$

with $0 \leq r \leq a$, $0 \leq \theta \leq 2\pi$ and

$$\begin{aligned}
\chi_{1m}(k_{fA} r) &= k_{fA} J'_m(k_{fA} r), \\
\chi_{2m}(k_{fA} r) &= \frac{1}{r} J_m(k_{fA} r), \\
\chi_{3m}(k_{fA} r) &= \left(-\frac{1}{2}k_{fT}^2 + \frac{M}{r^2}\right) J_m(k_{fA} r) - \frac{1}{r} k_{fA} J'_m(k_{fA} r), \\
\chi_{4m}(k_{fA} r) &= \frac{1}{r}\left[-\frac{1}{r} J_m(k_{fA} r) + k_{fA} J'_m(k_{fA} r)\right] \qquad (A = L, T;\ M = m^2).
\end{aligned} \tag{39}$$

For the solution of the equations of the shell theory we use the distribution of unknown functions in the Fourier series over the angular variable θ. However, there must be taken into consideration that these functions and their first derivates are continuous, possibly except the discontinuities of the first kind at point $\theta = \theta_0$. Therefore,

$$f(\theta) = \sum_{m=-\infty}^{\infty} f_m e^{-im\theta} \quad (0 \leq \theta \leq 2\pi), \tag{40}$$

such that

$$f_m = \frac{1}{2\pi} \lim_{\delta \to 0} \left[\int_0^{\theta_0-\delta} f(\theta) e^{im\theta}\,\mathrm{d}\theta + \int_{\theta_0+\delta}^{2\pi} f(\theta) e^{im\theta}\,\mathrm{d}\theta\right] \qquad (m = 0, \pm 1, \pm 2, ...). \tag{41}$$

For this reason, applying the operator $\int_0^{2\pi} (...) e^{im\theta}\,\mathrm{d}\theta$ to the Eqs. (6) and (7) we obtain (Piddubniak, 1995)

$$2\pi N_{2m} - [Q_2] e^{im\theta_0} + 2\pi i m Q_{2m} = 2\pi(\rho_s \omega^2 a h w_m + a q_{rm}), \tag{42}$$

$$[N_2] e^{im\theta_0} - 2\pi i m N_{2m} + \frac{1}{a}[M_2] e^{im\theta_0} - \frac{2\pi i m}{a} M_{2m} = -2\pi(\rho_s \omega^2 a h v_m + a q_{\theta m}), \tag{43}$$

where $[f] = f(\theta_0 - 0) - f(\theta_0 + 0)$ is the jump of function $f(\theta)$ resulting from transition through the slit in the shell.

From Eqs. (8)–(11), the following equations can be obtained in the same way:

$$2\pi N_{2m} = \frac{D_1}{a}\left([v] e^{im\theta_0} - 2\pi i m v_m + 2\pi w_m\right), \tag{44}$$

$$2\pi M_{2m} = -\frac{D_2}{a}\left([\vartheta_2] e^{im\theta_0} - 2\pi i m \vartheta_{2m}\right), \tag{45}$$

$$2\pi Q_{2m} = \frac{1}{a}\left([M_2] e^{im\theta_0} - 2\pi i m M_{2m}\right), \tag{46}$$

$$2\pi \vartheta_{2m} = \frac{1}{a}\left([w] e^{im\theta_0} - 2\pi i m w_m - 2\pi v_m\right). \tag{47}$$

The Eqs. (42), (43) and (46) contain the jumps of normal stress resultant $N_2(\theta,\omega)$, the stress couple $M_2(\theta,\omega)$ and shear stress resultant $Q_2(\theta,\omega)$, which in consequence of carrying out the boundary conditions (27), are zeros:

$$[N_2] = [M_2] = [Q_2] = 0. \tag{48}$$

Next, we introduce the definitions

$$\begin{aligned} W_m &= \frac{1}{2\pi}[w]e^{im\theta_0}, \\ V_m &= \frac{1}{2\pi}[v]e^{im\theta_0}, \\ T_m &= \frac{a}{2\pi}[\vartheta_2]e^{im\theta_0}, \\ \Theta_m &= T_m - imW_m. \end{aligned} \tag{49}$$

Then taking into account the Eqs. (42)–(48), we obtain the following system of equations:

$$\begin{aligned} &v_m - im(1+\varepsilon M)w_m \\ &\qquad = imV_m - im\varepsilon\Theta_m - \frac{a^2}{D_1}q_{\theta m}, \\ &im(1+\varepsilon M)v_m + (x_{10}^2 - 1 - \varepsilon M^2)w_m \\ &\qquad = V_m - \varepsilon M\Theta_m - \frac{a^2}{D_1}q_{rm}, \end{aligned} \tag{50}$$

where

$$\begin{aligned} &\varepsilon = \frac{h^2}{12a^2}, \qquad x_{10} = k_{10}a, \qquad k_{10} = \frac{\omega}{c_{10}}, \\ &c_{10} = \sqrt{\frac{E}{\rho_s(1-v^2)}} = 2c_T\sqrt{1 - \frac{c_T^2}{c_L^2}}, \end{aligned} \tag{51}$$

c_{10} is the velocity of the shell elastic wave connected with the plate mode of shell vibrations (Metsaveer *et al.*, 1979), k_{10} is the wave number for this mode.

Now, we write the expressions for the quantities $q_{\theta m}$ and q_{rm}. On the basis of the boundary conditions (22), (23) and Eqs. (26_1), (29), (31), (37), (38), (40), (41), we find

$$\begin{aligned} q_{rm} = -\{&p_0 i^m J_m(x) + p_{sm}H_m^{(1)}(x) \\ &+ 2\mu_f[\varPhi_m\chi_{3m}(x_{fL}) + M\varPsi_m\chi_{4m}(x_{fT})]\}, \end{aligned} \tag{52}$$

$$q_{\theta m} = -2i\mu_{fm}[\varPhi_m\chi_{4m}(x_{fL}) + \varPsi_m\chi_{3m}(x_{fT})]\}, \tag{53}$$

where $x = ka$, $x_{fA} = k_{fA}a$ $(A = L, T)$.

Next, from the conditions (24), (25) and Eqs. (30), (32), (35), (36) we have

$$w_{tot,m} = w_m = \frac{1}{\rho c\omega}[p_0 i^m J'_m(x) + p_{sm}H_m^{(1)'}(x)], \tag{54}$$

$$\begin{aligned} w_{fm} &= w_m \\ &= \frac{1}{a}[\varPhi_m x_{fL}J'_m(x_{fL}) + M\varPsi_m J_m(x_{fT})], \end{aligned} \tag{55}$$

$$\begin{aligned} v_{fm} &= v_m \\ &= -\frac{im}{a}[\varPhi_m J_m(x_{fL}) + \varPsi_m x_{fT}J'_m(x_{fT})]. \end{aligned} \tag{56}$$

From the Eq. (54), the quantities p_{sm} are obtained as

$$p_{sm} = \frac{1}{H_m^{(1)'}(x)}[\rho c\omega w_m - p_0 i^m J'_m(x)] \tag{57}$$

and from the system of equations (55) and (56) the quantities $\varPhi_{sm}$ and $\varPsi_{sm}$ may be written as

$$\varPhi_m = \frac{1}{\Delta_m}[w_m\chi_{1m}(x_{fT}) - imv_m\chi_{2m}(x_{fL})], \tag{58}$$

$$\varPsi_m = \frac{1}{\Delta_m}\left[-w_m\chi_{2m}(x_{fT}) + \frac{i}{m}v_m\chi_{1m}(x_{fL})\right] \qquad (m \neq 0), \tag{59}$$

where

$$\begin{aligned} \Delta_m = a^2[&\chi_{1m}(x_{fL})\chi_{1m}(x_{fT}) \\ &- M\chi_{2m}(x_{fL})\chi_{2m}(x_{fT})]. \end{aligned} \tag{60}$$

Substituting $\varPhi_{sm}$ and $\varPsi_{sm}$ into the expressions for the quantities q_{rm} and $q_{\theta m}$ (52), (53) we obtain after some transforms:

$$\begin{aligned} q_{rm} = &-[p_0 i^m J_m(x) + p_{sm}H_m^{(1)}(x)] \\ &- \frac{2\mu_f}{\Delta_m}[w_m f_{1m}(x_{fT}, x_{fL}) \\ &+ imv_m f_{2m}(x_{fT}, x_{fL})], \end{aligned} \tag{61}$$

$$\begin{aligned} q_{\theta m} = &-\frac{2\mu_f}{\Delta_m}[imw_m f_{2m}(x_{fL}, x_{fT}) \\ &- v_m f_{1m}(x_{fL}, x_{fT})] \end{aligned} \tag{62}$$

with

$$\begin{aligned} f_{1m}(x_{fA}, x_{fB}) &= a^3[\chi_{1m}(x_{fA})\chi_{3m}(x_{fB}) \\ &\qquad - M\chi_{2m}(x_{fA})\chi_{4m}(x_{fB})], \\ f_{2m}(x_{fA}, x_{fB}) &= a^3[-\chi_{2m}(x_{fA})\chi_{3m}(x_{fB}) \\ &\qquad + \chi_{1m}(x_{fA})\chi_{4m}(x_{fB})] \\ &\qquad (A, B = L, T;\ A \neq B). \end{aligned} \tag{63}$$

Now, using the expressions (57) for p_{sm} and the expressions (61), (62) for q_{rm} and $q_{\theta m}$, the equations (50) can be reduced to the systems of equations in v_m and w_m:

$$\begin{aligned} L_{11m}v_m + L_{12m}w_m &= imV_m - im\varepsilon\Theta_m, \\ L_{21m}v_m + L_{22m}^0 w_m &= V_m - \varepsilon M\Theta_m + g_m, \end{aligned} \tag{64}$$

where

$$L_{11m} = x_{10}^2 - (1+\varepsilon)M + \frac{2a\xi_{f0}}{\Delta_m} f_{1m}(x_{fL}, x_{fT}),$$

$$L_{12m} = -im\left[1 + \varepsilon M + \frac{2a\xi_{f0}}{\Delta_m} f_{2m}(x_{fL}, x_{fT})\right],$$

$$L_{21m} = im\left[1 + \varepsilon M - \frac{2a\xi_{f0}}{\Delta_m} f_{2m}(x_{fT}, x_{fL})\right],$$

$$L_{22m} = x_{10}^2 - 1 - \varepsilon M^2 - \frac{2a\xi_{f0}}{\Delta_m} f_{1m}(x_{fT}, x_{fL}),$$

$$L_{22m}^0 = L_{22m} + z_m, \qquad z_m = -x\xi_0 \frac{H_m^{(1)}(x)}{H_m^{(1)'}(x)}, \tag{65}$$

$$g_m = \kappa_0 \widetilde{g}_m, \qquad \widetilde{g}_m = \frac{i^m}{H_m^{(1)'}(x)},$$

$$\kappa_0 = \frac{2ip_0a^2}{\pi D_1 x}, \qquad \xi_0 = \frac{a}{h} N_s \left(\frac{c}{c_{10}}\right)^2,$$

$$\xi_{f0} = \frac{a}{h} N_{fs} \left(\frac{c_{fT}}{c_{10}}\right)^2,$$

$$N_s = \frac{\rho}{\rho_s}, \qquad N_{fs} = \frac{\rho_f}{\rho_s}.$$

Similarly as the expression for g_m, the unknown characteristics can be written as

$$\{v_m, w_m, \vartheta_m, V_m, \Theta_m\} = \kappa_0\{\widetilde{v}_m, \widetilde{w}_m, \widetilde{\vartheta}_m, \widetilde{V}_m, \widetilde{\Theta}_m\}. \tag{66}$$

After transformation, the system of Eqs. (64) leads to

$$\begin{aligned} L_{11m}\widetilde{v}_m + L_{12m}\widetilde{w}_m &= im\widetilde{V}_m - im\varepsilon\widetilde{\Theta}_m, \\ L_{21m}\widetilde{v}_m + L_{22m}\widetilde{w}_m &= \widetilde{V}_m - \varepsilon M\widetilde{\Theta}_m + \widetilde{g}_m. \end{aligned} \tag{67}$$

Solving these equations we obtain the connections between the quantities $\widetilde{v}_m$ and $\widetilde{w}_m$, on the one hand, and the characteristics $\widetilde{V}_m$ and $\widetilde{\Theta}_m$, on the other hand

$$\widetilde{v}_m = \frac{1}{D_m}(D_{vm} - L_{12m}\widetilde{g}_m), \tag{68}$$

$$\widetilde{w}_m = \frac{1}{D_m}(D_{wm} + L_{11m}\widetilde{g}_m), \tag{69}$$

where

$$\begin{aligned} D_m &= -\frac{1}{H_m^{(1)'}(x)}[x\xi_0 L_{11m} H_m^{(1)}(x) \\ &\quad - D_m^0 H_m^{(1)'}(x)], \\ D_{vm} &= (imL_{22m}^0 - L_{12m})\widetilde{V}_m \\ &\quad - (imL_{22m}^0 - ML_{12m})\varepsilon\widetilde{\Theta}_m, \\ D_{wm} &= (L_{11m} - imL_{21m})\widetilde{V}_m \\ &\quad - (ML_{11m} - imL_{21m})\varepsilon\widetilde{\Theta}_m, \\ D_m^0 &= L_{11m}L_{22m} - L_{12m}L_{21m}, \end{aligned} \tag{70}$$

The substitution of w_m into the expression for p_{sm} (57) yields

$$p_{sm} = p_{sm}^0 + \frac{2ip_0\xi_0}{\pi H_m^{(1)'}(x)} \frac{D_{wm}}{D_m}, \tag{71}$$

where the quantities

$$p_{sm}^0 = -p_0 i^m \frac{\xi_0 x L_{11m} J_m(x) - D_m^0 J_m'(x)}{\xi_0 x L_{11m} H_m^{(1)}(x) - D_m^0 H_m^{(1)'}(x)} \tag{72}$$

represent the case of the shell without slit.

For the estimation the influence of the slit on the spectral structure of the acoustical echo-signal, it is necessary to find the quantities $\widetilde{V}_m$ and $\widetilde{\Theta}_m$ ($\widetilde{W}_m$, $\widetilde{T}_m$), which are contained in the expressions for D_{vm} and D_{wm}. The conditions, with the help of which these quantities may be determined, are obtained from Eq. (27).

First, let us calculate the quantities N_{2m}, M_{2m} and Q_{2m} from Eqs. (44)–(46), (49) and next from the Eqs. (66), (68)–(70) and (40). The system of linear algebraic equations with unknown quantities $\widetilde{V}_m$, $\widetilde{\Theta}_m$ ($\widetilde{W}_m$, $\widetilde{T}_m$) is obtained:

$$\begin{aligned} &\sum_{m=-\infty}^{\infty} [A_{NVm}\widetilde{V}_m + A_{N\Theta m}\widetilde{\Theta}_m \\ &\qquad + A_{Npm}\widetilde{g}_m]e^{-im\theta_0} = 0, \\ &\sum_{m=-\infty}^{\infty} [A_{MVm}\widetilde{V}_m + A_{M\Theta m}\widetilde{\Theta}_m \\ &\qquad + A_{Mpm}\widetilde{g}_m]e^{-im\theta_0} = 0, \\ &\sum_{m=-\infty}^{\infty} m[A_{MVm}\widetilde{V}_m + A_{M\Theta m}\widetilde{\Theta}_m \\ &\qquad + A_{Mpm}\widetilde{g}_m]e^{-im\theta_0} = 0, \end{aligned} \tag{73}$$

where

$$\begin{aligned} A_{NVm} &= 1 + \frac{1}{D_m}[ML_{22m}^0 + im \\ &\quad \cdot (L_{12m} - L_{21m}) + L_{11m}], \\ A_{N\Theta m} &= \varepsilon A_{MVm}, \\ A_{MVm} &= -\frac{1}{D_m}[ML_{22m}^0 + im \\ &\quad \cdot (ML_{12m} - L_{21m}) + ML_{11m}], \\ A_{Npm} &= \frac{1}{D_m}(imL_{12m} + L_{11m}), \\ A_{Mpm} &= -\frac{1}{D_m}(imL_{12m} + ML_{11m}) \\ A_{M\Theta m} &= 1 + \frac{\varepsilon M}{D_m}[L_{22m}^0 + im \\ &\quad \cdot (L_{12m} - L_{21m}) + ML_{11m}]. \end{aligned} \tag{74}$$

From the definitions (49) and (66), it follows that

$$\{\widetilde{V}_m, \widetilde{W}_m, \widetilde{T}_m\}e^{-im\theta_0} = \frac{1}{2\pi}[\widetilde{v}, \widetilde{w}, \widetilde{\vartheta_2}] = \{\widetilde{V}_0, \widetilde{W}_0, \widetilde{T}_0\}. \tag{75}$$

Then, from the Eqs. (73) we obtain the system of equations with the quantities $\widetilde{V}_0$, $\widetilde{T}_0$, $\widetilde{W}_0$:

$$\begin{aligned} A_{11}\widetilde{V}_0 + A_{12}\widetilde{T}_0 &= B_1, \\ A_{21}\widetilde{V}_0 + A_{22}\widetilde{T}_0 &= B_2, \\ A_{33}\widetilde{W}_0 &= B_3, \end{aligned} \tag{76}$$

where

$$\begin{aligned} A_{11} &= \sum_{m=0}^{\infty} \varepsilon_m A_{MVm}, \\ A_{12} &= \sum_{m=1}^{\infty} A_{N\Theta m} = \varepsilon A_{21}, \\ A_{22} &= \sum_{m=0}^{\infty} \varepsilon_m A_{M\Theta m}, \\ A_{33} &= \sum_{m=1}^{\infty} M A_{M\Theta m}, \\ B_1 &= -\sum_{m=0}^{\infty} \varepsilon_m A_{Npm}\widetilde{g}_m \cos(m\theta_0), \\ B_2 &= -\sum_{m=1}^{\infty} A_{Mpm}\widetilde{g}_m \cos(m\theta_0), \\ B_3 &= -\sum_{m=1}^{\infty} m A_{Mpm}\widetilde{g}_m \sin(m\theta_0). \end{aligned} \tag{77}$$

Here $\varepsilon_m = 1-0.5\delta_{m0}$, δ_{m0} is the Kronecker symbol, and following properties are used as well:

$$\begin{aligned} &A_{NV,-m} = A_{NVm}, \qquad A_{MV,-m} = A_{MVm}, \\ &A_{N\Theta,-m} = A_{N\Theta m}, \qquad A_{M\Theta,-m} = A_{M\Theta m}, \\ &A_{Np,-m} = A_{Npm}, \qquad A_{Mp,-m} = A_{Mpm}, \\ &A_{MV0} = 0, \qquad A_{N\Theta 0} = 0, \\ &A_{Mp0} = 0. \end{aligned} \tag{78}$$

Solving the Eqs. (76) and (77) we obtain

$$\begin{aligned} \widetilde{V}_0 &= \frac{B_1 A_{22} - \varepsilon B_2 A_{21}}{A_{11}A_{22} - \varepsilon A_{21}^2}, \\ \widetilde{T}_0 &= -\frac{B_1 A_{21} - B_2 A_{11}}{A_{11}A_{22} - \varepsilon A_{21}^2}, \\ \widetilde{W}_0 &= \frac{B_3}{A_{33}}. \end{aligned} \tag{79}$$

Having the expressions for quantities $\widetilde{V}_0$, $\widetilde{W}_0$ and $\widetilde{T}_0$, from the Eqs. (31), (70)–(72), (75), (79), we can determine the complex amplitude of the acoustic pressure in the scattered sound wave:

$$\begin{aligned} p_{\mathrm{sc}}(r,\theta,\omega) &= 2\sum_{m=0}^{\infty} \varepsilon_m p_{sm}^0 \cos(m\theta) \\ &+ \frac{2}{\pi} i p_0 \xi_0 \sum_{m=0}^{\infty} \frac{H_m^{(1)}(kr)}{H_m^{(1)\prime}(x) D_m} \\ &\cdot \{[(\varepsilon_m L_{11m} - imL_{21m})\widetilde{V}_0 \\ &- \varepsilon(ML_{11m} - imL_{21m})\widetilde{T}_0] \cos[m(\theta-\theta_0)] \\ &+ \varepsilon m(ML_{11m} - imL_{21m})\widetilde{W}_0 \sin[m(\theta-\theta_0)]\}. \end{aligned} \tag{80}$$

This formula is obtained taking into consideration the Bessel function property in the Eq. (72) and the equality $p_{s,-m}^0 = (-1)^m p_{sm}^0$.

For the farfield case ($r \to \infty$) the following asymptote for the Hankel function of first kind must be used (Bateman, Erdélyi, 1953):

$$H_m^{(1)}(kr) \approx \frac{2(-i)^m}{\sqrt{\pi x i}} \sqrt{\frac{a}{2r}} e^{ikr}. \tag{81}$$

Then, for the acoustic pressure in the scattered field we have

$$p_{\mathrm{sc}}(r,\theta,\omega) \approx p_0 \sqrt{\frac{a}{2r}} f(\theta,k) e^{ikr}, \tag{82}$$

where $f(\theta,k)$ is the scattering amplitude:

$$f(\theta,k) = f_0(\theta,k) + f_v(\theta,k) + f_\vartheta(\theta,k) + f_w(\theta,k). \tag{83}$$

Here $f_0(\theta,k)$ is the scattering amplitude for the case of the shell without slit:

$$f_0(\theta,k) = -\frac{4}{\sqrt{\pi i x}} \sum_{m=0}^{\infty} \varepsilon_m \cdot \frac{\xi_0 x L_{11m} J_m(x) - D_m^0 J_m'(x)}{\xi_0 x L_{11m} H_m^{(1)}(x) - D_m^0 H_m^{(1)\prime}(x)} \cos(m\theta) \tag{84}$$

and $f_v(\theta,k)$, $f_\vartheta(\theta,k)$, $f_w(\theta,k)$ are the disturbances in the scattering amplitude caused by the tangential, v, angular, ϑ, and radial, w, displacements of the shell edges on the slit, respectively:

$$f_v(\theta,k) = -\frac{8i\xi_0}{\pi\sqrt{\pi i x}} \widetilde{V}_0 \sum_{m=0}^{\infty} (-i)^m \cdot \frac{(\varepsilon_m L_{11m} - imL_{21m}) \cos[m(\theta-\theta_0)]}{\xi_0 x L_{11m} H_m^{(1)}(x) - D_m^0 H_m^{(1)\prime}(x)}, \tag{85}$$

$$f_\vartheta(\theta,k) = \frac{8i\xi_0\varepsilon}{\pi\sqrt{\pi i x}}\widetilde{T}_0\sum_{m=1}^{\infty}(-i)^m \cdot\frac{(ML_{11m}-imL_{21m})\cos[m(\theta-\theta_0)]}{\xi_0 x L_{11m}H_m^{(1)}(x)-D_m^0 H_m^{(1)\prime}(x)}, \tag{86}$$

$$f_w(\theta,k) = -\frac{8i\xi_0\varepsilon}{\pi\sqrt{\pi i x}}\widetilde{W}_0\sum_{m=1}^{\infty}(-i)^m \cdot\frac{m(ML_{11m}-imL_{21m})\sin[m(\theta-\theta_0)]}{\xi_0 x L_{11m}H_m^{(1)}(x)-D_m^0 H_m^{(1)\prime}(x)}. \tag{87}$$

It should be noted that here

$$\xi_0\varepsilon = \frac{h}{12a}N_s\frac{c^2}{c_{10}^2}.$$

4. Numerical calculations and analysis of results

The numerical calculations have been performed for the case of the steel shell with radius $a = 1$ m and wall thickness $h = 0.025$ m, for which $\rho_s = 7900$ kg/m^3, $c_L = 5240$ m/s, $c_T = 2978$ m/s, $c_{10} = 4901$ m/s (Anson, Chivers, 1981).

The shell is immersed in seawater of parameters: $\rho = 1000$ kg/m^3, $c = 1410$ m/c (Hickling, Means, 1968; Artobolevski, 1976).

The shell has been filled with an oil. In the general case, the density of the viscous fluid and the sound velocity in this substance depend on temperature, pressure and frequency of vibrations (Litovitz, Davis, 1965; Meng *et al.*, 2006; Dukhin, Goetz, 2009; Tittmann, 2011). The density of this fluid had varied in the limits from 650 to 1040 kg/m^3. We select the middle value from this range $\rho_f = 870$ kg/m^3 corresponding to the oil of the 30WeightOil type for room temperature 25°C[1]. For this temperature, the dynamical viscosity equals $\eta_f = 0.110$ Pa·s. In addition, $c_f = 1300$ m/s (Åseng, 2006).

In respect to the volume viscosity, it the approximate equality $\zeta_f \approx 4\eta_f/3$ may be used for oil (Taşköprülü *et al.*, 1961). Then, from Eqs. (13) we obtain

$$\lambda_f(\omega) = \rho_f\left(c_f^2 - \frac{2}{3}i\omega\nu_f\right), \qquad \mu_f(\omega) = -i\omega\rho_f\nu_f, \tag{88}$$

where $\nu_f = \eta_f/\rho_f$ is the kinematic viscosity: $\nu_f = 1.26\cdot 10^{-4}$ m^2/s.

Next, from the Eqs. (18) the wave velocities in a viscous fluid may be written as

$$c_{fL} = \sqrt{c_f^2 - \frac{8}{3}i\omega\nu_f}, \qquad c_{fT} = \sqrt{-i\omega\nu_f}. \tag{89}$$

[1]Oil Viscosity/Zplus$^{\mathrm{TM}}$ Tech Brief #13, 2008, June 29, 1–11, www.zddplus.com/TechBrief13%20-%20Oil%20Viscosity.pdf.

Next, we obtain the dimensionless wave numbers for the viscous fluid in the complex form (Dwight, 1957):

$$x_{fL} = \frac{\omega a}{c_{fL}} = \frac{x_f}{\sqrt{1-(8/3)ix_f n_f}} = \frac{x_f}{\sqrt{2}\sqrt{1+(8x_f n_f/3)^2}} \times\left[\sqrt{\sqrt{1+(8x_f n_f/3)^2}+1} + i\sqrt{\sqrt{1+(8x_f n_f/3)^2}-1}\right], \tag{90}$$

$$x_{fT} = \sqrt{\frac{x_f}{2n_f}}(1+i), \qquad x_f = \frac{\omega a}{c_f}, \tag{91}$$

where $n_f = \nu_f/(c_f a)$ is the dimensionless kinematic viscosity.

It should be noted that performing the calculations we have applied the technique of elimination of the numerical instabilities of the Bessel functions with complex arguments in the same manner as it was done by Anson, Chivers (1993).

Figures 2 a and b present the dependence of the real and imaginary parts of the dimensionless longitudinal wave numbers x_{fL} for the oil *versus* the dimensionless wave numbers for seawater. As seen the imaginary part

a)

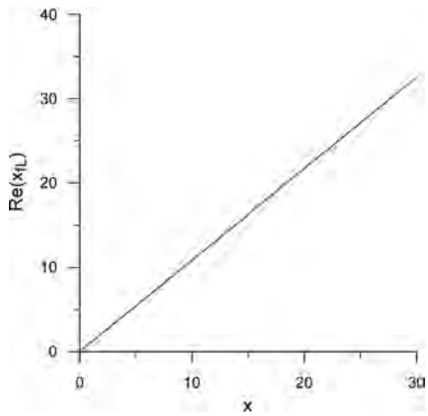

b)

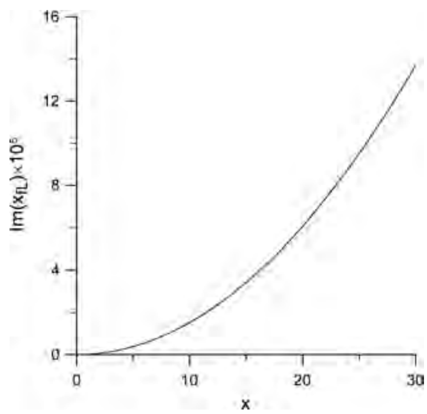

Fig. 2. The dependences of dimensionless complex longitudinal wave number x_{fL} in the oil on the dimensionless wave number in seawater x: a) Re(x_{fL}); b) Im(x_{fL}).

is very small in the considered frequency range, i.e. the attenuation of longitudinal waves is slight. Another type of behavior are observe in Fig. 3, where a similar dependence is presented for the dimensionless shear wave numbers. In this case, the real and imaginary parts of the wave numbers have the same values and increase quickly as the sound frequency increases (proportional to the square root of the frequency). Thus, the shear waves are characterized by great attenuation.

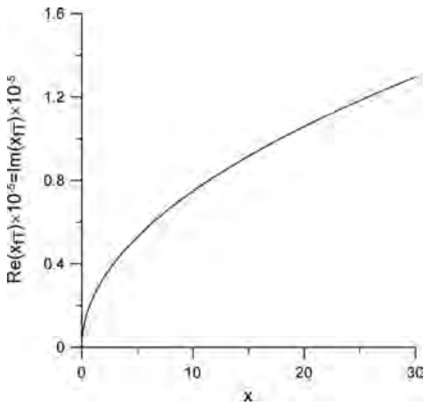

Fig. 3. The dependence of dimensionless complex shear wave number x_{fT} in the oil on the dimensionless wave number in seawater x: $\mathrm{Re}(x_{fT}) = \mathrm{Im}(x_{fT})$.

The module of the scattering amplitude $|f(\theta, k)|$ (it is known as "form-function") calculated in the "back" direction, i.e. for $\theta = 180°$ *versus* dimensionless frequency in the range $0 < x < 30$ for the case of shell without a slit, is shown in Fig. 4. It is seen that this amplitude contains many oscillations caused by superposition of the scattered waves arriving to the observation point with the difference phases. Another feature characterizing the sound scattering is the large quality of sharp peaks and dips aroused by the contribution of vibrations of the shell with a viscous liquid filler to the eigen frequencies. Thus, the figure shows the effects of the resonance acoustic scattering (Gaunaurd, Werby, 1990; Veksler, 1993; Kaplunov *et al.*, 1994, 1998; Belov *et al.*, 1999).

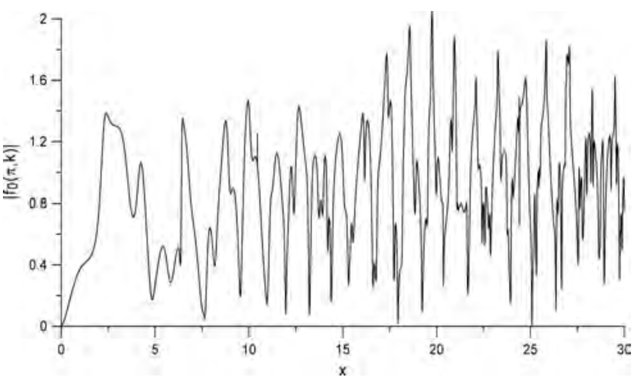

Fig. 4. Form-function $|f_0(\pi, k)|$ of non-defected steel shell filled with oil and surrounded in seawater vs $x = ka$.

The same characteristics, but for the case of the shell weakened by a slit, aregiven in Figs. 5–9 for $\theta_0 = 0°$, $45°$, $90°$, $135°$, and $180°$, respectively. The comparison of the plots in these figures and Fig. 4 demonstrates the resonance nature of the sound wave diffraction from objects of both types. However, large differences must be noted in the resonance amplitudes excited in consequence of the present slit and the vibrations of the elastic shell edges. Moreover, additional resonances arise that are caused by the surface wave propagation on the elastic shell. These waves, running on the shell periphery from one slit boundary to the other one, radiate sound energy into the surroundings including the "back" direction. The amplitudes of these resonances depend on the slit location.

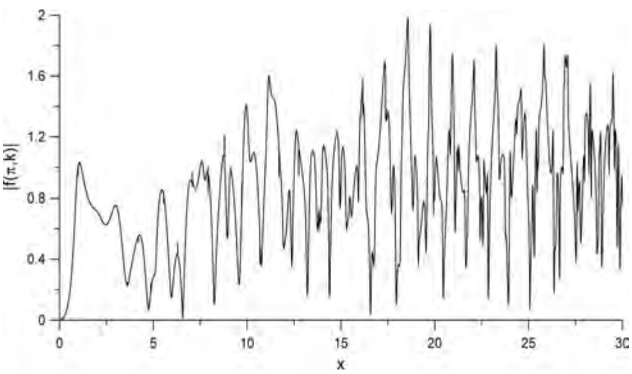

Fig. 5. Form-function $|f(\pi, k)|$ of defected steel shell filled with oil and surrounded in seawater vs $x = ka$ ($\theta_0 = 0°$).

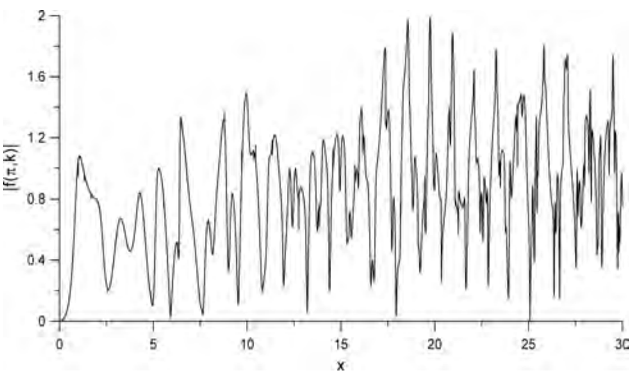

Fig. 6. Form-function $|f(\pi, k)|$ for $\theta_0 = 45°$.

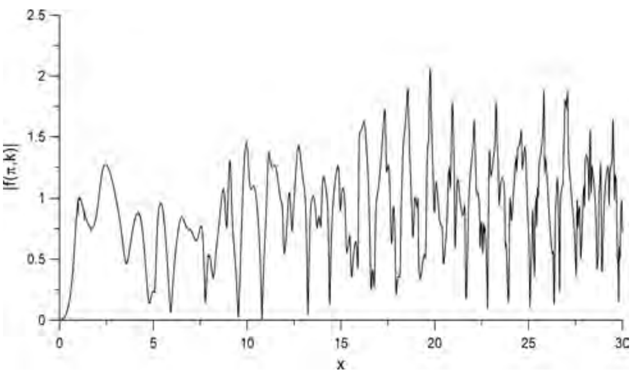

Fig. 7. Form-function $|f(\pi, k)|$ for $\theta_0 = 90°$.

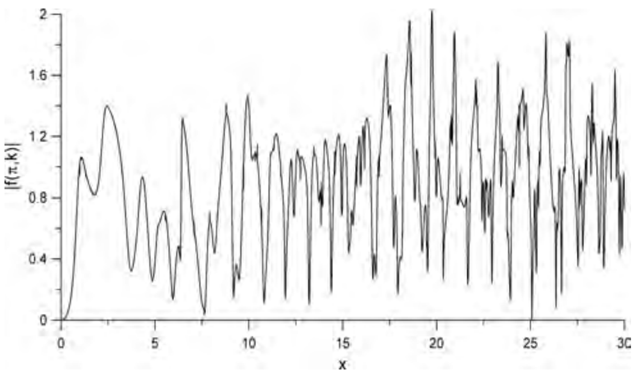

Fig. 8. Form-function $|f(\pi, k)|$ for $\theta_0 = 135°$.

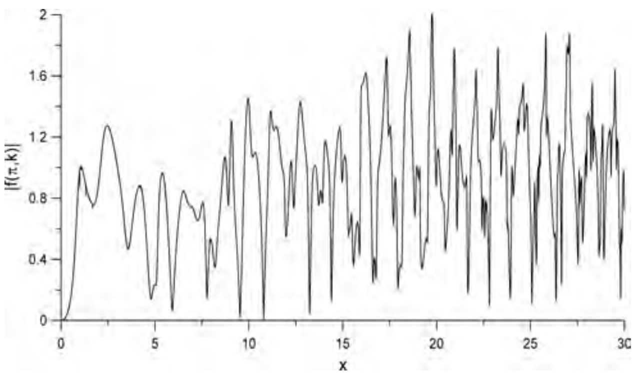

Fig. 9. Form-function $|f(\pi, k)|$ for $\theta_0 = 180°$.

Figures 10–15 show the phase of the scattering amplitude $\phi(\theta, k) = \arctan[\mathrm{Im}f(\theta, k)/\mathrm{Re}f(\theta, k)]$, from which visually can be noted the resonance character of the sound diffraction and crack influence on the scattering process.

The influence of slit orientation on the spectral wave structure is illustrated in more detail in Fig. 16 for the scattering function phase portraits calculated for the "back" direction and the frequency range $0.001 \leq x \leq 30$. From these plots it is seen how the localization of the defect is reflected in the phase of echo-signal. The small loops in the displayed plots (in the form of small "circulars") for the case of shell with defect correspond to the signals with small amplitude and are caused by the particular vibrations of the shell edges.

Figures 17 represent the space distribution of the form-function $|f(\theta, k))|$ (in dB) at one of resonance frequency $x = 5.459$ for the case of shell without and with defect for some slit positions: $\theta_0 = 0°$, $45°$, $90°$, $135°$, $180°$. For the case of the cracked shell this characteristic is non-symmetrical with respect to the direction $\theta = 180°$ (or for $\theta = 0°$) and the asymmetry is most noted in "light" side of the object.

The directivity patterns $D(\theta, k) = |f(\theta, k)|/|f(\pi, k)|$ are presented in Figs. 18. The numerical calculations have been performed using the same parameters as above. We see here that the main part of the scattered acoustic energy is located in the "forward"

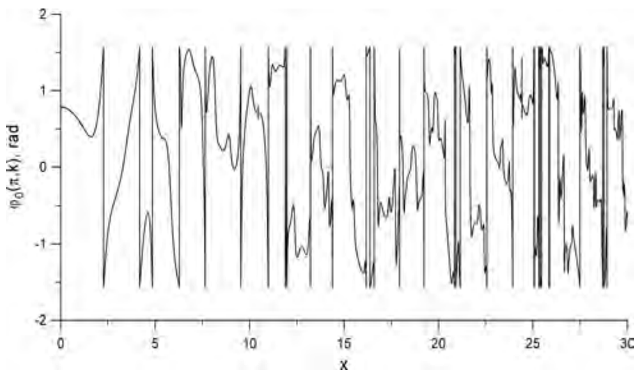

Fig. 10. Phase of backscattering far-field amplitude $\phi_0(\pi, k) = \mathrm{arctg}[\mathrm{Im}f_0(\pi, k)/\mathrm{Re}f_0(\pi, k)]|$ of non-defected shell vs $x = ka$.

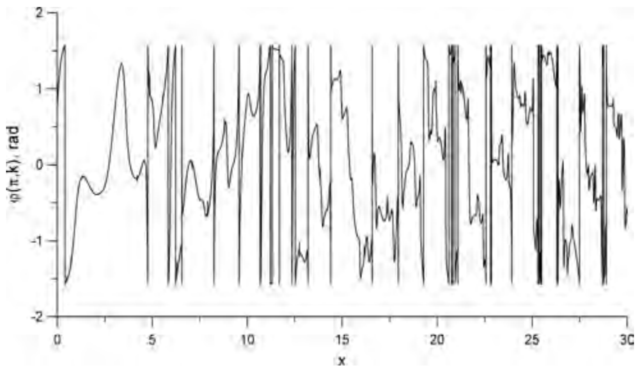

Fig. 11. Phase $\phi(\pi, k) = \mathrm{arctg}[\mathrm{Im}f(\pi, k)/\mathrm{Re}f(\pi, k)]|$ of defected shell vs $x = ka$ ($\theta_0 = 0°$).

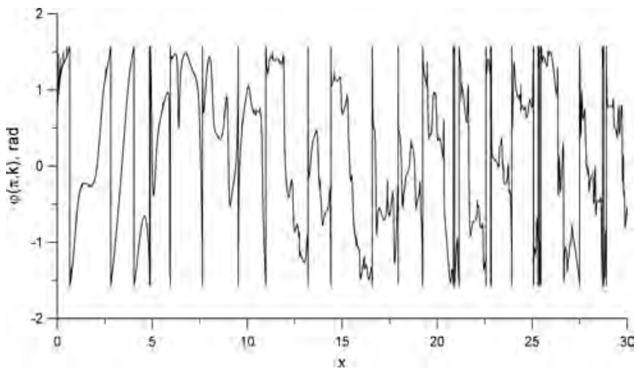

Fig. 12. Phase $\phi(\pi, k) = \mathrm{arctg}[\mathrm{Im}f(\pi, k)/\mathrm{Re}f(\pi, k)]|$ for $\theta_\circ = 45°$.

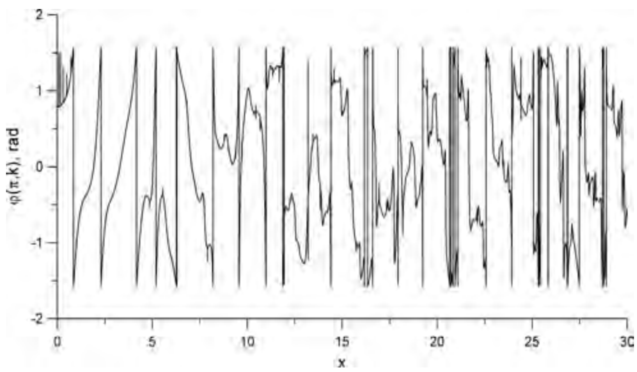

Fig. 13. Phase $\phi(\pi, k) = \mathrm{arctg}[\mathrm{Im}f(\pi, k)/\mathrm{Re}f(\pi, k)]|$ for $\theta_0 = 90°$.

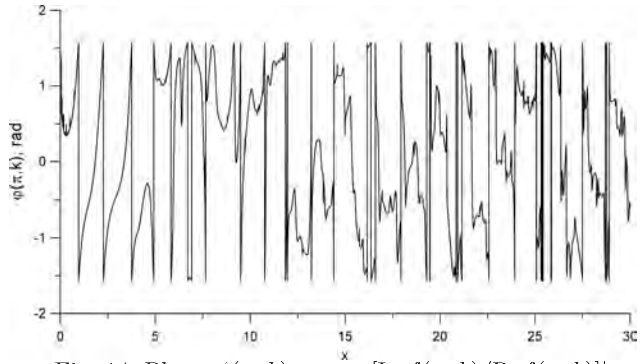

Fig. 14. Phase $\phi(\pi, k)$ =arctg[Im$f(\pi,k)$/Re$f(\pi,k)$]| for $\theta_0 = 135°$.

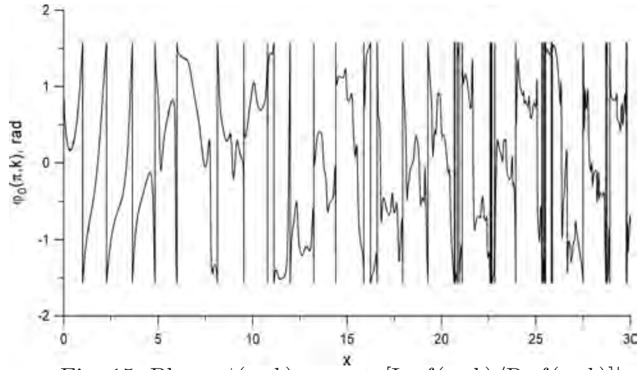

Fig. 15. Phase $\phi(\pi, k)$ = arctg[Im$f(\pi,k)$/Re$f(\pi,k)$]| for $\theta_0 = 180°$.

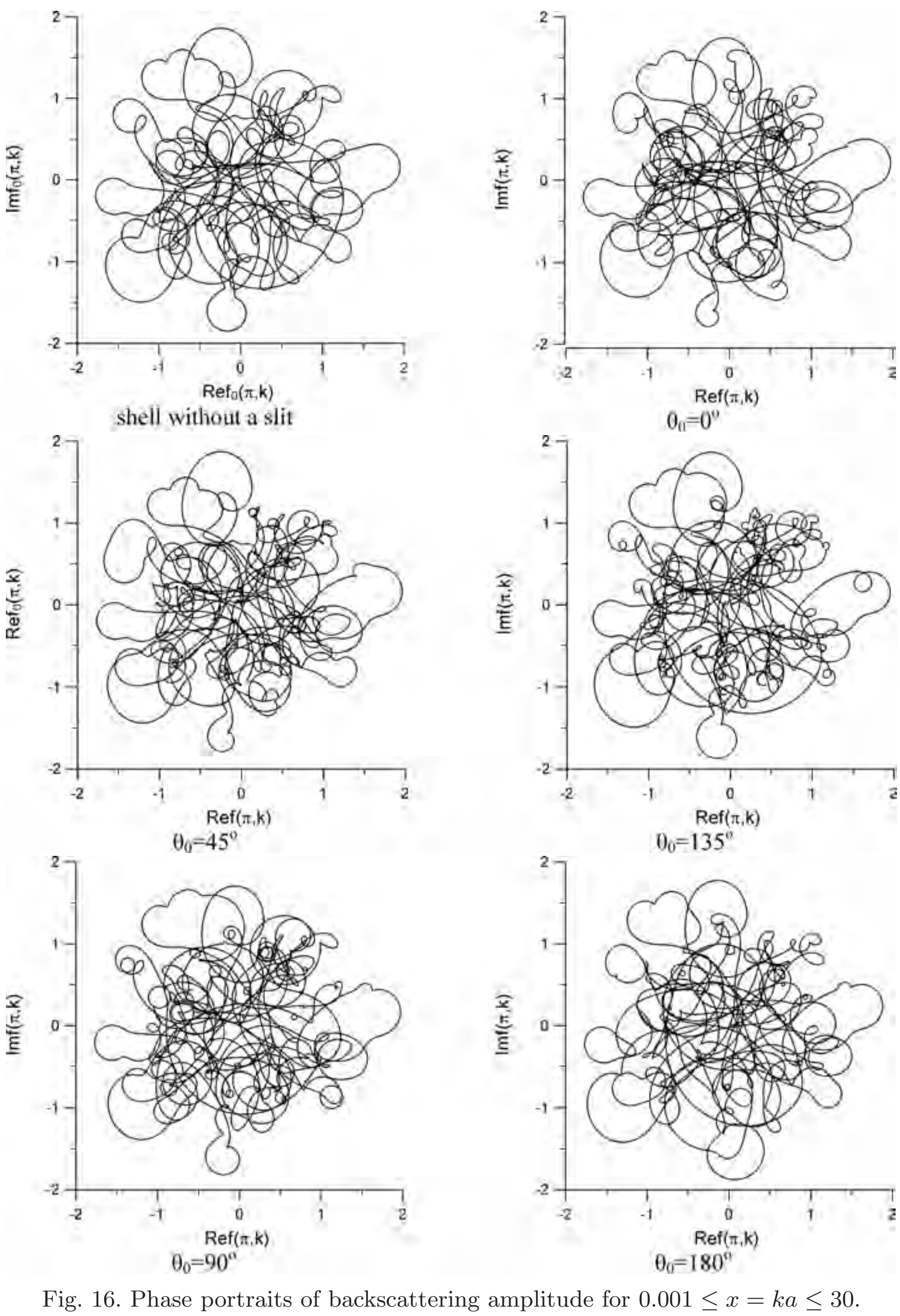

Fig. 16. Phase portraits of backscattering amplitude for $0.001 \leq x = ka \leq 30$.

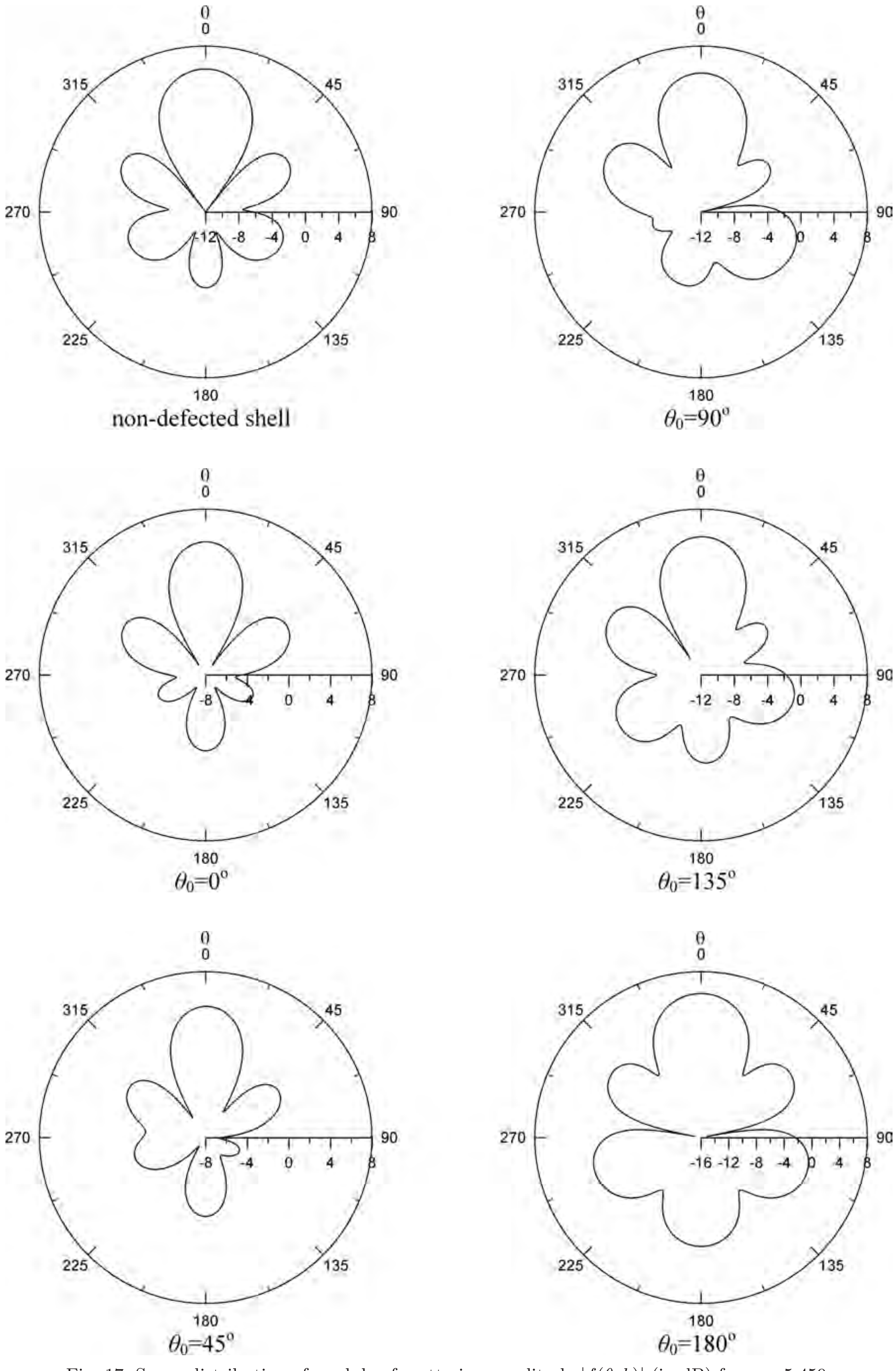

Fig. 17. Space distribution of module of scattering amplitude $|f(\theta, k)|$ (in dB) for $x = 5.459$.

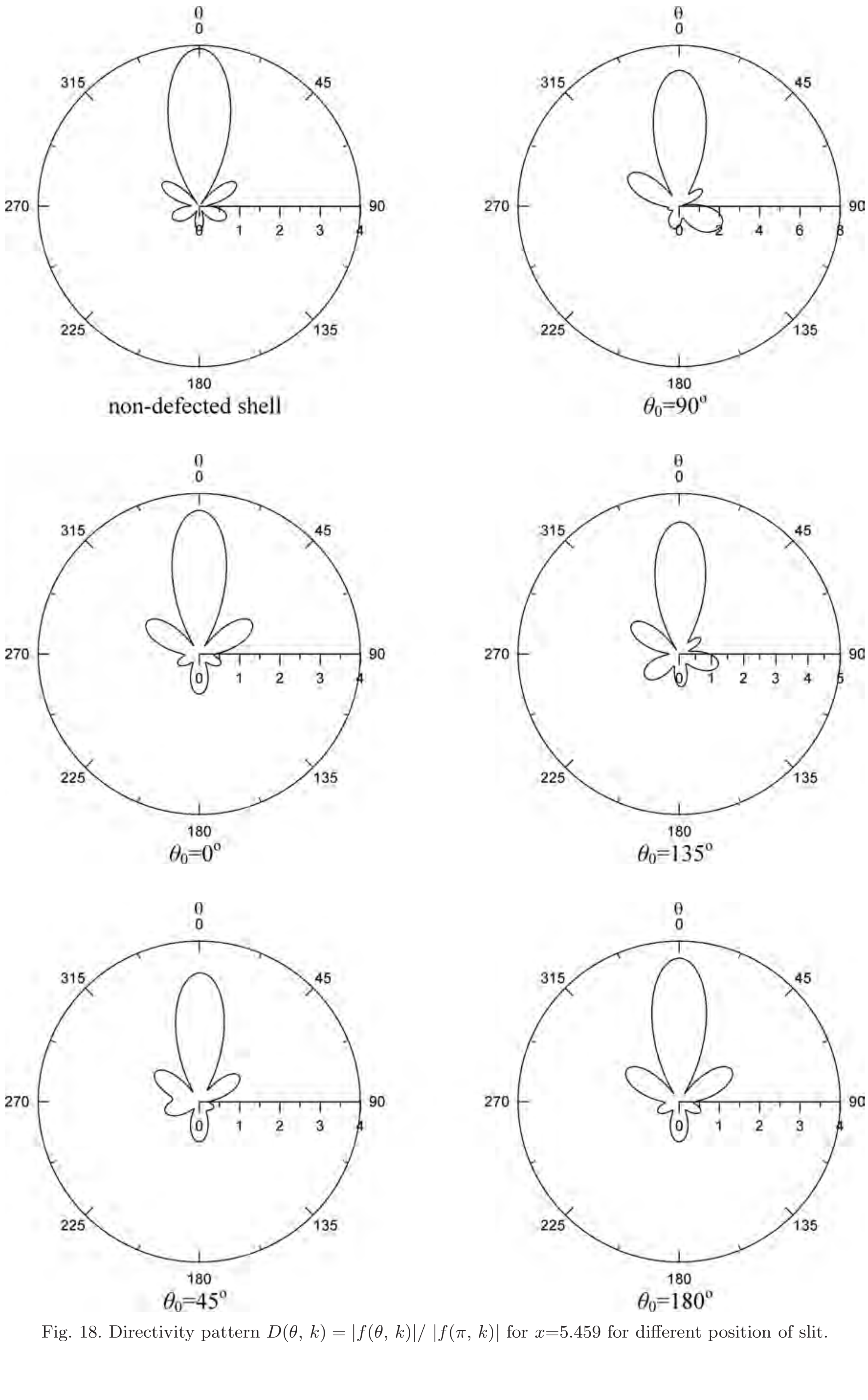

Fig. 18. Directivity pattern $D(\theta,\, k) = |f(\theta,\, k)|/\ |f(\pi,\, k)|$ for x=5.459 for different position of slit.

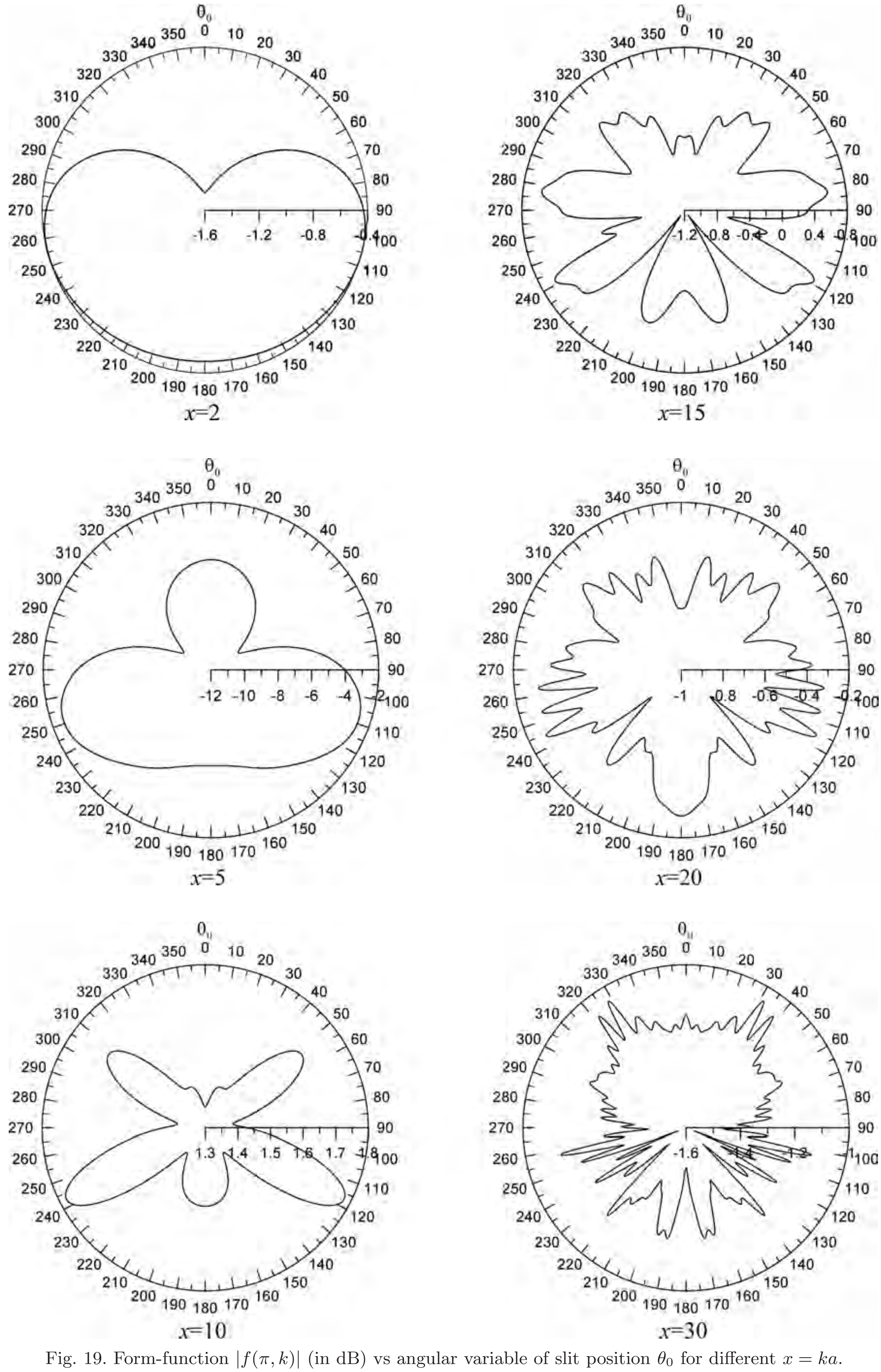

Fig. 19. Form-function $|f(\pi, k)|$ (in dB) vs angular variable of slit position θ_0 for different $x = ka$.

direction. The calculation also indicates that directivity pattern reaches its maximum for $\theta_0 = 90°$. In this case the side lobes of this characteristic are the most ones as well.

One further approach, which have been applied consists in the calculation of the form-function $|f(\theta, k)|$ (in dB) in the "back" direction *versus* the slit location θ_0. From the plots displayed in Figs. 19 for different frequencies $x = 2, 5, 10, 15, 20, 30$, it follows that having the value of the echo-signal amplitude on the transducer the slit location on the shell may be determined with very precision.

5. Conclusions

In this article we have presented the mathematical model of the scattering of plane harmonic sound waves from thin elastic cylindrical shells filled with a compressible viscous fluid and weakened by a long linear crack. The exact solution, i.e. the complex amplitude of the acoustic pressure, is found in the form of infinite Fourier-Bessel series.

On the basis of the solution obtained and the numerical calculations carried out for the case of the steel shell filled with oil and surrounded by seawater, it is shown that the spectrum of the scattered acoustic pressure is formed as the result of the resonance wave reflection from the object. These resonances are caused by shell vibrations on the eigen frequencies. The new additional effects are contributions to the resonance scattering caused by tangential, angular and radial vibrations of the free shell edges of the slit.

The numerical calculations show also that the presence of the slit is most visible in the low dimensionless frequency range, i.e. approximately in the range $0 < x < 10$.

The analysis of amplitudes and phases of the scattered sound pressure, the pattern directivity and influence of slit location on the scattering characteristics show the possibility of distance acoustic identification of cracked shells of the oil pipeline.

References

1. Achenbach J.D. (1973), *Wave propagation in elastic solids*, North-Holland Publ. Co., Amer. Elsevier Publ. Co., Inc., Amsterdam, London, New York.
2. Anson L.W., Chivers R.C. (1981), *Frequency dependence of the acoustic radiation force function (Yp) for spherical targets for a wire range of materials*, J. Acoust. Soc. Amer., **69**, 6, 1618–1623.
3. Anson L.W., Chivers R.C. (1993), *Ultrasonic scattering from spherical shells including viscous and thermal effects*, J. Acoust. Soc. Amer., **93**, Pt. 1, 4, 1687–1699.
4. Artobolevski I.I. (main Ed.) (1976), *Polytechnical Dictionary* [in Russian], Sov. Encyclopedia, Moscow.
5. Åseng V. (2006), *Compressibility and sound speed*, Diploma thesis; Norwegian University of Science and Technology, Trondheim. – www.ipt.ntnu.no/~jsg/studenter/diplom/2006VidarAAseng.pdf
6. Bateman H., Erdélyi A. (1953), *Higher transcendental functions. Vol. 2*, Mc Graw-Hill Book Co., Inc., New York, Toronto, London.
7. Belov A.V., Kaplunov J.D., Nolde E.V. (1999), *A refined asymptotic model of fluid-structure interaction in scattering by elastic shells*, Flow, Turbulence and Combustion, **61**, 1–4, 255–267.
8. Brekhovskikh L.M., Godin O.A. (1989), *Acoustics of layered media* [in Russian], Nauka, Moscow.
9. Dukhin A.S., Goetz P.J. (2009), *Bulk viscosity and compressibility measurement using acoustic spectroscopy*, J. Chem. Physics, **130**, 12, 124519-1-124519-13.
10. Dwight H.B. (1957), *Tables of integrals and other mathematical data*, The Macmillan Co., New York.
11. Felsen L., Markuvitz N. (1973), *Radiation and scattering of waves*, Prentice-Hall, Inc., Englewood Cliffs, New Jersey.
12. Gaunaurd G., Werby M.F. (1990), *Acoustic resonance scattering by submerged elastic shells*, Appl. Mech. Rev., **43**, 171–208.
13. Goldsberry T.G. (1967), *Reflection of circumferential waves from a slit in a thin-walled cylinder*, J. Acoust. Soc. Amer., **42**, 6, 1298–1305.
14. Hasheminejad S.M., Safari N. (2003), *Dynamic viscoelastic effects on sound wave diffraction by spherical and cylindrical shells submerged in and filled with viscous compressible fluids*, Shock and Vibration, **10**, 5/6, 339–363.
15. Hickling R., Means R.W. (1968), *Scattering frequency-modulated pulses by spherical elastic shells in water*, J. Acoust. Soc. Amer., **44**, 5, 1246–1252.
16. Kachaenko O.B., Pal'ko L.S., Shul'ga N.A. (1990), *Acoustic wave diffraction by an elastic cylindrical shell with viscous filling*, Int. Applied Mech., **25**, 7, 662–667 [transl. from Russian: Prikladnaya Mekhanika (1989), **25**, 7, 38–44].
17. Kaplunov J.D., Kossovich L.Yu., Nolde E.V. (1998), *Dynamics of thin walled elastic bodies*, Academic Press, San Diego, Calif.
18. Kaplunov J.D., Nolde E.V., Veksler N.D. (1994), *Asymptotic formulae for the modal resonance of peripheral waves in the scattering of an obliquely incident plane acoustic wave by a cylindrical shell*, Acustica, **80**, 3, 280–293.
19. Kerbrat E., Clorennec D., Prada C., Royer D., Cassereau D., Fink M. (2002), *Detection of cracks in a thin air-filled hollow cylinder by application of the DORT method to elastic components of the echo*, Ultrasonics, **40**, 715–720.
20. Kubenko V.D., Ryabukha Yu.N., Savina I.V. (1989), *Acoustic wave diffraction by coaxial piezoceramic shells with a viscous fluid*, Int. Applied Mech., **24**, 10, 961–966 [transl. from Russian: Prikladnaya Mekhanika (1988), **24**, 10, 28–34].

21. Landau L.D., Lifsitz E.M. (1987), *Fluid mechanics. Vol. 6 (Course of theoretical physics)*, Butterworth-Heinemann, Oxford.

22. Litovitz T.A., Davis C.M. (1965), *Structural and shear relaxation in liquids*, Physical Acoustics, Vol. 2, Part A: Properties of gases, liquids, and solutions, Academic Press, New York.

23. Makino H., Kubo T., Shiwaku T., Endo S., Inoue T., Kawaguchi Y., Matsumoto Y., Machida S. (2001), *Prediction for crack propagation and arrest of shear fracture in ultra-high pressure natural gas pipelines*, ISIJ Int., **41**, 4, 381–388.

24. Meng G., Jaworski A.J., White N.M. (2006), *Composition measurements of crude oil and process water emulsions using thick-film ultrasonic transducers*, Chem. Engineering and Processing, **45**, 383–391.

25. Metsaveer Ja.A., Veksler N.D., Stulov A.S. (1979), *Diffraction of acoustic pulses by elastic bodies* [in Russian], Nauka, Moscow.

26. Mohamed N., Jawhar I., Al-Jaroodi J., Zhang L. (2011), *Sensor network architectures for monitoring underwater pipelines*, Sensors, **11**, 11, 10738–10764.

27. Piddubniak O.P. (1995), *Frequency characteristics of sound waves scattered by an elastic circular cylindrical shell with a slit along generating line* [in Ukrainian], Proc. Nat. Acad. Sci. Ukraine, 9, 38–40.

28. Piddubniak O.P., Piddubniak N., Karnicki K. (2009), *Acoustic echo-signal from a thin cylindrical shell with a slit*, DIPED-2009: Direct and Inverse Problems of Electromagnetic and Acoustic Wave Theory: Proc. XIVth Int. Seminar/Workshop, Lviv, Sept. 21–24, 2009, 24–30, Lviv.

29. Pidstryhach Ja.S., Piddubniak O.P. (1986), *Scattering of the sound beams from the elastic bodies of spherical and cylindrical forms* [in Russian], Naukova Dumka, Kyiv.

30. Pidstryhach Ja.S., Shvetz R.M. (1978), *Thermoelasticity of thin shells* [in Russian], Naukova Dumka, Kyiv.

31. Porokhovski V.V. (2008), *Plane problem of interaction of elastic longitudinal wave and cylindrical shell with an axial slit* [in Ukrainian], Math. Methods and Physicomech. Fields, **51**, 1, 131–137.

32. Taşköprülü N.Ş., Barlow A.J., Lamb J. (1961), *Ultrasonic and visco-elastic relaxation in a lubricating oil*, J. Acoust. Soc. Amer., **33**, 3, 278–285.

33. Tittmann B.R. (2011), *Ultrasonic sensor viscosity of mineral oil for built-in pipe applications*, Sensor+Test Conference, 7–9 June 2011, Nürnberg, Germany, 171–176.

34. Veksler N.D. (1993), *Resonance acoustic spectroscopy*, Springer-Verlag, Berlin, New York.

35. Vollmann J., Dual J. (1997), *High-resolution analysis of the complex wave spectrum in a cylindrical shell containing a viscoelastic medium. Part I. Theory and numerical results*, J. Acoust. Soc. Amer., **102**, 2, pt. 1, 896–908.

36. Yeh C. (1968), *Diffraction of sound waves by a moving fluid cylinder*, J. Acoust. Soc. Amer., **44**, 5, 1216–1219.

37. Zhang Han, Chimenti D.E. (1997), *Ultrasonic beam reflection from lossy layered cylindrical shells*, Ultrasonics, **35**, 441–450.

PAN
ARCHIVES OF ACOUSTICS
Vol. **38**, No. 3, pp. 351–356 (2013)

DOI: 10.2478/aoa-2013-0041

Underwater Noise Generated by a Small Ship in the Shallow Sea

Grażyna GRELOWSKA[(1),(2)], Eugeniusz KOZACZKA[(2),(1)],
Sławomir KOZACZKA[(1)], Wojciech SZYMCZAK[(1)]

[(1)] *Polish Naval Academy*
Śmidowicza 69, 81-103 Gdynia, Poland; e-mail: g.grelowska@amw.gdynia.pl

[(2)] *Gdańsk University of Technology*
Narutowicza 11/12, 80-233 Gdańsk, Poland

(*received October 24, 2012; accepted April 10, 2013*)

Study of the sea noise has been a subject of interest for many years. The first works in this scope were published at the turn of the twentieth century by Knudsen (Knudsen *et al.*, 1948) and G. Wenz (Wenz, 1962). Disturbances called "shipping noise" are one of the important components of the sea noise.

In this work the results of an experimental research of underwater noise produced by a small ship of a classic propulsion are presented. A linear receiving antenna composed of two orthogonal components was used in the investigation. Identification of the main sources of acoustic waves related with the ship was achieved. In addition, the intensity of the wave was measured. The research was performed in conditions of the shallow sea.

Keywords: signal processing, sound propagation, underwater ship noise, propagation in the shallow sea.

1. Introduction

Problems of generation and noise control in the air are well recognized in general, and in certain cases noise limitation gives satisfying results. Because of direct disadvantageous influence of noise on humans, noise control is topical and stimulates activity of State and NGO organizations. Their main goal is reducing to minimum the impact of undesirable vibroacoustical effects on man.

We are confronted with a considerably worse situation in the water environment (Hildebrand, 2009). Binding laws of particular states or the EU Directives concerning care for the natural environment lack clear rules forcing owners of technical devices to limit the level of underwater noise (Arveson, VenditTIS, 2000).

The only exception, however, loosely connected with care for the natural environment, is the limitation of underwater noise produced by warships (Kozaczka, Grelowska, 2004). Military techniques utilize phenomena of generation and propagation in water of the acoustic waves produced by ships (Kozaczka, 1978; Ross, 1976) for monitoring their movement in a fixed sea area (Kozaczka *et al.*, 2007a; 2007b) with the possibility of their classification and identification (Grelowska *et al.*, 2012). This fact forces the users of military equipment to lower the noise produced by their individual ships to the spectral level of the environmental noise (Urick, 1975). Besides, in use also are various manners and methods of changes in time and spectral structure of noise generated by the ships, so as to make their immediate classification and detection difficult or even impossible (Kozaczka, Grelowska, 2004).

Taking into account that this paper does not deal with military utilization of noise produced by ships and other underwater sources, we shall pay our attention mostly to quantitative characterization of this noise with indication of its disadvantageous influence on the natural underwater environment. It is commonly known that impact of noise on organisms living in water is harmful, similarly to that of noise in the aerial environment on any living organism, not only on man (Committee…, 2003, Richardson *et al.*, 1995).

The passing and underwater moving objects produce the noise of variable intensity, which significantly increases the overall level of noise in the sea (Arveson, VenditTIS, 2000; Hildebrand, 2009; Kozaczka, Grelowska, 2004; 2011; Ross, 2005). This applies to both the sonic and ultrasonic range. The excessive levels of underwater noise adversely affect the so-called underwater acoustic climate and are the reason why this phenomenon has been intensively investigated for the number of years (Hildebrand, 2009).

The results of experimental work conducted in the sea conditions and connected with the small ship are presented in this paper. Their primary aim is a detailed analysis of the phenomenon of generation and propagation of acoustic waves produced by vessels. The detailed analysis of the acoustic signals illustrated in the form of spectrograms is presented. The influence of the boundary conditions (shallow sea) on the shape of acoustic characteristics will be also considered. The receiving antenna which allows to designate the direction and, in certain circumstances, distance from the sources of acoustic waves was used in the majority of studies.

Elaborated research methods can be applied for diagnostics, identification, and classification of sources of underwater acoustic waves.

2. General features of noise produced by ships

Using the classic classification of noise produced by ships it is possible to segregate them into (Arveson, Vendittis, 2000; Kozaczka *et al.*, 2007a; Ross, 1976):

- noise generated by devices active dynamically, placed inside and on the surface of the hull, mainly by engines, propulsion, and auxiliary, and system of transport of mechanical energy – shafting,
- noise produced by the ship propellers,
- acoustic effects connected with cavitation of the propellers and flow around the underwater part of the hull.

At the low speed the ship's service generator is the main source of the underwater noise generated by the ship. It radiates tonal components that contribute almost all of the radiated noise power of the ship. They are independent of the ship's speed. Few of components are strong enough to be contributors to the high-speed signature. The tonal levels of ship's service diesel generator are nearly stable in amplitude and frequency (Kozaczka *et al.*, 2007a). The wide-band energy of the noise generated by the ship's service generator is proportional to the square of generated power (Urick, 1975).

Discrete components that could be associated with the mechanical activity of propulsion engines, as well as propellers, appear at a higher speed of the ship in the spectrum of the underwater noise. They are mainly noticed in the frequency range up to 100 Hz (Arveson, Vendittis, 2000).

3. Noise generated by a propulsion engine

The propulsion engine is the main source of the underwater noise for moderate speeds of the ship. In general, the tonal level is not stable because of variations of loading the propeller for different sea states. The radiated power at the fundamental firing rate frequency is related to the engine horsepower and can be estimated up to 0.1% of the total engine power. The tonal components are connected with the firing rate. For the two-stroke x-cylinder diesel engine the firing rate is defined as (Urick, 1975):

$$\mathrm{FR} = \frac{x}{60} \quad [\mathrm{rpm}], \tag{1}$$

where FR is the firing rate, x is the number of cylinders, revolutions per minute.

The tonal level is not stable in general because of variations of loading, as it is the case with the propeller for different sea states (Kozaczka, 1978). The radiated acoustic power at the fundamental firing rate frequency F is related to the engine horsepower H as (Urick, 1975):

$$W \sim (HF)^2. \tag{2}$$

Analyzing the vibration caused by the diesel engine that is converted into acoustic energy one should take into account the possibility of occurring of structural

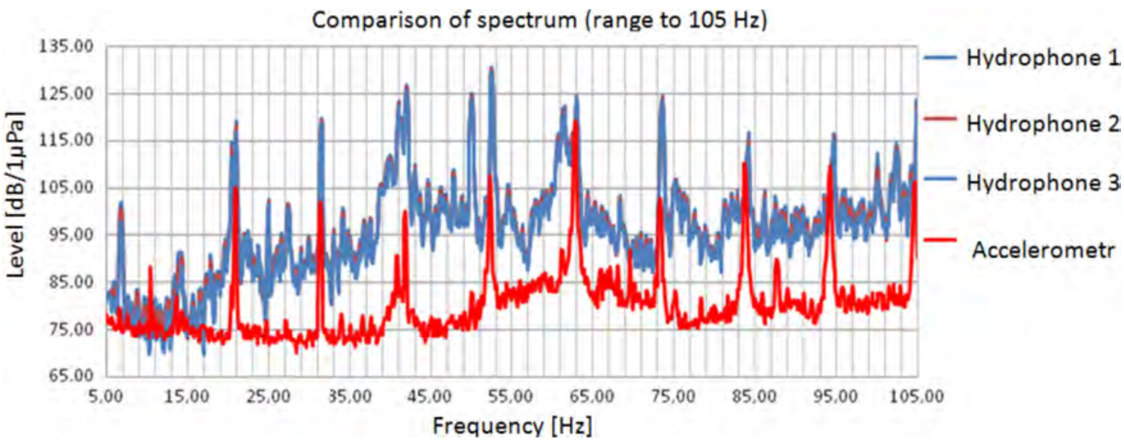

Fig. 1. Spectra of the underwater noise produced by a moving small ship measured by 3 hydrophones (H1, H2, and H3) 2.4 m distant form each other and the spectrum of the vibration of the main engine.

resonances. These may play a great role in determining the radiation efficiency of the ship's engine tones. Comparison of the spectrum of the underwater noise and the spectrum of vibration of the engine allows to determine the components in the underwater noise caused by the engine activity (Fig. 1).

4. Noise generated by a propeller

The most efficient underwater noise source on the ship is the propeller noise. One part of it is the blade rate, which is a signal at the blade passing frequency and its harmonics. This usually gives the dominant contribution to the low frequency tonal level at high speeds of the ship, when the propeller is heavily cavitating (Kozaczka, 1978; 1986).

In view of the fact that the work of the propeller is near the hull, the inflow velocity is reduced significantly near the top of the propeller. A propeller of the surface of the ship operates behind the hull, which creates a nonuniform distribution of the water flow velocity in the screw disk. Additionally, variation of the sea surface due to wind causes that the upper part of the propeller blades during their motion is usually in the area of the lowest pressure. For the high rotation speed a cavity can be formed. It collapses when the pressure increases during the blade movement downwards. Because the collapse of a cavity occurs every time, a blade passes through the region of the low pressure. The noise that appears in this case has fundamental harmonics equal to those of the blade rate.

Estimation of the sound pressure generated by the cavitating area can be done by assuming that the pulsation of the cavity may be approximated by a monopole source. Because the process takes place in the vicinity of the free-pressure surface, the nearly perfect reflections of the sound waves occur as the second source. As a result, the radiation pattern of the propeller noise has a dipole character with a dipole directivity pattern. The simple expression describing the dipole pressure P_d is as follows (Ross, 1976):

$$P_d(t) = \frac{d\rho}{2\pi rc} \frac{\mathrm{d}^3 V(t)}{\mathrm{d}t^3}, \tag{3}$$

where r is the distance from the source, ρ is the density, d is the source depth, c is the speed of the sound, $V(t)$ is the instantaneous cavity volume, t is the time.

In the spectrum of the underwater noise components whose origin can be directly linked to the activity of the mechanisms of the ship can be distinguished. In Fig. 2 the consecutive spectra of the underwater noise of the small ship calculated for particular sections of the track length of 1 kilometer and the averaged spectrum for the track are shown.

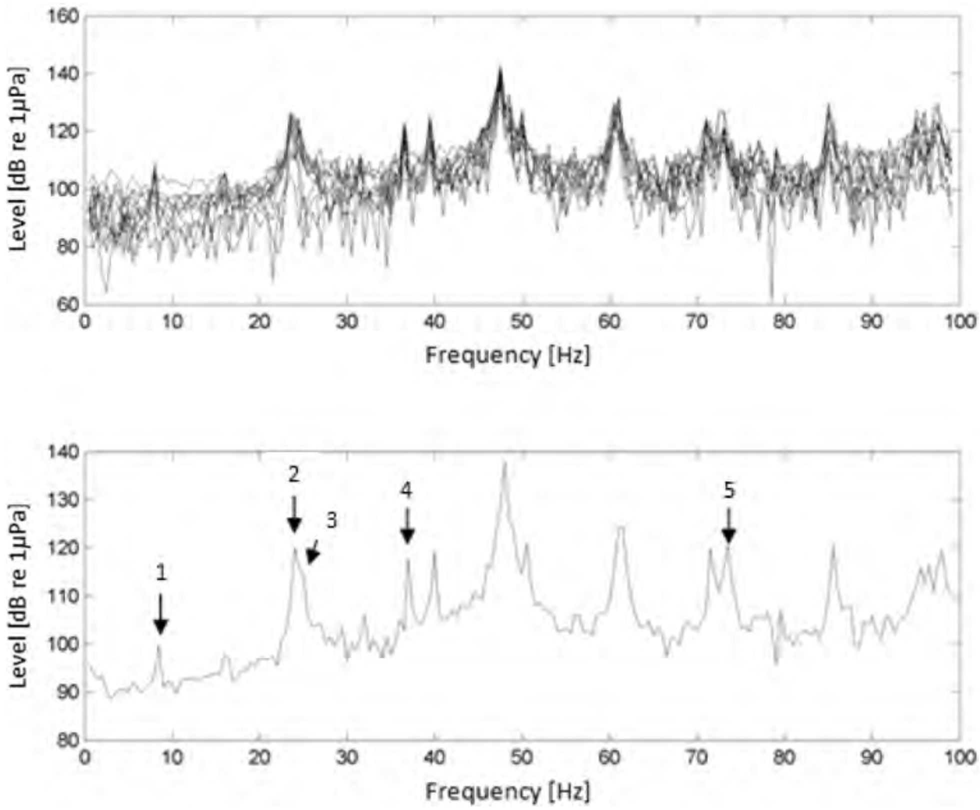

Fig. 2. Consecutive spectra (top) and spectrum averaged (bottom) for the 1 km track of the small ship: 1 – shaft, 2 – proppeler – fundamental frequency, 3 – unbalance of the proppeler, 4 – detonation combustion of fuel in the cylinders, 5 – proppeler – 3rd harmonic.

5. Measurements method and results

As it has been mentioned above, the ship is a broadband underwater source and in the spectrum of the noise generated by her, the low frequency band is of a significant importance. In this case we have to consider propagation of waves with the length comparable to the depth of the sea, according to the theory elaborated for the shallow sea (Brekhovskikh *et al.*, 1992). In such a situation, the transmission losses of waves with the length of λ that satisfy the condition:

$$10\lambda < h, \tag{4}$$

where h is the depth of the sea, has to be calculated under the assumption that the kind of propagation changes with the distance from the source. The kind of bottom sediments has an impact on the phenomenon of wave propagation in the shallow sea (Kozaczka, 2013).

The shape of forming wave mods and the range of propagation of disturbances, in general, is influenced by boundary conditions. Mainly, it refers to the boundary condition at the sea bottom.

Considering the fact that the ship noise is a broadband noise in the low frequency range, in the shallow water conditions the impact of the sound speed distribution, and, thereby, the refraction, is of little importance. However, the influence of the ambient background noise affects the detection range of the target.

In order to minimize the influence of the boundary condition, one can choose the optimal location for measurement, taking into account the depth and the kind of sediments. Nevertheless, the transmission losses for low frequencies were determined according to the shallow sea propagation rules.

The best location for the measurement facility, used in evaluation of hydroacoustic characteristics of noise radiated by classical ships as well as underwater ships, is in places where the ambient noise is the smallest and the depth of the sea is high enough so that the bottom could be treated as reflectionless.

In the measurements of the acoustic pressure vertical and horizontal arrays of hydrophones are used, mounted in such a way so that the impact of the environment motion, especially waved sea surface, is minimized. Signals from the acoustic transducers are transmitted to the registering and analyzing devices. On the basis of the results of these measurements, a set of characteristics that determine individual distinctive features of the examined source is obtained.

Among others, the set of characteristics contains:

- instantaneous spectra of the underwater noise of the ship,
- characteristics illustrating changes in the pressure level with the distance from the ship at a fixed depth,
- a set of correlation and coherence functions and directivity patterns.

Moreover, for each measurement spectrograms that combine features of the spectral characteristics and functions connected with changing of position of the source relative to the receiving antenna are determined.

At the same time, on-board measurement of the vibration of the main engine, as well as the service diesel generator, are carried out. On the basis of the results of these measurements one can determine the bandwidth of the noise produced by the ship, diesel engine cylinder pressure spectra, engine vibration transmis-

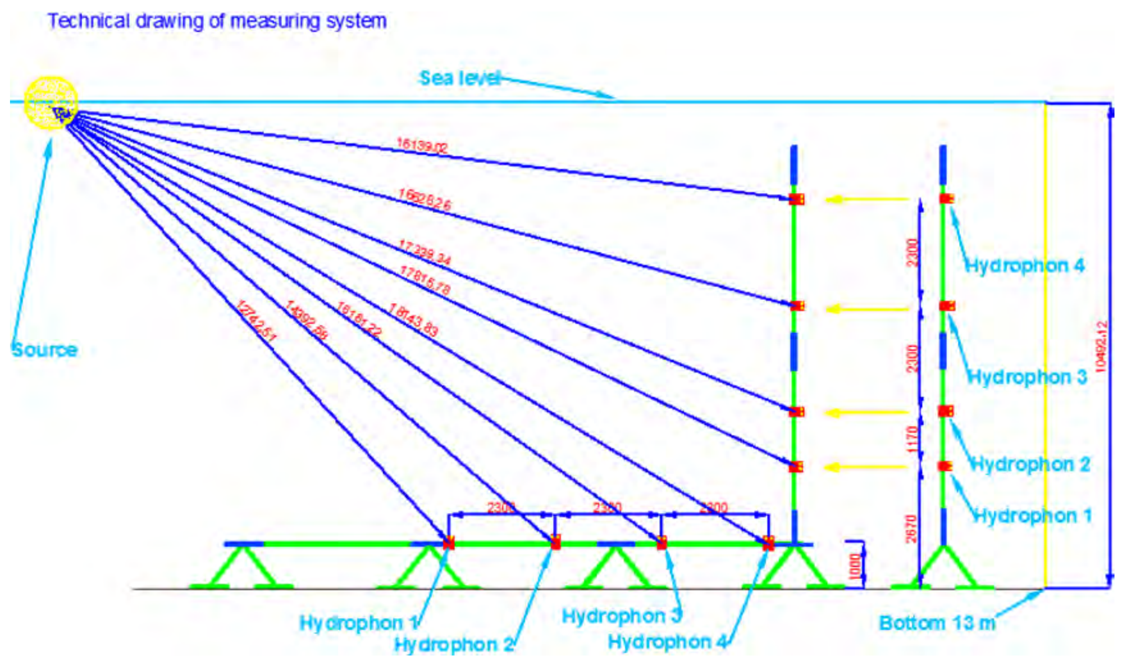

Fig. 3. Technical drawing of the measuring system.

sion paths, the ship hull "beam mode" response, and, at last, the transfer function between the on-board installed sources of vibration and outside radiation level.

Fig. 4. Small ship used in the experiment.

All of these characteristics should reflect individual features of the source that is a moving ship. Knowledge of them gives information about what steps should be taken to obtain the specified characteristics of the source. Besides, the characteristics allow to assess which factors are the most disadvantageous to the surrounding and whether their reduction is possible without changes of operational variables of the ship.

Some measurements carried out during the investigation of the ship noise are illustrated in this text. In Figs. 1 and 2 spectra determined for the frequency range up to 100 Hz, where characteristic components linked to the activity of the main ship's devices are well visible, are shown. The acoustic effects connected with cavitation of the propeller and flow around the underwater part of the hull are observed in the range of higher frequencies, approximately 300–1500 Hz. It depends on the type of ship and its speed. An example of the spectrogram where the mentioned acoustical effects are pointed is shown in Fig. 5. Below is given the spectrum of noise when the ship is over the receiving antenna.

Applying the linear antenna composed both of vertically and horizontally placed hydrophones allows us to determine experimentally the spatial distribution of noise produced by a moving ship. It is a great advantage of the examined measurement set up that distinguishes it from others, typically composed of hydrophones placed on the sea bottom. Moreover, the configuration of hydrophones allows to determine the intensity of the sound (Kozaczka *et al.*, 2007b). An example of the spatial distribution of the sound intensity of noise produced by a moving ship determined experimentally is shown in Fig. 6. This makes it possible to determine the area of a given level of intensity.

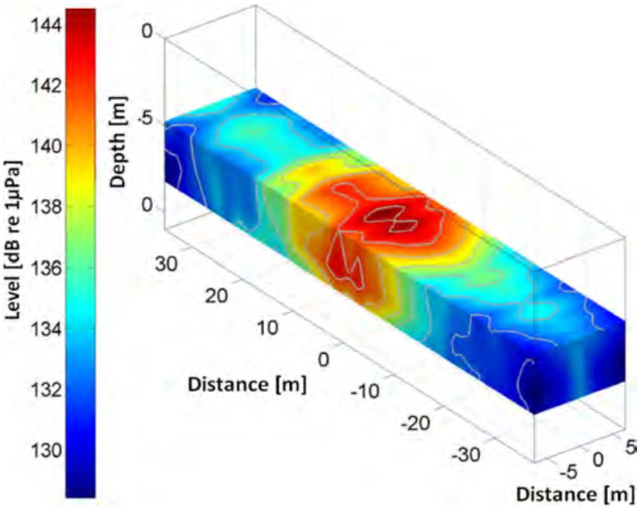

Fig. 6. Distribution of sound intensity of noise produced by a small ship determined experimentally.

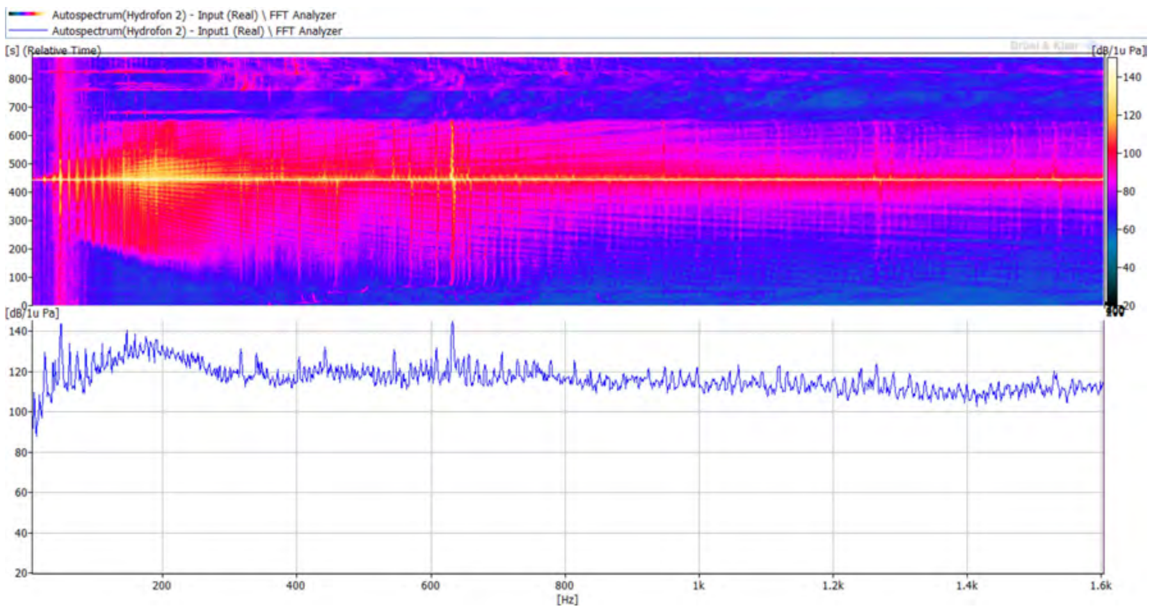

Fig. 5. Spectrogram and spectrum of a small ship.

6. Conclusions

Investigations of the acoustic signature of ships are very expensive and time consuming procedures. These investigations should be carried out at the same time on-board and out-board. This allows to determine connections between sources installed on-board and near the hull (ship propeller) and radiated level, as well as their spectra.

Basing on the measurements of underwater noise generated by a ship it is possible to get information about sources of underwater noise and technical state of ship's mechanisms. The knowledge of the levels and structures of the underwater noise radiated by ships is important for monitoring self-noise and the technical state of their mechanisms.

The noise of a moving vessel is connected with the way of mounting and vibration of the machines and next transmission in various paths into the water as underwater sound.

Applying the sound intensity measuring method, one can carry out the measurements in the near field of a source of acoustic waves. It is very important in the cases when there is a need to measure the ship's noise in the shallow sea. Otherwise, on the basis of intensity characteristics one can determine the direction of movement.

The presented measuring set up composed of linear arrays allows to obtain experimental data about the spatial distribution of the sound field of moving objects. In spectral characteristics of the ship presented in the paper, the following elements can be distinguished:

1) individual components in the band pass up to 200 Hz connected to the activity of the ship's mechanisms;
2) broadband noise in the band from 200 to 700 Hz, as a result of flow of the hull and cavitation;
3) component of frequency 500 Hz, independent of the speed of the ship.

The results of measurements are influenced by the ambient noise, especially in the low band frequency range. This was due to the vicinity of a harbor and shipyard, as well as marine traffic.

Acknowledgments

The investigation was partially supported by the National Centre for Research and Development, Grant No. O R00 0089 09 and Grant No. 0007/R/IDI/2011/01.

References

1. Arveson P.T., Vendittis D.T. (2000), *Radiated noise characteristics of modern cargo ship*, J. Acoust. Soc. Am., **107**, 1, 118–129.
2. Brekhovskikh L.M., Godin O.A. (1992), Acoustics of Layered Media II, Springer-Verlag, Berlin.
3. Committee on Potential Impacts of Ambient Noise in the Ocean on Marine Mammals (2003), *Ocean noise and marine mammals*, National Academies Press, Washington, DC.
4. Grelowska G., Kozaczka E., Kozaczka S., Szymczak W. (2012), *Some aspects of noise generated by a small ship in the shallow sea*, Proceedings of the 11th European Conference on Underwater Acoustics.
5. Hildebrand J.A. (2009), *Anthropogenic and natural sources of ambient noise in the ocean*, Marine Ecology Progress Series, 395, 5–20.
6. Knudsen V.O., Alford R.S., Emling J.W. (1948), *Underwater ambient noise*, J. Mar. Res., **7**, 410–429.
7. Kozaczka E. (1978), *Investigations of underwater disturbances generated by the ship propeller*, Arch. Acoust., **13**, 2, 133–152.
8. Kozaczka E. (1986), *Acoustical activity of cavitation bubbles produced by the ship propeller*, Journal of Applied Mechanics, **4**, 431–438.
9. Kozaczka E. (2013), *The Propagation of the Acoustic Disturbances in the Shallow Water*, [in:] *Hydroacoustics of Shallow Water*, Grelowska G., Kozaczka E. [Eds.] (in print), Institute of Fundamental Technological Research PAN, Warszawa.
10. Kozaczka E., Domagalski J., Grelowska G., Gloza I. (2007a), Identification of hydroacoustic waves emitted from floating units during mooring tests, Polish Maritime Research, **14**, 4, 40–46.
11. Kozaczka E., Grelowska G., Gloza I. (2007b), *Sound intensity in ships noise measuring*, Proc. 19th ICA, 6 pp. CD, Madrid.
12. Kozaczka E., Grelowska G. (2004), *Shipping noise*, Arch. Acoust., **29**, 2, 169–176.
13. Kozaczka E., Grelowska G. (2011), *Shipping low frequency noise and its propagation in shallow water*, Acta Physica Polonica A, **119**, 1009–1012.
14. Richardson W., Greene C., Malme C., Thomson D. (1995), *Marine Mammals and Noise*, Academic Press, San Diego, CA.
15. Ross D. (1976), *Mechanics of Underwater Noise*, Pergamon, New York.
16. Ross D. (2005), *Ship sources of ambient noise*, IEEE Journal of Oceanic Engineering, **30**, 257–261.
17. Urick R.J. (1975), *Principles of Underwater Sound*, Chap. 10, Me Graw-Hill, New York.
18. Wenz G.M. (1962), *Acoustic ambient noise in the ocean: spectra and sources*, J. Acoust. Soc. Am., **34**, 1936–1956.

PAN ARCHIVES OF ACOUSTICS
Vol. **38**, No. 3, pp. 357–362 (2013)

DOI: 10.2478/aoa-2013-0042

Features of Nonlinear Sound Propagation in Vibrationally Excited Gases

Anna PERELOMOVA(1), Magdalena KUSMIREK(2)

(1) *Gdansk University of Technology*
Faculty of Applied Physics and Mathematics
Narutowicza 11/12, 80-233 Gdańsk, Poland; e-mail: anpe@mif.pg.gda.pl

(2) *Ship Design and Research Center*
Wały Piastowskie 1, 80-958 Gdańsk, Poland; e-mail: magdalena.kusmirek@cto.gda.pl

(*received June 20, 2012; accepted April 22, 2013*)

Weakly nonlinear sound propagation in a gas where molecular vibrational relaxation takes place is studied. New equations which govern the sound in media where the irreversible relaxation may take place are derived and discussed. Their form depends on the regime of excitation of oscillatory degrees of freedom, equilibrium (reversible) or non-equilibrium (irreversible), and on the comparative frequency of the sound in relation to the inverse time of relaxation. Additional nonlinear terms increase standard nonlinearity of the high-frequency sound in the equilibrium regime of vibrational excitation and decrease otherwise. As for the nonlinearity of the low-frequency sound, the conclusions are opposite. Appearance of a non-oscillating additional part which is a linear function of the distance from the transducer is an unusual property of nonlinear distortions of harmonic at the transducer high-frequency sound.

Keywords: Nonlinear acoustics, parameter of nonlinearity, non-equilibrium media, vibrationally excited gas.
PACS numbers: 43.35.Fj, 43.25, 43.28.Py.

1. Introduction. Basic equations and starting points

The non-equilibrium physics was born and started to rapidly develop in the sixties of the XX-th century in connection with the need of a deeper study of unusual hydrodynamics of media where irreverible processes take place (Zeldovich, Raizer, 1966; Gordiets *et al.*, 1973; Osipov, Uvarov, 1992). The most important of them are gases with excited degrees of oscillatory freedom of molecules. Non-equilibrium processes are established as well in discharge plasma, the rarified levels of the upper atmosphere, interstellar media, and so on. There was reported relaxation of rotational, translational, and electronic degrees of freedom of a molecule. Difference in relaxation times follows from difference of probabilities of various elementary events. Chemically reacting media are also relaxing; the duration of reaction is the characteristic time of relaxation. If a chemical reaction is irreversible, the sound propagates over the reacting medium unusually. The irreversible relaxation results in anomalous dispersion and absorption of ultrasonics waves in such media (Zeldovich, Raizer, 1966; Osipov, Uvarov, 1992; Kogan, Molevich, 1986; Molevich *et al.*, 2005). Interest in the non-equilibrium phenomena in the physics of gases was originally connected with the study of these anomalies.

This paper is devoted to the nonlinear features of sound propagation in the low-frequency (when the characteristic frequency of the sound, ω, is much smaller than the inverse time of relaxation, $1/\tau$) and high-frequency regimes in the vibrationally relaxing gas. It is well-known, that dispersion, due to reversible relaxation, leads to an increase in the phase speed with enlargement in the sound frequency. Vice versa, in the non-equilibrium regime, the phase speed decreases. The nonlinear features of sound propagation depend on the frequency of the sound and on the type of vibrational excitation, equilibrium or not. The nonlinear distortion is not longer determined by the standard parameter of nonlinearity; and the type of distortion differs from the standard one.

We consider a gas whose steady state is maintained by pumping energy into the vibrational degrees of freedom by power I and heat withdrawal from the translational degrees of freedom of power Q, while both I and Q refer to the unit mass (Sec. 2). The relaxation equation for the vibrational energy per unit mass complements the system of conservation equations in the differential form. It takes the form:

$$\frac{\mathrm{d}\varepsilon}{\mathrm{d}t} = -\frac{\varepsilon - \varepsilon_{eq}(T)}{\tau(\rho, T)} + I. \tag{1}$$

The equilibrium value for the vibrational energy at the given temperature T is denoted by $\varepsilon_{eq}(T)$, and $\tau(\rho, T)$ is the vibrational relaxation time. The mass, momentum, and energy conservation equations governing thermoviscous flow in a vibrationally relaxing gas read (Osipov, Uvarov, 1992):

$$\begin{gathered}\frac{\partial \rho}{\partial t} + \boldsymbol{\nabla}\cdot(\rho\mathbf{v}) = 0,\\ \rho\left[\frac{\partial \mathbf{v}}{\partial t} + (\mathbf{v}\cdot\boldsymbol{\nabla})\mathbf{v}\right] = -\boldsymbol{\nabla}p,\\ \rho\left[\frac{\partial(e+\varepsilon)}{\partial t} + (\mathbf{v}\cdot\boldsymbol{\nabla})(e+\varepsilon)\right] + p\,(\boldsymbol{\nabla}\cdot\mathbf{v}) = \rho(I-Q),\end{gathered} \tag{2}$$

where $\mathbf{v}$ denotes the velocity of fluid, ρ, p are the density and pressure, e marks the internal energy per unit mass of translation motion of molecules, x_i $(i = 1, 2, 3)$ are space coordinates. The system (2) may be complemented by the terms which account for viscosity and thermal conductivity but they are insignificant in the studies of nonlinear distortions of the sound. We will consider only effects relating to the oscillatory relaxation. Two thermodynamic functions $e(p, \rho)$, $T(p, \rho)$ complete the system (2). Thermodynamics of ideal gases provides the equalities:

$$e(p,\rho) = \frac{R}{\mu(\gamma-1)}, \qquad T(p,\rho) = \frac{p}{(\gamma-1)\rho}, \tag{3}$$

where $\gamma = C_{P,\infty}/C_{V,\infty}$ is the isentropic exponent without account for vibrational degrees of freedom ($C_{P,\infty}$ and $C_{V,\infty}$ denote "frozen" heat capacities correspondent to very quick processes), R is the universal gas constant, and μ is the molar mass of a gas.

2. Fundamentals of modes' designation and derivation of dynamic equations

Let start by considering a motion of a gas with an infinitely small magnitude in the case $I = Q$. Every quantity q is represented as a sum of unperturbed value q_0 (in absence of the background flows, $v_0 = 0$) and its variation q'. The flow is supposed to be one-dimensional along axis Ox. Following Molevich and Makaryan (Molevich, 2003; 2004; Makaryan, Molevich, 2007), we consider weak transversal pumping which may alter the background quantities in the transversal direction of axis Ox. It is assumed that the background stationary quantities are constant along axis Ox.

The system of conservation equations including the quadratic nonlinear terms, which are of major importance in the nonlinear acoustics, with the account of Eqs. (3), takes the form (Perelomova, 2012):

$$\begin{aligned}
&\frac{\partial v'}{\partial t} + \frac{1}{\rho_0}\frac{\partial p'}{\partial x} = -v'\frac{\partial v'}{\partial x} + \frac{\rho'}{\rho_0^2}\frac{\partial p'}{\partial x},\\
&\frac{\partial p'}{\partial t} + \gamma p_0\frac{\partial v'}{\partial x} - (\gamma-1)\rho_0\frac{\varepsilon'}{\tau}\\
&\quad + (\gamma-1)\rho_0 T_0 \Phi_1\left(\frac{p'}{p_0} - \frac{\rho'}{\rho_0}\right) = -v'\frac{\partial p'}{\partial x}\\
&\quad - \gamma p'\frac{\partial v'}{\partial x} + (\gamma-1)\rho'\left(\frac{\varepsilon'}{\tau} - T_0\Phi_1\left(\frac{p'}{p_0} - \frac{\rho'}{\rho_0}\right)\right)\\
&\quad - (\gamma-1)\rho_0\left(T_0\left(\frac{1}{\tau^2}\frac{d\tau}{dT}\right)_0 \varepsilon'\left(\frac{p'}{p_0} - \frac{\rho'}{\rho_0}\right)\right.\\
&\quad \left. + T_0\Phi_1\left(\frac{\rho'^2}{\rho_0^2} - \frac{p'\rho'}{p_0\rho_0}\right) + T_0\Phi_2\left(\frac{p'}{p_0} - \frac{\rho'}{\rho_0}\right)^2\right),\\
&\frac{\partial \rho'}{\partial t} + \rho_0\frac{\partial v'}{\partial x} = -v'\frac{\partial \rho'}{\partial x} - \rho'\frac{\partial v'}{\partial x},\\
&\frac{\partial \varepsilon'}{\partial t} + \frac{\varepsilon'}{\tau} - T_0\Phi_1\left(\frac{p'}{p_0} - \frac{\rho'}{\rho_0}\right)\\
&\qquad = T_0\left(\frac{1}{\tau^2}\frac{d\tau}{dT}\right)_0 \varepsilon'\left(\frac{p'}{p_0} - \frac{\rho'}{\rho_0}\right)\\
&\qquad + T_0\Phi_1\left(\frac{\rho'^2}{\rho_0^2} - \frac{p'\rho'}{p_0\rho_0}\right)\\
&\qquad + T_0\Phi_2\left(\frac{p'}{p_0} - \frac{\rho'}{\rho_0}\right)^2 - v'\frac{\partial \varepsilon'}{\partial x},
\end{aligned} \tag{4}$$

where

$$\begin{aligned}
&\Phi_1 = \left(\frac{C_{V,eq}}{\tau} + \frac{\varepsilon - \varepsilon_{eq}}{\tau^2}\frac{\mathrm{d}\tau}{\mathrm{d}T}\right)_0,\\
&C_{V,eq} = \left(\frac{\mathrm{d}\varepsilon_{eq}}{\mathrm{d}T}\right)_0,\\
&\Phi_2 = T_0\left(-\frac{1}{\tau^2}C_{V,eq}\frac{\mathrm{d}\tau}{\mathrm{d}T} - \frac{(\varepsilon_0 - \varepsilon_{eq})}{\tau^3}\left(\frac{\mathrm{d}\tau}{\mathrm{d}T}\right)^2\right.\\
&\qquad \left. + \frac{1}{2\tau}\frac{\mathrm{d}C_{V,eq}}{\mathrm{d}T} + \frac{(\varepsilon_0 - \varepsilon_{eq})}{2\tau^2}\frac{d^2\tau}{\mathrm{d}T^2}\right)_0.
\end{aligned} \tag{5}$$

The relaxation time in the most important cases may be thought as a function of temperature accordingly to Landau and Teller, $\tau(T) = A\exp(BT^{-1/3})$, where A and B are some positive constants. That gives negative values of $\mathrm{d}\tau/\mathrm{d}T$ (Zeldovich, Raizer, 1966; Gordiets *et al.*, 1973; Osipov, Uvarov, 1992) which may correspond to a negative value of Φ_1. The dispersion equation follows from the linear version of Eqs. (4):

$$\omega\left(i\Phi_1(\gamma-1)T_0\tau(c_\infty^2k^2-\gamma\omega^2) + c_\infty^2(c_\infty^2k^2-\omega^2)(i-\omega\tau)\right)=0, \quad (6)$$

where

$$c_\infty=\sqrt{\frac{\gamma RT_0}{\mu}}=\sqrt{\gamma\frac{p_0}{\rho_0}}$$

is the "frozen", infinitely small-signal sound speed in the ideal uniform gas.

The approximate roots of dispersion equation for both acoustic branches, progressive in the positive and negative directions of axis Ox, are well known under the simplifying condition $\omega\tau\gg 1$, which restricts consideration by the high-frequency sound (Osipov, Uvarov, 1992; Molevich, 2003)

$$\begin{aligned}\omega_{1,\infty}&=c_\infty k+\frac{i}{2}\frac{(\gamma-1)^2T_0}{c_\infty^2}\Phi_1,\\ \omega_{2,\infty}&=-c_\infty k+\frac{i}{2}\frac{(\gamma-1)^2T_0}{c_\infty^2}\Phi_1.\end{aligned} \quad (7)$$

The last term in both dispersion relations manifests amplification of the sound in the non-equilibrium regime (if $\Phi_1<0$) which does not depend on the wave number k. The approximate roots of dispersion equation for both acoustic branches, progressive in the positive or negative directions of axis Ox in the low-frequency domain $\omega\tau\ll 1$, are as follows (see also (Molevich, 2003; 2004)):

$$\omega_{1,0}=c_0k, \qquad \omega_{2,0}=-c_0k, \quad (8)$$

where

$$c_0=c_\infty-\frac{(\gamma-1)^2T_0\tau}{2c_\infty}\Phi_1.$$

The two last roots of the dispersive equation, estimated without the limitation $\omega\tau\gg 1$ or, $\omega\tau\ll 1$, sound:

$$\begin{aligned}\omega_3&=i\left(\frac{1}{\tau}+\frac{(\gamma-1)(\gamma+c_\infty^2k^2\tau^2)T_0}{c_\infty^2(1+c_\infty^2k^2\tau^2)}\Phi_1\right),\\ \omega_4&=0.\end{aligned} \quad (9)$$

These last two roots manifest slow varying and stationary, non-wave motions of a gas. Accordingly, perturbation in the velocity, pressure or energy of every dynamic variable may be expressed in terms of specific excess densities. The overall excess velocity, pressure, density, and internal energy are sums of specific parts:

$$\begin{aligned}v'(x,t)&=\sum_{n=1}^4 v'_n(x,t), \quad p'(x,t)=\sum_{n=1}^4 p'_n(x,t),\\ \rho'(x,t)&=\sum_{n=1}^4 \rho'_n(x,t), \quad \varepsilon'(x,t)=\sum_{n=1}^4 \varepsilon'_n(x,t).\end{aligned} \quad (10)$$

Relations of acoustic rightwards propagating wave in the high-frequency regime ($\omega_1 k\gg 1$ or, alternatively, $c_\infty k\tau\gg 1$) follow from the dispersion relation $\omega_1(k)$ (Perelomova, 2012):

$$\begin{aligned}v'_{1,h}(x,t)&=\frac{c_\infty}{\rho_0}\left(1-B\int \mathrm{d}x\right)\rho'_{1,h}(x,t),\\ p'_{1,h}(x,t)&=c_\infty^2\left(1-2B\int \mathrm{d}x\right)\rho'_{1,h}(x,t),\\ \varepsilon'_{1,h}(x,t)&=\frac{2Bc_\infty^2}{(\gamma-1)\rho_0}\int \mathrm{d}x\rho'_{1,h}(x,t),\end{aligned} \quad (11)$$

where

$$B=-\frac{(\gamma-1)^2T_0}{2c_\infty^3}\Phi_1. \quad (12)$$

The sound is imposed to be a wave process, so that it attenuates (or amplifies, in dependence on the sign of B) weakly over the wavelength, $|B|k^{-1}\ll 1$. In the low-frequency regime, the relations take the leading-order form (Perelomova, 2010a):

$$\begin{aligned}v'_{1,l}(x,t)&=\frac{c_0}{\rho_0}\rho'_{1,l}(x,t),\\ p'_{1,l}(x,t)&=c_0^2\rho'_{1,l}(x,t),\\ \varepsilon'_{1,l}(x,t)&=\frac{2Bc_0^2}{(\gamma-1)\rho_0}\int dx\rho'_{1,l}(x,t).\end{aligned} \quad (13)$$

Relations (11), (13), along with the linear property of superposition, Eqs. (10), point out a way of combination of four equations from (4) in order to get dynamic equations describing perturbation of only one specific mode. Formally, that may be done by means of the complete set of orthogonal projectors. The remarkable property of projectors is to decompose the dynamic equations governing the correspondent mode by immediate appliance on the linear system. The details of establishing of the projectors in the low- and high-frequency regimes may be found in the papers by one of the authors (Perelomova, 2003; 2006; 2008). Application of the matrix operator on the vector of overall perturbations ($v'\ \ p'\ \ \rho'\ \ \varepsilon'$) actually decomposes the correspondent specific mode:

$$P_n\begin{pmatrix}v'(x,t)\\ p'(x,t)\\ \rho'(x,t)\\ \varepsilon'(x,t)\end{pmatrix}=\begin{pmatrix}v'_n(x,t)\\ p'_n(x,t)\\ \rho'_n(x,t)\\ \varepsilon'_n(x,t)\end{pmatrix}, \quad n=1,\ldots,4. \quad (14)$$

Within the accuracy up to the terms of the first order in $(c_\infty k\tau)^{-1}$, $|B|k^{-1}$, the third row of projector $P_{1,h}$, which projects the overall vector of perturbations into an excess density belonging to the first high-frequency acoustic mode, takes the following form:

$$\left(\frac{\rho_0}{2c_\infty}+\frac{B\rho_0}{c_\infty}\int \mathrm{d}x \qquad \frac{1}{2c_\infty^2}+\frac{B(\gamma-3)}{2(\gamma-1)c_\infty^2}\int \mathrm{d}x \right.$$
$$\left. \frac{B}{(\gamma-1)}\int \mathrm{d}x \qquad \frac{(\gamma-1)\rho_0}{2c_\infty^3\tau}\int \mathrm{d}x\right). \tag{15}$$

The row which projects the overall vector of perturbations into the first branch of the low-frequency sound, calculated with the accuracy up to the terms of the first order in $(c_0k\tau)^1$, $|B|k^{-1}$, is

$$\left(\frac{\rho_0}{2c_0}-\frac{B\rho_0}{c_0}\int \mathrm{d}x \qquad \frac{1}{2c_0^2}+\frac{B\tau}{(\gamma-1)c_0}\right.$$
$$\left. -\frac{Bc_0\tau}{(\gamma-1)} \qquad \frac{(\gamma-1)\rho_0}{2c_0^2}-\frac{B(\gamma-2)\rho_0\tau}{c_0}\right). \tag{16}$$

Both rows include operators. Employment of the first row on the linearized system (4), i.e., application of the first operator on the first equation from this set, the second operator on the second one, and so on, and calculation of the sum of all four equalities, result in the dynamic equation for an excess density of the first acoustic high-frequency mode:

$$\frac{\partial\rho_{1,h}}{\partial t}+c_\infty\frac{\partial\rho_{1,h}}{\partial x}-c_\infty B\rho_{1,h}=0, \tag{17}$$

where $\rho_{1,h}$ is the excess acoustic density, ρ_1', in the case of the high-frequency sound. Application of the second row on the system (4) yields the dynamic equation for the first low-frequency acoustic mode:

$$\frac{\partial\rho_{1,l}}{\partial t}+c_0\frac{\partial\rho_{1,l}}{\partial x}=0, \tag{18}$$

where $\rho_{1,l}$ is the excess acoustic density in the case of the low-frequency sound. Equations (17), (18) obviously coincide with the roots of the dispersion relation $\omega_{1,0}$ and $\omega_{1,\infty}$ from Eqs. (7), (8). It may be readily established that terms relating to all other modes become reduced. That follows from the properties of projectors.

Applying projectors on the nonlinear vector of system (4) yields quadratic nonlinear corrections in the final dynamic equations originating from the right-hand side of Eqs. (4). We will keep among all of them only those belonging to the progressive in the positive direction of axis Ox sound. That is valid over spatial and temporal domains, where magnitude of this branch of sound is much larger than that of other modes.

3. Nonlinear features of sound propagation

3.1. The high-frequency sound

Application of the row (15) at the column of nonlinear equations (4) and account for the links (11) results, after some ordering, in the equation governing the first sound branch. The term proportional to B^0 in the right-hand side of the equation takes the form:

$$-\frac{c_\infty(\gamma+1)}{2\rho_0}\rho_{1,h}\frac{\partial\rho_{1,h}}{\partial x}. \tag{19}$$

The term associated with the corrections of order B^1 in the operators, is:

$$-\frac{Bc_\infty(\gamma-1)}{2\rho_0}\int\rho_{1,h}\frac{\partial\rho_{1,h}}{\partial x}\,\mathrm{d}x=-\frac{Bc_\infty(\gamma-1)}{4\rho_0}\rho_{1,h}^2, \tag{20}$$

and the terms originated from the links between acoustic perturbations (15), are:

$$\frac{Bc_\infty(\gamma+1)}{2\rho_0}\left(\rho_{1,h}^2+2\frac{\partial\rho_{1,h}}{\partial x}\int\rho_{1,h}\,\mathrm{d}x\right)$$
$$-\frac{T_0\Phi_2(\gamma-1)^3}{\rho_0}\rho_{1,h}^2. \tag{21}$$

The overall weakly nonlinear equation governing sound contains the sum of all nonlinear terms:

$$\frac{\partial\rho_{1,h}}{\partial t}+c_\infty\frac{\partial\rho_{1,h}}{\partial x}+\frac{c_\infty(\gamma+1)}{2\rho_0}\rho_{1,h}\frac{\partial\rho_{1,h}}{\partial x}-c_\infty B\rho_{1,h}$$
$$=\frac{Bc_\infty}{2\rho_0}\left(\frac{\gamma+3}{2}\rho_{1,h}^2+2(\gamma+1)\frac{\partial\rho_{1,h}}{\partial x}\int\rho_{1,h}\,\mathrm{d}x\right)$$
$$-\frac{T_0\Phi_2(\gamma-1)^3}{\rho_0}\rho_{1,h}^2. \tag{22}$$

The limiting case of Eq. (22) when $B=0$ and $\Phi_2=0$ is the famous Earnshaw equation for a simple wave in non-viscous ideal gas (Rudenko, Soluyan, 1977). The analysis of Eq. (22) may be readily proceeded by means of the standard method of successive approximations. In order to establish pure nonlinear distortions, we put the linear term proportional to B in the left-hand side of Eq. (22) equal to zero. If a transducer placed at $x=0$ transmits a harmonic wave,

$$\rho_{1,h}(x=0,t)=R_A\sin(\omega t), \tag{23}$$

the spectrum is enriched at some distances from the transducer due to nonlinearity of the medium. Simple evaluations yield the approximate solution:

$$\begin{aligned}\rho_{1,h}(x,t) = {} & R_A\sin(\omega t-kx)\\ & +\frac{x(\gamma+1)\omega R_A^2}{4c_\infty\rho_0}\sin(2\omega t-2kx)\\ & +\frac{xR_A^2(\alpha+\beta)}{2c_\infty\rho_0}\cos(2\omega t-2kx)\\ & +\frac{xR_A^2(-\alpha+\beta)}{2c_\infty\rho_0},\end{aligned} \tag{24}$$

where

$$\begin{aligned}\alpha &= -\frac{Bc_\infty(\gamma+3)}{4}+T_0\Phi_2(\gamma-1)^3,\\ \beta &= -Bc_\infty(\gamma+1).\end{aligned} \tag{25}$$

The second term in the right-hand side of Eq. (24) reflects the "standard" weakly nonlinear distortions. The third one originates from the vibrational relaxation, it also varies with time. Assuming that the sign of B is more important than that of Φ_2, one may conclude that the magnitude of nonlinear distortions relating to this oscillating term decrease with x for the positive B and increase otherwise. The last monotonic term, analogously, decreases when B is positive. It causes the non-zero mean value of perturbations in the periodic sound wave. Thus, the conclusion is that the non-equilibrium gases possess unusual nonlinearity which gets smaller with the increase in the degree of disequilibrium. Equilibrium media, *vice versa*, makes the nonlinearity larger. For any periodic in time acoustic wave, the averaged over the sound period term in the right-hand side of Eq. (22) takes the leading-order form:

$$\frac{-\alpha+\beta}{\rho_0}\langle\rho_{1,h}^2\rangle. \tag{26}$$

It differs from the "standard" nonlinearity, $\frac{c_\infty(\gamma+1)}{2\rho_0}\rho_{1,h}\frac{\partial\rho_{1,h}}{\partial x}$, which is zero on average in the leading order. As for the momentum of the acoustic impulse, it is known that it is constant independent on the distance from a transducer before or after formation of a discontinuity in a simple wave. Integrating Eq. (22) from $x=-\infty$ till $x=\infty$ and assuming that excess acoustic density and all its spatial derivatives tend to zero at infinities, we finally arrive at the dynamic equation describing the momentum,

$$\frac{\partial P_{1,h}}{\partial t} = c_\infty B P_{1,h} + \frac{(-\alpha+\beta)c_\infty}{\rho_0}\int\limits_{-\infty}^{\infty}\rho_{1,h}^2\,\mathrm{d}x, \tag{27}$$

where

$$P_{1,h} = c_\infty\int\limits_{-\infty}^{\infty}\rho_{1,h}\,\mathrm{d}x \tag{28}$$

is the density of the acoustic momentum. If we would not consider nonlinearity associated with excitation of vibrational degrees of a molecule freedom, the last term in the right-hand side of Eq. (27) were zero and the acoustic momentum would vary with time proportionally to $\exp(c_\infty Bt)$. It would increase for a positive B, in the non-equilibrium case, and decrease otherwise. Dependence of the acoustic momentum on time is connected with exchange of the momentum of internal and external degrees of molecules of a relaxing gas. Account for nonlinearity makes variations of P with time faster in the equilibrium regime, in view of the fact that the integral in the right-hand side of Eq. (27) is always positive.

If the vibrational relaxation is equilibrium, the discontinuity in the sound wave may not form at all. That happens for enough large $|B|$. Without account for nonlinearity connected with vibrational relaxation, for initially sinusoidal wave, the front forms if (Perelomova, Wojda, 2011)

$$\frac{2\rho_0 c_\infty B\pi}{R_A(\gamma+1)\omega} < -1. \tag{29}$$

One may expect that the threshold of the discontinuity appearance is even lower in view of additional nonlinearity. Vice versa, in the non-equilibrium regime, for the positive B, discontinuity always forms. Account for the specific nonlinearity originating from relaxation predicts larger distances from a transducer where that happens.

3.2. The low-frequency sound

As for the low-frequency sound, taking into account relations (13) along with the application of row (16) on the nonlinear right-hand side of Eqs. (4) yields:

$$\frac{\partial\rho_{1,l}}{\partial t} + c_0\frac{\partial\rho_{1,l}}{\partial x} + \frac{c_0(\gamma+1)}{2\rho_0}\rho_{1,l}\frac{\partial\rho_{1,l}}{\partial x} = \frac{B}{\rho_0\tau}\rho_{1,l}\int\rho_{1,l}\,\mathrm{d}x. \tag{30}$$

For an excess acoustic density at a transducer being a harmonic function of time, the approximate solution at some distances from the transducer takes the form:

$$\begin{aligned}\rho_{1,l}(x,t) = {} & R_A\sin(\omega t-kx) \\ & + \frac{x(\gamma+1)\omega R_A^2}{4c_0\rho_0}\sin(2\omega t-2kx) \\ & + \frac{xBR_A^2}{2\omega\tau\rho_0}\sin(2\omega t-2kx).\end{aligned} \tag{31}$$

Also, in this case, there is a part oscillating at a double frequency which associates with the standard nonlinearity and one which reflects the effects of relaxation. In the non-equilibrium regime, if $B>0$, the nonlinearity enhances, and it decreases otherwise. Thus, conclusions are opposite to those of the high-frequency sound. Also, perturbations in the sound remain zero on average. For any periodic in time acoustic wave, the averaged over the sound period term in the right-hand side of Eq. (30) takes the leading-order form:

$$\frac{B}{2\rho_0\tau}\left\langle\left(\int\rho_{1,l}\,\mathrm{d}x\right)^2\right\rangle, \tag{32}$$

and the conclusion about enhancement of nonlinearity in the non-equilibrium regime of excitation is valid. This type of non-linearity differs both from that in the simple wave and that in the high-frequency case described by Eq. (26).

As for the acoustic momentum, it varies with time in accordance to the following dynamic equation:

$$\frac{\partial P_{1,l}}{\partial t} = \frac{Bc_\infty}{2\rho_0\tau}\left(\int\rho_{1,l}\,\mathrm{d}x\right)^2. \tag{33}$$

It enlarges in the non-equilibrium regime and decreases otherwise.

The unusual feature is that in contrast to the high-frequency sound where the ratio of nonlinear terms associated with the vibrational relaxation and the standard one is of the order $|B|k^{-1}$ is much less than unity, the ratio of the similar terms in the low-frequency regime in the evolution equation (30) is of the order of the ratio of two small parameters, $|B|k^{-1}$ and $\omega\tau$. It is not rigorously small and may make the nonlinear term originating from the vibrational relaxation larger than the standard one.

4. Concluding remarks

In this study we consider the nonlinear distortions of the sound associated with the equilibrium or non-equilibrium type of relaxation. The linear effect of relaxation is in increase (or unusual decrease, if $B > 0$) in the phase speed of a signal in equilibrium relaxation, while its frequency enlarges. Accordingly, sound enhances in the non-equilibrium regime. As for nonlinear distortions, they depend also on the domain of the sound frequency emitted by a transducer and on the type of relaxation. In addition to standard nonlinearity, there appear terms which enlarge nonlinearity or make it smaller. The main conclusion is that nonlinear distortion of the high-frequency sound decreases and that of the low-frequency regime increases, while sound propagates over a gas in vibrational nonequilibrium. This may be of especial importance in the low-frequency domain because the relative magnitude of the term associated with relaxation is proportional to the ratio of small parameters, $|B|k^{-1}$ and $\omega\tau$. Since the low-frequency sound almost does not attenuate linearly, this may lead to unusual short (if $B > 0$) or large (if $B < 0$) distances from a transducer where the sawtooth wave forms. In the equilibrium gases, vise versa, nonlinear distortion of the high-frequency sound enhances and nonlinear distortion of the low-frequency sound declines.

Gases, where vibrational relaxation of the internal degrees of molecules takes place, are just one example among fluids with different thermodynamic relaxation processes which may occur in an irreversible way. In spite of that, flows over these relaxing fluids are described quantatively by different parameters, the equations governing sound and relative nonlinear phenomena, are quite similar (Molevich, 1986). The nonlinear effects caused by the sound in a chemically reacting gas are discussed in the papers by one of the authors (Perelomova, 2010b). Thus, the conclusions of this study may be expanded over a wide class of fluids with thermodynamical relaxation processes of different kinds. Theoretical predictions hopefully will allow to conclude about qualitative and quantitative relaxation processes in a gas remotely, basing on data on nonlinear distortions of the sound and on variations in its momentum during propagation over a gas.

References

1. Gordiets A.I., Osipov A.I., Stupochenko E.V., Shelepin L.A. (1973), *Vibrational relaxation in gases and molecular lasers*, Soviet Physics Uspekhi, **15**, 6, 759–785.
2. Kogan Ye.A., Molevich N.E. (1986), *Acoustical wave in nonequilibrium molecular gas*, Russian Physics Journ, **29**, 7, 53–58.
3. Makaryan V.G., Molevich N.E. (2007), *Stationary shock waves in nonequilibrium media*, Plasma Sources Sci. Technol., **16**, 124–131.
4. Molevich N.E. (2003), *Sound velocity dispersion and second viscosity in media with nonequilibrium chemical reactions*, Acoustical Physics, **49**, 2, 229–232.
5. Molevich N.E. (2004), *Acoustical properties of nonequilibrium media* 42 AIAA Aerospace Sciences Meeting and Exhibit (Reno, NV), Paper AIAA-2004-1020.
6. Molevich N.E., Klimov A.I., Makaryan V.G. (2005), *Influence of thermodynamic nonequilibrium on acoustical properties of gas*, Intern. Journ. Aeroacoustics, **4**, 3–4, 345–355.
7. Osipov A.I., Uvarov A.V. (1992), *Kinetic and gasdynamic processes in nonequilibrium molecular physics*, Sov. Phys. Usp., **35**, 11, 903–923.
8. Perelomova A. (2003), *Acoustic radiation force and streaming caused by non-periodic acoustic source*, Acta Acustica united with Acustica, **89**, 754–763.
9. Perelomova A. (2006), *Development of linear projecting in studies of non-linear flow. Acoustic heating induced by non-periodic sound*, Physics Letters A, **357**, 42–47.
10. Perelomova A. (2008), *Acoustic heating in a weakly dispersive fluid flow*, Acta Acustica, **94**, 3, 382–387.
11. Perelomova A. (2010a), *Nonlinear generation of non-acoustic modes by low-frequency sound in a vibrationally relaxing gas*, Canadian Journal of Physics, **88**, 4, 293–300.
12. Perelomova A. (2010b), *Interaction of acoustic and thermal modes in the gas with nonequilibrium chemical reactions. Possibilities of acoustic cooling*, Acta Acustica united with Acustica, **96**, 43–48.
13. Perelomova A. (2012), *Nonlinear influence of sound on vibrational energy of molecules in relaxing gas*, Archives of Acoustics, **37**, 1, 89–96.
14. Perelomova A., Wojda P. (2011), *Generation of the vorticity motion by sound in a chemically reacting gas. Inversion of acoustic streaming in the non-equilibrium regime*, Central European Journal of Physics, **9**, 3, 740–750
15. Rudenko O.V., Soluyan S.I. (1977), *Theoretical foundations of nonlinear acoustics*, Plenum, New York.
16. Zeldovich Ya.B., Raizer Yu.P. (1966), *Physics of shock waves and high temperature hydrodynamic phenomena*, Academic Press, New York.

PAN
ARCHIVES OF ACOUSTICS
Vol. **38**, No. 3, pp. 363–373 (2013)

DOI: 10.2478/aoa-2013-0043

Estimation of the Fundamental Frequency of the Speech Signal Compressed by MP3 Algorithm

Zoran N. MILIVOJEVIĆ[(1)], Darko BRODIĆ[(2)]

[(1)] *Technical College*
Aleksandra Medvedeva 20, 18000 Nis, Serbia; e-mail: zoran.milivojevic@vtsnis.edu.rs

[(2)] *Technical Faculty in Bor, University of Belgrade*
Vojske Jugoslavije 12, 19210 Bor, Serbia; e-mail: dbrodic@tf.bor.ac.rs

(*received September 28, 2012; accepted May 17, 2013*)

The paper analyzes the estimation of the fundamental frequency from the real speech signal which is obtained by recording the speaker in the real acoustic environment modeled by the MP3 method. The estimation was performed by the Picking-Peaks algorithm with implemented parametric cubic convolution (PCC) interpolation. The efficiency of PCC was tested for Catmull-Rom, Greville, and Greville two-parametric kernel. Depending on MSE, a window that gives optimal results was chosen.

Keywords: fundamental frequency, speech compression, speech processing, signal representation, MP3.

Notations

α_{opt} – optimal kernel parameter,
α – kernel parameter,
x – audio or speech signal,
X – spectrum,
w – window function,
r – interpolation kernel,
p – interpolation function,
n – time lag, $0 \leq n \leq N-1$,
N – window length,
M – number of points between two samples in spectrum,
L – kernel length, $4 \leq L \leq 8$,
k – spectrum lag, $0 \leq k \leq N-1$,
K – number of harmonics,
f_s – sampling frequency,
$f_{\max}$ – maximum of the interpolated frequency,
f_e – estimated fundamental frequency,
f – frequency,
β_{opt} – optimal kernel parameter,
β – kernel parameter,
s – MP3 coded audio or speech signal.

1. Introduction

The rising trend of multimedia communications has imposed the need for archiving and transferring the audiovisual information. The amount of data which is archived or transferred, is very large (Brandenburg *et al.*, 1992; ISO/IEC, 1992; ISO/IEC 13818-3, 1994). For instance, audio record rate in stereo technique at the sampling frequency f_s = 44.1 kHz is 10.584 MB/min. Transferring that number of bits is a very slow process even in very fast communication media. Hence, the development of compressing techniques is mandatory. A number of algorithms for audio signal compressing has been appeared. Most of them used MP3 algorithm with a compression degree of 1:12. Such compression ratio enables archiving a digitalized audio signal as well as transferring it by multimedia systems. Accordingly, MP3 became especially popular in internet applications (Hacker, 2000; McCandless, 1999). MP3 is a shortened name for coding algorithm derived from the standard MPEG-1, Layer III, developed by the German Technology Group. It was standardized by International Standards Organization (ISO) (ISO/IEC, 1992). MP3 does the compression tasks eliminating redundancy. It is similar to zip algorithm in accordance with a psycho-acoustic model that describes mechanisms of the human sound perception. Technically, MPEG-1 Layer III and MPEG-2 Layer III are declared as MP3 standard. MPEG-1 Layer III is used for 32 kHz, 44.1 kHz, and 48 kHz of sampling frequency, while MPEG-2 Layer III is used for 16 kHz, 22.05 kHz, and 24 kHz of sampling frequency. The standard broadening with a sign MPEG 2.5 is used for 8 kHz and 11 kHz (Hacker, 2000). MP3 compression algorithm is based on the combination of several techniques the function of which is to maximize the relation between the perceived quality and the necessary file size. Spectrum of an audio signal is divided into 32 equally spaced frequency sub-bands. After that, a Modified Discrete Cosine Transformation (MDCT) is applied (Britanak, 2011). Precision of MDCT coefficient is reduced by the process of quantization. Further, the signal is processed according to the psychoacoustic model. This model emulates the human perception, i.e. the masking effects, which represent auditory and temporal masking (Hacker, 2000). After the signal processing according to the psychoacoustic model, Huffman's coding is performed. This coding additionally performs reduction of file size for 20%. In the name of copyright, the algorithms for inserting audio watermarks have been developed (Yeo, Kim, 2003; Wang, Hong, 2006; Dhar, Echizen, 2011). Latest advances in MP3 incorporate DFT-based MP3 multichannel audio system (Moon, 2012). The parametric multi-channel audio coding concept enables the legacy system to reproduce stereo audio as well as the advanced system to reproduce multi-channel audio.

A number of the old music and speech records are digitalized and compressed by MP3 algorithm. However, there was a need for re-recording the significant historical and musical materials previously made by analog medium (magnetic tapes, vinyl records 78 rpm, LP, ...). The main deficiency of the analog sound recording is a high level of noise. In vinyl recordings, degradation effects come from imperfections and subsequent mechanical damage to the recording medium, and manifest themselves as clicks, sputtering, and noise from scratches. There is a need for this kind of processing as well as for restoration of the audio signals (Avila, Biscainho, 2012).

In many multimedia applications, it is necessary to process audio records in order to improve the quality, intelligibility of speech, verification of the speaker, etc. A typical example is the quality improvement of the speech signal by reducing dissonant frequencies (Joen *et al.*, 2003; Kang, 2004; Kang, Kim, 2006). Besides analyzing the trajectories of fundamental frequency, it is possible to classify the emotional state of a man (sadness, anger, joy, ...) (Ayadi *et al.*, 2011), evaluate health status, and the conditions of hypoxia, which is manifested as a decrease in the concentration of oxygen in the blood (due to incidents during a flight, working in the mines, tunnels, etc.) (Milivojevic *et al.*, 2012). In processing of music and speech signal, it is necessary to determine the fundamental frequencies. Music signals are characterized by a fundamental frequency and the series of harmonic components that are integer multiples of fundamental frequency, i.e. partials.

In musical strings instruments, harmonic shifts occurrence leads to inharmonocity of an instrument. It is defined through the inharmonicity coefficient. Determining the inharmonicity coefficient requires an accurate estimation of the fundamental frequency (Barbancho *et al.*, 2012). Digital processing of the music signal is possible for string instruments (e.g. guitar). Accordingly, it plays an estimate note, in which the string is played (E, H, G, D, A, E) as a fret. The more complex algorithms can detect the chords and form the score music (Fragoulis *et al.*, 2006).

The authors of this paper asked themselves: "What is the degradation of the fundamental frequency for MP3 encoding and decoding speech signals?"

In order to answer this question, the authors have conducted a number of experiments by applying the algorithms to estimate the fundamental frequency (F_0) in the frequency domain. After the calculation of DFT, the Picking-Picks is made. The highest peak represents the fundamental frequency. Particular attention is devoted to the application of parametric cubic convolution (PCC) algorithm in order to increase the precision of fundamental frequency estimation, when it is located between the spectral components on which DFT is calculated. The experiments were based on the time-domain (application of the window functions) and the frequency-domain processing, which implemented the cubic convolution kernels (Catmull-Rom, Greville, and Greville two-parametric kernel). Retrieval of the maximum position in the continuous convolution interpolation function is a mathematically complex and time-consuming process. Analytical expressions for the calculation of F_0 according to Keys kernel is proposed in (Pang *et al.*, 2000), while for the calculation of F_0 for Greville and Greville two-parametric (G2P) kernel is given in (Milivojevic, Brodic, 2011).

In this paper, the authors present the results of the fundamental frequency assessment for:

a) mathematically generated sine signal proposed in (Pang *et al.*, 2000) and
b) real speech signals recorded in a real environment proposed in (Milivojevic, Brodic, 2011).

The results will be analyzed by the mean square error (MSE) method. Finally, comparative analysis of the estimation accuracy F_0 by MP3 algorithm SYMPES (Yarman *et al.*, 2006; Milivojevic, Mirkovic, 2009) and G.3.721 (Milivojevic, Brodic, 2011) will be made.

This paper is organized as follows: Sec. 2 presents the previous works in the field. Section 3 describes the PCC algorithm. Subsection 3.1 defines the interpolation kernels. Subsection 3.2 presents the algorithm for determination of the optimal kernel parameters. Subsection 3.3 defines the test signals. Section 4 presents MSE results for the fundamental frequency estimation of the real speech signal modeled by the MP3 method. Section 5 shows the comparative analysis as well as the optimal kernel and window function selection. Section 6 gives the conclusion.

2. Previous works

The estimation of the fundamental frequency has received immense interest from different speech research areas, such as speech segregation, speech synthesis, speech coding, speech and speaker recognition, and speech articulation training for the deaf (Griffin, Lim, 1988; Atal, 1972; Kawahara *et al.*, 1999). A number of algorithms for determining the fundamental frequency has been developed. Theirs processing is performed in the time-domain (TD) and frequency-domain (FD) methods (Kawahara, 2002; Sekhar, Sreenivas, 2004; Hussain, Boashash, 2002; Kacha, Benmahammed, 2005; Veprek, Scordilis, 2002; Klapuri, 2003). In TD methods, one or more speech features (the fundamental harmonic, a quasi-periodic time structure, an alternation of high and low amplitudes, and points of discontinuities in the speech waveform) are identified first, and then the pitch markers or epochs are obtained in a pitch synchronous manner. In FD methods, a short-time frame or block of speech samples is transformed into spectral or frequency-domain in order to enhance the periodicity information contained in the speech. These methods determine an average pitch from several contiguous periods in the analysis frame. The performance of TD methods compared to FD methods depends more on the shape of the time waveform of speech (Resch *et al.*, 2007). The autocorrelation function (ACF) (Rabiner, 1977) and the average magnitude difference function (AMDF) (Ross *et al.*, 1974) have been commonly employed for pitch estimation. In (Kawahara, 2002), an estimator named YIN has been proposed, where a series of modifications (a difference function formulation, normalization, and parabolic interpolation) has been introduced to decrease the error rates in pitch estimation from a clean speech (Shahnaz *et al.*, 2012).

The widespread method for determination of the fundamental frequency is based on Picking Peaks of the amplitude characteristic in the specific frequency range. This method is used for analyzing the signal values in the spectrum at frequencies on which the Discrete Fourier Transform (DFT) was calculated. Usually, the real value of the fundamental frequency is not there at the frequencies where DFT is calculated. In contrast, it lies between the two spectrum samples. That causes the frequency estimation error that lies in the interval $[-(f_s/(2N)\text{ Hz}, (f_s/(2N)\text{ Hz}]$, where f_s is the sampling frequency and N is the DFT window size. One way of reducing the error is determination of the interpolation function and estimation of the spectrum characteristics in the interval between two samples. This procedure gives the reconstruction of the spectrum on the base of DFT. The spectrum parameters are then determined by analytic procedures (differentiation, integration, extreme values, etc).

The calculation of the interpolation function by using PCC was represented in (Keys, 1981; Park, Schowengerdt, 1983). The special case of PCC interpolation applied in computer graphics has been called the Catmull-Rom interpolation (Meijering, Unser, 2003). Pang *et al.* (2000) give detailed analysis of the fundamental frequency estimation and show the advantage of PCC interpolation. The application of PCC interpolation for determining the fundamental frequency in specific conditions is presented in (Milivojevic *et al.*, 2004). The efficiency of the algorithm for the evaluation of the fundamental frequency is determined by the simulation. As a quality measure of the algorithm, the mean square error (MSE) has been used. The best results were shown by the algorithm with the implemented Blackman window. The analysis of the algorithm efficiency where the signal-to-noise relation (SNR) is changeable according to the presence of the important harmonics in the fundamental function, is shown in (Mirkovic *et al.*, 2004). It confirmed the efficiency of the algorithm with the Blackman window. In (Mirkovic *et al.*, 2006), an analysis of PCC interpolation algorithm efficiency is made for the case where Greville two-parametric cubic convolution kernel (G2P) was implemented. The window was determined and the kernel parameters (α, β) were calculated where the minimum MSE was generated (in relation to Caltmull-Rom kernel the error was smaller by 58.1%). The new method of speech signal modeling called "A Novel Systematic Procedure to Model Speech Signals via Predefined Envelope and Signature Sequences" (SYMPES) is presented in the paper (Yarman *et al.*, 2006). The results of the fundamental frequency estimation of the speech signal modeled by SYMPES method are shown in (Milivojevic, Mirkovic, 2009). Furthermore, the results of the fundamental frequency estimation for the speech signal coded by G.3.721 method are shown in (Milivojevic, Brodic, 2011).

3. Proposed algorithms

Algorithm for the estimation of the fundamental frequency, based on the algorithm from (Pang *et al.*, 2000), is presented in Fig. 1.

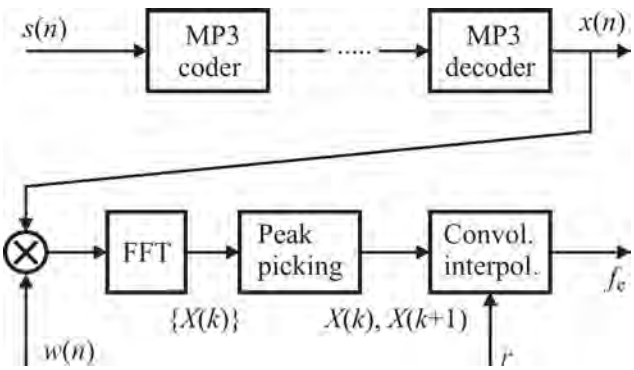

Fig. 1. Algorithm for the estimation of the fundamental frequency.

This algorithm is realized as follows:
Step 1: Audio or speech signal $s(n)$ is coded by MP3 coder.
Step 2: Coded signal is decoded by MP3 decoder and formed as signal $x(n)$.
Step 3: Window $w(n)$, length of which is N, is applied to decoded signal $x(n)$.
Step 4: Spectrum $X(k)$ is calculated by using DFT:

$$X(k) = \mathrm{DFT}(x(n)). \tag{1}$$

The spectrum is calculated in discrete points $k = 0, ..., N-1$, where N is the length of DFT. The real spectrum of signals $x(n)$ is continuous, whereas DFT defines the values of the spectrum at some discrete points.
Step 5: The maximum of the real spectrum that is between k-th and $(k+1)$-th samples is determined by using the Picking-Peak algorithm. The values $X(k)$ and $X(k+1)$ are the highest in the specified domain.
Step 6: The maximum of the spectrum is calculated by PCC interpolation. The reconstructed function is:

$$X_r(f) = \sum_{i=k-L/2+1}^{k+L/2} p_i \cdot r(f-i), \qquad k \le f \le k+1, \tag{2}$$

where $p_i = X_r(i)$, $r(f)$ is the kernel of interpolation, and L is the number of samples that participate in the interpolation.
Step 7: By differentiation $X_r(f)$ and zero adjustment, the position of the maximum is determined. It represents the estimated fundamental frequency f_e.

The quality of the algorithm for the fundamental frequency estimation can be also expressed by MSE:

$$\mathrm{MSE} = \overline{(f - f_e)^2}, \tag{3}$$

where f is true fundamental frequency and f_e is estimated fundamental frequency.

3.1. Interpolation kernel

The definitions of the interpolation kernels, which are tested in this paper, are:

a) Keys interpolation kernel (Keys, 1981; Park, Schowengerdt, 1983):

$$r(f)=\begin{cases}(\alpha+2)\,|f|^3-(\alpha+3)\,|f|^2+1, & |f|\le 1,\\[2mm] \alpha\,|f|^3-5\alpha\,|f|^2+8\alpha\,|f|-4\alpha, & 1<|f|\le 2,\\[2mm] 0, & \text{otherwise.}\end{cases} \tag{4}$$

For $L = 4$, from Eq. (2), the position of maximum is determined:

$$f_{\max} = \begin{cases} k - \dfrac{c}{2b}, & a = 0,\\[2mm] k + \dfrac{-b -+ \sqrt{b^2 - ac}}{a}, & a \ne 0, \end{cases} \tag{5}$$

where

$$\begin{aligned} a &= 2\left(\alpha p_{k-1} + (\alpha+2)p_k \right.\\ &\quad\left. - (\alpha+2)p_{k+1} - \alpha p_{k+2}\right),\\ b &= -2\alpha p_{k-1} - (\alpha+3)p_k + (2\alpha+3)p_{k+1}\\ &\quad + \alpha p_{k+2},\\ c &= -\alpha p_{k-1} - \alpha p_{k+1}, \end{aligned} \tag{6}$$

b) Greville interpolation kernel (Meijering, Unser, 2003):

$$r(f) = \begin{cases} \left(\alpha + \dfrac{3}{2}\right)|f|^3 - \left(\alpha + \dfrac{5}{2}\right)|f|^2 + 1; & \text{if } \ 0 \le |f| \le 1,\\[2mm] \dfrac{1}{2}(\alpha-1)|f|^3 - \left(3\alpha - \dfrac{5}{2}\right)|f|^2 + \left(\dfrac{11}{2}\alpha - 4\right)|f| - (3\alpha - 2); & \text{if } \ 1 \le |f| \le 2,\\[2mm] -\dfrac{1}{2}\alpha|f|^3 + 4\alpha|f|^2 - \dfrac{21}{2}\alpha|f| + 9\alpha; & \text{if } \ 2 \le |f| \le 3,\\[2mm] 0; & \text{if } \ 3 \le |f|. \end{cases} \tag{7}$$

For $L = 6$, from Eqs. (2) and (7), the position of maximum is determined according to Eq. (5), where

$$\begin{aligned} a &= -\frac{3}{2}\alpha p_{k-2} + \frac{3}{2}(\alpha-1)\,p_{k-1}\\ &\quad + 3\left(\alpha + \frac{3}{2}\right)p_k - 3\left(\alpha + \frac{3}{2}\right)p_{k+1}\\ &\quad - \frac{3}{2}(\alpha-1)\,p_{k+2} + \frac{3}{2}\alpha p_{k+3},\\ b &= -2\alpha p_{k-2} + (-3\alpha+2)\,p_{k-1} - (2\alpha+5)\,p_k\\ &\quad + 4(\alpha+1)\,p_{k+1} - p_{k+2} - \alpha p_{k+3},\\ c &= -\frac{1}{2}\alpha p_{k-2} + \left(\alpha - \frac{1}{2}\right)p_{k-1}\\ &\quad - \left(\alpha - \frac{1}{2}\right)p_{k+1} + \frac{1}{2}\alpha p_{k+2}, \end{aligned} \tag{8}$$

c) Greville two-parametric cubic convolution kernel (G2P) (Meijering, Unser, 2003):

$$r(f)=\begin{cases}\left(\alpha-\frac{5}{2}\beta+\frac{3}{2}\right)\cdot|f|^3 \\ \quad -\left(\alpha-\frac{5}{2}\beta+\frac{5}{2}\right)\cdot|f|^2+1; \\ \qquad 0\le|f|\le 1, \\ \frac{1}{2}(\alpha-\beta-1)\cdot|f|^3 \\ \quad -\left(3\alpha-\frac{9}{2}\beta-\frac{5}{2}\right)\cdot|f|^2 \\ \quad +\left(\frac{11}{2}\alpha-10\beta-4\right)\cdot|f| \\ \quad -(3\alpha-6\beta-2); \\ \qquad 1\le|f|\le 2, \\ -\frac{1}{2}(\alpha-3\beta)\cdot|f|^3 \\ \quad +\left(4\alpha-\frac{25}{2}\beta\right)\cdot|f|^2 \\ \quad -\left(\frac{21}{2}\alpha-34\beta\right)\cdot|f| \\ \quad +(9\alpha-30\beta); \\ \qquad 2\le|f|\le 3, \\ -\frac{1}{2}\beta\cdot|f|^3+\frac{11}{2}\beta\cdot|f|^2 \\ \quad -20\beta\cdot|f|+24\beta; \\ \qquad 4\le|f|.\end{cases} \tag{9}$$

For $L=8$, from Eqs. (2) and (9), the position of maximum is determined according to Eq. (5), where

$$\begin{aligned} a=&-\frac{3}{2}\beta p_{k-3}-\frac{3}{2}(\alpha-3\beta)p_{k-2} \\ &+\frac{3}{2}(\alpha-\beta-1)p_{k-1}+3\left(\alpha-\frac{5}{2}\beta+\frac{3}{2}\right)p_k \\ &-3\left(\alpha-\frac{5}{2}\beta+\frac{3}{2}\right)p_{k+1}-\frac{3}{2}(\alpha-\beta-1)p_{k+2} \\ &+-\frac{3}{2}(\alpha-3\beta)p_{k+3}+\frac{3}{2}\beta p_{k+4}; \\ b=&-2\beta p_{k-3}-(2\alpha-7\beta)p_{k-2} \\ &+(-3\alpha+6\beta+2)p_{k-1}-\left(2\alpha-5\beta+\frac{5}{2}\right)p_k \\ &+(4\alpha-10\beta+1)p_{k+1}+(3\beta-1)p_{k+2} \\ &+(-\alpha+2\beta)\alpha p_{k+3}-\beta p_{k+4}; \\ c=&-\frac{1}{2}\beta p_{k-3}+\left(-\frac{1}{2}\alpha+2\beta\right)p_{k-2} \\ &+\left(\alpha-\frac{5}{2}\beta-\frac{1}{2}\right)p_{k-1}-\left(\alpha+\frac{5}{2}\beta+\frac{1}{2}\right)p_{k+1} \\ &+\left(\frac{1}{2}\alpha-2\beta\right)p_{k+2}+\frac{1}{2}\beta p_{k-3}. \end{aligned} \tag{10}$$

In Eqs. (4)–(10), there are α and β parameters. The optimal values of these parameters will be determined by the minimum value of MSE, for Keys, Greville, and G2P kernel. For the first two of them

$$\alpha_{\text{opt}}=\arg\min_{\alpha}(\text{MSE}), \tag{11}$$

and for the G2P kernel,

$$(\alpha_{\text{opt}},\beta_{\text{opt}})=\arg\min_{\alpha,\beta}(\text{MSE}). \tag{12}$$

The detailed analysis in (Pang *et al.*, 2000; Milivojevic *et al.*, 2004; 2006; Mirkovic *et al.*, 2004; Yarman *et al.*, 2006; Milivojevic, Mirkovic, 2009; Milivojevic, Brodic, 2011) showed that the minimum value of MSE depends on the application of window by which signal processing $x(n)$ is carried out in time domain. MSE will be defined for: (a) Hamming, (b) Hanning, (c) Blackman, (d) Rectangular, (e) Kaiser, and (f) Triangular window.

3.2. Interpolation kernel parameters

The algorithm for determination of interpolation kernel parameters α and β is realized as follows:
Step 1: Signal $x(n)$, which was previously coded and decoded by MP3 algorithm, is modified by the window function $w(n)$, length of which is N.
Step 2: Spectrum $X(k)$ is determined by application of DFT.
Step 3: Reconstruction of the continual function that represents spectrum $X(f)$ is performed by application of PCC interpolation.
Step 4: MSE is calculated for various values of parameters α and β depending on the implemented window.
Step 5: α_{opt} and β_{opt} are determined for which the minimum value of MSE is obtained.

3.3. Test signals

PCC algorithm of the fundamental frequency estimation will be applied to:

a) simulation sine test signal and
b) real speech test signal.

Simulation sine signal for testing of PCC algorithm is defined in (Pang *et al.*, 2000):

$$s(t)=\sum_{i=1}^{K}\sum_{g=0}^{M}a_i\sin\left(2\pi i\left(f_o+g\frac{f_s}{NM}\right)t+\theta_i\right), \tag{13}$$

where f_0 is fundamental frequency, θ_i and a_i are phase and amplitude of the i-th harmonic, respectively, K is the number of harmonics, and M is the number of points between the two samples in spectrum where PCC interpolation is being made. The real speech test signal is obtained by recording of a speaker in the real acoustic environment.

PCC algorithm will be applied to:
a) uncoded real speech test signals and
b) real speech test signals coded and decoded by MP3 algorithm.

The results will be summarized and comparative analysis will be established in accordance to MP3 algorithm applied to the sine test signal.

4. Experimental results and discussion

4.1. Testing parameters

In the simulation process, f_0 and θ_i are random variables with uniform distribution in the range [G2 (97.99 Hz), G5 (783.99 Hz)] and $[0, 2\pi]$ with sine and real speech test signals. Signal frequency of sampling is $f_s = 8$ kHz, and the length of window is $N = 256$, which assures the analysis of subsequences that last 32 ms. Furthermore, the results will relate to $f_0 =$ 125–140.625 Hz (frequencies between the 8-th and 9-th DFT components). Number of frequencies in the specified range, for which the estimation is done, is $M = 100$. The sine test signal is with $K = 10$ harmonics. All further analyses will relate to: (a) Hamming, (b) Hanning, (c) Blackman, (d) Rectangular, (e) Kaiser, and (f) Triangular window.

4.2. Experimental results

4.2.1. Keys kernel

By applying the algorithm for determination of Keys interpolation kernel parameters, some diagrams MSE(α) are drawn (Fig. 2 and Fig. 3), the minimum value $\mathrm{MSEK_{min}}$ is determined, and on the base of it, the optimum value of Keys kernel α_{opt} is determined for: (a) Hamming, (b) Hanning, (c) Blackman, (d) Kaiser, and (e) Triangular window functions. Values $\mathrm{MSEK_{min}}$ and α_{opt} are presented in Table 1 (uncoded sine test signal $\mathrm{MSEK_{min}}$, MP3 coded sine test signal MSEK_MP3min) and Table 2 (real speech test signal $\mathrm{MSE_{KSPmin}}$, MP3 coded real sine test signal $\mathrm{MSE_{KSP\_MP3min}}$).

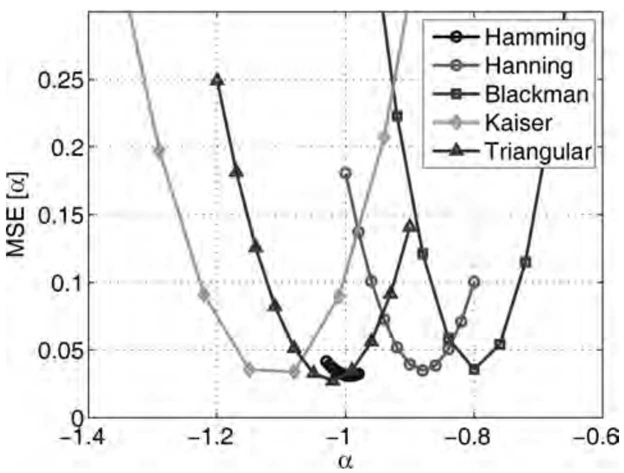

Fig. 2. MSE(α) for Keys kernel and uncompressed real speech test signal.

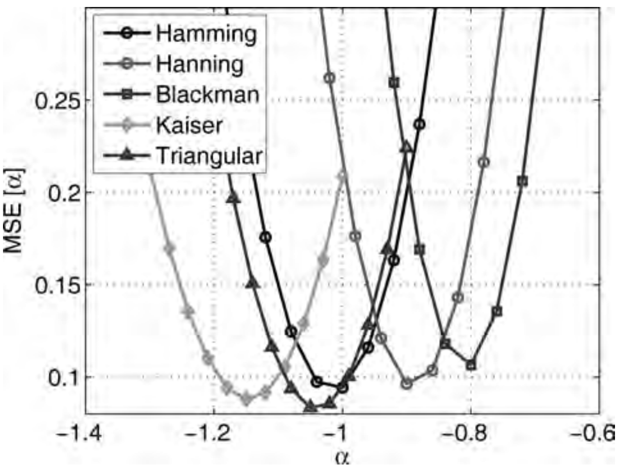

Fig. 3. MSE(α) for Keys kernel and MP3 compressed real speech test signal.

Table 1. Minimum MSE and α_{opt} for sine test signal (Keys kernel).

	Uncoded signal		Signal coded by MP3 algorithm	
	α_{opt}	$\mathrm{MSE_{Kmin}}$	α_{opt}	$\mathrm{MSE_{K\_MP3min}}$
Hamming	−1.005	0.023	−1.0100	0.0320
Hanning	−0.885	0.004	−0.8825	0.0031
Blackman	−1.801	0.001	−0.8024	0.0028
Rectangular	−2.61	0.515	−2.5500	0.4388
Kaiser	−1.125	0.02	−1.1250	0.0203
Triangular	−1.028	0.0028	−1.0280	0.0068

Table 2. Minimum MSE and α_{opt} for real speech test signal (Keys kernel).

	Uncoded signal		Signal coded by MP3 algorithm	
	α_{opt}	$\mathrm{MSE_{KSPmin}}$	α_{opt}	$\mathrm{MSE_{KSP\_MP3min}}$
Hamming	−0.995	0.0310	−1	0.0943
Hanning	−0.880	0.0349	−0.9000	0.0965
Blackman	−0.800	0.0358	−0.8000	0.1067
Rectangular	−2.400	0.4323	−2.3000	0.7011
Kaiser	−1.080	0.0339	−1.1500	0.0880
Triangular	−1.030	0.0277	−1.0500	0.0835

According to the results presented in Tables 1 and 2, it is obvious that:

a) At sine test signal, the greatest precision of fundamental frequency estimation is when Blackman window ($\mathrm{MSE_{Kmin}} = 0.001$) is applied. At MP3 coded sine test signal, the greatest precision of estimation is in Blackman ($\mathrm{MSE_{K\_MP3min}} = 0.0028$) window. When MP3 coding is applied, the precision of the fundamental frequency estimation is $\text{MSE}_{\text{K\_MP3min}}/\text{MSE}_{\text{KGmin}} = 0.0028/0.001 = 2.8$ times lower.

b) At real speech test signal, the greatest precision is in triangular window ($\text{MSE}_{\text{KSPmin}} = 0.0277$). At MP3 coded real speech signal, the greatest precision is in triangular window ($\text{MSE}_{\text{KSP\_MP3min}} = 0.0835$). When coding is applied, the precision of the fundamental frequency estimation is $\text{MSE}_{\text{KSP\_MP3min}}/\text{MSE}_{\text{KSPmin}} = 0.0835/0.0277 = 3.0144$ times lower.

c) At coded real speech signal in relation to coded sine signal, the non-precision of the fundamental frequency estimation is $\text{MSE}_{\text{KSP\_MP3min}}/\text{MSE}_{\text{K\_MP3min}} = 0.0835/0.0028 = 29.821$ times higher.

4.2.2. Greville kernel

By applying the algorithm for determination of Greville interpolation kernel parameters, some diagrams MSE(α) are drawn (Fig. 4 and Fig. 5), minimum value MSE_{Gmin} is determined, and on the base of it, the optimum value of Greville kernel parameters α_{opt} is determined for: (a) Hamming, (b) Hanning, (c) Blackman, (d) Kaiser, and (e) Triangular window. Values MSE_{min} and α_{opt} are presented in Table 3 (uncoded sine test signal MSE_{Gmin}, coded sine test signal $\text{MSE}_{\text{G\_MP3min}}$) and Table 4 (real speech test signal $\text{MSE}_{\text{GSPmin}}$, coded real speech test signal $\text{MSE}_{\text{GSP\_MP3min}}$).

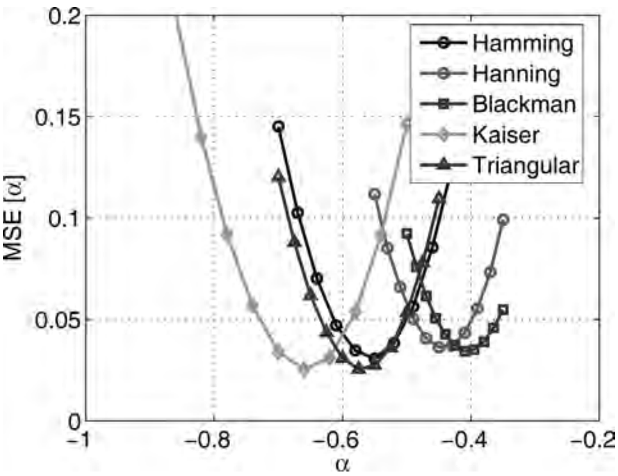

Fig. 4. MSE(α) for Greville kernel and uncompressed real speech test signal.

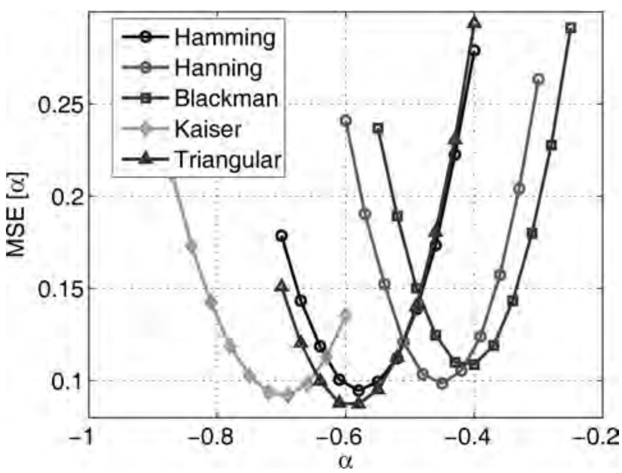

Fig. 5. MSE(α) for Greville kernel and MP3 compressed real speech test signal.

Table 3. Minimum MSE and α_{opt} for sine test signal (Greville kernel).

	Uncoded signal		Signal coded by MP3 algorithm	
	α_{opt}	MSE_{Gmin}	α_{opt}	$\text{MSE}_{\text{G\_MP3min}}$
Hamming	−0.57	0.0175	−0.5750	0.0272
Hanning	−0.449	0.0027	−0.4500	0.0032
Blackman	−0.415	0.0009	−0.4200	0.0037
Rectangular	−2.254	0.4054	−2.2000	0.3966
Kaiser	−0.6676	0.0124	−0.6600	0.0207
Triangular	−0.575	0.002	−0.5750	0.0064

Table 4. Minimum MSE and α_{opt} for real speech test signal (Greville kernel).

	Uncoded signal		Signal coded by MP3 algorithm	
	α_{opt}	$\text{MSE}_{\text{GSPmin}}$	α_{opt}	$\text{MSE}_{\text{GSP\_MP3min}}$
Hamming	−0.560	0.0310	−0.5800	0.0947
Hanning	−0.450	0.0363	−0.4500	0.0986
Blackman	−0.410	0.0344	−0.4000	0.1088
Rectangular	−2.100	0.2016	−2.2000	0.3481
Kaiser	−0.660	0.0255	−0.6900	0.0922
Triangular	−0.575	0.0256	−0.5800	0.0874

According to the results presented in Tables 3 and 4, it is obvious that:

a) At sine test signal, the greatest precision of fundamental frequency estimation is when Blackman ($\text{MSE}_{\text{Gmin}} = 0.0009$) window is applied. At MP3 coded sine test signal, the greatest precision of estimation is in Hanning window ($\text{MSE}_{\text{G\_MP3min}} = 0.0032$). When coding is applied, the precision of the fundamental frequency estimation is $\text{MSE}_{\text{G\_MP3min}}/\text{MSE}_{\text{Gmin}} = 0.0032/0.0009 = 3.55$ times lower.

b) At real speech test signal, the greatest precision is in Kaiser window ($\text{MSE}_{\text{GSPmin}} = 0.0255$). At coded real speech signal, the greatest precision is in triangular window ($\text{MSE}_{\text{GSP\_MP3min}} = 0.0874$). When coding is applied, the precision of the fundamental frequency estimation is $\text{MSE}_{\text{GSP\_MP3min}}/\text{MSE}_{\text{GSPmin}} = 0.0874/0.0255 = 3.427$ times lower.

c) At coded real speech signal in relation to coded sine signal, the non-precision of the fundamental frequency is $\mathrm{MSE}_{\mathrm{GSP\_MP3min}}/\mathrm{MSE}_{\mathrm{G\_MP3min}} = 0.0874/0.0032 = 27.31$ times higher.

4.2.3. G2P kernel

By applying the algorithm for determination of Greville two-parametric interpolation kernel parameters, some diagrams MSE(α) are drawn and minimum values $\mathrm{MSE}_{\mathrm{G2Pmin}}$ are determined for windows with the smallest MSE. Three-dimensional MSE(α, β) graphics are drawn for uncompressed real speech test signal (Fig. 6a), the shift of minimum $\mathrm{MSE}_{\mathrm{min}}$ in (α, β) level (Fig. 6b) for Blackman window, and real speech test signal coded by MP3 (Fig. 7a), the shift of minimum $\mathrm{MSE}_{\mathrm{min}}$ in (α, β) level (Fig. 7b) for Kaiser window. In Figs. 6b and 7b, positions of $\mathrm{MSE}_{\mathrm{min}} = \mathrm{MSE}(\alpha_{\mathrm{opt}}, \beta_{\mathrm{opt}})$ minimum in (α, β) plane for Greville (point **A**) and G2P (point **B**) interpolation kernel are shown. Vector **AB** shows the position change of the minimum (MSE(α_{opt}, β_{opt})). The determined parameters α_{opt} and β_{opt} are presented in Table 5.

a)

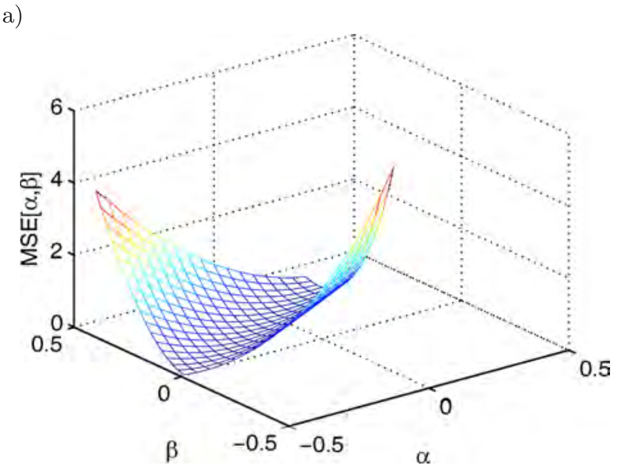

b)

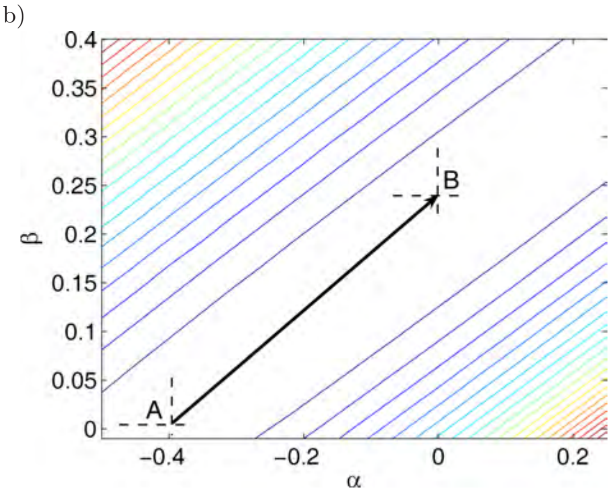

Fig. 6. Real speech test signal with the application of Blackman window without compression: a) MSE(α, β) for the application of G2P PCC interpolation; b) positions of min(MSE(α_{opt}, β_{opt})) in plane (α, β) for Greville (point **A**) and G2P PCC (point **B**) interpolation.

a)

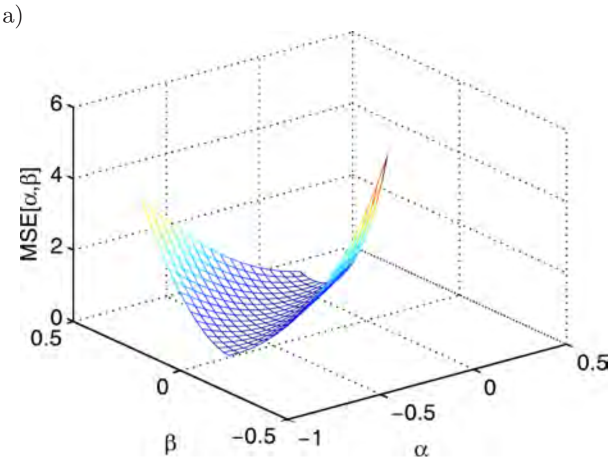

b)

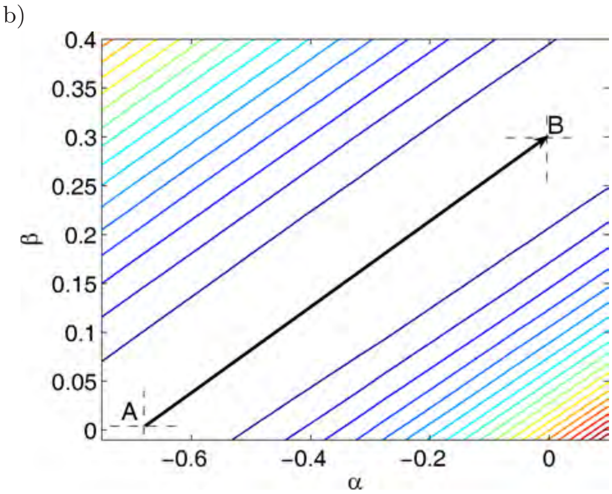

Fig. 7. Real speech test signal with the application of Kaiser window with MP3 compression: a) MSE(α, β) for the application of G2P PCC interpolation; b) positions of min(MSE(α_{opt}, β_{opt})) in plane (α, β) for Greville (point **A**) and G2P PCC (point **B**) interpolation.

According to the results presented in Table 5, it is obvious that:

a) At real speech test signal with G2P kernel comparing with Greville kernel, the precision of the fundamental frequency estimation ($\mathrm{MSE}_{\mathrm{GSP\_MP3min}}/\mathrm{MSE}_{\mathrm{G2PSP\_MP3min}}$) is: (a) 1.57 (Hamming), (b) 1.76 (Hanning), (c) 1.83 (Blackman), (d) 1.75 (Kaiser), and (e) 1.5 (Triangular) times higher.

b) At real speech test signal, the greatest precision is in Blackman window ($\mathrm{MSE}_{\mathrm{GSPmin}} = 0.0009$). At MP3 coded real speech signal, the greatest precision is in Kaiser window ($\mathrm{MSE}_{\mathrm{G2PSP\_MP2min}} = 0.0524$). When MP3 coding with G2P kernel is applied, the precision of the fundamental frequency estimation is $\mathrm{MSE}_{\mathrm{G2PSP\_MP3min}}/\mathrm{MSE}_{\mathrm{GSPmin}} = 0.0524/0.0009 = 58.22$ times lower.

c) At MP3 coded real speech with Greville kernel, the greatest precision is in Triangular window ($\mathrm{MSE}_{\mathrm{GSPmin}} = 0.0874$). At MP3 coded real speech

Table 5. Minimum MSE, α_{opt}, and β_{opt} (G2P kernel).

Sine test signal (uncoded)			
Window	α_{opt}	β_{opt}	$\mathrm{MSE}_{\mathrm{G2Pmin}}$
Hamming	−0.55	0.03	0.0046
Hanning	0.5	0.015	0.0018
Blackman	−0.42	0.002	0.000377
Kaiser	−0.681	0.001	0.0096
Triangular	0.6	−0.001	0.001
Sine test signal (coded by MP3 algorithm)			
Window	α_{opt}	β_{opt}	$\mathrm{MSE}_{\mathrm{G2P\_MP3min}}$
Hamming	−0.5900	−0.0060	0.0270
Hanning	−0.4600	−0.0060	0.0029
Blackman	−0.4200	−0.0020	0.0022
Kaiser	−0.6600	0.0060	0.0178
Triangular	−0.5680	0.0030	0.0060
Real speech test signal (uncoded)			
Window	α_{opt}	β_{opt}	$\mathrm{MSE}_{\mathrm{G2PSPmin}}$
Hamming	0.1	0.2975	0.0072
Hanning	0.1531	0.2719	0.0025
Blackman	0.0625	0.2463	0.001
Kaiser	−0.1	0.2463	0.0075
Triangular	−0.3219	0.1181	0.0016
Real speech test signal (coded by MP3 algorithm)			
Window	α_{opt}	α_{opt}	$\mathrm{MSE}_{\mathrm{G2PSP\_MP3min}}$
Hamming	0.0687	0.2788	0.0600
Hanning	0.0625	0.2375	0.0559
Blackman	−0.0625	0.1738	0.0592
Kaiser	−0.0062	0.2975	0.0524
Triangular	−0.3500	0.1194	0.0581

signal with G2P kernel, the greatest precision is in Kaiser window ($\mathrm{MSE}_{\mathrm{G2PSP\_MPmin}} = 0.0524$). When MP3 coding with G2P kernel is applied, the precision of the fundamental frequency estimation is $\mathrm{MSE}_{\mathrm{GSPmin}}/\ \mathrm{MSE}_{\mathrm{G2PSP\_MP3min}} = 0.0874/0.0524 = 1.66$ times higher.

5. Comparative analysis

The comparative analysis of the estimated fundamental frequency for the sine test signal and the real speech test signal, without and with MP3 compression, will be performed on the base of MSE minimum values. The minimum value of MSE is determined on the base of the diagram in the Figs. 2 and 3 (Keys), Figs. 4 and 5 (Greville), and Figs. 6 and 7 (G2P). It is presented in Table 1 ($\mathrm{MSE}_{\mathrm{Kmin}}$, $\mathrm{MSE}_{\mathrm{K\_MP3min}}$), Table 2 ($\mathrm{MSE}_{\mathrm{KSPmin}}$, $\mathrm{MSE}_{\mathrm{KSP\_MP3min}}$), Table 3 ($\mathrm{MSE}_{\mathrm{Gmin}}$, $\mathrm{MSE}_{\mathrm{G\_MP3min}}$), Table 4 ($\mathrm{MSE}_{\mathrm{GSPmin}}$, $\mathrm{MSE}_{\mathrm{GSP\_MP3min}}$), and Table 5 ($\mathrm{MSE}_{\mathrm{G2Pmin}}$, $\mathrm{MSE}_{\mathrm{G2P\_MP3min}}$, $\mathrm{MSE}_{G2PSPmin}$, $\mathrm{MSE}_{\mathrm{G2PSP\_MP3min}}$), respectively.

Comparing the values $\mathrm{MSE}_{\mathrm{min}}$ from Tables 1–5, it can be concluded that:

a) The optimum choice for sine test signal is Blackman window for all interpolation kernels. G2P interpolation kernel, which generates MSE by 60.05% less than Keys and 55.55% less than Greville kernel, showed the best results.

b) The optimum choice for real speech test signal is G2P kernel with Blackman window, which generates MSE by 96.387% less than Keys kernel (Triangular window), and 96.07% less than Greville kernel (Kaiser window).

c) The optimum choice for sine test signal coded by MP3 algorithm is G2P interpolation kernel with Blackman window, which generates MSE by 21.43% less than Keys (Blackman window) and 31.25% less than Greville kernel (Kaiser window), showed the best results.

d) The optimum choice for real speech test signal coded by MP3 algorithm is G2P interpolation kernel with Kaiser window, which generates MSE by 37.27% less than Keys (Triangular window) and 43.16% less than Greville kernel (Kaiser window), showed the best results.

e) Comparing MSE for G2P kernel for uncoded real speech test signal (Blackman window, $\mathrm{MSE}_{\mathrm{G2PSPmin}} = 0.0022$) and MP3 coded real speech test signal (Kaiser window, $\mathrm{MSE}_{\mathrm{G2PSP\_MP3min}} = 0.0524$), relation $\mathrm{MSE}_{\mathrm{G2PSP\_MP3min}}/\mathrm{MSE}_{\mathrm{G2PSPmin}} = 0.0524/\ 0.0022 = 23.818$ has been obtained.

Comparison of the estimation of the fundamental frequency for the signal coded with SYMPES algorithm (Milivojevic, Mirkovic, 2009), G.723.1 algorithm (Milivojevic, Brodic, 2011), and MP3 algorithm with real speech test signal given in this paper shows that the proposed algorithm has the least MSE values. Accordingly, the obtained results recommend the use of PCC algorithm with G2P kernel in preprocessing signals which are compressed by MP3 method. Hence, it is recommended for further processing by algorithms that require a precise determination of the fundamental frequency (automatic verification of a speaker, recognition of the speech, etc.).

6. Conclusions

This paper presents the comparative analysis of the fundamental frequency estimation for the real speech signal modeled by MP3 method. The estimation of the fundamental frequency has been made by the Picking-Peaks algorithm with implemented PCC interpolation. Experiments have been performed with Keys, Greville, and Greville two-parametric kernels. In order to minimize MSE, different windows have been implemented. The detailed analysis has shown that the optimal choice is Greville two-parametric kernel and the Kaiser window implemented in PCC algorithm. The optimum choice for real speech test signal coded by MP3 algorithm is G2P interpolation kernel with Kaiser window, which generates MSE by 37.27% less than Keys (Triangular window) and 43.16% less than Greville kernel (Kaiser window). Comparing these results with the results of the estimation of the fundamental frequency in the real speech signal that is not modeled by MP3 method, the relation of minimum MSEs 23.818 has been obtained. Comparison between algorithms shows MSE for SYMPES ($\text{MSE}_{\min} = 3.174$) and G.723.1 algorithm ($\text{MSE}_{\min} = 0.2898$), and for the proposed MP3 algorithm ($\text{MSE}_{\min} = 0.0524$). These results prove the quality of the proposed solution. Hence, the obtained results recommend the use of PCC algorithm with G2P kernel in preprocessing of signals compressed by MP3 method for further processing by algorithms which require a precise determination of the fundamental frequency.

References

1. Atal B. (1972), *Automatic speaker recognition based on pitch contours*, Journal of the Acoustical Society of America, **52**, 6, 1687–1697.
2. Avila F., Biscainho L. (2012), *Bayesian Restoration of Audio Signals Degraded by Impulsive Noise Modeled as Individual Pulses*, IEEE Transactions On Audio, Speech, And Language Processing, **20**, 9, 2470–2481.
3. Ayadi M., Kamel M., Karray F. (2011), *Survey on speech emotion recognition: Features, classification schemes, and databases*, Pattern Recognition, **44**, 572–587.
4. Barbancho I., Tardon L., Sammartino S., Barbancho A. (2012), *Inharmonicity-Based Method for the Automatic Generation of Guitar Tablature*, IEEE Transactions On Audio, Speech, And Language Processing, **20**, 6, 1857–1868.
5. Brandenburg K., Stoll G., Dehery Y.F., Johnston J.D., Kerkhof L.V., Schroeder E.F. (1992), *The ISO/MPEG Audio Codec: A Generic Standard for Coding of High Quality Digital Audio*, 92nd. AES-convention, preprint 3336, Vienna.
6. Britanak V. (2011), *A survey of efficient MDCT implementations in MP3 audio coding standard: Retrospective and state-of-the-art*, Signal Processing, **91**, 624–672.
7. Dhar P.K., Echizen I. (2011), *Robust FFT Based Watermarking Scheme for Copyright Protection of Digital Audio Data*, Seventh International Conference on Intelligent Information Hiding and Multimedia Signal Processing (IIH-MSP), 181–184.
8. Fragoulis D., Papaodysseus C., Exarhos M., Roussopoulos G., Panagopoulos T., Kamarotos D. (2006), *Automated classification of piano-guitar notes*, IEEE Transactions On Audio, Speech, And Language Processing, **14**, 3, 1040–1050.
9. Griffin D., Lim J. (1988), *Multiband excitation vocoder*, IEEE Transactions On Audio, Speech, And Language Processing, **36**, 8, 1223–1235.
10. Hacker S. (2000), *MP3: The Definitive Guide*, O'Reilly & Associates, Sebastopol, CA 95472.
11. Hussain Z.M., Boashash B. (2002), *Adaptive instantaneous frequency estimation of multicomponent signals using quadratic time-frequency distributions*, IEEE Transaction on Signal Processing. **50**, 8, 1866–1876.
12. ISO/IEC (1992), *Information Technology – Coding of Moving Pictures and Associated Audio for Digital Storage Media at up to about 1.5 Mbit/s, Part3: Audio*, ISO/IEC JTC1/SC29/WG11 MPEG, International Standard 11172-3 (MPEG-1).
13. ISO/IEC 13818-3 (1994), *Information Technology. Generic Coding of Moving Pictures and Associated Audio: Audio.* ISO/IEC JTC1/SC29/WG11 MPEG, International Standard 13818-3(MPEG-2), 1994.
14. Joen B., Kang S., Baek S.J., Sung K.M. (2003), *Filtering of a Dissonant Frequency Based on Improved Fundamental Frequency Estimation for Speech Enhancement*, IEICE Trans. Fundamentals, E86-A, **8**, 2063–2064.
15. Kacha F., Benmahammed G.K. (2005), *Time–frequency analysis and instantaneous frequency estimation using two-sided linear prediction*, IEEE Signal Processing, **85**, 491–503.
16. Kang S. (2004),*Dissonant frequency filtering technique for improving perceptual quality of noisy speech and husky voice*, IEEE Signal Processing, **84**, 431–433.
17. Kang S., Kim Y. (2006), *A Dissonant Frequency Filtering for Enhanced Clarity of Husky Voice Signals*, Lecture Notes Comp Science, **4188**, Berlin Springer, 517–522.
18. Kawahara H., Katsuse I., Cheveigne A. (1999), *Restructuring speech representations using a pitch-adaptive time-frequency smoothing and an instantaneous-frequency-based f0 extraction: Possible role of a repetitive structure in sounds*, Speech Communication, **27**, 3–4, 187–207.
19. Kawahara C.H. (2002), *YIN, a fundamental frequency estimator for speech and music*, Journal of the Acoustical Society of America, **111**, 4, 1917–1930.
20. Keys R.G. (1981), *Cubic convolution interpolation for digital image processing*, IEEE Transaction on Acoustics, Speech & Signal Processing, **29**, 6, 1153–1160.
21. Klapuri A. (2003), *Multiple fundamental frequency estimation based on harmonicity and spectral smoothness*, IEEE Transactions On Audio, Speech, And Language Processing, **11**, 6, 804–816.
22. McCandless M. (1999), *The MP3 revolution*, IEEE Intelligent Systems and their Applications, **14**, 3, 8–9.

23. Meijering E., Unser M. (2003), *A Note on Cubic Convolution Interpolation*, IEEE Transaction on Image Processing, **12**, 4, 447–479.

24. Milivojevic Z., Mirkovic D. (2009), *Estimation of the fundamental frequency of the speech signal modeled by the SYMPES method*, International Journal of Electronics and Communications (AEU), **63**, 200–208.

25. Milivojevic Z., Mirkovic M., Rajkovic P. (2004), *Estimating of the fundamental frequency by the using of the parametric cubic convolution interpolation*, Proceedings of International Scientific Conference UNITECH '04, 138–141, Gabrovo, Bulgaria.

26. Milivojevic Z., Brodic D. (2011), *Estimation of the Fundamental Frequency of the Speech Signal Compressed by G.723.1 Algorithm Applying PCC Interpolation*, Journal of Electrical Engineering, **62**, 4, 181–189.

27. Milivojevic Z., Mirkovic M., Milivojevic S. (2006), *An Estimate of Fundamental Frequency Using PCC Interpolation – Comparative Analysis*, Infornation Technology and Control, **35**, 2, 131–136.

28. Milivojevic Z., Milivojevic M., Brodic D. (2012), *The Effects of the Acute Hypoxia to the Fundamental Frequency of the Speech Signal*, Advances in Electrical and Computer Engineering, **12**, 2, 57–60.

29. Mirkovic M., Milivojevic Z., Rajkovic P. (2004), *Performances of the system with the implemented PCC algorithm for the fundamental frequency estimation*, Proceedings of XII Telecommunications Forum TELFOR '04, Section 7, Signal processing, Beograd.

30. Moon H. (2012), A Low-Complexity Design for an MP3 Multi-Channel Audio Decoding System, IEEE Transactions On Audio, Speech, and Language Processing, **20**, 1, 314–321.

31. Pang H.S., Baek S.J., Sung K.M. (2000), *Improved Fundamental Frequency Estimation Using Parametric Cubic Convolution*, IEICE Trans. Fund., **E83-A**, 12, 2747–2750.

32. Park K.S., Schowengerdt R.A. (1983), *Image reconstruction by parametric cubic convolution*, Computing, Vision, Graphics & Image Processing, **23**, 258–272.

33. Rabiner L. (1977), *On the use of autocorrelation analysis for pitch detection*, IEEE Transactions On Acoustic, Speech, Signal Processing, ASSP-25, 1, 24–33.

34. Resch B., Nilsson M., Ekman A., Kleijn W. (2007), *Estimation of the instantaneous pitch of speech*, IEEE Transactions On Audio, Speech, And Language Processing, **15**, 3, 813–822.

35. Ross M., Schafer H., Cohen A., Freudberg R., Manley H. (1974), *Average magnitude difference function pitch extractor*, IEEE Transactions On Acoustic, Speech, Signal Processing, ASSP-22, 5, 353–362.

36. Sekhar S.C., Sreenivas T.V. (2004), *Effect of interpolation on PWVD computation and instantaneous frequency estimation*, IEEE Signal Processing, **84**, 107–116.

37. Shahnaz C., Zhu W., Ahmad M. (2012), *Pitch Estimation Based on a Harmonic Sinusoidal Autocorrelation Model and a Time-Domain Matching Scheme*, IEEE Transactions On Audio, Speech, And Language Processing, **20**, 1, 310–323.

38. Veprek P., Scordilis M. (2002), *Analysis, enhancement and evaluation of five pitch determination techniques*, Speech Communication, **37**, 3–4, 249–270.

39. Wang X., Hong H. (2006), *A Novel Synchronization Invariant Audio Watermarking Scheme Based on DWT and DCT*, IEEE Transactions on Signal Processing, **54**, 12, 4835–4840.

40. Yarman B., Guz U., Gurkan H. (2006), *On the comparative results of SYMPES: A new method of speech modeling*, International Journal of Electronics and Communications (AEU), **60**, 421–427.

41. Yeo I., Kim H.J. (2003), *Modified patchwork algorithm: a novel audio watermarking scheme*, IEEE Transactions on Speech and Audio Processing, **11**, 4, 381–386.

PAN ARCHIVES OF ACOUSTICS
Vol. **38**, No. 3, pp. 375–381 (2013)

DOI: 10.2478/aoa-2013-0044

Pitch Processing of Speech: Comparison of Psychoacoustic and Electrophysiological Data

Małgorzata WRZOSEK[(1)], Justyna MACULEWICZ[(1)], Honorata HAFKE-DYS[(2)], Agnieszka NOWIK[(3)], Anna PREIS[(2)], Grzegorz KROLICZAK[(4)]

[(1)] *Institute of Psychology, Adam Mickiewicz University*
Szamarzewskiego 89, 60-568 Poznań, Poland; e-mail: wrzosek.gosia@gmail.com

[(2)] *Institute of Acoustics, Adam Mickiewicz University*
Umultowska 85, 61-614 Poznań, Poland

[(3)] *Department of Biophysics, Poznań University of Medical Sciences*
Fredry 10, 61-701 Poznań, Poland

[(4)] *Institute of Psychology, Cognitive Science Program, Head, Action, Cognition Laboratory, Adam Mickiewicz University*
Szamarzewskiego 89B, 60-568 Poznań, Poland

(*received September 30, 2012; accepted June 14, 2013*)

The present study consisted of two experiments. The goal of the first experiment was to establish the just noticeable differences for the fundamental frequency of the vowel /u/ by using the 2AFC method. We obtained the threshold value for 27 cents. This value is larger than the motor reaction values which had been observed in previous experiments (e.g. 9 or 19 cents). The second experiment was intended to provide neurophysiological confirmation of the detection of shifts in a frequency, using event-related potentials (ERPs). We concentrated on the mismatch negativity (MMN) – the component elicited by the change in the pattern of stimuli. Its occurrence is correlated with the discrimination threshold. In our study, MMN was observed for changes greater than 27 cents – shifts of ±50 and 100 cents (effect size – Cohen's $d = 2.259$). MMN did not appear for changes of ±10 and 20 cents. The results showed that the values for which motor responses can be observed are indeed lower than those for perceptual thresholds.

Keywords: pitch processing of speech, auditory perception-motor dissociation, mismatch negativity.

1. Introduction

The idea that there is a co-existence of two processing pathways in the visual cortex was first postulated in 1969 by Schneider. Thirteen years later, the hypothesis was developed by Ungerleider and Mishkin who consolidated the division of the visual processing systems into the ventral pathway – *what*, responsible for identifying visual objects, and the dorsal pathway – *where*, responsible for locating the stimulus (Ungerleider, Mishkin, 1982). The famous study of Patient D.F., a woman with damage in the brain region called the lateral occipital complex (LOC), enriched this attitude towards vision, in particular with regard to the visually guided action (Milner, Goodale, 1995; Goodale, Milner, 2004).

Growing interest in the functional organization of the auditory cortex has led to increased interest in whether or not there are two processing pathways in the auditory modality. Some researchers decided to try to find auditory systems similar to those found in the visual domain. Despite the consensus on what tasks the ventral pathway performs (involvement in the perception of sound source attributes), the role of the dorsal pathway is still controversial, dividing the researchers into two groups – those who view the pathway as being involved in the perceptual location of sounds and those who view the pathway as a functional auditory system responsible for motor activity. Researchers from the latter group claim that the dorsal pathway does more than merely localize sound sources and is in fact involved in the planning and output of motor response (in speech or body movements). According to the present state of research, this function is mainly carried out in speech (Hickok, Poeppel, 2004; Warren *et al.*, 2005; Hafke, 2008; 2009) or rhythm control (Repp, 2000; 2006).

Demonstrating the existence of the action pathway seems to be most effective in the case of automatic responses to perceptually unnoticed stimuli or to perceptually undetected changes in the sound stimuli reaching our auditory system. A variety of studies have demonstrated that the introduction of changes to real time auditory feedback (to self-generated sounds during vocalization) elicits compensative reactions with a latency of 100–150 ms in listeners, with speech sounds (Xu *et al.*, 2004; Chen *et al.*, 2007), consonants (Donath *et al.*, 2002; Natke, Kalveram, 2001; Natke *et al.*, 2003), and vowels (Burnett *et al.*, 1998; Larson *et al.*, 1996; Larson, 1998; Burnett, Larson, 2002; Sivasankar *et al.*, 2005; Liu, Larson, 2007; Hafke, 2008). It has been shown that compensative reactions to shifts in fundamental frequency remain the same when the listeners follow instructions not to respond to changes in feedback (Hain *et al.*, 2000). In the aforementioned studies, various interval values were used to introduce changes in the voice fundamental frequency. The easily noticed shift of 100 cents (one semitone) was most commonly used (Natke, Kalveram, 2001; Burnett, Larson, 2002; Donath *et al.*, 2002; Sivasankar *et al.*, 2005). A compensative reaction to much smaller shifts in auditory feedback was demonstrated in more recent studies (Liu, Larson, 2007; Hafke, 2008; Jones, Keough, 2009). The authors managed to observe a complete compensation for shifts as small as 9 cents (Hafke, 2008) and 10 cents (Liu, Larson, 2007). The main question is whether these minor frequency changes were consciously perceived, or whether they were due to their location being below the perception threshold and processed by a separate system. Hafke's study (Hafke, 2008) checked if the changes by ±9, 19, 50 and 100 cents introduced in feedback were perceived by listeners. The perceptual threshold of 26 cents was established, indicating that shifts of ±9 and 19 cents were not consciously perceived, yet while motor reactions were observed for them. To confirm Hafke's hypothesis that some compensative reactions are not followed by a conscious detection of change, the authors decided to also test brain responses to changes of 10, 20, 50 and 100 cents in both directions (±) by using the mismatch negativity (MMN) component. The aim of this part of the study was to test whether this EEG component, which occurs when a change in the pattern is perceived (Näätänen *et al.*, 1978; 2007; Näätänen, Alho, 1995; Picton *et al.*, 2000), would appear for changes in the fundamental frequency of the recorded vowel /u/ which, according to Hafke, are not consciously perceived. Positive verification – lack of an MMN response to changes of 10 and 20 cents – may suggest the existence of a separate pathway in the auditory system, unrelated to the perception motor pathway and designed to unconsciously control self-generated sounds.

The authors decided to perform a combined experiment (with two groups of participants – one for the psychophysical part, and one for the electrophysiological part) in order to: (1) determine the threshold of discrimination for the fundamental frequency (psychoacoustic approach); and (2) test whether the MMN component would appear for shifts in the fundamental frequency of vowel /u/ which, according to Hafke, are not perceived (electrophysiological approach).

2. Psychophysical experiment

2.1. Participants

Twenty-four listeners (9 men, 15 women), aged between 19 and 28, took part in the psychoacoustic part of this study. All the listeners were classified as having normal hearing, with normal hearing defined as the audiometric threshold of 20 dB (or better) hearing level for the range from 250 Hz to 8000 Hz (American National Standards Institute [ANSI], 1996). No neurological defects, speech disorders, or voice disorders were reported.

2.2. Procedure

In the first part of this study, an adaptive two-alternative forced choice (2AFC) procedure was used (Kingdom, Prins, 2010; Blauert, 2012; Blauert, Jekosch, 2012). Due to the previous use of the vowel /u/ in order to determine motor reactions (Hafke 2008; Liu, Larson, 2007), recordings of this vowel used were again as the stimulus. The recordings were prepared in an acoustically treated lecture booth using a G.R.A.S. 40AN omnidirectional microphone placed 40 cm from the mouth. A 44,100 Hz sampling frequency with 24 bits resolution was chosen to record the signals, using an RME DIGI96 PRO audio interface. The phase vocoder based on algorithm written in the MATLAB environment (Laroche, Dolson, 1999) served as the modifier of the pitch of the speech material. Two different recordings of female voices (vowel /u/) with the frequency of 247 Hz were used. The recordings only varied in timbre in order to ensure that the listeners did not adapt to one specific timbre. The duration of all stimuli was 2 s (the fragment of vocalization with the smallest deviation). The interval between the presented sounds was set to 0.5 s. All recordings were provided with 50 ms Hanning amplitude ramps at the beginning and the end of each stimulus. In each trial, sound examples were randomly chosen. All the stimuli had the same fundamental frequency and an equal RMS level. Before each trial, one of the two speakers was randomly chosen (for the testing and reference sound). The probability of the reference sound to be presented was equal: either as the first or second of the two sounds. The task required the listeners to decide which of the two sounds had the higher frequency. A single training session of 20 trials was used with feedback (information whether or not their answers were correct) in order to familiarize the listeners with the signals used. During the experiment, no feedback was provided. Starting with the difference of 100 cents between the sounds in a pair, the "2-yes 1-no" variant of the 2AFC procedure was used. The choice of this method resulted in decreasing the difference between sounds after two consecutive correct answers and increasing after each incorrect answer. A discrimination threshold was established, corresponding to a 70.07% probability of being correct. Multiplicative steps were used in the procedure, with two values of 1.5 and 1.25, respectively. At the beginning of the experiment, changes were introduced with the bigger step, and after the second reversal any further changes were made with the smaller step. Until the 12th reversal was reached, trials for each of the threshold values were continued. A single threshold value was calculated for each subject as an average of the values at the 8 final reversals. Three adaptive runs served as the basis for the final threshold value. All the signals were rendered on a PC connected with an equalizer (HEAD acoustics PEQ V) and presented over Sennheiser HD600 headphones. This part of the study was conducted in an acoustically treated listening booth.

3. Electrophysiological experiment

3.1. Participants

The EEG part of the study included seven participants (3 males, 4 females) with the mean age of 24.2 years (SD = 1.9). All the listeners were classified as having normal hearing, defined as the audiometric threshold of 20 dB (or better) hearing level for the range from 250 Hz to 8000 Hz (ANSI, 1996). Results from one person were excluded from further analyzes due to an error in the data file. Eventually, five right-handed participants and one left-handed participant were included in the analysis. No neurological deficits or serious head injuries in the past were reported. Only one person had had a musical education. This part of the study was conducted at the Action and Cognition Laboratory at the Institute of Psychology at Adam Mickiewicz University in Poznan, with the approval of the Ethics Committee of the Institute of Psychology at Adam Mickiewicz University in Poznan.

3.2. Procedure

During the experiment, participants were sitting in chairs with armrests at a distance of 80 cm from the fixation point which was located at the eye level. In the experiment, there were 960 repetitions of 9 types of recordings of the vocalized vowel /u/ (the same stimuli provided by Hafke (2008)). The recordings were presented in random order to the listeners. The whole presentation consisted of 720 repetitions of standard stimuli with a fundamental frequency of 247 Hz and 240 deviant stimuli with positive and negative shifts in frequencies of 10, 20, 50 or 100 cents.

The stimulus duration was set to 250 ms, with the interval between stimuli of 140 ms. The experiment was controlled by the Presentation 0.52 (Neurobehavioral System) software and the sounds were presented binaurally through ER-2 Etymotic Research headphones. Participants were instructed to focus their attention on a fixation point.

Electrophysiological brain responses were collected using the BioSemi ActiveTwo system. The 64 electrodes with DC amplifiers were set in accordance with the 10–20 system (Jasper, 1958). The EEG signal was recorded with a sampling rate of 1024 Hz. The removal of artifacts related to eye-movement signals was based on electrooculography (EOG). The EOG signal was recorded bipolarly with electrodes placed at the outer left and right lateral canthus (hEOG), above and below (vEOG) the left eye. During acquisition, reference was averaged across all the channels.

The EEG analysis was performed using Brain Vision Analyzer 2 (Brain Products GmbH, Munich, Germany). At the beginning, the signal was re-referenced off-line into two electrodes placed at the left and right mastoid. The filter band-pass set to 0.1–30 Hz (12 dB octave/slope) was used. The registered EEG signal was divided into segments with a length of 400 ms (from 50 ms before stimulus onset to 100 ms after stimulus offset, with a stimulus which lasted 250 ms). Baseline correction was performed by averaging the signal within the interval of 50 ms before presentation of the stimulus. The time window for MMN was set for the 160–220 ms after stimulus onset (Luck, 2005).

4. Results

The results of the experiments are presented in Fig. 1. In the psychophysical part of the study, the average frequency threshold value amounts to 27 cents (Fig. 1a). For comparison, Fig. 1a additionally includes the values obtained in the previous experiment (Hafke, 2008).

The distribution of results for the female and male listener groups can be treated as normally distributed, as shown in the Shapiro-Wilk test. Statistical differ-

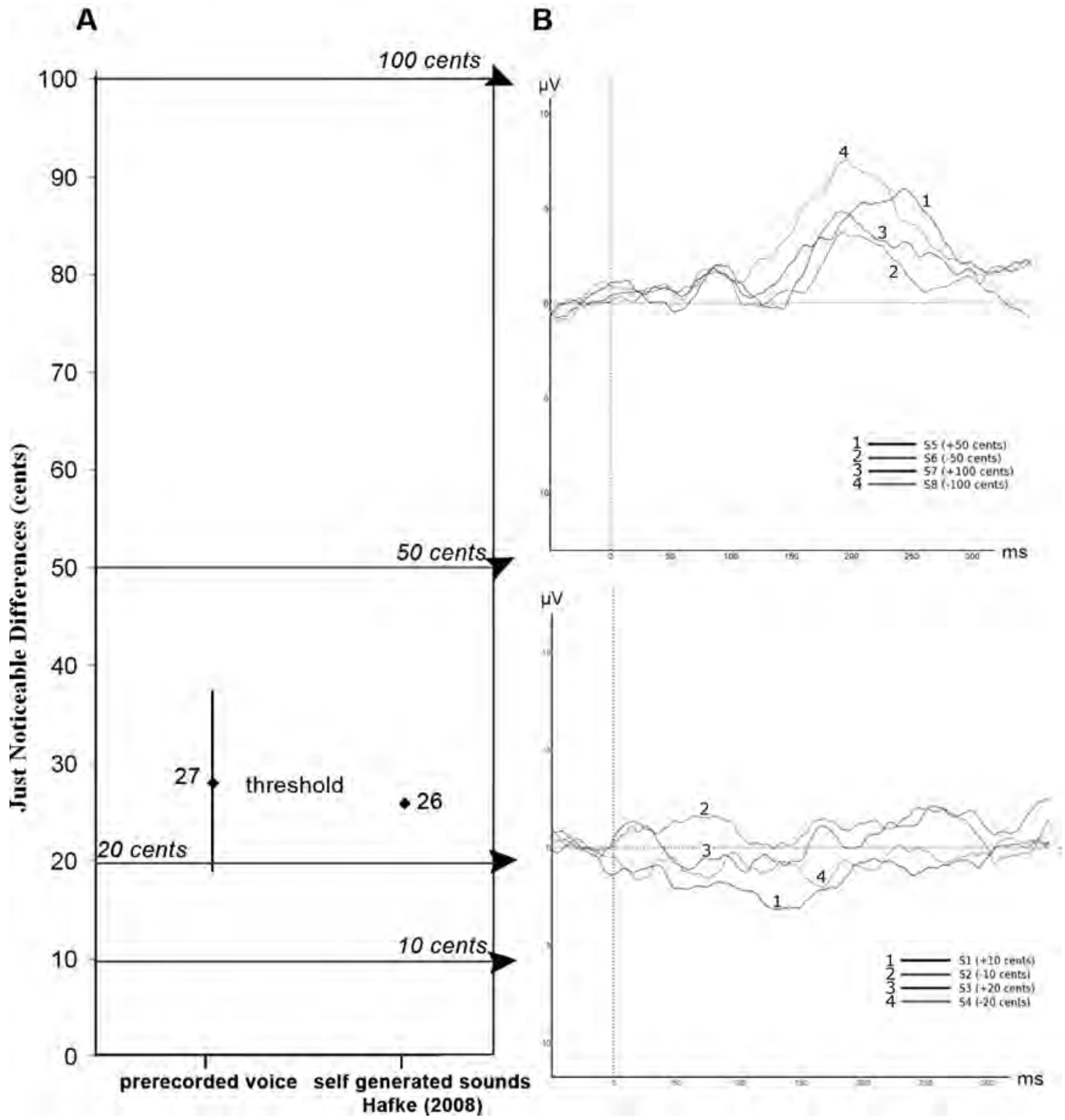

Fig. 1. Results: (**A**) The psychophysical part – the discrimination threshold established for 27 cents with confidence interval marked (value of 26 cents obtained in the previous experiment (Hafke, 2008) is on the right-hand side of the diagram); horizontal lines refer to shifts (of 10, 20, 50 and 100 cents) used in the EEG part – shifts of 50 and 100 cents and each shift larger than 27 cents are noticeable and should elicit MMN response; shifts of 10 and 20 cents are unnoticeable. (**B**) EEG part – deviant-minus-standard grand average difference waveforms at electrode Fz for noticeable (upper panel: ±50, 100 cents) and not noticeable shifts (lower panel: ±10 and 20 cents).

ences between the responses of the two gender groups ($F(1,\ 44) = 0.01$; $p = 0.93$) were not observed.

The occurrence of MMN for shifts of ±50 and ±100 cents is interpreted as a proof that changes in the frequency of vowel /u/ were detected. Any significant appearance of mismatch negativity was not recorded for undetected shifts (±10 and 20 cents) (Fig. 1b).

The obtained results were subjected to statistical analysis in IBM SPSS Statistics 20.0. The average MMN amplitude for stimuli containing a perceptually detectable shift was – 6.166 μV (SD = 3.172, SE = 0.647). The average amplitude for wave with the MMN-like latency for stimuli containing perceptually undetectable shifts (MMN was not elicited for these shifts) was – 1.582 μV (SD = 2.347, SE = 0.479). The average amplitude for the standard was – 0.732 μV (SD = 1.229, SE = 0.502). The average MMN or MMN-like latency for all stimuli was 195.245 ms (SD = 21.512, SE = 2.928).

Statistically significant differences ($F(8,\ 40) = 8.362$, $p < 0.001$) between the amplitudes of particular stimuli were observed, as shown in general linear model, repeated measures. Analysis of contrasts indicated that amplitudes for deviants with a change of +50, +100 and −100 cents comparing to standard stimuli were statistically significant (respectively:

$F(1, 5) = 24.475$, $p = 0.004$; $F(1, 5) = 15.387$, $p = 0.011$; $F(1, 5) = 27.373$, $p = 0.003$). When a 50 cent negative change was obtained, the result did not differ significantly from the standard ($F(1, 5) = 5.267$, $p = 0.07$). The same analysis of contrasts showed that changes of +10, −10, +20 and −20 cents did not elicit a statistically significant change in MMN amplitude when compared to the standard ($F(1, 5) = 0.050$, $p = 0.833$; $F(1, 5) = 2.415$, $p = 0.181$; $F(1, 5) = 5.448$, $p = 0.067$; $F(1, 5) = 0.742$, $p = 0.429$, respectively).

There were no significant differences in the amplitude of the mismatch negativity between the participants ($F(5, 48) = 0.936$, $p = 0.466$). The significance of differences in amplitudes of stimuli belonging to one from the three post-hoc one-way ANOVA groups – one containing shifts of ±10 and 20 cents (which did not elicit MMN response), the second containing shifts of ±50 and 100 cents (which elicited the MMN response) and the third containing standard stimuli (no shift) – was investigated. This relation was significant ($F(2, 51) = 21.250$, $p < 0.001$). A post-hoc two-sided Dunnett's Test was used to show that (1) these groups were significantly different from each other; (2) stimuli with detectable shifts (±50 and ±100 cents) differed significantly from the standard ($p < 0.001$); (3) deviants with shifts of 10 and 20 cents (undetectable shifts) did not differ significantly from the standard ($p = 0.646$); and (4) stimuli with detectable shifts differed significantly from stimuli with undetectable shifts ($p < 0.001$).

Cohen's d was calculated to demonstrate the effect size. In the case of the group containing undetectable shifts in comparison to the group containing standard stimuli, $d = 0.454$, while in the case of the group containing detectable shifts in comparison to the group containing standard stimuli, $d = 2.259$.

5. Discussion

In the previous experiment (2008), Hafke established for the fundamental frequency of self-generated sounds a perceptual threshold of 26 cents, using the method of the constant stimuli. In the psychoacoustic part of the present study there was no need for the subjects to produce speech sounds; participants were asked only to listen to speech that was generated externally. Although different experimental conditions and different psychophysical methods were used, the obtained perceptual threshold was almost the same.

The psychoacoustic part of the present study suggests that the motor reactions observed in the previous experiments were not associated with conscious perception of the introduced pitch changes. In summary, regardless of whether we look at the perception threshold for self-generated sounds (Hafke, 2008) or externally generated sounds (the present study), and regardless of the psychophysical method used, the perception threshold is always greater than the value for which motor reactions can be observed.

The independent confirmation was delivered by the second part of the present study. It turned out that the mismatch negativity (MMN), a component whose appearance is related to the detection of a perceptual deviation from a standard, was observed only for changes in the frequency of the vowel /u/ placed above the detection threshold established in the psychophysical part of the experiment. This result could be considered as a confirmation of the conclusion from the previous study (Hafke, 2008) about the occurrence of a compensatory motor response to non-perceived changes in the fundamental frequency. The mismatch negativity component was elicited by changes of 50 and 100 cents in both directions. For smaller shifts (10 and 20 cents), MMN was not observed.

In a study similar to the present one, Hawco *et al.* (2009) observed MMN in reaction to positive changes of 50, 100 and 200 cents in the vocalized vowel /a/. For the change of 25 cents, no MMN was observed, while a compensation response was noted. The present study constitutes an extension of Hawco's experiment and delivers a confirmation of the common parts. In the light of this study and the previous experiment (Hafke, 2008), the value of 25 cents can be considered subliminal to perception and classified as under the detection threshold. Table 1 presents the shifts used in the present study and by Hawco *et al.* (2009) with information whether the MMN component was present or not for these shift values. A compensative motor reaction was observed for all these shifts.

Table 1. The frequency shifts (in cents) used in the present study and by Hawco *et al.* (2009) – column 1, and the MMN responses for the fundamental frequency of vowel /u/ – column 2, and vowel /a/ – column 3, respectively.

Shifts (cents)	MMN – vowel /u/	MMN – vowel /a/
10	no MMN	–
20	no MMN	–
25	–	no MMN
50	MMN present	MMN present
100	MMN present	MMN present
200	–	MMN present

Note: '–' indicates changes not tested in particular experiment.

The results from the psychophysical part, as well as those of the electrophysiological part, suggest that the motor reactions observed in the previous studies (Liu, Larson, 2007; Hafke, 2008; Jones, Keough,

2009) occur for stimuli below the perceptual threshold. This may lead to the conclusion that there are two processing pathways co-existing in the auditory cortex.

The reader should take into account the fact that in the electrophysiological part of the study, the authors tested only 6 participants. This is not a common practice in EEG research. The authors consider this part of the present experiment as a preliminary study giving the insight into the problem and intend to extend this area in future research.

References

1. American National Standards Inst. (1996), ANSI S3.6-1996, *Specifications for Audiometers*, American National Standards Institute, New York.
2. Blauert J. (2012), *A perceptionist's view on psychoacoustics*, Arch. Acoust., **37**, 3, 365–372.
3. Blauert J., Jekosch U. (2012), *A Layer Model of Sound Quality*, J. Audio Eng. Soc., **60**, 1/2, 412.
4. Burnett T.A., Freedland M.B., Larson C.R., Hain T.C. (1998), *Voice F0 responses to manipulations in pitch feedback*, J. Acoust. Soc. Am., **103**, 6, 3153–3161.
5. Burnett T.A., Larson C.R. (2002), *Early pitch shift response is active in both steady and dynamic voice pitch control*, J. Acoust. Soc. Am., **112**, 1058–1063.
6. Chen S.H., Liu H., Xu Y., Larson C.R. (2007), *Voice F0 responses to pitch-shifted voice feedback during English speech*, J. Acoust. Soc. Am., **121**, 1157–1163.
7. Donath T.M., Natke U., Kalveram K.T. (2002), *Effects of frequency-shifted auditory feedback on voice F0 contours in syllables*, J. Acoust. Soc. Am., **111**, 357–366.
8. Goodale M.A., Milner M.A. (2004), *Sight Unseen: An Exploration of Conscious and Nonconscious Vision*, Oxford University Press, Oxford.
9. Hafke H.Z. (2008), *Nonconscious control of fundamental voice frequency*, J. Acoust. Soc. Am., **123**, 1, 273–278.
10. Hafke H.Z. (2009), *Nonconscious control of voice intensity during vocalization*, Archives of Acoustics, **34**, 4, 407–414.
11. Hain T.C., Burnett T.A., Kiran S., Larson C.R., Singh S., Kenney M.K. (2000), *Instructing subjects to make a voluntary response reveals the presence of two components to the audio-vocal reflex*, Exp. Brain Res., **130**, 133–141.
12. Hawco C.S., Jones J.A., Ferretti T.R., Keough D. (2009), *ERP correlates of online monitoring of auditory feedback during vocalization*, Psychophysiology, **46**, 1216–1225.
13. Hickok G., Poeppel D. (2004), *Dorsal and ventral pathways: a framework for understanding aspects of the functional anatomy of language*, Cognition, **92**, 1–2, 67–99.
14. Jasper H.H. (1958), *Report of the Committee on Methods of Clinical Examination in Electroencephalography*, Electroenceph. Clin. Neurophysiol., **10**, 370–371.
15. Jones J.A., Keough D. (2009), *The sensitivity of auditory-motor representations to subtle changes in auditory feedback while singing*, J. Acoust. Soc. Am., **126**, 2, 837–846.
16. Kingdom F.A.A., Prins N. (2010) *Psychophysics: A practical introduction*, Amsterdam: Academic Press.
17. Laroche J., Dolson M. (1999), *New Phase-Vocoder Techniques are Real-Time Pitch Shifting, Chorusing, Harmonizing, and Other Exotic Audio Modifications*, JAES, **47**, 11, 928–936.
18. Larson C.R. (1998), *Cross-modality influences in speech motor control: The use of pitchshifting for the study of F0 control*, J. Commun. Disorders, **31**, 489–503.
19. Larson C.R., White J.P., Freedland M.B., Burnett T.A. (1996), *Interactions Between Voluntary Modulations and Pitch-Shifted Feedback Signals: Implications for Neural Control of Voice Pitch*, [in:] *Vocal Fold Physiology: Controlling Complexity and Chaos*, P.J. Davis and N.H. Fletcher [Eds.], pp. 279–289, Singular, San Diego.
20. Liu H., Larson C.R. (2007), *Effects of perturbation magnitude and voice F0 level on the pitch-shift reflex*, J. Acoust. Soc. Am., **122**, 6, 3671–3677.
21. Luck S. (2005), *An Introduction to the Event-Related Potential Technique*, MIT Press, Massachusetts Institute of Technology.
22. Milner A.D., Goodale M.A. (1995), *The Visual Brain in Action*, Oxford University Press, Oxford.
23. Natke U., Donath T.M., Kalveram K.T. (2003), *Control of voice fundamental frequency in speaking versus singing*, J. Acoust. Soc. Am., **113**, 3, 1587–1593.
24. Natke U., Kalveram K.T. (2001), *Effects of frequency-shifted auditory feedback on fundamental frequency of long stressed and unstressed syllables*, J. Speech Lang. Hear. Res., **44**, 577–584.
25. Näätänen R., Gaillard A.W.K., Mäntysalo S. (1978), *Early selective-attention effect on evoked potential reinterpreted*, Acta Psychologica, **42**, 313–329.
26. Näätänen R., Alho K. (1995), *Mismatch negativity the unique measure of sensory processing in audition*, International Journal of Neuroscience, **80**, 317–337.
27. Näätänen R., Päävilänen P., Rinne T., Alho K. (2007), *The mismatch negativity (MMN) in basic re-*

search of central auditory processing: A review, Clin. Neurophysiol., **118**, 2544–2590.

28. Picton T.W., Alain C., Otten L., Ritter W., Achim A. (2000), *Mismatch negativity: Different water in the same river*, Audiology and Neuro-otology, **5**, 111–139.

29. Repp B.H. (2000), *Compensation for subliminal timing perturbations in perceptual-motor synchronization*, Psychological Research, **63**, 106–128.

30. Repp B.H. (2006), *Does an auditory perceptual illusion affect on-line auditory action control? The case of (de)accentuation and synchronization*, Exp. Brain Res., **168**, 493–504.

31. Sivasankar M., Bauer J.J., Babu T., Larson C.R. (2005), *Voice responses to changes in pitch of voice or tone auditory feedback*, J. Acoust. Soc. Am., **117**, 2, 850–857.

32. Ungerleider L.G., Mishkin M. (1982), *Two cortical visual systems. Analysis of visual behavior*, [in:] *Analysis of Visual Behavior*, Ingle D.J., Goodale M.A., Mansfield R.J.W. [Eds.], pp. 549–586, MIT Press, Cambridge.

33. Warren J.E., Wise R.J.S., Warren J.D. (2005), *Sounds do-able: auditory-motor transformations and the posterior temporal plane*, Trends in Neurosciences, **28**, 12, 636–643.

34. Xu Y., Larson C.R., Bauer J.J., Hain T.C. (2004), *Compensation for pitch-shifted auditory feedback during the production of Mandarin tone sequences*, J. Acoust. Soc. Am., **116**, 2, 1168–1178.

PAN
ARCHIVES OF ACOUSTICS
Vol. **38**, No. 3, pp. 383–387 (2013)

DOI: 10.2478/aoa-2013-0045

Preliminary Study on the Influence of Headphones for Listening Music on Hearing Loss of Young People

Andrzej B. DOBRUCKI, Maurycy J. KIN, Bartłomiej KRUK

Chair of Acoustics and Multimedia, Faculty of Electronics, Wrocław University of Technology
Wybrzeże Wyspiańskiego 27,50-370 Wrocław, Poland;
e-mail: {*andrzej.dobrucki, maurycy.kin, bartlomiej.kruk*}*@pwr.wroc.pl*

(*received April 19, 2013; accepted June 18, 2013*)

The paper presents results of hearing loss measurements provided for 81 young people (from 16 to 25 years old). The main aim of the work was to find the influence of headphones of the types used (closed, semi-open, open and in-ear) on the hearing losses. The first part of the research was to answer questions about the influence of: time of listening, loudness of music, other noise exposures as well as the type of the headphones used. It turned out that all factors mentioned above influence thresholds of hearing but the found dependencies are not explicit. The greatest hearing losses were observed for people who work as sound reinforcement engineers and, moreover, no influence of the headphone types was found for them. It turned out that the use of in-ear headphones causes the greatest hearing losses for some subjects (thresholds shifted up to about 20 dB HL at 4 kHz). The daily time of a listening also affected the hearing thresholds. It was found that for users of in-ear and close headphones, an average time of musical exposure of three hours causes the hearing loss of 10–15 dB HL at higher frequencies. The use of open as well as semi-open headphones has no influence on the hearing damage. Thus it would be stated that these kinds are safety in use. Almost 15% of the investigated young people have their thresholds shifted up at higher frequencies, particularly at 4 kHz, which means that they have the first symptoms of a permanent hearing damage.

Keywords: hearing threshold, headphones.

1. Introduction

In the past few years, the tendencies of sound production caused an increase of loudness of sound for communication, particularly for musical recordings. Many radio stations as well as record companies have applied increasing amounts of dynamic range compression and other means of the recording process in order to be perceived in the today noisy world (Katz, 2007). Radio stations may adjust the dynamic ranges in attempt to trade off a louder sound, which may attract listeners searching for a station. The trend called as "loudness wars" has been reflected in the higher subjective impressions in the psychological domain, and the slogans "louder means better" and "louder sounds are sold better" have come true (Vickers, 2011). Many young people want to separate their minds of different backgrounds by the use of special kinds of headphones and they listen to the sound material louder, beside of the fact that the listened material is louder in comparison to the recordings made in the previous century. The contemporary designed and produced equipment allows the listeners to consume music in accordance with their way of life. On the other hand, young people say: we listen to the music that sounds nicely for us and it is not alike as noise, so why may it be dangerous for our hearing? Sometimes, one could find many pieces of classical music from the XXth century, which are very loud while performed. The main differences between classical and pop-music are in the time of continuous exposition to the sound, the character of musical structure and spectral consistence of stimuli. In popular music, the way used very often during musical production process is based on the sound compression, and this compression itself may increase the potential for hearing damage. Moreover, the way of stimuli presentation (via headphones or loudspeaker, or naturally listening to the event) seems to be an important thing causing the hearing loss. Young people do not take into account that popular or rock music causes effects like that of higher and longtime exposure to noise when the earphones are used for listening due to the average sound level and duration of exposure, which simply leads to a listening fatigue (Moore, 1997). Of course, the higher hearing thresholds induce difficulties in receiving many information from human environment that influences the sense of safety and causes changes in the way of thinking and living together in a society (Strelau, 2000). It also may be interesting while the European Standard EN ISO 7029 still remains actual in the light of youngsters' way of life and this aspect was the aim of the research presented.

2. Experimental research

The results of audiometric measurements of 81 young people aged between 16 and 25 years are presented. The subjects declared frequent listening to loud music on headphones. None of them complained of hearing problems. The participants were asked to fill out the questionnaire sheet and to answer the following questions: the type of the used headphones, the daily listening time, the preferred levels of listening and the kind of music. Additionally, they have to point on other conditions concerning the noise exposure at the work, the background noise connected with the place of living, the work activity etc. The research was made for the inhabitants of Wroclaw.

Some of the people under investigation are working for an entertainment industry in a professional way so they were divided into three groups reflecting their activities:

- young classical musicians or music academy students,
- sound reinforcement engineers of FOH/PA systems (Front of House / Public Address sound system),
- sound engineers working in recording studios.

The ordinary young users of portable audio equipment were representative as the reference group for this range of age.

Characteristics of the study population obtained on the base of the questionnaires are as follows:

- 81 people (including 26 women),
- the average age: 22.5 years (between 16 and 25),
- average daily time of using of the headphones: 32 h (from 2 to 7 hours, 1 person declared 14 hours),
- other noise exposures: 4.9 hours per week (for example loud rock concerts).

The noise exposure occurred in the group of professionals.

According to the questionnaires, taking into account the subjects' activities, the whole group of the 81 persons was divided into the following four subgroups:

- young classical musicians or music academy students (26 people including 10 women),
- sound engineers of FOH/PA systems (10 men only),
- sound engineers working in recording studios (11 people including 3 women),
- users of audio equipment involved not professionally with the entertainment industry (34 people, including 13 women).

The first three subgroups were considered later separately.

The young musicians usually practice individually being exposed to noise for a long time (up to 8 hours per day). An equivalent level weighted during practicing with A curve that does not exceed 70 dB and is not harmful to hearing. On the other hand, this an important fact in their work is a symphony orchestra in that the rehearsal unweight peak levels can be as high as 110 dB SPL and the equivalent level A may be even of 85 dB. These are facts often overlooked and very reluctantly discussed by directors of operas and symphony orchestras due to the damages for musicians.

The second type of division of the whole population is defined by different types of earphones used by the subjects as declared in questionnaire what resulted in four subgroups:

- in-ear headphones – 23 users,
- open headphones – 18 users,
- closed – 22 users,
- semi-open – 18 users.

In this case each group consists of almost the same number of women and men. The most of the subjects (80%) declared that they listened to very loud music and the daily time of the headphone use was 3.2 h, which results in a weekly exposure of more than 22 h. The results of the questionnaires did not allow indicating any other factors that could influence the hearing threshold values because of their different representatives within each subgroup.

After the interviews and spoken instructions the people were measured by means of audiometers. The audiometric tests were conducted in an anechoic chamber and in the recording studio of the Wrocław University of Technology. These places meet the requirements of a maximum allowable amount of the background sound pressure level (ISO 8253-1:2010). Therefore, during the tests any masking phenomenon from outer signals does not occur (PN-EN 26189, ISO 8253-1:2010, ISO 7029:2000). Before the measurements, all the audiometers had been basically calibrated and checked aurally, they had also been calibrated subjectively in accordance with the ISO recommendations (PN-EN 26189). The threshold of hearing levels were determined by the air conduction audiometry with the

Maico M 53 audiometers. The measurements were carried out according to the applicable standards (PN-EN 26189) by ascending methods and with the use of continuous sinusoidal signals with steps of 2 dB. All measurement points were repeated twice in order to eliminate random errors for inexperienced subjects.

3. Analysis of the results

3.1. Average hearing threshold

Figure 1 shows the values of the hearing threshold for the left and right ears of the population tested. These values have been averaged over results obtained for 81 listeners. It can be easily seen that the threshold of hearing is uniformly shifted by about 6–7 dB. The statistical treatment by means of the Bartlett test (Greń, 1978) showed that the variances of the results obtained were homogenous ($\chi^2 = 24.893 < \chi^2_\alpha = 39.977$, at $\alpha = 0.05$) for all frequencies.

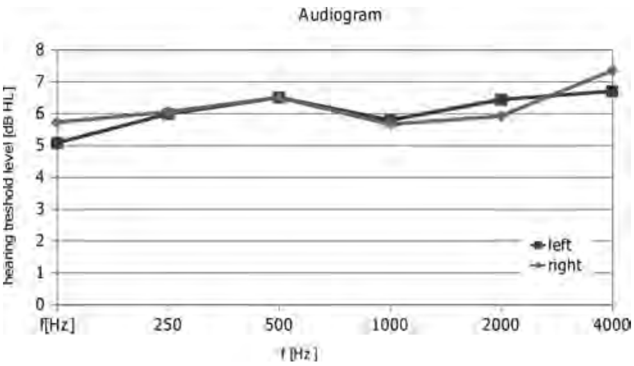

Fig. 1. Average values of the threshold of hearing (dB HL) for the tested population.

According to classification of BIAP (BIAP Recommendation 02/1), the young people tested belong to the group of normal hearing, but the shift in the threshold of hearing points to a slow tendency of the beginning of a permanent damage of hearing. These values, however, are the average ones and the greatest hearing losses can be balanced by the results for the people with otological normal values shown in Table 1 as values of standard deviations, especially for higher frequencies. Thus, it was decided to divide the whole group into categories which could influence the obtained results and reflect the real hearing loss for some specific nature of work as well as kinds of equipment used by the people.

Table 1. The average values and standard deviations for hearing thresholds (dB HL) for the left and right ears, respectively, measured for all of 81 subjects.

Frequency [Hz]	250	500	1000	2000	4000	8000
$\overline{x}_L$	5.1	6.0	6.5	5.8	6.4	6.7
σ_L	7.2	6.9	6.1	6.6	10.2	11.1
$\overline{x}_R$	5.7	6.0	6.5	5.6	5.9	7.3
σ_R	5.5	6.4	5.7	7.4	11.5	10.8

3.2. The influence of different kinds of headphones on the threshold of hearing

In this section, the results of pure tone audiometry for users of different types of headphones are presented. These results present "the worse" ear (left or right) for each subject and these values have been averaged over the people which use particular types of headphones. They are shown in the Fig. 2.

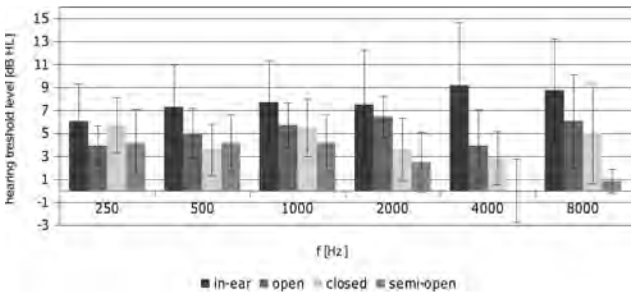

Fig. 2. Influence of different kinds of headphones on the threshold of hearing (dB HL). Standard deviation values are presented as vertical lines on the tops of the bars.

It turned out that except for the frequency of 4 kHz there is no relationship between the types of the preferred headphones and the shift of the hearing thresholds ($F < F_\alpha = 2.75$, where F, F_α – calculated and critical values of the F-Snedecor test, respectively, at $\alpha = 0.05$). For the frequency of 4 kHz, a statistically important influence of the headphone type on the threshold values was observed ($F = 3.35 > F_\alpha$). This means that most unfavorable for the hearing are inner earphones, especially at high frequencies for which our hearing system is most sensitive. The air in the ear canal is a natural protection from high sound pressure. Using inside earphones the length of the channel is reduced whereby the natural protection becomes less effective and the sound level in ear channel increases by 6 dB. Good alternatives are semi-open headphones that in a small way can isolate us from the outside noise. They additionally ensure good hygiene of the ear and by their design they are a protection from very high sound pressures acting directly on the ear membrane. The results of the hearing threshold values obtained for the frequency of 4 kHz are presented in Table 2.

Table 2. The average values of hearing thresholds at 4 kHz for various types of headphones, in dB HL.

Type of headphones	in-ear	open	closed	semi-open
Hearing threshold [dB HL]	9.2	3.9	2.9	0.1

In order to determine how the particular kinds of headphones are injurious for listening conditions, the structure index test (Greń, 1978) was applied as a statistical treatment for the series which reflects the degree of the hearing damage caused by the type of the used headphones, with $u_\alpha = 1.96$ at $\alpha = 0.05$. It turned out that for the frequency of 4 kHz the most dangerous for the hearing threshold is the inner-ear headphone type ($|u| = 4.73$), while the influence of the semi-open type is statistically inessential ($|u| = 1.05 < u_\alpha$). The degrees of injuries of the hearing damage obtained for the open and the closed headphones are lower than those for the in-ear headphones ($|u| = 2.52$ and $|u| = 2.12$, respectively).

3.3. Threshold of hearing in terms of professional work

In this section, only the professional group is analyzed (the three first subgroups listed in Sec. 2). The number of people in this group is equal to 47. Among them 35 persons have been working in the profession up to 7 years. By analyzing these data it can be concluded that even 3–4 years of working at an entertainment industry, especially as the front-of-house engineers may cause a slight loss of hearing ability. Comparing the other professional groups, it can be assumed that the results coincide to a large extent and the type of work (noise level) have no longer such effect on the threshold of hearing. In Fig. 3 hearing thresholds depending on the profession are presented. These results present "the worse" ear (left or right) for each subject, and these values have been averaged over the people within the particular group of profession.

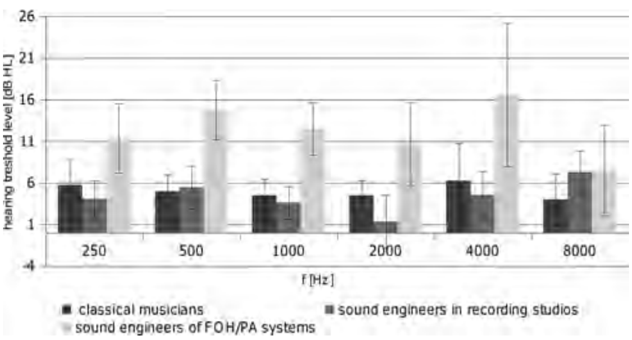

Fig. 3. Thresholds of hearing (dB HL) depending on the profession. Standard deviation values are presented as vertical lines on the tops of the bars.

As in the previous case it was decided to use the single-factor statistical treatment and on the base of the analysis of variance, it turned out that for frequency values of 500 Hz, 1 kHz as well as 4 kHz an influence of the working activity on the threshold of hearing has been observed ($F > F_\alpha = 3.29$, where F, F_α – calculated and critical values of the F-Snedecor test, respectively, at $\alpha = 0.05$). For other frequencies there is no relationship between the profession of work and the shift of the hearing threshold values. As mentioned in the previous chapter, the hearing loss at 4 kHz can be interpreted as the beginning of a permanent hearing damage that results from the exposure to sounds at high levels while the upward threshold shifts appearing for lower frequencies (500 Hz and 1000 Hz) result from the exposure to hyper-compressed musical sounds in these frequency bands, especially occurring on the stage situation in order to increase the total loudness impression.

4. Conclusions

On the base of the results presented it would be fairer to say that the most dangerous kind of headphones is the in-ear headphone set which causes the upward threshold shift of 9 dB HL at the frequency of 4 kHz. When the music would be played very loud and as long as declared at a level of approximately 100 dB SPL, a permanent hearing damage will occur after no more than 4 years of using such devices. Another factor influencing the hearing condition system is the professional activity connected to the exposure to loud signals. The presented results have also shown that working as reinforcement engineers with FOH/PA systems can permanently destroy the hearing system because an activity as long as 3–4 years causes the upward threshold shifts even of 16 dB HL at 500 Hz and 4 kHz. These values may mean the beginning of a permanent hearing damage and have to be taken into consideration by the industrial health protection. The results of the other researches (Chiou-Jong *et al.*, 2007; Gulati, 2011) conclude that it is enough to listen to loud music on MP3 players one hour a day for five years to ruin the hearing system permanently.

Hearing care professionals skeptical to listening to music with headphones admit that only a moderate volume for up to 8 hours a day is no longer a risk of hearing loss.

It was clearly shown what kind of problems we are dealing with. Listening to music is becoming a disease primarily among young people, but this fact is ignored in the media. The biggest problem is the type of headphones used for the every day listening. Most of young people listen to music through inside earphones what causes that the length of the ear canal is reduced, and as a consequence, the natural protection becomes less effective. The body does not give us a sign that the process of destroying the hearing has just began, and once damaged the hearing cells would never regenerate.

From the sociological point of view, young people like this kind of earphones because they take up little space and can be always carried in a pocket, however on the other hand, they are the worst ones for our hearing. Research has shown that 2–3 years of using this type of headphones leads to a slight hearing damage resulting in an incomprehensibility of whisper or quiet voice.

References

1. BIAP Recommendation 02/1 bis: *Automatic classification of hearing impairment,* Oct. 26, 1996.
2. Chiou-Jong Ch., Yu-Tung D., Yih-Min S., Yi-Chang L., Yow-Jer J. (2007), *Evaluation of Auditory Fatigue in Combined Noise, Heat and Workload Exposure,* Industrial Health, **45**, 4, 527–534.
3. Gulati S. (2011), *Hearing loss from headphones and earphones*, http://www.symptomfind.com/health/hearing-loss-from-headphones.htm.
4. Greń J. (1978), *Mathematical Statistics. Models and Exercises* [in Polish], PWN, Warszawa.
5. ISO 7029:2000, *Acoustics Statistical distribution of hearing threshold as a function of age.*
6. ISO 8253-1:2010, *Acoustics – Audiometric test methods – Part 1: Pure-tone air and bone conduction audiometry.*
7. Katz B. (2007), *Mastering Audio: The Art and the Science*, Focal Press, Oxford.
8. Moore B.C.J. (1997), *An Introduction to the Psychology of Hearing*, Academic Press, London.
9. PN-EN 26189, *The measurements of hearing threshold by audiometric air conduction for hearing protection* [in Polish].
10. Strelau J. (2000), *Psychology* [in Polish], Gdańskie Wyd. Psychologiczne, Gdańsk.
11. Vickers E. (2011), *The Loudness War – Do Louder, Hypercompressed Recordings Sell Better?*, J. Audio Eng. Soc., **59**, 5, 346–352.

PAN ARCHIVES OF ACOUSTICS
Vol. **38**, No. 3, pp. 389–395 (2013)

DOI: 10.2478/aoa-2013-0046

Road Traffic Noise Attenuation by Vegetation Belts at Some Sites in the Tarai Region of India

Vikrant TYAGI[(1)], Krishan KUMAR[(2)], V.K. JAIN[(2)]

[(1)] *Urban Management Masters Programme, Ethiopian Civil Service College*
P.Box No. 5648, Addis Ababa, Ethiopia

[(2)] *School of Environmental Sciences, Jawaharlal Nehru University*
New Delhi, India; e-mail: krishan_kumar@mail.jnu.ac.in

(*received March 18, 2013; accepted July 12, 2013*)

Noise measurements have been carried out at eleven different sites located in three prominent cities of the Tarai region of India to evaluate the effectiveness of vegetation belts in reducing traffic noise along the roadsides. Attenuation per doubling of distance has been computed for each site and excess attenuation at different 1/3 octave frequencies has been estimated. The average excess attenuation is found to be approximately 15 dB over the low frequencies (200 Hz to 500 Hz) and between 15 dB to 20 dB over the high frequencies (8 kHz to 12.5 kHz). Over the critical middle frequencies (1–4 kHz), the average excess attenuation (between 10–15 dB) though not as high, is still significant, with a number of sites showing an excess attenuation of 15 dB or more at 1 kHz. The results indicate that sufficiently dense vegetation belts along the roadsides may prove as effective noise barriers and significant attenuation may be achieved over the critical middle frequencies (1–4 kHz).

Keywords: noise, attenuation, traffic, frequency, vegetation belt, Tarai.

1. Introduction

Land, in most cities, is a scarce resource due to which houses and buildings are generally built quite close to the road. As a result, the population living/working along the roadsides is often exposed to noise levels that are significantly greater than the prescribed standards. Thus, there is a need of taking ameliorative measures for reducing noise levels along the roadsides. Providing noise barriers along the roadsides is a typical measure adopted worldwide in this regard. Though noise barriers may be made of different kinds of construction materials, thick plantations along the roadsides are a relatively inexpensive and aesthetically more pleasing alternative. As a result, a number of authors (Cook, Van Haverbeke, 1971; Aylor, 1972; Linskens *et al.*, 1976; Carlson *et al.*, 1977; Martens, 1980; Bullen, Fricke, 1982; Price *et al.*, 1988; Huddart, 1990; Kumar *et al.*, 1998; Fang, Ling, 2003; Tyagi *et al.*, 2006; Maleki *et al.*, 2010) across the world have focused their attention on the attenuation of road traffic noise by vegetation belts.

However, there is little in common in these studies in terms of the measurement procedures used or the results obtained. Consequently, there is a considerable divergence of opinion on the effectiveness of vegetation as a noise barrier. In the Indian context, surprisingly, very few noteworthy attempts (Kumar *et al.*, 1998; Pal *et al.*, 2000; Tyagi *et al.*, 2006; Pathak *et al.*, 2008; Garg *et al.*, 2012) have been made to investigate the role of vegetation in the attenuation of traffic noise. It is pertinent here to mention that the potential of vegetation belts in reducing road side noise levels remains unexploited in the Indian context despite the fact that many plant species in India do not shed the foliage throughout the year quite unlike the plant species in the temperate regions of the world. In their earlier studies Kumar *et al.* (1998) and Tyagi *et al.* (2006) have reported in the context of Delhi that vegetation belts could play a significant role in attenuating roadside noise levels due to road traffic. The present study is a continuation of their efforts to assess the effectiveness of vegetation in reducing road traffic noise levels in the Indian context by obtaining the sound attenuation spectrum of vegetation at some sites located in the Tarai region of India.

2. Methodology

In the present study, field experiments were conducted to evaluate the performance of vegetation barriers in reducing noise levels along the roadsides at eleven sites located in Dehradun, Pantnagar, and Haridwar, which are some of the prominent cities of the Tarai region in India. Each of the sites chosen had straight and level roads, carrying freely flowing traffic with average speed of $\geq$40 km/hour. The traffic consisted of two wheelers, autos, cars, jeeps, buses, light and heavy commercial vehicles. The depth of vegetation belt at each site was approximately 15 m. Generally, at all the sites, the vegetation belt started at 1–1.5 meters from the edge of the road. Most of the sites were dominated mainly by shrub type of vegetation interspersed with some trees. The details of species composition at each site are provided in Appendix. As these were natural vegetation belts, their height was variable but was 2 meters or more at most of the sites. Each site had an optical density such that a vegetation belt of 15 m thickness provided zero visibility across it at least up to a height of 2–3 meters. This criterion of selecting vegetation belt was based on ISO9613-2 A.1 according to which the foliage of trees and shrubs provides a small amount of attenuation but only if it is sufficiently dense to completely block the view along the propagation path, i.e. when it is impossible to see a short distance through the foliage.

For making the noise measurements, two type-I SVAN 945 sound level meters with the facility of integration, spectrum analysis, and data logging in real time were used. The equipment was mounted on tripod stands at a height of 1.5 m above the ground level on either side (front and rear) of the belt, close to the vegetation stand. The equipment in the front side was placed at 1.0 m from the kerbside of the road, approximately at a distance of 5.0 m from the centreline of the road (Fig. 1). No buildings were present in the vicinity of the measurement sites. The noise levels at all the sites were measured on calm and clear sunny days. The meteorological data (temperature and humidity) corresponding to each site is given in Appendix.

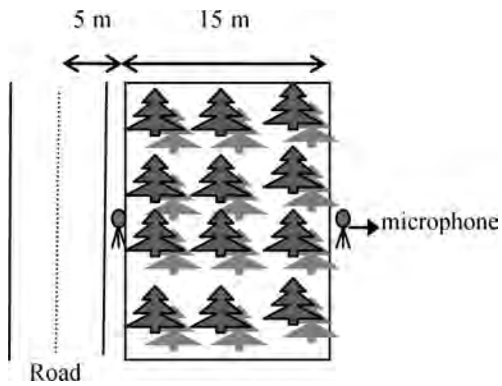

Fig. 1. Schematic diagram of the experimental set-up.

At each site, traffic noise measurements were made for a period of 30 minutes at the sampling rate of one observation/second. During each observation, the instrument recorded noise levels (in a linear mode) at different 1/3 octave frequencies (in the range of 40 Hz to 20000 Hz) as well as the A-weighted noise levels. This means that the instrument recorded time sequences consisting of 1800 values of noise levels at each 1/3 octave frequency along with the time sequence of A-weighted noise levels. The clocks of both pieces of the equipment were synchronized, so that they recorded the same sound signal. The data recorded at each site was downloaded with the help of RS 232 cable and analyzed using SVANPC interface software.

Noise attenuation at each site was evaluated from the time sequence plots of noise levels in the front and rear sides of the vegetation belt. A typical time series plot of A-weighted noise levels in the front and rear side of a vegetation belt is presented in Fig. 2. In the time sequence plots of noise levels at each site, there were time instants when noise levels in front of the noise barrier were at their background levels. At these time instants it is improper to compute attenuation since the background noise levels in the front and rear sides of the vegetation barrier would be approximately the same.

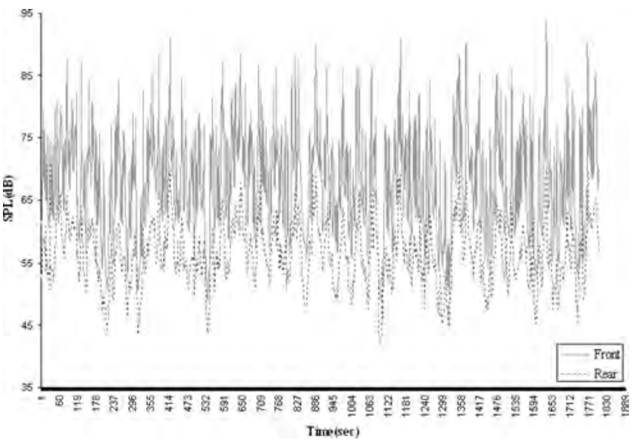

Fig. 2. A-weighted noise levels in the front and rear side of the vegetation belt.

A closer examination of the time series plots of the noise levels at each site revealed that the noise levels at the rear side of the noise barrier were a bit higher than or comparable in magnitude to the levels at the front side at some discrete time instants. This aberration, in fact, might have been due to extraneous factors such as chirping of birds near the microphone at the rear side of the noise barrier during the quiet sampling intervals. For this reason, noise attenuation for each site was recomputed by considering only those time instants when noise events occurred. The noise events at each site were identified on the basis of noise levels exceeding L_1 and L_{10} values of the time series respectively. While L_1 is the value that is exceeded only 1% of the time in the data, L_{10} is the value that is exceeded 10% of the time. Noise levels exceeding these values were considered as noise events in the context of the present study.

At the discrete time instants when noise events occurred, noise attenuation of overall A-weighted noise levels was computed for each site. For this purpose, A-weighted noise levels in the rear side of the barrier were subtracted from the corresponding levels at the front side at the time instants of occurrence of the noise events identified on the basis of L_1/L_{10} levels. This gave the overall attenuation of noise achieved by the barrier.

A similar approach was adopted to evaluate average overall noise attenuation at each 1/3 octave frequency at time instants of occurrence of noise events identified on the basis of L_1 levels. However, since noise also attenuates due to geometrical divergence (distance effect) and atmospheric absorption, excess attenuation at each 1/3 octave frequency was computed by applying appropriate corrections in order to assess the effectiveness of the barrier at each site. Excess attenuation is defined as the attenuation which is not accounted for by geometrical divergence and atmospheric absorption. In the present study, the correction for attenuation by geometrical divergence was applied by considering the moving live traffic as a line source, i.e. by considering the attenuation due to divergence to be proportional to 1/distance (Huddart, 1990). Atmospheric attenuation at each frequency for given conditions of temperature and relative humidity were computed following the calculation procedure given in ISO9613-1 (1992).

3. Results and discussion

Attenuation results of overall A-weighted noise levels identified on the basis of L_1/L_{10} levels at different sites are presented in Table 1. It can be seen that attenuation of A-weighted noise events identified on the basis of L_{10} levels varies from about 10 dBA to about 21 dBA at different sites. Attenuation of noise events identified on the basis of L_1 levels is found to vary between 13 dBA to 26 dBA.

To compare these results with those obtained by Huddart (1990), attenuation per doubling of distance (dd) was computed for each site using the following equation (Huddart, 1990):

$$L_p = L_x - k \log(r_p/r_x), \qquad (1)$$

where L_p is the noise level in dB at a distance r_p from the source, L_x is the noise level in dB at a distance r_x from the source, and k is a constant which is dependent on ground and vegetation characteristics.

While Huddart (1990) reports a variation of $5.4L_{10}$ dBA to $9.3L_{10}$ dBA in the attenuation per doubling of distance (dd) over seven different sites, attenuation per doubling of distance in the present study (Table 2) is found to vary between $5.1L_{10}$ dBA to $10.9L_{10}$ dBA over eleven different sites. Out of these, five sites have the attenuation/dd of $9L_{10}$ dBA or more. In the study by Huddart (1990), only one of the sites (site-4) has the attenuation/dd of $9L_{10}$ dBA or more.

Table 1. Attenuation of A-weighted noise levels for noise events identified on the basis of L_1/L_{10} levels.

S.No.	Name of experimental site	Attenuation of A-weighted noise levels for noise events based on L_{50}, L_{10} and L_1		
		L_{50} dBA±s.d. [dBA]	L_{10} dBA±s.d. [dBA]	L_1 dBA±s.d. [dBA]
1	Site-1 (Lachhiwala, Dehradun)	10.5±3.9	12.8±3.66	13.7±2.96
2	Site-2 (near Saung River, Dehradun)	7.3±4.8	13.1±3.47	16.4±2.40
3	Site-3 (Laltapar, Dehradun)	7.9±3.8	10.1±2.86	14.8±2.60
4	Site-4 (near Limekiln site, Dehradun)	11.5±4.3	15.6±3.60	17.2±4.32
5	Site-5 (Raiwala, Dehradun)	14.6±4.2	18.7±3.12	22±1.92
6	Site-6 (Doiwala, Dehradun)	11.2±3.0	13.8±2.64	15.6±3.43
7	Site-7 (Patharchatta, Pantnagar)	11.3±5.9	18.5±4.48	24±3.44
8	Site-8 (Tanda, Pantnagar)	11.9±5.4	18.7±4.54	22.8±3.07
9	Site-9 (Saptarishi Ashram, Haridwar)	15.5±4.6	19.9±4.39	23.5±4.86
10	Site-10 (Bhadrabad Road, Haridwar)	10.5±4.3	14.6±4.30	16.6±5.56
11	Site-11 (GK University, Haridwar)	15.8±4.7	21.7±3.16	26.1±2.78

Note: L_{50} dBA, L_{10} dBA, and L_1 dBA are the average attenuation of the A-weighted noise levels computed for the noise events identified on the basis of L_{50}, L_{10}, and L_1 levels respectively in the front side of the vegetation belt during the measurement period.

Table 2. Attenuation per doubling of distance.

Site name	Attenuation/dd L_{50} dBA	Attenuation/dd L_{10} dBA	Attenuation/dd L_1 dBA
Site-1 (Lachhiwala, Dehradun)	5.2	6.4	6.85
Site-2 (near Saung River, Dehradun)	3.6	6.55	8.2
Site-3 (Laltapar, Dehradun)	3.9	5.05	7.4
Site-4 (near Limekiln site, Dehradun)	5.8	7.8	8.6
Site-5 (Raiwala, Dehradun)	7.3	9.35	11
Site-6 (Doiwala, Dehradun)	5.6	6.9	7.8
Site-7 (Patharchatta, Pantnagar)	5.6	9.25	12
Site-8 (Tanda, Pantnagar)	5.9	9.35	11.4
Site-9 (Saptarishi Ashram, Haridwar)	7.7	9.95	11.75
Site-10 (Bhadrabad Road, Haridwar)	5.3	7.3	8.3
Site-11 (GK University, Haridwar)	7.9	10.85	13.05

Note: L_{50} dBA, L_{10} dBA, and L_1 dBA are the average attenuation of the A-weighted noise levels computed for the noise events identified on the basis of L_{50}, L_{10}, and L_1 levels respectively in the front side of the vegetation belt during the measurement period.

Figures 3–5 represent the excess attenuation at different 1/3 octave frequencies for various sites in the present study. It may be seen that not only have the vegetation belts differed from each other in terms of the magnitude of attenuation, they have also shown variations in terms of their spectral behavior in reducing the noise levels. Nevertheless, certain inferences may be drawn with a reasonable degree of confidence regarding the attenuation behavior of the vegetation belts.

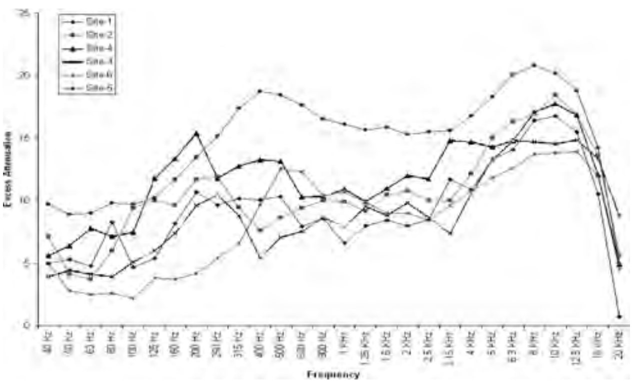

Fig. 3. Excess attenuation at different 1/3 octave frequencies at vegetation belt sites in Dehradun.

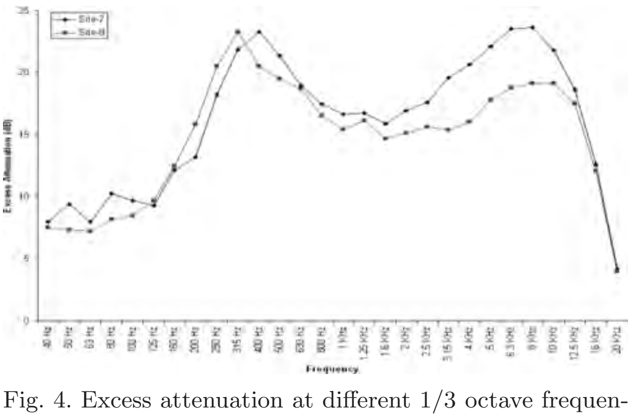

Fig. 4. Excess attenuation at different 1/3 octave frequencies at vegetation belt sites in Pantnagar.

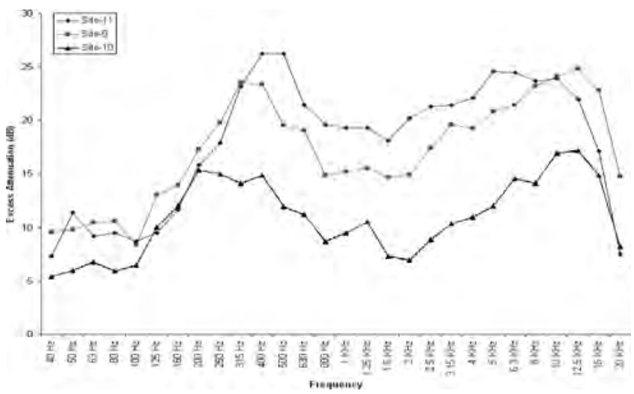

Fig. 5. Excess attenuation at different 1/3 octave frequencies at vegetation belt sites in Haridwar.

A close examination of the attenuation plots reveals that a peak in attenuation exists in the low frequency region in the range of 200 Hz to 500 Hz in the case of most vegetation belts. Similar peaks in attenuation at low frequencies have been reported by Aylor (1972), Carlson *et al.* (1977), and Martens (1981). The peak attenuation at low frequencies is due to interaction of the sound field with the ground. Attenuation as a result of this interaction between the sound waves and the ground surface is termed "the ground effect" (Attenborough 1988). Bullen and Fricke (1982), however, suggest that vegetation might reduce the benefit of the ground effect since the phases of the sound waves arriving at a point in the rear side of the vegetation belt would be random and as such the interference effects caused by the ground are destroyed. Huddart

(1990), on the other hand, suggests that soft porous ground surfaces are the best attenuators of sound over low frequencies and that the vegetation plays an important role in supplying a deep covering of plant debris which, together with the development of the plant root system, maintains a soft porous surface necessary for good ground absorption of sound. In the context of the present study, a significant low frequency peak in attenuation, varying from 12dB to more than 20 dB, is observed at almost all the sites. This indicates that vegetation does not reduce the benefit of the ground effect over low frequencies.

With regards to attenuation over the middle frequencies, most vegetation belts in the present study are found to cause a reasonable degree of attenuation though it may not be as high as the attenuation achieved over the low (200 Hz to 500 Hz) and high frequencies (8 kHz to 12.5 kHz). From Figs. 3–5, it is inferred that a minimum excess attenuation in the middle frequencies exists in the range of 1 kHz to 2 kHz. Martens (1981) reports a similar result and suggests the existence of an acoustic window from 1000 Hz to 2000 Hz for some species. Scattering by trunks and branches of vegetation seems to be an important mechanism of attenuation at middle frequencies. Aylor (1972) suggested that attenuation predicted by the scattering theory agreed well with field observations when

$$\frac{2\pi\, a}{\lambda} \geq 1,$$

where a – the radius of a trunk, λ – wavelength of the sound.

This implies that a trunk/branch diameter of ∼11 cm or more is required for scattering sound at 1000 Hz. The trunk/branch/twig diameters of vegetation at different sites in the present study were highly variable. However, most sites in the present study were dominated by the shrub type vegetation. In such vegetation, a trunk/branch diameter of 11 cm would generally lie in the extreme right of the size distribution of trunk/branches and as such the frequency of occurrence of trunks/branches with the diameter of 11 cm would be comparatively lower than trunks/branches of smaller diameters. Scattering of sound by trunks/branches of the shrub type of vegetation in the vicinity of 1000 Hz, therefore, is not as pronounced as it is at higher frequencies for which trunk/branches of a smaller diameter are required. The scattering by trunks/branches/twigs, therefore, is a plausible explanation for the observed attenuation behaviour at the middle and high frequencies. The minimum excess attenuation observed over the middle frequencies (1 kHz to 2 kHz) is found to vary from 6 dB to approximately 15 dB in the cases of some sites.

Another important result obtained regarding attenuation of sound by vegetation belts in the present study is the peak observed over high frequencies in the range of 8 kHz to 12.5 kHz. Though most studies report the maximum attenuation at high frequencies, there exist some variations regarding the frequency intervals in which such peaks are observed. In this respect, the results of the present study are quite close to some of the earlier studies (Aylor, 1972b; Yamada *et al.*, 1977; Linskens, 1976). Whereas Aylor (1972b) reports the high frequency peak attenuation at a frequency of 10 kHz, Yamada *et al.* (1977) observed the maximum attenuation at 8 kHz. The authenticity of their observation, however, is affected by the fact that they did not study the attenuation behavior in the entire audible spectrum. While Aylor (1972b) studied excess attenuation in the frequency range of 100 Hz to 10000 Hz, Yamada *et al.* (1977) observed excess attenuation in the range of 125 Hz to 8000 Hz. Linskens (1976), on the other hand, studied excess attenuation in the frequency range of 125 Hz to 16000 Hz and reported high frequency peak attenuation in the frequency range of 8000 Hz to 12500 Hz, which is similar to the results obtained in the present study. Other authors such as Huddart (1990) report the high frequency maximum in the range of 3000 Hz to 7000 Hz. Studies (Martens, 1980) have indicated that foliage is primarily responsible in attenuating sound at high frequencies and that the frequency of peak attenuation is influenced by foliage characteristics. Sites in the present study had mainly the shrub type of vegetation with variable leaf sizes. Figures 3–5 reveal that the high frequency (8 kHz to 12.5 kHz) peak attenuation is found to vary from less than 15 dB to more than 20 dB at different sites.

Figure 6 represents the average excess attenuation of all the eleven sites in the present study. The average excess attenuation at the low frequency peak due to the ground effect is approximately 15 dB. Though a dip is observed over the middle frequencies, excess attenuation is still significant (between 10 dB and 15 dB) enough. The average excess attenuation is found to be the maximum (between 15 dB and 20 dB) in the high frequency range (8 kHz to 12.5 kHz), owing to scattering and absorption by vegetation. Further, it can also be seen that there exists a variability in the atten-

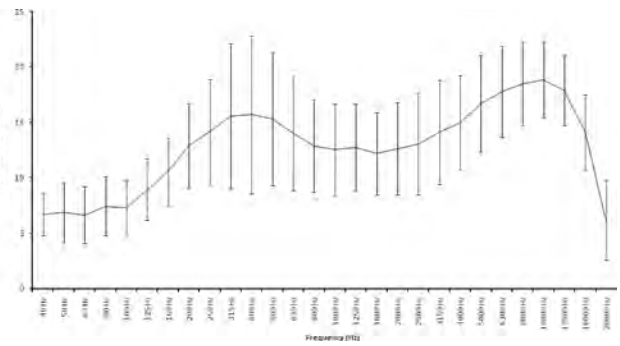

Fig. 6. Excess attenuation based upon the average taken from all the eleven sites with standard deviations represented as vertical error bars.

uation behavior of vegetation belts. Whereas the low frequency attenuation may have been influenced by the variation in the physical properties of the ground surface, the variation over the middle and high frequencies may have been due to the variation in the vegetation belt characteristics such as species composition, dominance, and density. The variability observed in the results, however, provides a sufficient basis for future research to investigate the effect of the factors mentioned above on excess attenuation.

4. Conclusions

The results of the present study indicate that sufficiently dense vegetation belts along the roadsides may prove as effective noise barriers and significant attenuation may be achieved even over the critical middle frequencies (1–4 kHz) if further research is conducted to evaluate contributions of individual plant species towards traffic noise attenuation. It is worthwhile here to mention that an excess attenuation of 15 dB or more is observed at 1 kHz for a number of sites in the context of the present study. Attenuation performance of vegetation belts in the low frequency range (200–500 Hz) and over the high frequency range (8–12.5 kHz) is found to be even better. The perceived benefits of vegetation barriers, in fact, are much more than merely reducing the noise levels. The aesthetic aspect provided by the vegetation barriers has a positive effect on human psychology, which is quite crucial for reducing the annoyance caused by exposure to the road traffic noise. Reduction of annoyance due to noise is very important since annoyance affects the psychological and hence the physiological health of human beings adversely. An additional benefit of vegetation belts along the roadsides is that the foliage cover of the vegetation provides surface for the aerosol particles to settle, thus mitigating the effect of air pollutants as well.

Appendix

Site number	Height of veg. belt	Temp.	RH	Species composition – type of vegetation
Site-1, Dehradun	9 ft	39°C	17%	Mallotus *phillipensis*, Cordia *dichotoma*, Morus *alba*, Adina *cordifolia*, Diospyros *tomentosa*, Azadirachta *indica*, Angoeissus *latifollia*, Symplocos *crataegeides*, Helicteres *isora*, Adhatoda *vassica*, Callicarpa *macrophyola*, Nerium *indicum*
Site-2, Dehradun	10 ft	39°C	18%	Adhatoda *vassica*, Mallotus *phillipensis*, Murraya *koeniggi*, Indigoferra *heterantha*, Arundo *donax*, Bauhinia *variegate*, Celtus *tetrandra*
Site-3 Dehradun	5–7 ft	27°C	26%	Lantana *camara*, Syzygium *cumini*, Thysanolena *agrostis*
Site-4, Dehradun	10–12 ft	27° C	26%	Broussonetia *papyrifera*, Lagerstroemia *parviflora*, Holarrhena *antidysenterica*, Mallotus *phillipensis*, Eulalliopsis *binata*, Themada *arundinacea*, Nerium *indicum*, Solanum *verbascifolium*, Murraya *kceniggi*
Site-5, Dehradun	12 ft	39°C	17%	Mallotus *phillipensis*, Lantana *camara*, Celtus *tetrandra*, Fiscus *racemosa*, Trema *orientalis*, Achyranthes *aspera*, Cryptolepis *buchanani*, Hiptage *bengalensis*, Saccharum *spontaneum*
Site-6, Dehradun	9 ft	39°C	18%	Mallotus *phillipensis*, Bauhinia *variegate*, Cryptolepis *buchanani*, Schleichera *oleosa*, Millettia *auriculata*, Saccharum *spontaneum*, Murraya *kceniggi*
Site-7, Pantnagar	10–12 ft	25° C	26%	Sal, Haplophragma *adenophyllum*, Adhatada *vassica*, Celtis *tetranda*, Bridelia *retusa*, Ehretia *laevis*, Litsea *glutinesa*, Bombax *ceiba*
Site-8, Pantnagar	14 ft	25°C	26%	Bauhinia *variegate*, Haloptelea *integrifolia*, Cassia *fistula*, Ehretia *laevis*, Coculus *laurifolius*, Mallotus *phillipensis*, Litsea *glutinesa*
Site-9, Haridwar	10 ft	40°C	16%	Moringa *oleifera*, Morus *alba*, Litsea *glutinesa*, Melia *azedarach*, Celastrus *paniculata*, Cuscuta *reflaxa*, Mangifera *indica*, Symplocos *crataegeides*
Site-10, Haridwar	6–7 ft	40°C	16%	Themeda *arundinacea*, Saccharum *spontaneum*, Cannabis *sativa*
Site-11, Hardwar	10 ft	40°C	16%	Themeda *arundinacea*, Lantana, Eulaliopsis *binata*, Cynadon *dactylon*, Vetiveria *zizanioides*

Acknowledgments

Two of the authors, Krishan Kumar and Vikrant Tyagi, would like thank the University Grants Commission, Government of India, for providing the financial assistance for carrying out this study.

References

1. Attenborough K. (1988), *Review of Ground Effects on Outdoor Sound Propagation from Continuous Broadband Sources*, Applied Acoustics, **24**, 289–319.
2. Aylor D. (1972), *Noise Reduction by Vegetation and Ground*, Journal of the Acoustical Society of America, **51**, 1, 197–205.
3. Aylor D. (1972), *Sound Propagation in Relation to Leaf Density, Leaf Width, and Breadth of Canopy*, Journal of the Acoustical Society of America, **1**, 1, 411–414.
4. Bullen F., Fricke F. (1982), *Sound Propagation through Vegetation*, Journal of Sound and Vibration, **80**, 1, 11–23.
5. Carlson D.E., Mc Daniel O.H., Reethof G. (1977), *Noise control by forest, In: Internoise international conference on noise control engineering*, Zurich, Switzerland, B567–86.
6. Cook D.I., Van Haverbeke D.F. (1971), *Trees and Shrubs for Noise Abatement, The forest service*, US Department of Agriculture, Research Bulletin, 246.
7. Fang C.F., Ling D.L. (2003), *Investigation of the noise reduction provided by tree belts*, Landscape Urban Plan, **63**, 187–95.
8. Garg N., Sharma O., Mohanan V., Maji S. (2012), *Passive noise control measures for traffic noise abatement in Delhi*, India, Journal of Scientific and Industrial Research, **71**, 226–234.
9. Huddart L. (1990), *The use of vegetation for traffic noise screening*, Department of transport TRRL report ISSN 0266-5247, Transport and Road Research Laboratory, Crowthorne.
10. ISO 9613-1 (1992), Acoustic – Attenuation of Sound during Propagation Outdoors, Part 1: Methods of calculation of the Attenuation of Sound by Atmospheric Absorption, International Organization for Standardization.
11. ISO 9613-2 (1992), Acoustic – Attenuation of Sound during Propagation Outdoors, Part 2: Methods of calculation of the Attenuation of Sound by Atmospheric Absorption, International Organization for Standardization.
12. Kumar K., Jain V.K., Rao D.N. (1998), *A predictive model of noise for Delhi*, J. Acoust. Soc. Am., **103**, 3, 1677–79.
13. Linskens H.F., Martens M.J.M., Hendriksen H.J.G.M., Reostenberg-Sinnige A.M., Brouwers W.A.J.M., Van Der Staak A.L.H.C., Strik-Jansen A.M.J. (1976), *The Acoustic Climate of Plant Communities*, Oecologia (Berl.), **23**, 165–177.
14. Martens M.J.M. (1980), *Foliage as a Low Pass Filter: Experiments with model Forests in a Anechoic Chamber*, Journal of Acoustical Society of America, 67, 1, 66–72.
15. Maleki K., Hosseini S.M., Nasiri P. (2010), *The Effect of Pure and Mixed Plantations of Robinia Pseudoacasia and Pinus Eldarica on Traffic Noise Decrease*, International Journal of Environmental Sciences, **1**, 213–224.
16. Martens M.J.M. (1981), *Noise Abatement in Plant Monocultures and Plant Community*, Applied Acoustics, **14**, 167–189.
17. Pal A.K., Kumar V., Saxena N.C. (2000), *Noise attenuation by green belts*, Journal of Sound and Vibration, **234**, 1, 149–165.
18. Pathak V., Tripathi B.D., Mishra V.K. (2008), *Dynamics of traffic noise in a tropical city Varanasi and its abatement through vegetation*, Environmental Monitoring Assessment, **146**, 67–75.
19. Price M.A., Attenborough K., Heap N. (1988), *Sound Attenuation through Trees – Measurements and Models*, Journal of Acoustical Society of America, **84**, 5, 1836–1844.
20. Tyagi V., Kumar K., Jain V.K. (2006), *A study of the spectral characteristics of traffic noise attenuation by vegetation belts in Delhi*, Applied Acoustics, **67**, 926–935.
21. Yamada S., Watanabe T., Nakamura S., Yokoyama H., Takeoka S. (1977), *Noise reduction by vegetation*, Internoise 77 – International Conference on Noise Control Engineering, Zurich, Switzerland, B599–B606.

PAN ARCHIVES OF ACOUSTICS
Vol. 38, No. 3, pp. 397–405 (2013)

DOI: 10.2478/aoa-2013-0047

Study of the Categorisation Method Using Long-term Measurements

Guillermo REY GOZALO[(1), (2)], Juan Miguel BARRIGÓN MORILLAS[(1)],
Valentín GÓMEZ ESCOBAR[(1)], Rosendo VÍLCHEZ-GÓMEZ[(1)],
Juan Antonio MÉNDEZ SIERRA[(1)], Francisco Javier CARMONA del RÍO[(1)],
Carlos PRIETO GAJARDO[(1)]

[(1)] *Laboratorio de Acústica, Departamento de Física Aplicada, E Politécnica, Universidad de Extremadura*
Avda. de la Universidad s/n, 10003 Cáceres, Spain;
e-mail: {guille, barrigon, valentin, vilchez, jmendez, jcarmona, carlosprieto}@unex.es

[(2)] *Universidad Autónoma de Chile*
5 Poniente 1670, Talca, Región del Maule, Chile; e-mail: greyg@uautonoma.cl

(*received March 7, 2012; accepted July 15, 2013*)

Previous studies concerning the categorisation method have been based on short daytime measurements. These studies demonstrated urban-noise stratification in the daytime. Nevertheless, legislation and standards refer to noise estimation throughout the day. This paper presents the first attempt to apply the categorisation method to indicators obtained through long-term measurements. The study was conducted in Plasencia, Extremadura (Spain) which has approximately 41,500 inhabitants. First, we conducted a stratification of the roads using the categorisation method. Second, long-term measurements (approximately one week) were conducted at different sampling locations across different categories of streets. The results were analysed by category. Moreover, the profile of the noise-level variation was analysed during the day. The results revealed a stratification of sound levels measured across the different categories. Furthermore, we found health risks due to the noise levels in this town. Short-term measurements were also conducted to complete the categorisation method suitability analysis.

Keywords: noise pollution, sampling methods, street categorisation.

1. Introduction

Noise pollution is an environmental problem present everywhere in developed society. Numerous publications alert us to the dangerous effects of noise (EEA, 2009; WHO, 2011).

Within concern for noise pollution, European legislation demands Member States to elaborate noise maps in population centres with more than 100,000 inhabitants (EU, 2002). Nevertheless, many Europeans live in small towns; thus, they are excluded from these studies. For example, in 2010, 60.2% of the Spanish population lived in towns with less than 100,000 inhabitants (INE, 2010).

The large percentage of people living in small towns makes devoting effort to these places necessary. For the current studies, our research group used a categorisation method to classify streets into different groups based on their use as communication routes. This *in situ* method has shown potential as a simpler and less resource-consuming method than grid-based experimental designs. Furthermore, it has revealed promising results in small (Rey Gozalo *et al.*, 2012) and medium-sized towns (Barrigón Morillas *et al.*, 2002; 2005a; 2005b; Carmona del Río *et al.*, 2011). Recent publications have shown other applications using this methodology (Barrigón Morillas *et al.*, 2010; Rey Gozalo *et al.*, 2013), and it has been compared with other *in situ* methodologies (Barrigón Morillas *et al.*, 2011).

Our previous studies have been based on short-term measurements from which we estimated sound levels during the day (L_{d}). However, the present study analyses, for the first time, the suitability of the categorisation definition by conducting long-term measurements to obtain the L_{d}, L_{e}, L_{n}, and L_{den} indices. Besides, relationships among short-term and long-term results are also analysed.

The main objective of this work was to study the performance of the categorisation method and the behaviour of city sound levels using long-term measurements (for approximately one week).

Besides, as a secondary objective, we analyse the acoustical situation of a small city in relation with international reference values.

2. Methods

2.1. Plasencia

Plasencia has a population of 41,500 inhabitants and is located in the north of the Extremadura region in south-western Spain. Despite its number of inhabitants, Plasencia is the second most populated town in the province and the fourth most populous in the region. The city's economy is based primarily on the trade and services sector which represents 68.3% of the employed population. It also contributes to the construction and industry sectors (19.3% and 8.7% of the employed population, respectively). The industry sector specialises in agricultural products. For over eight centuries, this village remained locked in a walled area and contact with the outside was conducted through doors and wall shutters. During the nineteenth century, the city grew outside the wall, primarily beside the Jerte River. As a consequence of this history (i.e. excessively narrow and elongated streets), there are problems with modern urban mobility.

2.2. Categorisation method

The categorisation method is based on the widely accepted assumption that road traffic is the primary source of noise in most streets. The category definitions used in the present study are the same as in a previous work (Barrigón Morillas *et al.*, 2005a). A summary of the steps needed to apply this method can also be found in this publication.

2.3. Street categorisation

The town categorisation consisted in classifying each street into one of six categories. This step required approximately one week: one to two days of study using a map and the assistance of one of the town's residents, and four to five days of *in situ* study.

The final categorisation of Plasencia is shown in Fig. 1. Only streets with housing were considered. All streets other than pedestrian, restricted-access, and so on not included in Categories 1 to 4 were included in Category 5.

2.4. Sampling point selection

Two types of measurements were conducted for the present study: short-term measurements and long-term measurements.

For the short-term measurements, once every street of the city had been assigned to one of five categories, ten sampling points were randomly selected in each category. Two methods were used: one for Categories 1 to 4 streets and the other for Category 5 streets. In the

Fig. 1. Map of Plasencia including the different categories and sampling points with both short- and long-term measurements.

former method, the total length of streets that belonged to each category was calculated and denoted by L_i, the length of category i ($i = 1, ..., 4$). Ten sampling points were located randomly between 0 and L_i. The only restriction was that equivalent points (i.e., those located on the same street section with no intersection between them) were avoided; thus, only 9 sampling points for Categories 1 and 2 were chosen because it was impossible to select more non-equivalent points. Another random strategy was used in the latter method due to the large number of streets involved in Category 5 (n_5). Each street was taken as a single potential sampling point (p_i, $i = 1, ..., n_5$) and ten sampling point selected randomly between 1 and n_5 and located in the middle of the segment that corresponded to the entire street. Locations of the 48 short-term measurement points are shown in Fig. 1 and are superimposed on the street categorisation.

For the long-term measurements, several non-equivalent points were selected for each of the categories to locate the maximum number of sampling points. Special care was taken when selecting these points to assure the security of the monitoring equipment with respect to adverse weather conditions and vandalism. The locations of the 18 long-term measurement locations are presented in Fig. 1.

Importantly, the categories do not have a standard size. Thus, to obtain average values for the entire city, each category was weighted by length. Table 1 shows the number of points measured in each category as well as the length percentage and the proportion of the population that lives in each category.

Table 1. The number of sampling points measured for each category. The percentage of each category's street length is determined with respect to the total street length of Plasencia and in proportion to the population that lives in each category.

Category	1	2	3	4	5
Number of long-term measurements	4	4	4	3	3
Number of short-term measurements	9	9	10	10	10
% Length	5.2	8.0	5.9	10.6	70.3
% Population	2.1	3.5	4.9	8.7	80.8

2.5. Measurement equipment and procedure

In-situ noise short-term measurements were made from Monday to Friday in the daytime. Daytime was defined by the European Directive 20002/49/EC (COM, 2002) as from 7:00 a.m. to 7:00 p.m. This period was divided into four 3-hour periods and one noise measurement of 15 minutes of duration was carried out in each period to obtain a set of four independent measurements for each sampling point. Using this method, only one measurement was performed at each location per day and never during the same time interval.

All measurements were conducted following the ISO 1996-2 guidelines (ISO 1996-2, 2007) using 2260 and 2238 Brüel & Kjær Type-1 sound level meters equipped with a tripod and a windshield. For the long-term measurements, a 2-metre extension pole separated the microphone from the building facade. For the short-term measurements, the sound level meter was located at a height of 1.5 metres and one metre from the curb. Calibration was performed using a 4231 Brüel & Kjær calibrator twice a day. The measurement lasted for approximately a week for the long-term measurements.

3. Results and discussion

3.1. Preliminary analysis of long-term measurements

In the first step, long-term measurements values were normalised to the reference height of 4 metres (EU, 2002). For these calculations, the normalisation effects of geometric divergence for open profile streets (considering streets as a source of line noise) were considered, whereas the French Standard *Guide du Bruit* corrected the data from streets with a U-shape (CETUR, 1980). Variation of long-term measurements values during a week are shown in Fig. 2 for four sampling points.

In the second step, due to the significant differences between the sound levels of the different categories found in previous studies for short-term measurements (Barrigón Morillas *et al.*, 2005a), we decided to use the long-term measurements to analyse the sound level during a full week to search for similarities, tendencies, differences among categories, and so on. For instance, we analysed the difference between the temporal structure of noise levels in each category in order to check if this structure was similar in all the categories or if, as it happens with noise values, there were differences between categories. For this purpose, we used continuous partial trend models (Tomé, Miranda, 2005a; 2005b). This technique allows for a multiple linear fit by fitting least-squares continuous line segments to a continuous series with a minimum mean square error. After observing the sound-pressure profile of the long-term measurements (Fig. 2) and adjusting calculations with regard to 3, 4, and 5 breakpoints, we decided to analyse each day independently using 3 breakpoints. Table 2 presents the average values of the different breakpoints and the slopes of the lines that join these points for each category.

Considering the time at which a breakpoint first occurs, we are able to observe similar behaviours for the different categories:

- Workdays: The first breakpoint occurs from 4:00–5:00 a.m., which coincides with the start of city

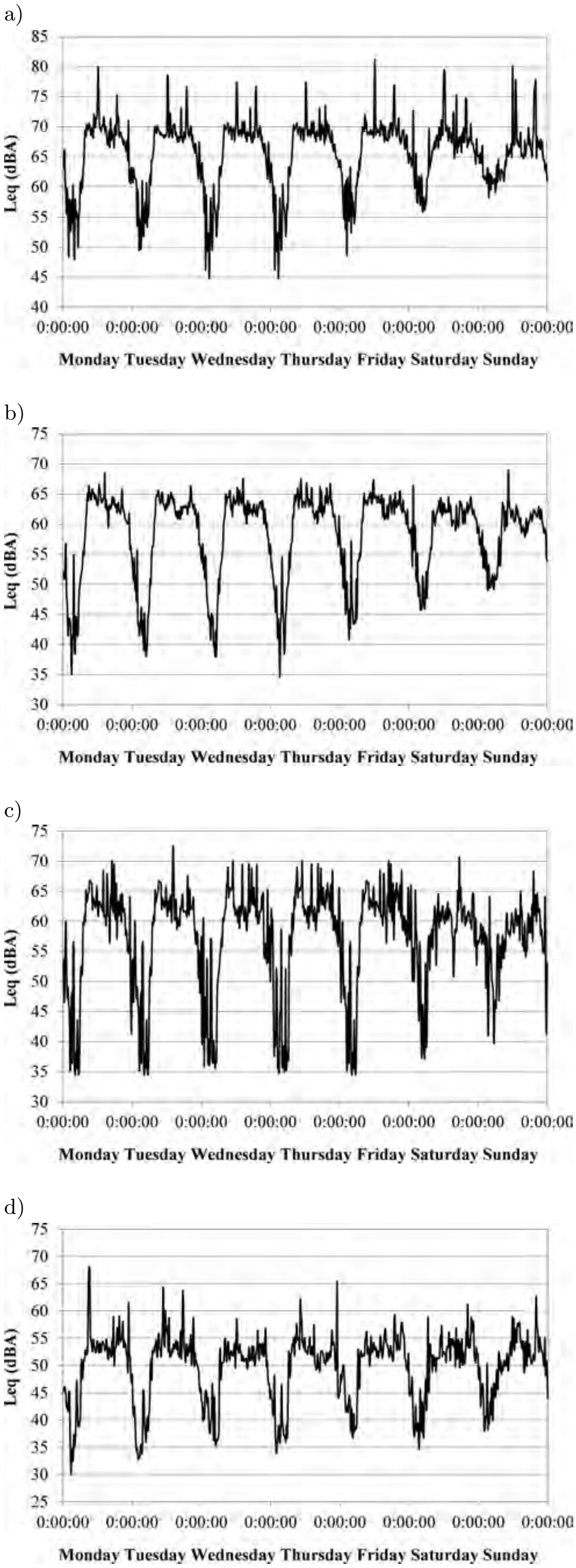

Fig. 2. The weeklong variation of L_{eq}, 15 min for some long-term sampling points: a) Point 1.01; b) Point 2.01; c) Point 4.01; and d) Point 5.01.

Table 2. Average breakpoints and slopes calculated from continuous partial trend models.

Category	Day	Breakpoint		Slope	
		Code	Finish hour	Code	Value
1	Workdays	1	4	1	−2.48
		2	9	2	4.06
		3	22	3	−0.07
	Weekend	1	6	1	−1.84
		2	11	2	1.92
		3	23	3	−0.12
2	Workdays	1	5	1	−2.86
		2	9	2	4.71
		3	22	3	−0.16
	Weekend	1	6	1	−2.83
		2	10	2	2.63
		3	23	3	0.11
3	Workdays	1	5	1	−2.76
		2	9	2	4.95
		3	22	3	0.01
	Weekend	1	5	1	−2.36
		2	11	2	1.68
		3	23	3	0.05
4	Workdays	1	5	1	−2.51
		2	9	2	5.52
		3	22	3	−0.06
	Weekend	1	6	1	−2.83
		2	10	2	2.61
		3	22	3	0.07
5	Workdays	1	5	1	−2.47
		2	8	2	6.25
		3	22	3	−0.14
	Weekend	1	5	1	−2.26
		2	9	2	3.68
		3	23	3	0.05

traffic (i.e. garbage trucks, the first human movements, and so on). The second breakpoint occurs from 8:00–9:00 a.m. when noise levels begin to rise. The third breakpoint occurs at 10:00 p.m. when sound levels stabilise and begin to decrease.

- Weekend: Human activity began later; thus, the first breakpoint is approximately at 5:00–6:00 a.m. Noise levels begin to rise at 10:00–11:00 a.m. (except in Category 5 in which noise rises at 9:00 a.m.). Finally, sound levels stabilise and start to decrease at 10:00–11:00 p.m.

Therefore, there were no important differences between the studied categories; however, we observed differences between workdays and weekend with respect to the breakpoints. Specifically, the first breakpoint occurs one to two hours later than in working days than weekends.

Then, considering the slope of the lines that join the breakpoints:

- Without considering the category, the slopes of Lines 1 (a reduction in noise levels from 10:00–11:00 p.m. to 4:00–6:00 a.m.) and 2 (an increase in noise levels from 4:00–6:00 a.m. to 8:00–11:00 a.m.) are more pronounced in workdays than weekends, whereas there was no difference with regard to the slope of Line 3. Line 3 has a slope value close to zero because the sound levels are approximately stable between 9:00 a.m. and 10:00 p.m.
- Comparing the slope means of the lines representing different categories, the slopes of Lines 1 and 3 do not differ across the different categories. Nevertheless, the slope of Line 2 increases when the category increases, especially on workdays.

Thus, the sound level variation profiles of the different categories have many similarities to each other during the day. In any case, according to our long-term measurements, the slope that corresponds to the increase of sound levels from the morning (between 4:00 and 6:00 a.m.) to the evening (between 8:00 and 10:00 p.m.) increases with the street category. This finding might indicate other differences between the categories that should be investigated in the future.

Finally, the L_{d}, L_{e}, L_{n}, and L_{den} long-term measurement indices were calculated for each category (Table 3 presents these values). Two indices were calculated for L_{d}: L_{d12} was calculated from 7:00 a.m. to 7:00 p.m., and L_{d16} was calculated from 7:00 a.m. to 11:00 p.m. Thus, considering the international reference values (e.g. 65 dBA, 55 dBA, or 45 dBA) and the average sonorous values for each category (Table 3), only the Category 5 L_{d16} was under 55 dBA, a level that the WHO considers as a serious annoyance (WHO, 1999). This represents the 19% of the population living in this town (see Table 1). L_{d16} levels above 65 dBA (the value that the OECD suggests as the daytime exposure limit; OECD, 1986) were exceeded by Category 1 and Category 2. At night, the L_{n} index was under 45 dBA (a value considered by the WHO as a reference value for sleep disturbance; WHO, 1999) at only in workdays in Category 5. Finally, 11% of the population live in "black acoustic zones" ($L_{\mathrm{den}} > 65$ dBA), 89% in "grey acoustic zones" (65 dBA $> L_{\mathrm{den}} >$ 55 dBA) and 0% in "white acoustic zones" ($L_{\mathrm{den}} < 55$ dBA), using the OECD criteria terminology (OECD, 1991).

Therefore, we conclude from the long-term measurement results that Plasencia, despite being a small city, has noise levels that might seriously affect the health and quality of life of a significant percentage of its population, especially at night.

Table 3. Average values of L_{d12}, L_{e}, L_{d16}, L_{n}, and L_{den} indices (in dBA) for each category.

Category	Sound Index	Average value (workdays) [dBA]	Average value (weekend) [dBA]	Average value (weekly) [dBA]
1	L_{d12}	67.7±2.8	66.0±3.0	67.3±2.8
	L_{e}	66.4±2.1	66.4±3.1	66.4±2.3
	L_{d16}	67.4±2.6	66.1±3.1	67.1±2.7
	L_{n}	58.1±3.2	61.2±2.6	59.3±2.8
	L_{den}	69.4±2.5	70.2±2.8	69.7±2.6
2	L_{d12}	66.1±0.8	63.2±0.9	65.4±0.8
	L_{e}	64.8±1.4	64.7±1.7	64.8±1.5
	L_{d16}	65.8±0.9	63.6±1.1	65.3±0.9
	L_{n}	55.3±1.5	59.2±1.0	56.8±1.3
	L_{den}	67.6±1.1	68.2±1.2	67.8±1.1
3	L_{d12}	63.2±2.6	60.5±1.5	62.6±2.3
	L_{e}	63.4±2.0	61.7±1.8	63.0±1.8
	L_{d16}	63.2±2.4	60.9±1.5	62.7±2.2
	L_{n}	54.1±1.8	57.1±1.3	55.2±1.5
	L_{den}	65.9±2.0	65.7±1.3	65.8±1.7
4	L_{d12}	60.5±2.4	57.9±1.5	59.9±2.3
	L_{e}	60.4±1.4	59.0±1.6	60.0±1.5
	L_{d16}	60.5±2.1	58.2±1.5	60.0±1.9
	L_{n}	50.8±1.5	53.0±3.1	51.6±2.1
	L_{den}	62.9±1.5	62.3±2.1	62.7±1.7
5	L_{d12}	53.6±0.5	50.8±1.1	53.0±0.4
	L_{e}	52.8±0.8	52.5±1.7	52.7±1.0
	L_{d16}	53.4±0.3	51.3±1.3	52.9±0.4
	L_{n}	44.5±3.0	46.2±0.3	45.2±2.0
	L_{den}	55.9±0.6	55.7±0.9	55.8±0.5

3.2. Analysis of categorisation method

As shown in Table 3, the long-term measurement average values of all the analysed indices decrease when the number of the category increases. These results seem to indicate the existence of noise-level stratification in the city. Nevertheless, sampling point locations are not similar and obtained values must to be normalised.

Thus, long-term measurements were used to obtain the sound power level per length of traffic source (assuming it is linear). This calculation was necessary to compare the long-term results with the short-term results because different distances to the source must be considered with the reflection effects (ISO 9613-2, 1996). The average power level was evaluated in each category after accounting for these divergence and reflection effects. One order of reflection was considered; reflections on vertical obstacles were treated with the help of image-sources, as used in several national calculation methods (EC, 2003). As shown in Table 4,

Table 4. Sound power levels (L_{w}, in dBA) of the linear traffic source for each category.

Category	L_{d16w} [dBA]			L_{nw} [dBA]			L_{d24w} [dBA]		
	Average value (workdays)	Average value (weekend)	Average value (weekly)	Average value (workdays)	Average value (weekend)	Average value (weekly)	Average value (workdays)	Average value (weekens)	Average value (weekly)
1	81.9±0.6	80.6±1.2	81.6±0.7	72.6±1.2	75.7±0.7	73.8±0.8	80.4±0.6	79.5±1.1	80.2±0.6
2	80.1±0.4	77.9±0.7	79.6±0.5	69.6±1.3	73.5±0.9	71.1±1.1	78.6±0.4	76.8±0.6	78.1±0.4
3	76.5±1.5	74.2±1.5	76.0±1.4	67.4±0.4	70.4±0.6	68.5±0.3	75.1±1.4	73.2±1.3	74.6±1.3
4	73.0±0.5	70.6±1.1	72.5±0.6	63.2±1.3	65.4±1.7	64.0±1.2	71.5±0.5	69.5±1.0	71.0±0.6
5	66.2±0.4	64.1±1.5	65.7±0.6	57.3±3.0	59.0±0.2	58.0±2.0	64.7±0.5	62.9±1.3	64.3±0.6

Category	L_{d12w} [dBA]			L_{ew} [dBA]		
	Average value (workdays)	Average value (Weekends)	Average value (weekly)	Average value (workdays)	Average value (Weekends)	Average value (weekly)
1	82.2±0.7	80.5±1.2	81.8±0.8	80.8±0.4	80.9±1.3	80.9±0.4
2	80.4±0.4	77.4±0.6	79.7±0.3	79.1±1.0	79.0±1.3	79.1±1.0
3	76.5±1.7	73.8±1.3	75.9±1.6	76.6±1.0	75.0±2.2	76.3±1.0
4	73.0±0.2	70.3±1.0	72.4±0.2	72.9±1.8	71.5±1.3	72.5±1.7
5	66.3±0.6	63.6±1.3	65.7±0.6	65.5±0.9	65.2±1.9	65.5±1.2

the sound power levels decrease when the category number increases, and there is practically no overlap. Table 4 clearly shows the existence of noise stratification in all of the time periods considered across the city. In addition, these results indicate that the categorisation method suitably characterises the noise stratification in the city. Nevertheless, the long-term measurements cannot statistically demonstrate that the categorisation method suitably discriminates this stratification due to the small number of sampling points (a maximum of four points per category). Thus, the existence of the mentioned stratification will be analysed using the results of the short-term measurements and checking the coherence among short-term and long-term results.

Short-term measurements allowed us to obtain a dataset large enough to statistically examine the possible differences between the measured sound levels. In previous studies, approximately 10 sampling points per category were sufficient to analyse the differences between five categories (Barrigón Morillas *et al.*, 2002; 2005a; 2011). Thus, as previously mentioned, 9–10 points were selected in Plasencia per category (see Table 1) to characterise the noise of the city that was not examined with the long-term measurements.

Table 5 shows the average L_{eq} values obtained for each category for short-term measurements and average sound power levels calculated both from short-term and long-term measurements (the latter being previously shown in Table 4). L_{eq} values were obtained as the arithmetic mean of the sound level values of the points of each category. Sound power per unit length values for short-term measurements were obtained as the arithmetic mean of the power values of the different points which were obtained from the measured sound pressure levels with the same calculation procedure used for long-term measurements.

Table 5. L_{d12h} and sound power levels obtained for short-term measurements. The L_{d12w} obtained for workdays is also shown.

Category	L_{d12} [dBA] Workdays Short-term measurements	L_{d12w} [dBA] Workdays Short-term measurements	L_{d12w} [dBA] Workdays Long-term measurements
1	71.5±0.8	81.6±0.8	82.2±0.7
2	69.5±0.8	79.9±0.7	80.4±0.4
3	67.1±1.5	77.0±1.2	76.5±1.7
4	64.7±1.3	73.3±2.5	73.0±0.2
5	59.7±3.2	68.1±3.3	66.3±0.6

As can be seen in Table 5, sound power values are similar between short-term measurements and long-term measurements. These results indicate that, when averaging by category, short-term sound levels provide a sufficient approximation of the weekly sound levels in daytime period.

We performed a statistical analysis of the sound power values obtained from the street to examine the differences in sound power levels among the five categories. We sought to determine whether these differences were significant at a 95% confidence interval.

We proposed the following hypotheses for the analysis below:

- H_0 = There were no significant differences among the sound power level means of the different categories.

- H_1 = There were significant differences among the sound power level means of the different categories.

Before conducting the appropriate statistical test to address the hypotheses, we analysed the normality of the data using the Shapiro-Wilk test (Shapiro, 1965). We obtained a p-value of 0.0072, indicating that these data significantly differed from a normal distribution. This lack of normality, together with the small number of data in each category, suggests the use of nonparametric tests because the results are less disputable.

Thus, we first analysed the different categories using the Kruskal-Wallis test (Kruskal, Wallis, 1952). We obtained a p-value of $1.037 \cdot 10^{-8}$ which indicates a significant difference among the categories. Then, we used the Mann-Whitney U test with a Bonferroni correction to perform multiple comparisons between different category pairs (Mann, Whitney, 1947; Martin, Altman, 1995). The results of this test are shown in Table 6.

As shown in Table 6, there were differences between all category pairs at a significance level less than or equal to 0.05. Thus, the categorisation method is a suitable method of studying the noise stratification in small cities.

As a second proof of this suitability, we used the ROC analysis (Hand, Till, 2001; Fawcett, 2006) to demonstrate the predictive capacity of this method. ROC has been previously and successfully used to support similar aims (Carmona del Río *et al.*, 2011). Table 7 shows the results of this analysis. As can be seen, the marks of the strata were close to the means of all categories. This proximity is indicative of the internal coherence of the category method.

ROC analysis sensitivity is a measure of the capacity to include the previously assigned streets in the stratum. The results presented in Table 7 are encouraging: the sensitivity was 100% in Stratum 1, and 70% or greater in the other strata. Consequently, the overall sensitivity of the method was over 85%: of a group of five streets, four presented sound values that corresponded to the stratum to which they were assigned in the initial categorisation (prior to measurement).

The nonspecificity measures the proportion of streets that were not initially assigned to a certain stratum but for which the ROC analysis indicates that they belong to that stratum. As shown in Table 7, only Strata 4 and 5 revealed a nonspecificity greater than 5%. These values were less than 3% for the rest of the strata. The overall nonspecificity was 14.6% which is consistent with the overall sensitivity. This result means that, on average, the ROC analysis assigned less than one of the five streets to a stratum that was different from the one to which the categorisation method had assigned it.

Finally, the predictive values of the different strata represent the proportion of the streets that the ROC analysis assigned to the stratum that matched the categories to which they were initially assigned, relative

Table 6. Mann-Whitney U test results with a Bonferroni correction: (***) $p < 0.001$, (**) $p < 0.01$, and (*) $p < 0.05$.

		Category			
		1	2	3	4
Category	2	0.00288(**)	–	–	–
	3	0.00022(***)	0.00152(**)	–	–
	4	0.00022(***)	0.00022(***)	0.00325(**)	–
	5	0.00022(***)	0.00022(***)	0.00011(***)	0.01505(*)

Table 7. ROC analysis results.

Stratum	1		2		3		4		5	all
Mark	81.5		79.4		77.1		73.9		66.9	
Upper limit	82.5		80.4		78.3		75.8		72.0	
Lower limit	80.4		78.3		75.8		72.0		61.8	
Amplitude	2.1		2.1		2.6		3.8		10.2	
AUC		0.96		0.96		0.94		0.90		
Sensitivity (n°)	9		8		8		7		9	41
Sensitivity (%)	100		88.9		80.0		70.0		90.0	85.4
Nonspecificity (n°)	1		1		1		2		2	7
Nonspecificity (%)	2.6		2.6		2.6		5.3		5.3	14.6
Predictive value (%)	90.0		88.9		88.9		77.8		81.8	85.4

to the total number of streets that the ROC analysis determined for the stratum. Table 7 shows that, except for Stratum 4, the predictive values were greater than 80%. The overall predictive value was 85%.

4. Conclusions

The primary conclusions of the present study are as follows:

- Considering that linear noise sources are similar for short and long-term measurements, the sound power levels in the daytime indicate that short-term measurements are sufficient when an adequate number of long-term measurements cannot be conducted.
- Significant short-term measurement differences were found among the different categories with regard to sound levels in the streets. This finding demonstrates the effectiveness of the categorisation method.
- We found a clear differentiation among the different categories with regard to the indices calculated from the long-term measurements.

From these conclusions, we surmise that the categorisation method can be expected to sufficiently estimate the long-term indicators recommended in the European Directive. Nevertheless, more studies are necessary to confirm this conclusion.

- We found that sound level variation behaves similarly throughout the day across the different categories. This finding implies that the city's sound is homogeneous across locations.
- The ROC analysis that examined the predictive capacity of the categorisation method in Plasencia found overall sensitivities and predictive values higher than 85% with regard to the categorisation method.

Acknowledgments

The University of Extremadura (Acción III. Plan Iniciación a la Investigación, Desarrollo Tecnológico e Innovación 2011), the European Social Fund, the European Regional Development Fund (ERDF), and Junta de Extremadura (Projects PRI06A271, PD10166, and GR10175), Consejería de Economía, Comercio e Innovación supported this work.

References

1. Barrigón Morillas J.M., Gómez Escobar V., Méndez Sierra J.A., Vílchez-Gómez R., Trujillo Carmona J. (2002), *An environmental noise study in the city of Cáceres, Spain*, Appl. Acoust., **63**, 1061–1070.
2. Barrigón Morillas J.M., Gómez Escobar V., Méndez Sierra J.A., Vílchez-Gómez R., Vaquero J.M., Trujillo Carmona J. (2005a), *A categorization method applied to the study of urban road traffic noise*, J. Acoust. Soc. Am., **117**, 2844–2852.
3. Barrigón Morillas J.M., Gómez Escobar V., Vaquero J.M, Méndez Sierra J.A., Vílchez-Gómez R. (2005b), *Measurements of noise pollution in Badajoz City, Spain*, Acta Acustica united with Acustica, **91**, 797–801.
4. Barrigón J.M., Gómez Escobar V., Rey Gozalo G., Vílchez-Gómez R. (2010), *Possible relation of noise levels in streets to the population of the municipalities in which they are located*, J. Acoust. Soc. Am., **128**, EL86–EL92.
5. Barrigón Morillas J.M., Gómez Escobar V., Méndez Sierra J.A., Vílchez-Gómez R., Carmona del Río J., Trujillo Carmona J. (2011), *Comparison of two procedures for the evaluation of urban noise*, Appl. Acoust., **71**, 760–771.
6. Carmona del Río F.J., Gómez Escobar V., Trujillo Carmona J., Vílchez-Gómez R., Méndez Sierra J.A., Rey Gozalo G., Barrigón Morillas J.M. (2011), *Application of a street categorization method to the study of urban noise: the Valladolid (Spain) study*, Environmental Engineering Science, **28**, 811–817.
7. CETUR, Centre d'Etudes des Transports Urbains (1980), *Guide du Bruit des Transports Terrestres. Prévision des niveaux sonores*, CETUR, France.
8. EC (European Commision) (2003), *Adaptation and revision of the interim noise computation methods for the purpose of strategic noise mapping*, European Commision DG Environment, reference: B4-3040/2001/329750/MAR/C1.
9. EU (European Union) (2002), *Directive 2002/49/EC relating to the Assessment and Management of Environmental Noise*, Official Journal of the European Communities, No. L 189.
10. Fawcett T. (2006), *An introduction to ROC analysis*, Pattern Recognition Letters, **27**, 861–874.
11. Hand D.J., Till R.J. (2001), *A simple generalisation of the area under the ROC curve for multiple class classification problems*, Machine Learning, **45**, 171–186.
12. INE, Instituto Nacional de Estadística (2010), *Padrón municipal: cifras oficiales de población*, INE, Madrid.
13. ISO 1996-2: 2007 (2007), *Description, measurement and assessment of environmental noise. Part 2: Determination of environmental noise levels*, International Organization for Standardization, Switzerland.
14. ISO 9613-2: 1996 (1996), *Acoustic-attenuation of sound during propagation outdoors. Part 2: General method of calculation*, International Organization for Standardization, Switzerland.

15. Kruskal W.H., Wallis W.A. (1952), *Use of ranks in one-criterion variance analysis*, Journal of American Statistical Association, **47**, 583–621.

16. Mann H.B., Whitney D.R. (1947), *On a test of whether one of two random variables is stochastically larger than the other*, Annals of Mathematical Statistics, **18**, 50–60.

17. Martin J., Altman D.G. (1995), *Statistic notes: Multiple significance test: the Bonferroni method*, British Medical Journal, **310**, 170.

18. OECD, Organization for Economic Cooperation and Development (1986), *Fighting Noise: Strengthening Noise Abatement Policies*, OECD Publications, Paris.

19. OECD, Organization for Economic Cooperation and Development (1991), *Fighting noise in 1990s*, OECD Publications, Paris.

20. Rey Gozalo G., Barrigón Morillas J.M., Gómez Escobar V. (2013), *Urban streets functionality as a tool for urban pollution management*, Science of the Total Environment, 461–462, 453-–461.

21. Rey Gozalo G., Barrigón Morillas J.M., Gómez Escobar V. (2012), *Analysis of noise exposure in two small towns*, Acta Acustica united with Acustica, **98**, 884–893.

22. Shapiro S.S. (1965), *An analysis of variance test for normality (complete samples)*, Biometrika, **52** (3–4), 591–611.

23. Tomé A.R., Miranda P.M.A. (2005a), *Continuous partial trends and low-frequency oscillations of time series*, Nonlinear Processes in Geophysics, **12**, 451–460.

24. Tomé A.R., Miranda P.M.A. (2005b), *Large scale spatial structure of observed temperature trends*, Proceeding 16th Conference on Climate Variability and Change, American Meteorological Society.

25. WHO, World Health Organization (1999), *Guidelines for Community Noise*, WHO, Geneva.

26. WHO, World Health Organization (2011), *Burden of disease from environmental noise. Quantification of healthy life years lost in Europe*, WHO, Geneva.

PAN ARCHIVES OF ACOUSTICS
Vol. 38, No. 3, pp. 407–415 (2013)

DOI: 10.2478/aoa-2013-0048

Technical Notes

Using Microphone Arrays to Detect Moving Vehicle Velocity

Ramón PERAL-ORTS, Emilio VELASCO-SÁNCHEZ,
Nuria CAMPILLO-DAVÓ, Héctor CAMPELLO-VICENTE

Acoustical Engineering and Vibration Research Group,
Department of Mechanical Engineering, University of Miguel Hernandez
Av Universidad S/N, 03202, Elche (Alicante), Spain; e-mail: ramon.peral@umh.es

(*received May 30, 2012; accepted February 26, 2013*)

The noise of motor vehicles is one of the most important problems as regards to pollution on main roads. However, this unpleasant characteristic could be used to determine vehicle speed by external observers. Building on this idea, the present study investigates the capabilities of a microphone array system to identify the position and velocity of a vehicle travelling on a previously established route. Such linear microphone array has been formed by a reduced number of microphones working at medium frequencies as compared to industrial microphone arrays built for location purposes, and operates with a processing algorithm that ultimately identifies the noise source location and reduces the error in velocity estimation.

Keywords: microphone array, sound location, moving sources, vehicle velocity.

1. Motivation and objective

Speed control and processing systems of road vehicles can currently determine traffic speed by using microwave radar systems. These devices can detect objects and determine distance and movement speed by using built-in emitting and receiving antennas. The mechanics of a microwave radar system are in essence simple: the emitting antennas project radio waves continuously onto the road and upon contact with the vehicle in transit, the radio waves are reflected and captured by the receiving antennas, which in turn trigger the start of an internal processing algorithm that produces an estimate of the velocity of the detected vehicle. In a similar fashion, other type of radars can be built based on the same idea, but using laser emitters and receivers. Although these systems have some advantages as they do not need to interrupt traffic for installation and are multilane data collection systems, they also have disadvantages like the possibility of some missed detections if tall vehicles occlude the more distant lanes and mainly that they are easily detected by antiradar systems.

Other systems, like "velocity cameras", have, in contrast, a slightly different approach to speed vehicle detection. They calculate the average velocity of a vehicle transiting between two points by processing the temporal delay of two or more snapshots of the vehicle taken along the stretch of the road under study. New control systems, such as the DUO and/or Mobile-Vision systems, play with the same principle of capturing images, but use a more advanced technology than the basic "speed camera" system. These systems have main problems with large vehicles, because they can mask trailing vehicles, moreover the presence of shadows, reflections from wet pavement, headlight beams, relative color of vehicles and background, or camera vibration can affect vehicles' detection.

All existing control devices currently in operation, as well as those that are being developed, aim to reliably detect the speed of road vehicles. Whereas vehicles are traditionally seen as significant noise pollutants, this negative and inherent characteristic could be used to locate and estimate their speed. The use of an acoustic microphone array as a traffic control tool would be an undetectable system which would avoid visual problems and be cheaper than most of those currently used.

As the modeling process and theoretical research of sound sources state, a moving source of real sound placed at a particular distance from the receiver can be considered as a point source, which can be identified by emitting a spherical wave from the physical center of the generating element. Locating the origin of this wave constantly would enable us to establish the position of the vehicle to be analyzed and then its velocity. Microphone array is the most suitable system to identify the angle of arrival of a wave emitted in a particular point of space as their set of sound sensors can determine the origin of a sound wave through gaps in signals received between the elements.

Building on the above idea, the present study investigates the creation of a linear microphone array formed by the fewest possible number of sound receivers to allow an easy installation and a manageable on-site use, but guaranteeing a reasonable degree of accuracy in the results. As one might expect, the reduction of the number of sensors in the array could cause an increase in the error of the results, but such increase can be controlled, as described in this article later on, by the application of a processing algorithm that adjusts the operating procedures and reduces the error to an acceptable limit. Such linear microphone array has been formed by a reduced number of microphones working at medium frequencies as compared to industrial microphone arrays (Kuhn *et al.*, 1998) or directional microphones (Danicki, 2005) built for location purposes.

2. Microphone array background

A microphone array consists of a grid of microphones sampling the sound field at discrete spatial positions. The angle of the array relative to the far field sound source and the strategic position of each microphone within the array cause the plane wave front to hit the receivers with a temporal delay, as Fig. 1 shows. The temporal recording of each microphone needs to be compared to ensure that the measuring signal is the same in every microphone regardless of the specific phase delay of each signal, which depends on the relative position between the transducer and the noise source. The capacity of locating a noise source is known as the Direction Of Arrival, DOA.

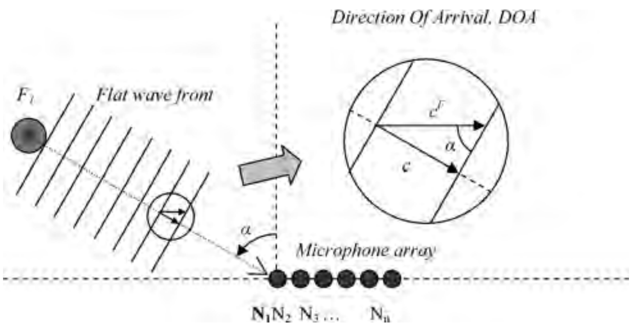

Fig. 1. Noise source wave front consideration for a linear array in the far field.

Developing the optimal microphone array configuration and finding novel applications for microphone arrays are some of the main goals pursued by contemporary scientists specialized in the matter. A clear example of this search is noted in the development of 2-dimensional antennas to detect and identify noise sources in near field, as marketed by Bruel&Kjaer (Christensen, Hald, 2004), and some other technology companies like Bswa Technology from China and Gfai Technology (Döbler *et al.*, 2008) from Germany.

Using simple antennas may give satisfying results. Lopez-Valcarce (2004) and Moran *et al.* (2007) carried out different tests to detect noise sources, localization, and speed through microphone antennas. Other authors (Kodera *et al.*, 2007) suggest a 4-microphone system to locate vehicles in the near field with the purpose of using it in road safety. Using a 2-microphone system (Perez-Gonzalez *et al.*, 2002) there is suggested an algorithmic calculation to detect the position and speed of moving sound sources emitting on a narrow broadband and then optimize results with the Monte Carlo series.

On the other hand, microphone antennas are suggested by Harmonoise work team to locate and identify noise sources of travelling vehicles as well as holographies in the near field by using linear and 2D antennas.

Some applications of microphone array in the far field have been published (Quaranta *et al.*, 2008) and they suggested a model for noise source localization in open spaces using sound sensors placed far away from each other. Other authors (Cigada *et al.*, 2007) developed an experimental test in order to validate a linear microphone array using the delay & sum algorithm.

3. Array design

Characteristics of the environmental test and the noise source determine, to a considerable degree, design restrictions of a microphone antenna as well as the method used to process the incoming data. Important design factors to be taken into account are listed below so the microphone antenna we suggested can achieve all the goals initially established.

3.1. Type of antenna

The spatial distribution of the microphones considered for the antenna designing process will condition its characteristics, its mathematical data processing, and its potential applications. Depending on how sensors are placed in space, systems can be divided into:

- Linear antennas: All sensors are placed on the same spatial line by keeping a distance sequence between each pair of sensors, such as a group of microphones uniformly distributed, Uniform Linear Array, ULA, or an array with a proportional distance between microphones.

- Planar antennas (2 dimensions): In this case, microphones are placed on the same work level. This kind of antennas is commonly used to create holograms in the near field.
- Spatial antennas (3 dimensions): Finally, in these antennas, the relative position between sensors varies depending on a particular volume, being able to detect noise sources moving in a specific volume.

As one of main objectives of this application is to work with the simplest solution and due to the first simulations shown good results, it was established that a linear antenna with uniformly placed microphones will be used, ULA.

3.2. Processing method

Bibliography is composed of an important variety of processing methods: narrowband methods such as "delay and sum"; Capon or MUSIC method; and broadband methods such as the Double Fourier Transform or Spatial Cross Spectrum method.

Results of other research works (Genescà *et al.*, 2009) and previous experiences (Peral, 2009) determine that the most suitable method is the Spatial Cross Spectrum, SCS (Boone, 1987) according to the frequency range of the sound source as well as to the needs of the angular resolution and the number of the antenna sensors.

3.3. Distance between microphones

Distance between microphones would be conditioned by testing frequency and it should fulfill Eq. (1) to avoid spatial aliasing:

$$d \leq \lambda/2 = c/(2f), \tag{1}$$

where d is the distance between microphones, λ is the wavelength of the expected signal, c is the speed of sound, and f is the frequency of the expected signal.

After analyzing spectral characteristics of an average group of passing vehicles (see Fig. 2), it has been detected that 1000 Hz was the frequency band that kept more sound power, which allowed us to determine that the distance between microphones for the narrow band system should be not more than 0.17 meters to avoid spatial aliasing.

3.4. Distance between source and receiver

To assure a correct identification, the proposed test should be carried out under the hypothesis based on a point source emitting in the far field. To do so, the minimum distance between source and receiver has to be established so these assumptions can be guaranteed. Different authors (Maekawa, 1970) state that a noise source can be considered a point-like one when the distance from the receiver shows a minimum value that depends on source size and the frequency of an emitted wave. Given all the size characteristics of the tested source and the location frequency, the reference distance between the microphone array and the closest

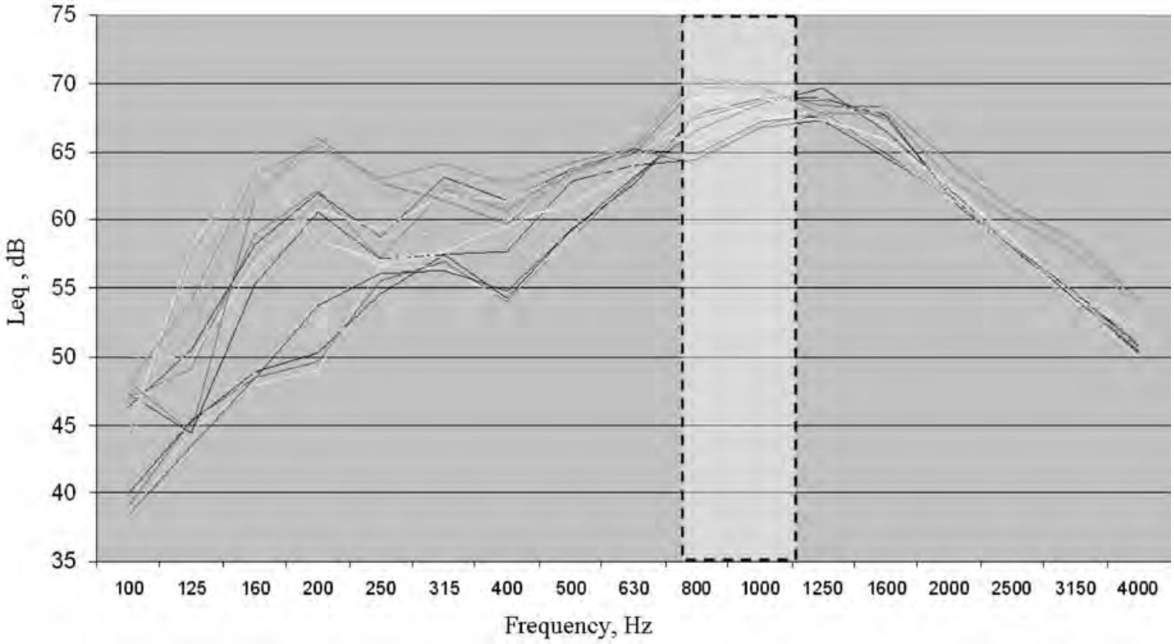

Fig. 2. 1/3 octave band noise spectrums of a measured group of passing vehicles with different characteristics used to detect main working frequency.

point to the travelling trajectory is 30 meters and the length of the test track in which the source will be detected is 300 meters (see Fig. 3).

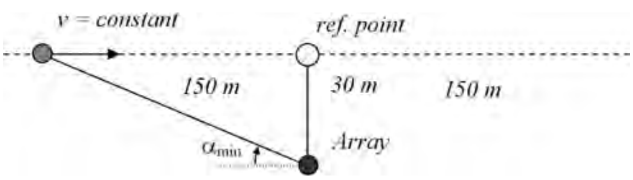

Fig. 3. Schematic sketch of the test and the minimum location angle.

3.5. Number of microphones and angular resolution

The angular resolution of a linear array will be determined by its total aperture or length capacity as well as the frequency of the captured signal. After establishing the distance between the sensors, the total aperture capacity will be directly determined by the total number of array microphones. When there are more sensors, the angular resolution of the array is less, which makes localization results even more reliable.

Angular resolution is determined by the antenna steering vector and it varies depending on the focal angle as well as on the processing method used. The angular resolution for SCS processing method will be as follows (Cigada *et al.*, 2007):

$$\Delta\alpha = \frac{\lambda}{Ap\cos(\alpha)} = \frac{c}{2L\,f\cos(\alpha)}, \tag{2}$$

where $\Delta\alpha$ is the angular resolution of the microphone array, Ap is the aperture of the array, L is the total length of the microphone array, f is the frequency of the signal, and α is the focal angle.

Considering that during the test, no other significant noise source would be in the stage and knowing that the extreme angle of the noise source will be, correspond with Fig. 3, $\alpha_{\min} = \arctan(30/150) = 0.197$ rad with respect to the antenna, the minimum length of the antenna should fulfil the condition

$$\frac{c}{2L_{\min}\,f\cos(\alpha_{\min})} \leq \alpha_{\min}, \tag{3}$$

giving, as a result,

$$L_{\min} \geq 0.89\ \text{m}. \tag{4}$$

Knowing that the distance between microphones is 0.17 m, the antenna should need at least 7 microphones to reach the minimum distance, $L_{7\text{-micros}} = 1.02$ m. The resulting beam pattern from a 7-microphone antenna at working frequency of 1000 Hz is shown in Fig. 4.

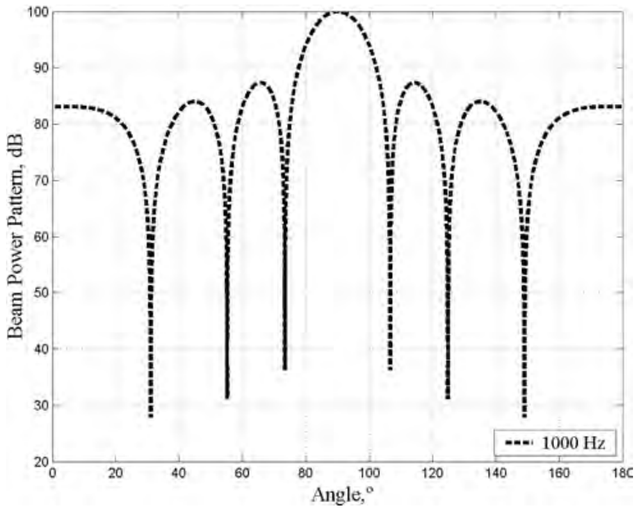

Fig. 4. Beam Pattern of the ULA of 7 microphones at 1 KHz, depending on the source location angles.

3.6. Linear antenna direction

To determine antenna direction that guarantees the best results on the angle of source arrival, angular variation of linear microphone distribution will be taken into consideration. Resolution of a linear antenna will decrease as the source focal point moves away from the zero angle (seen itself as the center of the trajectory of the travelling vehicle to the perpendicular direction). Two alternatives were then suggested for the linear layout: sensor system in a perpendicular line to the vehicle trajectory, *Perp*, and antenna parallel to the travelling trajectory, *Parl*. Both layouts have been tried out to determine the most suitable one for the proposed test, as shown in Fig. 5.

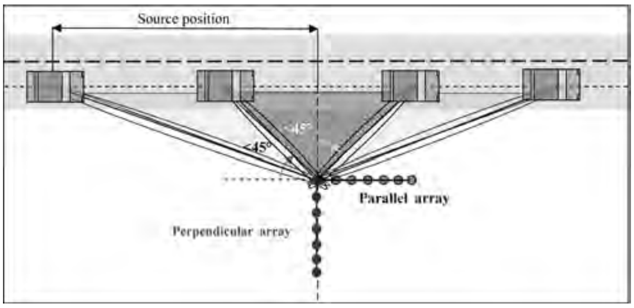

Fig. 5. Trial zone for the two different microphone positions.

3.7. Sampling frequency

As the main location frequency was considered to be 1000 Hz, a sampling frequency, f_s, of 10000 Hz would be enough for testing purposes. This way we would avoid problems such as temporal aliasing and using vectors with a too large data content which would make it difficult to obtain data as well as its subsequent processing.

4. Data processing

Figure 6 shows the process diagram of data processing.

Each sensor of the operating antenna will provide a data vector, $S\prime_n(t)$. These will then be filtered and processed to obtain the instant velocity of the sound source. Signals will initially be filtered, $S_n(t)$. Taking into account the range in which the vehicle will provide us with the highest amount of sound energy, like the Doppler Effect, a FIR filtering called "band-pass" is carried out between 940 and 1060 Hz frequencies for each signal captured by each transducer.

All signals obtained are divided into K snapshot blocks (see Eq. (5)), which will be analyzed separately assuming a fixed position of the source when capturing. Each block will have an enough number of snapshots to carry out the correct analysis and will be as small as possible to minimize source movement when capturing. To stop the source from varying its position abruptly, and knowing that a Hanning window will subsequently be used to reduce values on extreme sides, samples of $0.1 f_s$ snapshots were taken (this amount of data guaranteed that the vehicle movement was less than 2 meters for every measuring instant):

$$K = \frac{\text{Time}}{0.1\, f_s}, \tag{5}$$

where Time is the testing total time, f_s is the sample frequency, and K is the number of snapshot blocks.

Each average time, t_a, will be the new reference time for data blocks. Namely, data block j, delimited by an initial time $t_{i,j}$ and a final time $t_{f,j}$, is associated with time $t_{a,j}$ defined as

$$t_{a,j} = \frac{(t_{i,j} + t_{f,j})}{2}, \tag{6}$$

where j takes values from 1 to K.

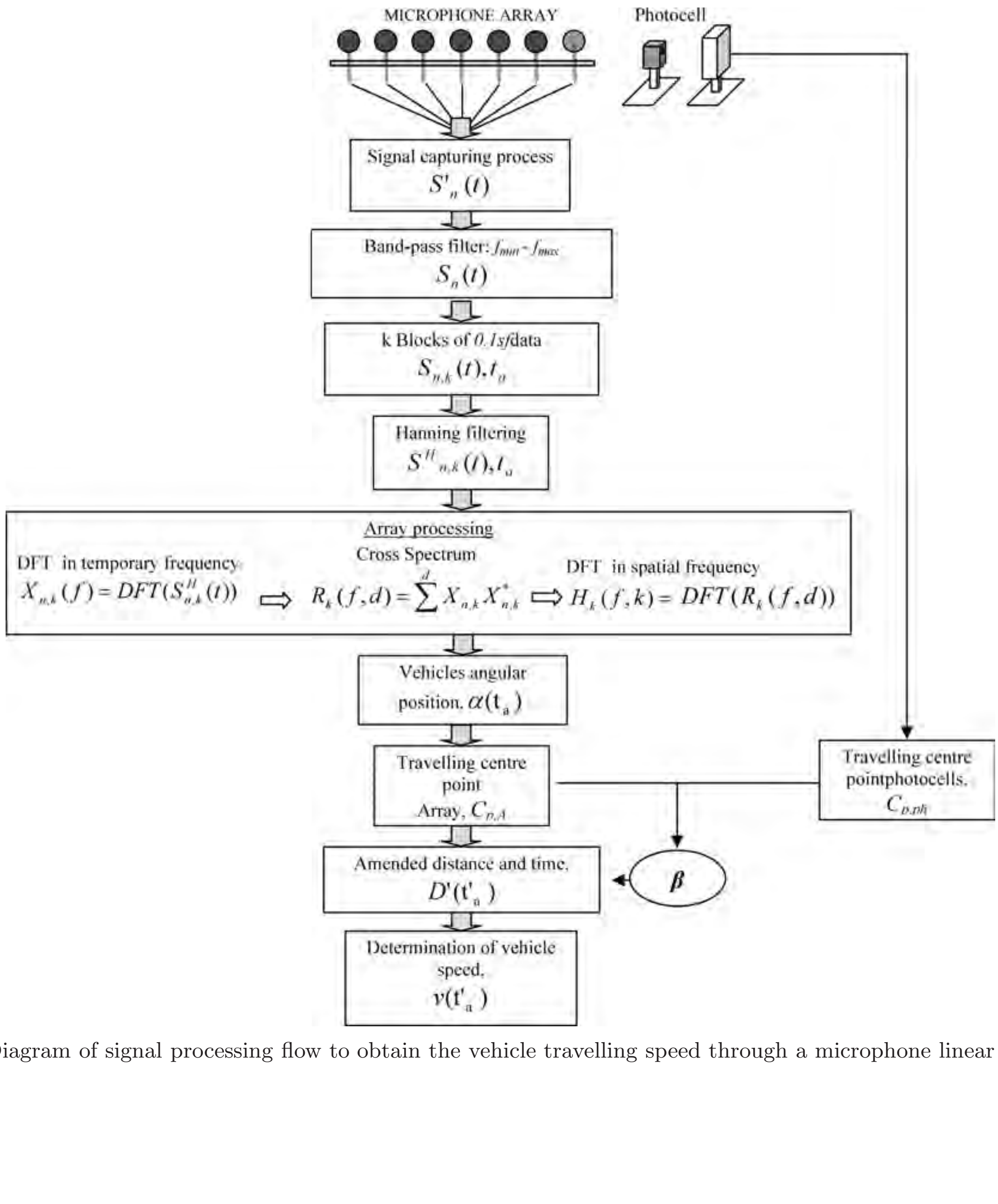

Fig. 6. Diagram of signal processing flow to obtain the vehicle travelling speed through a microphone linear antenna.

Each block then goes through an IIR filter, of the Hanning window type, to avoid leakage problems before going through Spatial Cross Spectrum algorithm (Jonhson, Dudgeon, 1993). As a response, the algorithm gives a localization function from which the direction of arrival of the main source can be inferred. Each block will therefore have the value of the direction of arrival of the signal, $\alpha(t_a)$.

The direction of arrival of the sound wave will lead to the travelling velocity of the vehicle during the test. Consequently, deviations in the source position are amended due to possible angular variation between the array and the travelling line of the sound source (to do so, a given time interval should be found by using a couple of photocells which will lead us to the exact vehicle position), wave displacement time from the emitting source to the array, and point sound sources in the area being able to move the antenna focalization away. To adjust these results, an algorithm has been implemented to locate the vehicle travelling line and get rid of all samples that have not detected it as main noise source, working as a 'clean function' (see Fig. 7).

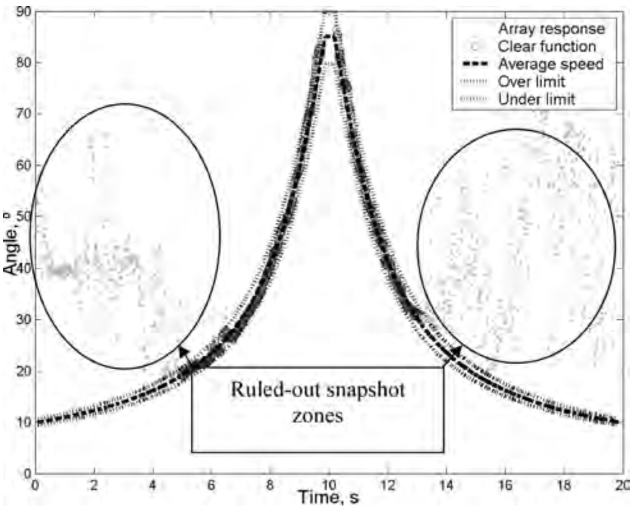

Fig. 7. The zones bounded by the vehicles average speed rule out points giving no information on sound source localization, *'clean function'*.

Given the vehicle trajectory and the angular position for any moment in time $\alpha(t_a)$, displacement will be obtained as

$$D(t_a) = \frac{dist}{\tan(\alpha(t_a))}, \tag{7}$$

where $D(t_a)$ is the theoretical displacement of the noise source, *dist* is the constant perpendicular distance between the microphone array and the source track, and $\alpha(t_a)$ is the focusing angle of the antenna of each data block.

After being adjusted as previously mentioned, the corrected value will be

$$D'(t_a) = \frac{D(t_a)\,\sin(\alpha(t_a))}{\sin(\pi - (\alpha(t_a) + \beta))} = \frac{\cos(\alpha(t_a))\,dist}{\sin(\pi - (\alpha(t_a) + \beta))}, \tag{8}$$

where $D'(t_a)$ is the real displacement of the noise source and β is the correction angle (angular difference between real direction and theoretical direction of the antenna, see Fig. 8).

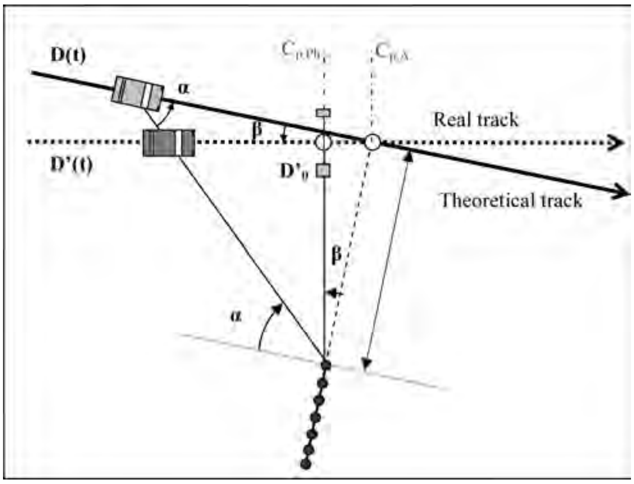

Fig. 8. Sketch of the angular correction to obtain the real displacement of the noise source.

Likewise, the theoretical distance R that the sound wave has to travel to arrive at the microphone antenna is

$$R(t_a) = \frac{dist}{\sin(\alpha(t_a))}. \tag{9}$$

But considering the correction angle, the real distance $R\prime$ between the sound source and the receptor is

$$R'(t_a) = \frac{dist}{\sin(\alpha(t_a))} \pm \frac{D'(t_a)\sin(\beta)}{\sin(\alpha(t_a))} = \frac{dist \pm (D'(t_a)\sin(\beta))}{\sin(\alpha(t_a))}. \tag{10}$$

So actually, the angular function will provide the position of the vehicle at the instant

$$t'_a = t_a - R'(t_a)/c = t_a - \frac{dist \pm (D'(t_a)\sin(\beta))}{c\,\sin(\alpha(t_a))}, \tag{11}$$

where c is again the speed of sound.

Linking this position with the moment in time in which the vehicle is traversing the center of the real travelling line reference D'_0, an average variation of the position will be obtained as

$$\Delta D'(t_a) = |D'(t_a) - D'_0|\,. \tag{12}$$

Taking the velocity definition into account,

$$v(t_a) = \frac{\Delta D'(t_a)}{\Delta t'_a} = \frac{|D'(t_a) - D'_0|}{|t'_a - t'_0|}. \tag{13}$$

Due to the antenna features and the test itself, results will fall into a margin of error which will be minimized by using an approximation of least squares. In order to achieve this, a speed value range between 10 and 30 m/s should be used and the obtained speed vector would be $v_k = [10, ..., 30]$.

Taking the center of the vehicle travelling line into account, the velocity value is established and minimizes the difference between squares of the snapshot block captured in 0.5 seconds.

Data processing was implemented in MATLAB and tested in a simulation as it is explained in the next section.

5. Simulation

To guarantee that this microphone system operates accurately, tests under different assumptions have been carried out. To achieve this, the simulation was based on a point sound source on the move emitting pink noise, proceeding all the way along a straight line at a constant velocity. The distance covered was 300 m and the microphone system placed at a distance of 30 m. During the simulation, parameters such as displacement velocity and sound intensity of background noise were varied. Figure 9 shows signals of the reference microphone (first microphone of the linear array) for the 3 assumptions.

Figures 10 and 11 show results of simulations obtained through the antenna placed perpendicularly and parallel to the vehicle travelling line. The background noise changes for each assumption as Table 1 shows, and affects source localization when it is placed far away from the capture system. In both cases, it is possible to find a limit angle from which the antenna results are not accepted because of high deviation between results and real source position. However, because of the area of low angular resolution, parallel antenna determines sources position during a lower time period.

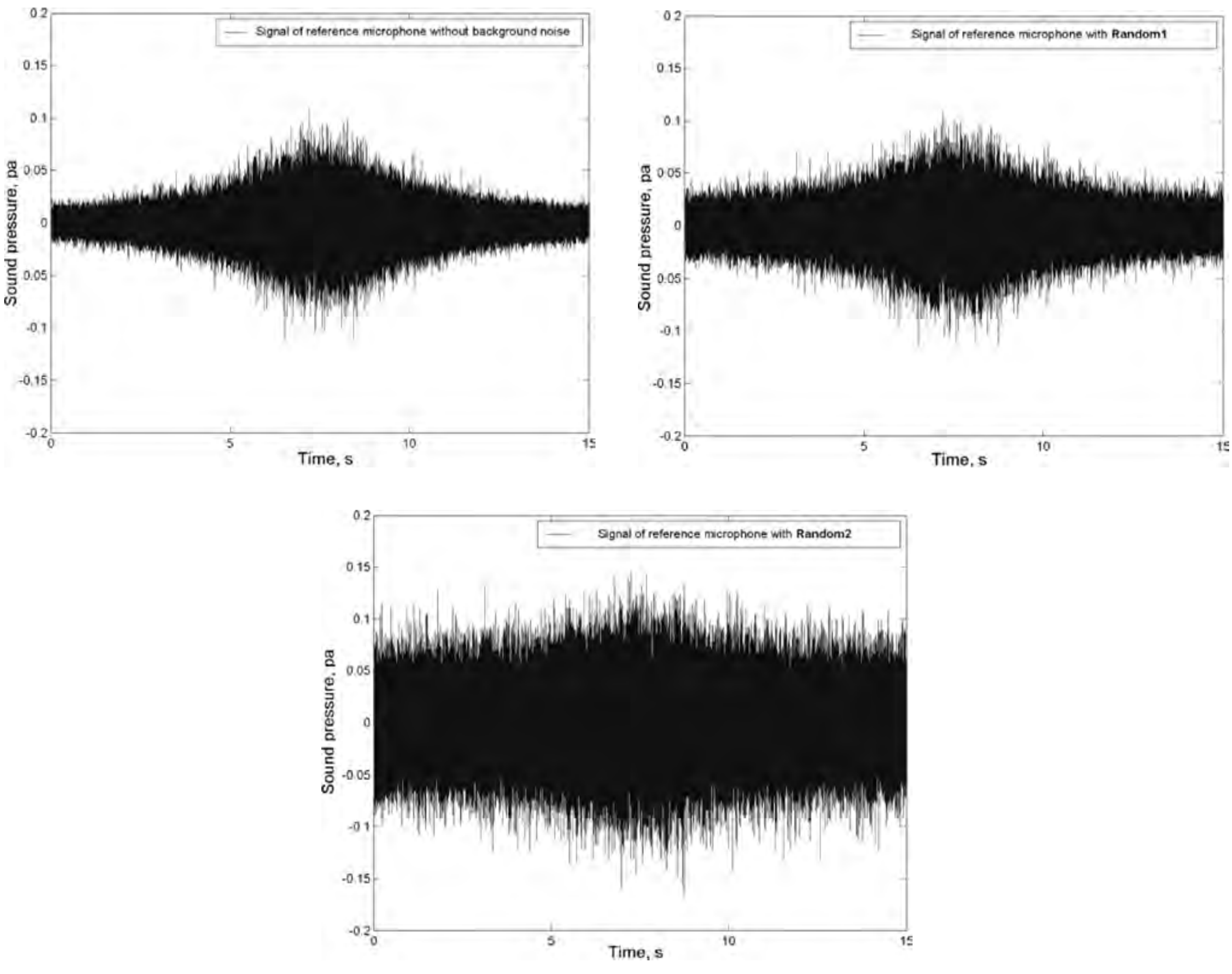

Fig. 9. Signals simulated.

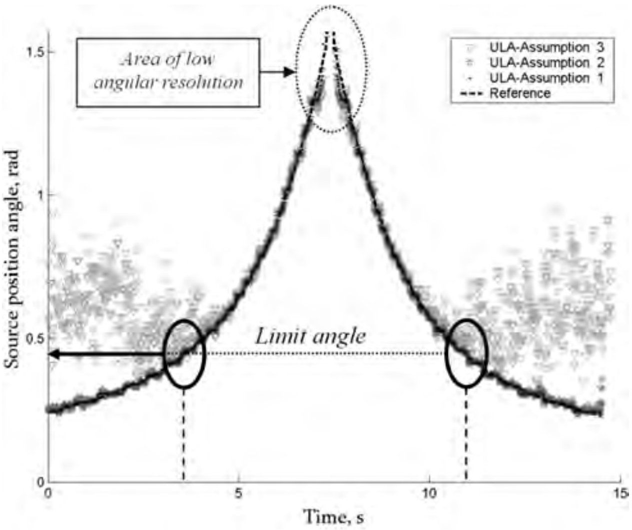

Fig. 10. Results of simulation of ULA-7 placed perpendicularly to the vehicle travelling line.

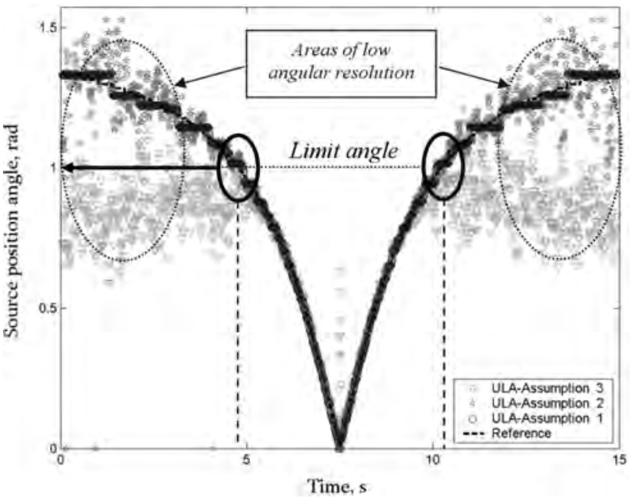

Fig. 11. Results of simulation of antenna parallel to the travelling trajectory.

Table 1. Assumptions simulated.

	Velocity [m/s]	Sampling Frequency [Hz]	Background noise
Assumption 1	20/30	10,000	*Null*
Assumption 2			*Random1* (9 dB lower than emitted in ref point)
Assumption 3			*Random2* (same level like emitted in ref point)

Table 2 contains the mean squared errors (10) of the results obtained from every simulation carried out. For each assumption, calculations have been performed

Table 2. Mean Squared Error obtained through both antennas and for each of the assumptions.

	ULA-L [rad]	ULA-II [rad]
Assumption 1	0.0149	0.016
Assumption 2	0.018	0.0942
Assumption 3	0.223	0.3041

by using the position values given by the algorithm which have been compared with the real source position:

$$MSE = \sqrt{\sum_{i=1}^{N} \frac{(\alpha_{\exp,i} - \alpha_{\text{real},i})^2}{N}}, \tag{14}$$

where MSE is the Mean Square Error, N is the number of results obtained, $\alpha_{\exp,\,i}$ is the experimental angle of each instant of time, and $\alpha_{\text{real},\,i}$ is the real angle of each instant of time.

Uniform linear array works better in orientation perpendicular to the vehicle travelling line, obtaining a narrow deviation in vehicle position for different background noise conditions.

Following the data processing procedure suggested, vehicle speed can be established if position data given by the system are considered. Finally, Fig. 12 presents speed values for assumption 2 as well as deviation observed at a constant speed of 20 m/s.

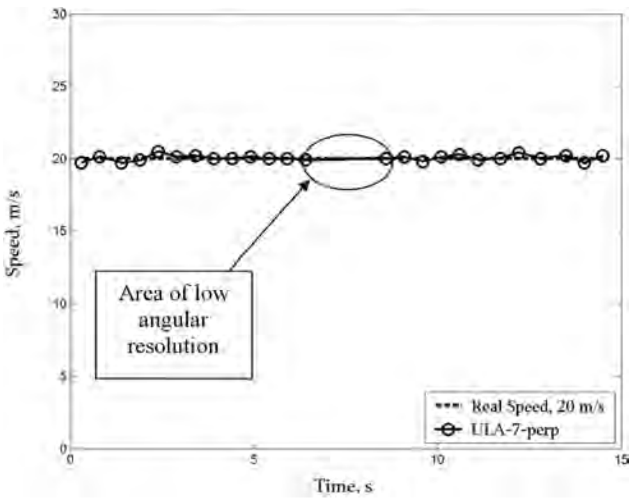

Fig. 12. Source speed obtained by processing results of ULA-7 with antenna perpendicular to the vehicle travelling line for assumption 2.

6. Conclusions

This article analyzes main aspects of the designing process of a linear microphone antenna for vehicle localization in higher speed traffic conditions. Design tasks included the study of different types of microphone arrays, distance and number of sensors, direction and distance of the antenna with respect to the travelling line of the sound source. The antenna eventually suggested has 7 omnidirectional microphones, strategically placed 0.17 meters away from each other, and set up perpendicularly to the travelling line 30 meters away from the closest point of it. The algorithm that has been designed for data processing is based on filtering and conditioning of signals captured by different microphones, implementation of signals through the calculation method *Spatial Cross Spectrum*, proposal for a system that reduces deviation of results, and obtaining instantaneous function with the velocity source based on mean squares.

Acknowledgments

Authors would like to thank the Government of Valencia Region for providing funding necessary in this research. Likewise, authors are indebted to the reviewers for their useful comments.

References

1. Boone R. (1987), *Design and development of a synthetic acoustic antenna for highly directional sound measurements*, Ph.D. Thesis, University of Delf, Netherland.
2. Christensen J.J., Hald J. (2004), *Beamforming, Technical review*, Bruel & Kjaer Sound and vibration measurement, Denmark, No. 1.
3. Cigada A., Ripamonti F., Vanali M. (2007), *The delay & sum algorithm applied to microphone array measurements: numerical analysis and experimental validation*, Mechanical Systems and Signal Processing, **21**, 2645–2664.
4. Danicki E. (2005), *Acoustic sniper location*, Archives of Acoustics, **30**, 2, 233–245.
5. Döbler D., Heilmann G., Schröder R. (2008), *Investigation of the depth of field in acoustic maps and its relation between focal distance and array design,* Proceedings of Internoise 2008, 654–660, Shanghai.
6. Genescà M., Romeu J., Pàmiesa T., Sánchez A. (2009), *Real time aircraft fly-over noise discrimination*, Journal of Sound and Vibration, **323**, 1/2, 112–129.
7. Jonhson D.H., Dudgeon D.E. (1993), *Array signal processing: Concepts and Techniques*, Prestice Hall Signal Processing Series, United States of America.
8. Kodera K., Itai A., Yasukawa H. (2007), *Sound localization of approaching vehicles using uniform microphone array.* Proceedings of 2007 IEEE, Intelligent Transportation Systems Conference, 1054–1058, Seattle.
9. Kuhn J.P., Bui B.C., Pieper G. (1998), *Acoustic sensor system for vehicle detection and multi-lane highway monitoring*, US Patent 5798983, 1998.
10. Lopez-Valcarce R. (2004), *Broadband analysis of a microphone array based road traffic speed estimator*, Sensor Array and Multichannel Signal Processing Workshop Proceedings, 533–537, Vigo, Spain.
11. Maekawa Z. (1970), *Noise reduction by distance from sources of various shapes*, Applied Acoustics, **3**, 3, 225–238.
12. Moran M., Greenfield R., Wilson K. (2007), *Acoustic array tracking performance under moderately complex environmental conditions*, Applied Acoustics, **68**, 1241–1262.
13. Peral R. (2009), *Test method to obtain horizontal sound directivity of a road vehicle at high speed conditions*, Ph.D. Thesis, Miguel Hernandez University, Spain.
14. Perez-Gonzalez F., Lopez-Valcarce R., Mosquera C. (2002), *Road vehicle speed estimation from a two-microphone array*, Acoustics, Speech, and Signal Processing (ICASSP), Proceedings of IEEE International Conference, 1321–1324.
15. Quaranta V., Dimino I., Benedetto C., Tassini C., D'Altrui G. (2008), *Digital terrain Model for far field noise localization with beam-forming technique*, Proceedings of Internoise 2008, 1278–1284, Shanghai.

PAN
ARCHIVES OF ACOUSTICS
Vol. **38**, No. 3, pp. 417–423 (2013)

DOI: 10.2478/aoa-2013-0049

Acoustic Absorption of Mortar Composites with Waste Material

Marco Aurélio STUMPF GONZÁLEZ, Fernanda FLACH,
Josiane RESCHKE PIRES, Marlova PIVA KULAKOWSKI

Civil Engineering Graduate Program (PPGEC), Universidade do Vale do Rio dos Sinos
Av. Unisinos, 950, 93022-000 — São Leopoldo, RS, Brazil;
e-mail: mgonzalez@unisinos.br; fernanda_flach@hotmail.com.br; josianepires@uol.com.br; marlovak@unisinos.br

(*received September 11, 2012; accepted March 21, 2013*)

This paper presents an investigation about acoustic absorption of mortars with partial replacement of sand by waste (plywood formwork, rice husk, and thermoplastic shoe counters), examining different levels of replacement (0%, 5%, 10%, 25%, and 50%). The measurement of acoustic absorption was performed using a plane wave impedance tube with 100 mm diameter, using mortar samples of 20 mm, in frequency range 200–2000 Hz. Results demonstrated that some composite with waste presented noise reduction coefficient (NRC) above the reference mortar (NRC = 0.0343), such as a composite with 50% rice husk (NRC = 0.2757) and other with 50% of plywood waste (NRC = 0.2052). Since there is virtually no cost or difficulty to use these residuals, it may be concluded that it is a sustainable alternative to improve the acoustic comfort and reduce the impact of the waste on the environment.

Keywords: acoustics, comfort, impedance tube, civil construction, waste.

1. Introduction

The quality of human life is aided by environmental conditions of comfort, such as thermal, acoustic, and luminous comforts. Noise can affect general comfort, sleep, and relationships between residents of the same building. Exposure to excessive noise for long periods can cause side effects such as interference in task performance and health problems: irritability, hypertension, headaches, insomnia, and stress (ABNT, 2010; Ferraz, 2008; Gerges, 2000).

Studies developed in Brazil show low acoustic insulation in buildings or some of its components (Duarte, Viveiros, 2007; Losso, Viveiros, 2004; Polli, Viveiros, 2007; Vianna, Roméro, 2002). Traditional solutions involve the increased thickness of slabs and the walls or insertion of special material for insulation and acoustic conditioning. Correction after construction finished usually is uneconomical, and even the expansion of the insulation in the design phase is difficult, due to the cost of traditional materials (Ferraz, 2008; Gerges, 2000; Porges, 1977).

On the other hand, construction industry is absorbing huge waste of the construction and other industries, for example through the inclusion of waste in bricks, mortar, and concrete, and so creating more sustainable materials. The replacement of part of aggregates or cement reduces the extraction of raw materials and reduces the energy consumed to produce the materials of construction (Rocha, John, 2003; Mehta, Monteiro, 2006).

Composites are materials made from the union of two or more elements in order to create a material with properties superior to those of their components alone. Mortars and concrete are the most common building materials worldwide (Mehta, Monteiro, 2006). Composites originated from mortars and concretes may receive mineral, synthetic, and biomass fibers or particles. Some studies examine the acoustic absorption of materials produced from the recycling or recovery of materials. Branco *et al.* (2010) produced mortars using different types of lightweight aggregate (expanded polystyrene, expanded clay, and expanded granulated cork), evaluating their performance in reducing noise levels caused by impact. Ramis *et al.* (2010) used hemp fibers. Sakamoto *et al.* (2011) examined rice husk, rice straw, and wheat husks. Del Rey *et al.* (2011) worked with polyester wool obtained by recycling PET bottles. Tutikian *et al.* (2012) investigated the noise performance of a composite material with recycled aggregates, ethylene vinyl acetate (EVA), as a substitute for conventional coarse aggregate in the production of lightweight concrete to use in subfloors in residential buildings. Yang *et al.* (2003) studied composites of rice husk and wood particles. Ersoy and Küçük (2009) examined tea-leaf fibers and Oldham *et al.* (2011) investigated several vegetal fibers, such as jute, sisal, flax, ramie, and hemp.

One alternative that has been studied in construction is the generation of new materials, combining common materials with waste. The region of study (Vale do Rio dos Sinos, Rio Grande do Sul, Southern Brazil) has difficulty to dispose some residuals, in particular: formwork to concrete made with plywood, rice husk, and shoe counters. About 80% of plywood used in formwork for structure become waste (Mosmann, 2012). Brazil produced 11.3 million tons of rice in 2010, and husk represents about 20% of the rice grain (Brazilian Institute for Statistics [IBGE], 2010; Kieling, 2009). Moreover, the region is a center of shoe production, generating several residues, such as EVA (already studied in acoustic applications by Tutikian *et al.*, 2012) and shoe counters (this part goes behind the heel and is used to reinforce the back part of the shoe, and to mould its structure) (Kazmierczak *et al.*, 2003).

This paper investigates the acoustic absorption in mortars produced with the addition of plywood waste, rice husk, and residuals of shoes. The methodology adopted is based on measuring samples in the impedance tube.

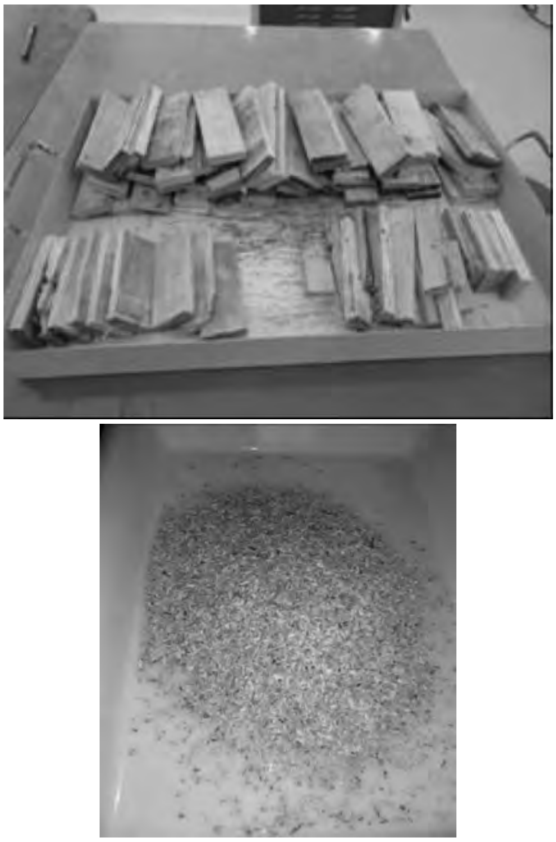

Fig. 1. Residue of plywood resin formwork: cut-off plates (top) and after grinding (bottom).

2. Materials and methods

Residues investigated were plywood resin, rice husk, and thermoplastic impregnated shoe counters. Mortar composites were investigated with partial replacement of sand by the waste, by volume (0%, 5%, 10%, 25%, and 50%). The impedance tube was evaluated as the most appropriate test method to perform the experiment, because it is necessary only a small sample of the material analyzed which allows testing with a greater quantity and variety of composites. Absorption coefficients were studied in the frequency range 200–2000 Hz. The measurements follow international standards ASTM E1050:2008 and ISO 10534-2:1998. The Noise Reduction Coefficient (NRC) was then obtained by calculating the average sound absorption coefficients at 250 Hz, 500 Hz, 1000 Hz, and 2000 Hz frequencies according to procedure ASTM C423-99A, but using 4 decimal places.

2.1. Preparation of the waste

Waste of plywood and shoe counters was cleaned and then ground in a knife mill. The particles were crushed. Figures 1 and 2 illustrate these materials. Time and effort to preparation are relatively small.

Fig. 2. Counter thermoplastic residue: waste received (top) and after grinding (bottom).

The preparation of rice husk residue consisted of verifying and segregate foreign particles manually, through the prior selection by removing impurities such as traces of gravel, straw, etc. (Fig. 3). Also in this case waste preparation is a simple activity.

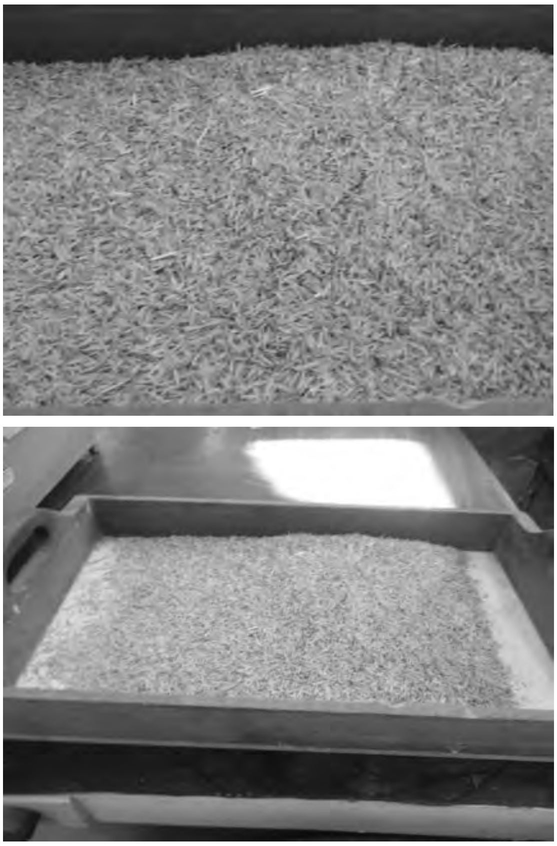

Fig. 3. Rice husk: waste received (top) and after cleaning (bottom).

2.2. Production of mortar

A selection of particles was carried out by preliminary screening using a sieve of 4.8 mm opening. This allowed the separation of materials, ensuring that particles larger than this dimension should be discarded, thus generating samples of aggregates that can provide blends with higher uniformity and higher workability.

The trace of mortar that was used in this study consisted of 1 : 4 (cement: sand) by volume. The consistency index pattern was fixed at 260 mm ±5 mm measured in the table consistency for the reference mortar. Experimental dosages with different amounts of cement (CP-IV), medium sand, and water were applied in separate mortars made with substitution of sand by waste until the proper consistency indexes were achieved.

The mortar composites had a curing time of 28 days and during the first 48 h ±24 h they remained in the molds in a climatic chamber with controlled temperature and relative humidity ($T = 20°\text{C} \pm 2°\text{C}$, $RH = 70\% \pm 10\%$) in the same room. After this period, the samples were demoulded and stored in containers with water and lime, in conditioned room, where they remained until fully cured. The pores influence the acoustic behaviour, therefore important for the healing of mortars and water content. After this period, they were removed from the water and stored in conditioned room until to stabilize the moisture and achieve constant mass, adopting the parameter of variation below 1% between measurements. They were weighted and measured, calculating sample density (in kg/m^3).

For all mortars produced we used the same procedure, without significant differences among mortars with different dosages of waste. We found minor differences among preparation of regular mortars and mortars with waste components.

3. Results and discussion

3.1. Absorption coefficients

3.1.1. Comparison between configurations with dosage of 5%

In Fig. 4, the graph shows the results of the sound absorption obtained for the dosing of mortars with 5% for different residues at frequencies tested. Examining the data, it can be seen that very approximate values were obtained in rice husk and counter shoes mortars. In both samples, the highest value of absorption coefficient occurred around 2 kHz, with 0.10 absorption coefficient. When using the residue of plywood, we found values of absorption coefficients larger than the previous ones, at almost all frequencies measured. However, for the three residues, the measured absorption did not exceed 0.10. Apparently the dosage of 5% addition of residue in the composites has little influenced on acoustic absorption, approaching the values found in the reference sample.

3.1.2. Comparison between configurations with dosage of 10%

In Fig. 5, the graph shows the values of sound absorption corresponding to 10% dosage. It is observed that the values of sound absorption to counter residues and rice husk are approximate, with sound absorption coefficient between 0 and 0.10. Plywood results are slightly higher, reaching a 0.13 absorption coefficient at 1.6 kHz, and rice husk has an increase at higher frequencies, with a 0.22 at 2 kHz.

3.1.3. Comparison between configurations with dosage of 25%

In Fig. 6, the graph shows the results found in the sound absorption coefficients configuration with 25% waste. It appears that the results of the residue of plywood showed more significant results, but the other

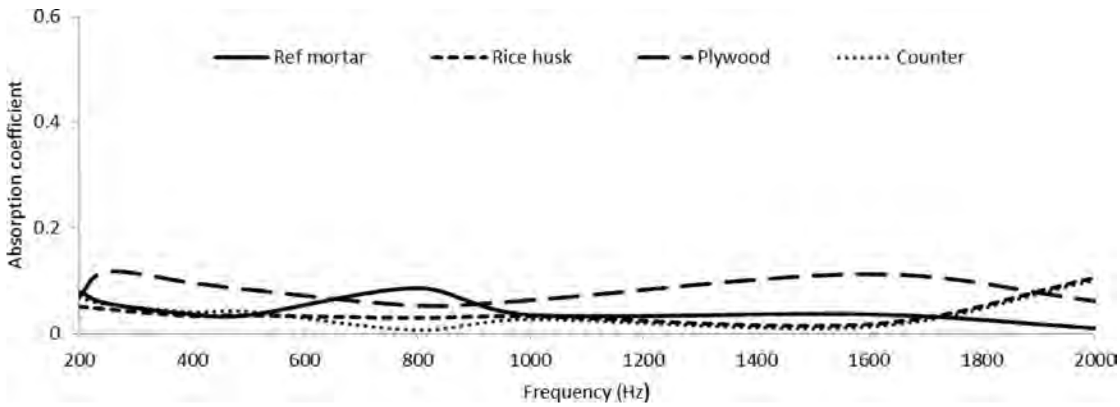

Fig. 4. Sound absorption coefficients – mortars with 5% of waste.

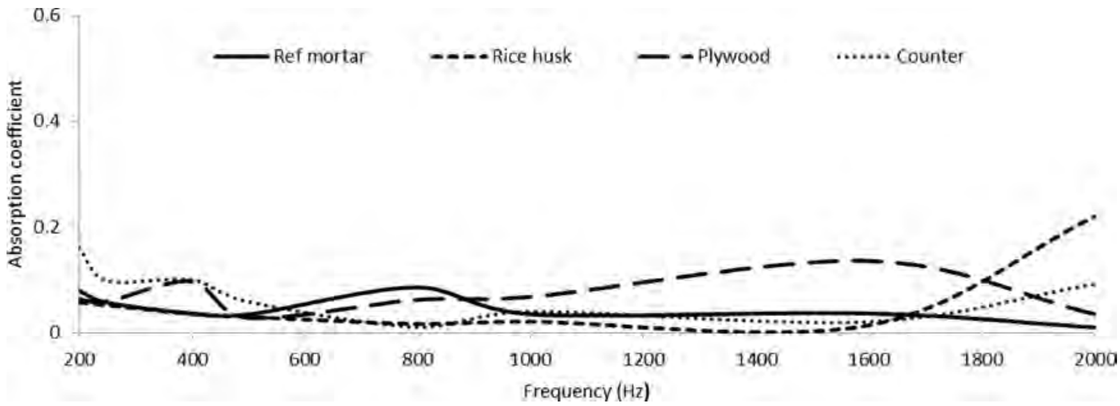

Fig. 5. Sound absorption coefficients – mortars with 10% of waste.

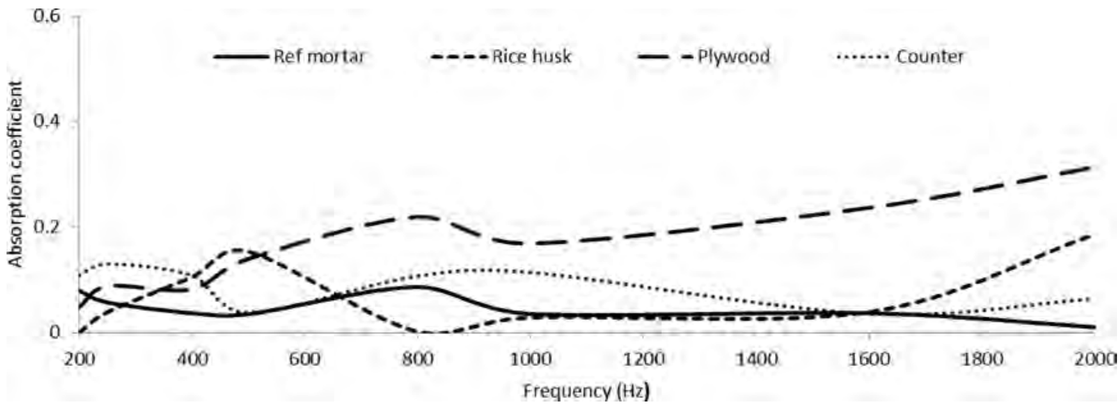

Fig. 6. Sound absorption coefficients – mortars with 25% of waste.

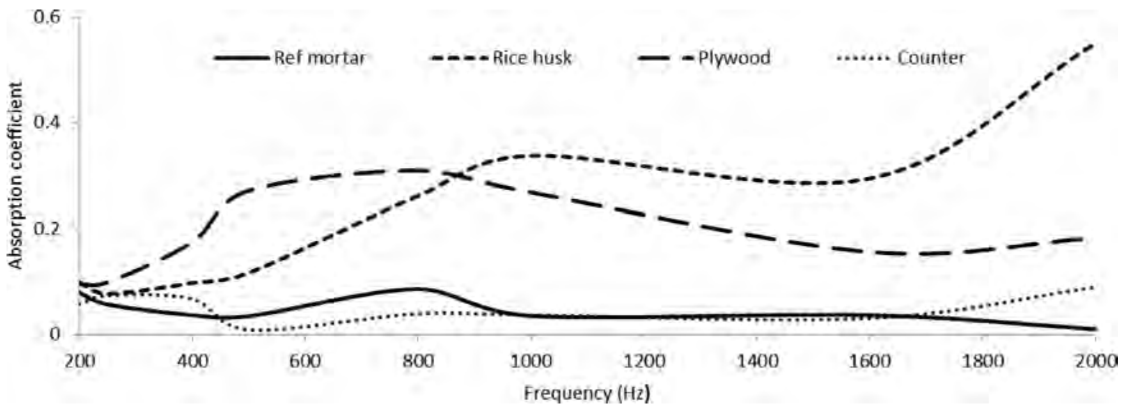

Fig. 7. Sound absorption coefficients – mortars with 50% of waste.

residues showed some resemblance. The counter mortar values are above the reference found in the mortars. Therefore the dosage of 25% represents a significant increase in sound absorption of the composites, reaching absorption coefficient values of about 0.30 for plywood.

3.1.4. Comparison between the configurations with a dosage of 50%

Values obtained for the dosing of 50% with various residues are presented in Fig. 7. The addition of fibers increases the behaviour of the samples. It has a reasonable increase in the absorption coefficient at higher frequencies, with peak absorption coefficient of 0.30 at 600–800 Hz for plywood, and 0.34 at 1 kHz and 0.55 at 2 Hz for rice husk. Results showed lower performance of shoe counter mortar, staying close to the reference mortar. In general, mortars with 50% waste have the major absorption coefficients.

3.1.5. Noise Reduction Coefficient (NRC)

Noise Reduction Coefficient (NRC) provides an overview of the results. NRC values are shown in Table 1 for reference mortar and samples with waste of plywood formwork, rice husk, and shoe counters. The reference configuration reached a NRC = 0.0343. It should be noted that this configuration was as expected, because there are studies that found that similar mortars showed a NRC = 0.0375 (Bistafa, 2006).

Table 1. Noise Reduction Coefficient (NRC).

Waste type	Waste dosage				
	0% (ref.)	5%	10%	25%	50%
Rice husk		0.0546	0.0863	0.1014	0.2757
Plywood formwork	0.0343	0.0813	0.0478	0.1773	0.2052
Shoe counters		0.0561	0.0723	0.0864	0.0523

At 5% of residuals, the NRC found shows the greatest value for plywood samples (NRC = 0.0813). For 10% dosage, the NRC demonstrate that the rice husk (NRC = 0.0863) showed greater performance. With 25% level, it was observed that the plywood mortar appeared highlighted (NRC = 0.1773). Finally, when dosage of waste was 50%, the comparison of the composites indicated that the rice husk (NRC = 0.2757) is offset above the resin (NRC = 0.2052) and shoe counters (NRC = 0.0523). In all cases, composites with waste were superior to reference mortar in terms of sound absorption.

3.2. Statistical analysis

We have not found in the literature any studies about absorption coefficient with statistical analysis, either using the techniques of analysis of variance (ANOVA) or regression analysis to prove their results. We investigated variable relationship through regression, creating a statistical model with which the behavior of NRC can be analyzed using a set of independent variables. Independent variables were: Dosage (in %), Density (in kg/m^3), and Type of waste. The Type was codified as a numeric variable, ranging from 0 to 3. Rice husk was considered as the residue with best acoustic performance, therefore it was assigned the value of 3, followed by plywood with value 1.5, shoe counters with the value 1 and, finally, reference mortar to the value zero. This scale was determined through simulations. The resulting model was the following:

$$\begin{aligned}\text{NRC} = 0.34114 - 0.000165 \cdot \text{Density} \\ + 0.02936 \cdot \text{Type of Waste}.\end{aligned} \tag{1}$$

The model was investigated according to the traditional procedures in regression analysis with good results. The analysis of variance using the F test showed significance above 95% level. Variable analysis performed by t test indicated that the Type and Density influence the NRC, while Dosage not significantly affects NRC, because this variable showed no significance at least 95% in the t test, and it remains out of model (1). The coefficient of determination (R^2) of the model was 0.69542, demonstrating that near 70% of the NRC variations are explained by the model (Eq. (1)). Therefore we can conclude that the regression model is significant and the statistical analysis confirms the results presented above.

3.3. Economic analysis

An analysis of the economic perspective of mortar produced with waste is necessary to verify the viability of these composites. Table 2 presents a survey of costs for conventional materials (glass wool and acoustical foam) and the reference mortar. For the residues incorporated was considered a relative value spent on work and electricity for drying, cutting, and grinding the materials. We considered the cases with 50% substitution for waste, because they have shown the best

Table 2. Survey of costs of conventional materials and composites studied.

Material	Costs (in Euros/m^3)
Glass wool	274.19
Acoustic foam	453.63
Reference mortar	115.32
Mortar with 50% plywood waste	80.40
Mortar with 50% rice husk	79.53
Mortar with 50% shoe counter waste	80.30

acoustic results. There is an advantage when using the composite in view of the cost far below the conventional mortar, representing a saving, besides that it improves reuses and recycling, and reduces costs of waste deposal in landfills.

3.4. Discussion

Measurements of sound absorption coefficient show that all configurations with partial substitution of sand by residues (5%, 10%, 25%, and 50%) had values of sound absorption superior to the composite reference, with similar distributions among them in the whole frequency range.

Apparently, the residues may interfere in sound absorption in mortar with waste. The results indicated that the plywood's NRC are superior to other waste, in settings of 5% and 25%, the values found to counter top at a dosage of 10%, and to rice husk at a dosage of 50%. Given the characteristics of waste, it was expected that the higher the percentage of residue added to the composite, the apparently greater number of cavities in the face of the composites and therefore, the greater sound absorption will be occurred. So, it can be assumed that the physical configuration (coming from the spaces cavities, pores, and structures of the fiber waste) influences the sound absorption. This hypothesis has support in the analysis of acoustic absorption of waste plywood resin and rice, as opposed to the shoe counter waste, which is impregnated by resin.

In the statistical analysis of regression, the variable Density had become more significant, followed by the variable Type of waste. Thus, it was also observed that the lower mass density, the higher the value of the NRC, therefore more embedded in the mortar residues potentially greater the sound absorption (within the limits investigated). This analysis shows that rice husk performance is up to three times greater when compared to the performance of composites with shoe counters and two times greater when compared to the composite using plywood.

4. Conclusion

This research produced mortars with regular cement and sand, with partial replacement of sand by waste, generating samples for analysis in the impedance tube, in 200–2000 Hz frequency range. Results show that the mortars with addition of waste have acoustic absorption above the reference specimens, giving this way an increase in sound absorption ability of these compounds. It is easy to prepare waste and to mould the mortars, and costs for incorporation of these residues are relatively low. Therefore, it was found that the present work to obtain satisfactory performance of composites with different residues with characteristics that qualify with potential for sound absorption, may be a sustainable option to use in the construction industry.

Acknowledgments

The authors wish to thank to Brazilian Research Councils CAPES, CNPq, and FAPERGS, as well as to UNISINOS to support the development of this project.

References

1. ABNT – Brazilian Standards Institute (2010), NBR15575-1 – *Performance of residential buildings up to five floors, Part 1: General requirements* [in Portuguese], ABNT, Rio de Janeiro.
2. Bistafa S.R. (2006), *Acoustics applied to noise control* [in Portuguese], Edgard Blücher, Sao Paulo.
3. Branco F.G., Godinho L., Tavares J.A. (2010), *Use of light mortars on reducing floor impact noise transmission* [in Portuguese], Proceedings of 3rd Portuguese Conference on Construction Mortars, APFAC, Lisbon.
4. Del Rey R., J., Alba J., Ramis J., Sanchís V.J. (2011), *New acoustic absorbing materials obtained from plastic bottles waste* [in Spanish], Materiales de Construccion, **61**, 304, 547–558.
5. Duarte E.A.C., Viveiros E.B. (2007), *Acoustic performance on Brazilian residential architecture: Sealing walls* [in Portuguese], Ambiente Construído, **7**, 3, 159–171.
6. Ersoy S., Küçük H. (2009), *Investigation of industrial tea-leaf-fibre waste material for its sound absorption properties*, Applied Acoustics, **70**, 215–220.
7. Ferraz R. (2008), *Impact noise attenuation on floors of multi-pavement buildings* [in Portuguese], Master Thesis, PPGEC, Universidade Federal de Minas Gerais, Belo Horizonte, Brasil.
8. Gerges S. (2000), *Noise: Fundamentals and control* [in Portuguese], 3rd ed., NR Editora, Florianópolis, Brasil.
9. IBGE — Brazilian National Statistical Institute (2010), *Results from Decennial Demographic Census*, IBGE, Rio de Janeiro.
10. Kazmierczak C.S., Kern A.P., Santos I.S.S., Ramires M.V.V., Silva H.C. (2003), *Thermoplastic of shoes waste from Leather-footwear industry* [in Portuguese], [in:] *Use of construction waste in residential buildings*, Rocha J.C, John V.M., ANTAC, Porto Alegre, Brasil.
11. Kieling A. (2009), *Influence of segregation on the performance of mortars with rice husk ash and pozzolans with adsorbent material* [in Portuguese], Master Thesis, PPGEC, Universidade do Vale do Rio dos Sinos, Sao Leopoldo, Brasil.
12. Losso M., Viveiros E.B. (2004), *Drywall and acoustic insulation: theory versus practice in Brazil* [in Portuguese], Proceedings of the 10th Brazilian Conference on Technology of Built Environment, ANTAC, Sao Paulo.

13. Mehta P.K., Monteiro P.J.M. (2006), *Concrete: microstructure, properties, and materials*, 3rd ed., McGraw-Hill, New York.

14. Mosmann A.S. (2012), *Proposal to use rationalization and waste management of building formwork wood* [in Portuguese], Master Thesis, PPGEC, Universidade do Vale do Rio dos Sinos, Sao Leopoldo, Brasil.

15. Oldham D.J., Egan C.A., Cookson R.D. (2011), *Sustainable acoustic absorbers from biomass*, Applied Acoustics, **72**, 350–363.

16. Polli T., Viveiros E.B. (2007), *When price no matters: Relationship among building costs and acoustics comfort* [in Portuguese], Proceedings of 9th Brazilian Conference on Comfort in Built Environment, ANTAC, Ouro Preto, Brasil.

17. Porges G. (1977), *Applied Acoustics*, Edward Arnold, London.

18. Ramis J., Alba J., Del Rey R., Escuder E., Sanchís V.J. (2010), *New sound absorbers materials based on Kenaf fiber* [in Spanish], Materiales de Construcción, **60**, 299, 133–143.

19. Rocha J.C., John V.M. (2003), *Use of construction waste in residential buildings* [in Portuguese], ANTAC, Porto Alegre, Brasil.

20. Sakamoto S., Takauchi Y., Yanagimoto K., Watanabe S. (2011), *Study for sound absorbing materials of biomass tubule etc. (Measured Result for Rice Straw, Rice Husks, and Buckwheat Husks)*, Journal of Environment and Engineering, **6**, 2, 352–364.

21. Tutikian B.F., Nunes M.F.O., Leal L.C., Marquetto L. (2012), *Impact sound insulation of lightweight concrete floor with EVA waste*, Building Acoustics, **19**, 2, 75–88.

22. Vianna N.S., Roméro M.A. (2002), *Methodology for assessing post-occupancy in low-income housing projects with an emphasis on environmental comfort* [in Portuguese], Ambiente Construído, **2**, 3, 71–84.

23. Yang H.-S., Kim D.-J., Kim H.-J. (2003), *Rice straw-wood particle composite for sound absorbing wooden construction materials*, Bioresource Technology, **86**, 2, 117–121.

ARCHIVES OF ACOUSTICS
Vol. **38**, No. 3, pp. 425–432 (2013)

DOI: 10.2478/aoa-2013-0050

A Clamped Bar Model for the Sompoton Vibrator

Tee Hao WONG[(1)], Jedol DAYOU[(1)], M.C.D. NGU[(1)],
Jackson H.W. CHANG[(1)], Willey Y.H. LIEW[(2)]

[(1)] *Energy, Sound and Vibration Research Group (e-VIBS)*
School of Science and Technology, University Malaysia Sabah
Jalan UMS, 88400 Kota Kinabalu, Sabah, Malaysia; e-mail: jed@ums.edu.my

[(2)] *School of Engineering and Information Technology, University Malaysia Sabah*
Jalan UMS, 88400 Kota Kinabalu, Sabah, Malaysia

(*received May 8, 2012; accepted March 22, 2013*)

The sompoton is one of famous traditional musical instruments in Sabah. This instrument consists of several parts with the vibrator being the most important one. In this paper, the vibrator is modeled as a clamped bar with a uniformly distributed mass. By means of this model, the fundamental frequency is analyzed with the use of an equivalent single degree of freedom system (SDOF) and exact analysis. The vibrator is made of aluminum in different sizes and is excited using a constant air jet to obtain its fundamental resonance frequency. The fundamental frequency obtained from the experimental measurement is compared with the theoretical values calculated based on the equivalent SDOF and exact analysis theories. It is found that the exact analysis gives a closer value to the experimental results as compared to the SDOF system. Although both the experimental and theoretical results exhibit the same trend, they are different in magnitude. To overcome the differences in both theories, a correction factor is added to account for the production errors.

Keywords: vibrator, clamped bar, single degree of freedom system, exact analysis, resonance frequency.

1. Introduction

Malaysia is a developing country and Sabah is the second largest state which is richly blessed with natural diversity and unique heritages. It is important to preserve the cultural heritage at the same time moving towards a developed country. Malaysia is renowned for its cultural diverse indigenous communities of more than 30 ethnic groups. The largest ethnic group in Sabah is KadazanDusun. The sompoton undoubtedly belongs to their cultural heritage and it also serves as an attraction in tourism. This traditional musical instrument consists of three parts: the acoustic chamber, vibrator, locally known as sodi, and bamboo pipes (Fig. 1).

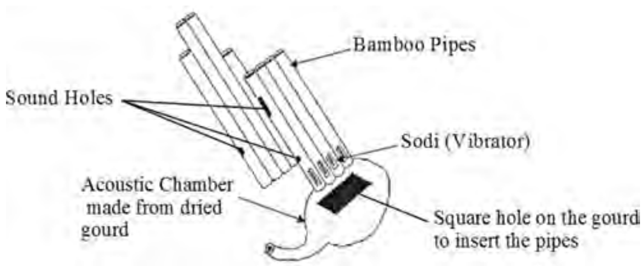

Fig. 1. Structure design of the sompoton (Marasan, 2003).

In the past, only a few studies scrutinized the sound production mechanism of musical instruments and even fewer studies dealt with traditional musical instruments. For example, Someya and Okamoto (2007) studied the measurement of the flow and vibration of the Japanese traditional bamboo flute using the dynamic PIV. They successfully visualized the air oscillation in the bamboo flute, which is useful to understand the important phenomena in sound production of the instrument. Rujinirum *et al.* (2005) characterized the acoustics properties for different types of wood used to make the Ranad (Thai traditional xylophone) and the resonator box. They managed to determine the dominant acoustic properties of the wood required to make good quality Ranad bars and resonator box. A wood with a high specific dynamic Young's modulus, density, and hardness is needed for the Ranad box. As for the resonator box, a high value of acoustic converting efficiency (ACE) is necessary.

Far in the west Finland, Erkut *et al.* (2002) analyzed the sound generated by a Finnish traditional musical instrument known as the kantele, based on measurements and analytical formulation. A synthesis model had been proposed to capture the nonlinear properties of the kantele tones. The sounds produced were proven in accordance with the measurements and analytical approximations.

Due to the increasing demands for high quality sound production, a lot of research effort has been focused on the modern musical instruments. For instance, Fouilhe *et al.* (2011) managed to understand the changes of the cello's sound as the tailpiece characteristics changes. They successfully identified 9 different vibration modes and the effects of the tailpiece shape and types of attachments to the sound characteristics. Carral *et al.* (2011) made a comparison between the single reed and double reed mouthpieces of oboe. Both mouthpieces were played by a professional player and the sound produced was compared and studied. Lohri *et al.* (2011) investigated the appearances of combination tones in violins by recording the sound using two methods – two tones played simultaneously by a violinist, and excited using shakers. The outcome of the study opens up some further questions regarding the significance of combined tones in the string instrument and its performance.

Skrodzka *et al.* (2011) performed the modal analysis and laser Doppler vibrometry (LDV) measurements of the bracing pattern of the soundboard on two incomplete and complete guitars. Their investigation outcome showed that the bracing pattern does not affect at least the first three low frequencies mode shape of the incomplete/complete guitars. However, it does affect the modal frequencies of the instruments.

In the western part of Malaysia, Ismail *et al.* (2006) studied the properties and characteristics of the sound produced by a Malay traditional musical instrument – the kompang and analyzed them using computer music synthesis. The kompang is noted as a pitchless musical instrument and it is similar to other vibrating circular membrane instruments. Similar research on pitchless instruments dedicated to the modal analysis of the batter head of the snare drum was done by Skrodzka *et al.* (2006). They performed measurements of the instrument's sound spectrum. The results showed that the batter head is not the strongest radiating element of the drum system, and the influence of other elements may also have a significant role in the sound radiation. In Sabah (east Malaysia), Ong and Dayou (2009) initiated the study of the frequency analysis of the sound from a local traditional musical instrument, the sompoton. They reported that the generation of harmonic frequency from the sompoton follows the open-end pipe model but the fundamental frequency does not comply with the same model.

The sompoton is played by blowing the air into the gourd (acoustic chamber) through the mouthpiece (Fig. 2). The air resonance in the gourd then acts as an airjet passing through the vibrator making it to vibrate and thus producing audible sound. Musicians can produce a melody by covering and uncovering the opening of the three shorter pipes with their right hand and small sound holes near the front and back pipes with their left hand.

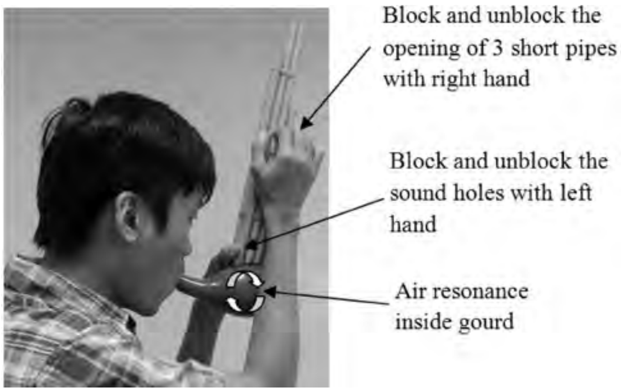

Fig. 2. Standard posture while playing the sompoton.

Up till now, very limited studies have considered the vibrator of the sompoton. In view of this, it is important to expand the studies in the effort to preserve this traditional musical instrument. The vibrator plays an important role in the sound production by the sompoton. The original vibrator is made of polod which is a kind of a palm tree found locally. The existing vibrator does not have fixed standard dimensions to produce a certain sound frequency. It depends on the expertise of the master. In this research, the vibrator is constructed using aluminum instead of polod, to provide a less complicated way to understand the sound production mechanism of the sompoton. To carry out this work, vibrators of different dimensions were produced and analyzed in order to determine the governing formulation of the fundamental frequency.

2. Clamped bar model and fundamental frequency analysis of the vibrator

2.1. Rayleigh's energy theory and SDOF system analysis

A clamped bar in mechanical constructions is called a cantilever beam, which is a bar supported at one end, whereas the other end can vibrate freely (Fig. 3a). It is widely found in construction designs such as cantilever bridges, balconies, and it is also applied in the aircraft wings design. Detailed inspection of the sompoton's vibrator in Fig. 3b shows that generally it has a similar design to the clamped bar (Fig. 3a), where one end of the vibrator is attached to the frame and the other end vibrates freely when it is subjected to a force.

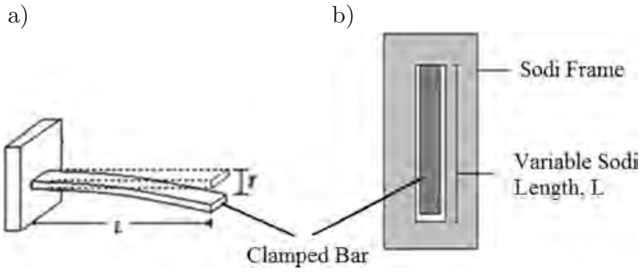

Fig. 3. Schematic diagram of the clamped bar and vibrator (sodi): a) clamped bar model, b) schematic drawing of the vibrator.

Although a clamped bar has many modes of vibration, the knowledge of its fundamental mode is of prime importance, as higher frequencies are the multiplication of this fundamental frequency. Therefore, in this paper, an equivalent single-degree-of-freedom system is adopted. The vibrator is modeled as a single mode clamped bar to predict its fundamental frequency.

The sompoton's vibrator has a uniform dimension and, therefore, can be modeled as a clamped bar with a uniformly distributed mass as shown in Fig. 4. When a uniformly distributed force is applied, Rayleigh energy theorem can be used to determine its fundamental sound frequency, according to which angular frequency of a vibrating system can be written as

$$\omega = \sqrt{\frac{k}{M}}\,, \tag{1}$$

where ω is the angular frequency in radian per second, k is the stiffness of the bar and M is the mass.

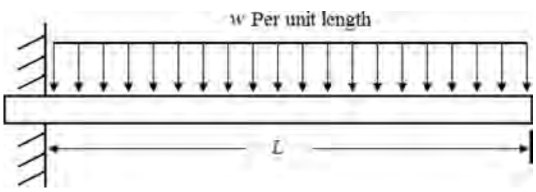

Fig. 4. Clamped bar of length L fixed at one end and carrying a uniformly distributed mass of w per unit length over the entire length of the bar.

The angular frequency can be expressed in the form of

$$\omega = 2\pi f. \tag{2}$$

Combining equation (1) and (2) gives

$$f = \frac{1}{2\pi}\sqrt{\frac{k}{M}}\,. \tag{3}$$

The maximum deflection of the clamped bar, y is given by (Gere, Goodno, 2009; Merriman, 1924)

$$y = \frac{wL^4}{8EI}\,, \tag{4}$$

where E is the modulus of elasticity, I is the second moment of inertia, L is the length, w is the uniform weight per unit length.

The stiffness of the bar system can be written as

$$k = \frac{F}{y} = \frac{wL}{y}\,, \tag{5}$$

where F is the total force acting on the bar.

Substitute Eq. (4) into Eq. (5) gives

$$k = \frac{8EI}{L^3}\,. \tag{6}$$

According to the Rayleigh energy theorem, the clamped bar system is analogous to the system of a spring mass. Therefore, the stiffness, k in Eq. (3) can be substituted by Eq. (6) to give the fundamental natural frequency of a uniformly distributed mass as

$$f = \frac{1}{2\pi}\sqrt{\frac{8EI}{ML^3}}\,, \tag{7}$$

where M is the mass of the bar which is calculated from the density value taken from the standard table of aluminum and L is the length of the bar.

2.2. Exact analysis

The free transverse vibration of the bar can be described as a differential equation of motion as

$$M\frac{\partial^2 y}{\partial t^2} + EI\frac{\partial^4 y}{\partial x^4} = 0, \tag{8}$$

where E, I, y, and M denotes Young modulus of elasticity, second moment of inertia, transverse deflection, and mass per unit length of the bar, respectively.

Using the method of separation of variables, we can write

$$\frac{EI}{M}\,\frac{1}{\varphi(x)}\,\frac{\mathrm{d}^4\varphi(x)}{\mathrm{d}x^4} = -\frac{1}{q}\,\frac{\mathrm{d}^2 q(t)}{\mathrm{d}t^2} = \omega^2, \tag{9}$$

where ω^2 is defined as constant.

This equation is then separated into separate differential equations as

$$\frac{\mathrm{d}^4\varphi(x)}{\mathrm{d}x^4} - \lambda^4\varphi(x) = 0, \qquad \frac{\mathrm{d}^2 q(t)}{\mathrm{d}t^2} + \omega^2 q(t) = 0, \tag{10}$$

where

$$\lambda^4 = \frac{\omega^2 M}{EI}\,. \tag{11}$$

The general solutions to the Eqs. (10) are

$$\begin{aligned} \varphi(x) &= C_1\cosh(\lambda x) + C_2\cos(\lambda x) \\ &\quad + C_3\sinh(\lambda x) + C_4\sin(\lambda x), \\ q(t) &= C_5\sin(\omega t) + C_6\cos(\omega t). \end{aligned} \tag{12}$$

Equation $(12)_1$ has four constants and requires four boundary conditions. For the case of a bar clamped at one end, the boundary conditions at the clamped end ($x = 0$) are that both deflection ($\varphi(x)$) and the slope $(\partial\varphi(x)/\partial x)$ should be equal to zero. On the other hand, at the free end, the bending moment $EI(\partial^2\varphi(x)/\partial x^2)$ and shear force $EI(\partial^3\varphi(x)/\partial x^3)$must both be zero (Morse, 1948).

After substituting the four boundary conditions into the Eq. $(12)_1$ and arranging it into the matrix form we have:

$$\begin{bmatrix} 1 & 1 & 0 & 0 \\ 0 & 0 & 1 & 1 \\ \cosh(\lambda L) & -\cos(\lambda L) & \sinh(\lambda L) & -\sin(\lambda L) \\ \sinh(\lambda L) & \sin(\lambda L) & \cosh(\lambda L) & -\cos(\lambda L) \end{bmatrix} \times \begin{bmatrix} C_1 \\ C_2 \\ C_3 \\ C_4 \end{bmatrix} = \begin{bmatrix} 0 \\ 0 \\ 0 \\ 0 \end{bmatrix} \tag{13}$$

or simply $[Q][C] = [0]$.

The constant matrix $[C]$ cannot be equal to zero (otherwise no vibration is present). Therefore, the determinant of $[Q] = 0$. The result of the determinant gives

$$\cosh(\lambda L)\cos(\lambda L) + 1 = 0, \tag{14}$$

which is the frequency equation.

The first four solutions for a clamped bar free vibration are given as

$$(\lambda L)_1 = 1.875104, \qquad (\lambda L)_2 = 4.694091,$$
$$(\lambda L)_3 = 7.854757, \qquad (\lambda L)_4 = 10.9955.$$

When the first value $\lambda L = 1.8751$ is substituted into Eq. (11) and rearrangement of the equation gives the fundamental frequency

$$\omega = 1.0150\frac{h}{L^2}\sqrt{\frac{E}{\rho}} \tag{15}$$

or

$$v = 0.1615\frac{h}{L^2}\sqrt{\frac{E}{\rho}}, \tag{16}$$

which gives values in Hz.

3. Experimental setup, results, and discussion

The aim of this paper is to establish a theoretical model that can explain the sound production mechanisms of the sompoton. In the previous section, a hypothesis was proposed that the sompoton's vibrator is similar to a clamped bar due to the similarity in their structural designs. In this section, experimental works were performed to verify this hypothesis and investigate the governing factors that may affect the sound emitted by the vibrator. To do this, vibrators of different lengths were produced from thin aluminum plate using Computer Numerical Control (CNC) machine to ensure uniformity. The width and thickness of the produced vibrators is fixed at 2 mm and 0.2 mm, respectively.

Figure 5 shows the experimental setup of this work. The vibrator was excited by using constant air jet pressure from an air compressor. The bar of the vibrator acts as an air gate that alternately blocks and un-blocks the passing air. This generates a vibration in the surrounding air and thus produces an audible tone (Hopkin, 1996). The sound generated by excitation of the vibrator was recorded using the Harmonie measurement system and later analysed using MATLAB to obtain the frequency spectrum. To avoid unwanted noise, the experiments were carried out in a noise free anechoic room. The aluminium vibrator was made with the modulus of elasticity $E = 70$ GPa, second moment of inertia $I = 1.333 \times 10^{-15}$ Nm, and density $\rho = 2700$ kg/m^3. The values of the modulus of elasticity and density are taken from the standard table for aluminum.

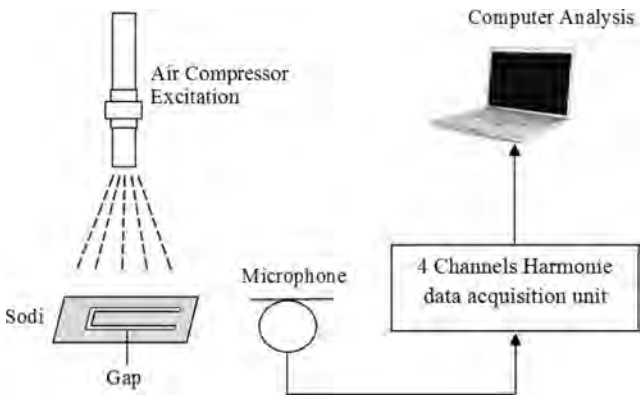

Fig. 5. Experimental setup of the sompoton's vibrator excitation and data analysis.

Table 1 shows the frequency values for different lengths of the vibrator obtained from the experimental measurements and theoretical calculation of SDOF system using Eq. (7). It should be noted that the sec-

Table 1. Experimental and theoretical value of SDOF fundamental frequency of the sound from aluminum vibrator.

Vibrator length L [mm]	Experimental frequency f_e [Hz]	SDOF system frequency f_t [Hz]	Percentage difference Δ [%]
17	572.0	457.9	19.95
18	567.0	408.4	27.97
19	520.0	366.6	29.50
20	505.7	330.8	34.59
21	413.0	300.1	27.34
22	392.4	273.4	30.33
23	359.0	250.2	30.31
24	338.0	229.8	32.01
25	304.1	211.7	30.38

ond moment of inertia I in the equation was calculated using the dimension of the aluminium vibrator, the mass M is the measured mass of the vibrator itself, and the length L is the length of the vibrator given in Table 1. It is clearly seen that both frequencies differ in magnitude. This is further visualized in a graphical comparison shown in Fig. 6 where the frequency obtained from measurement is always higher as compared to the theoretical value. Detailed inspection of Fig. 6 also shows that although they differ in magnitude, both data shared an identical trend – the sound frequency decreases as the vibrator length increases in a similar proportion. Errors occurring during production are a possible reason to explain the differences in the results. During the cutting process, the CNC machine's cutter defects the vibrator's bar and leaves a little curvature shape on the bar. Therefore, each vibrator experienced similar defects in production with the same proportion.

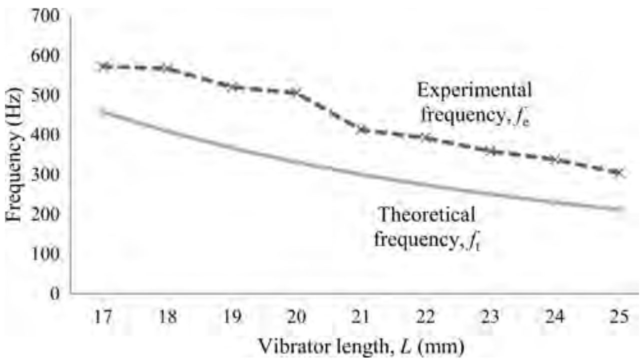

Fig. 6. Comparison between the theoretical SDOF using Eq. (7) and experimental values of the fundamental frequency of the aluminum vibrator of different lengths.

To account for the production errors, a correction factor must be added into the theoretical formula to determine the actual frequency. The linear scale graph in Fig. 6 is first rescaled into a semilog of y-axis as shown in Fig. 7.

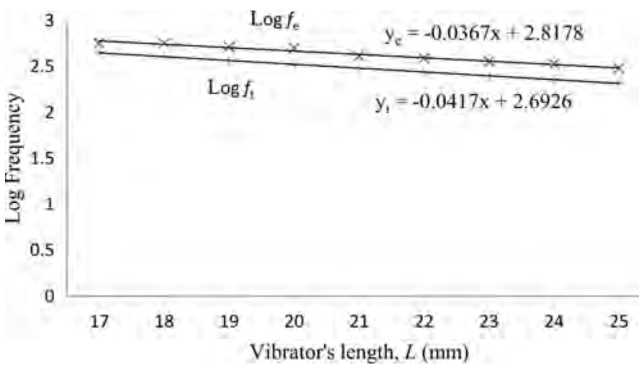

Fig. 7. Conversion of the graph in Fig. 6 into a logarithm form.

It can be seen now that the data obtained from the experimental work ($\log f_e$) and theoretical prediction ($\log f_t$) are in the linear proportion. For clarity, both equations are written in the following way:

$$\log f_e = -0.0367x + 2.817, \tag{17}$$

$$\log f_t = -0.0417x + 2.692. \tag{18}$$

Substituting Eq. (17) into (18) for x gives, after rearrangement:

$$\log f_t - 1.1362 \log f_e = -0.5091. \tag{19}$$

This can also be rewritten as

$$\log\left(\frac{f_t}{f_e^{1.1362}}\right) = -0.5091. \tag{20}$$

From the log identity, it can be written that

$$\frac{f_t}{f_e^{1.1362}} = 0.3097 \tag{21}$$

or

$$f_t = 0.3097 f_e^{1.1362}. \tag{22}$$

Rearranging the equation gives

$$f_e = \sqrt[1.1362]{3.229 f_t}, \tag{23}$$

which gives the final equation as

$$f_e = 2.81 f_t^{0.88}, \tag{24}$$

rounded to two decimal points, where f_t is the theoretical value of frequency of the produced vibrator given in Eq. (7).

Equation (24) relates the experimental and theoretical values of the vibrator's frequency. It is the corresponding equation that gives the actual frequency in terms of a theoretical equation with the correction factor. This means that using the same CNC machine setting, the required thickness of the vibrator has to be adjusted according to this equation and not to the theoretical formulation in Eq. (7).

In order to validate this new formula, the theoretical value of the frequency of the produced vibrator in Table 1 was substituted into Eq. (24) and then compared with the actual measurement. Table 2 shows the comparison between the two values. The table shows that the two set of values are in a close agreement with a maximum deviation of 8.37%. It can also be seen in Fig. 8 that the corrected frequency now closely matches the experimental frequency. Both graphs show a similar decreasing trend as the vibrator's length decreases.

In comparison with the previous analysis using the equivalent SDOF system, theoretical frequency values using the exact solution have been calculated. It was found that the fundamental frequency obtained from the exact analysis shows a closer agreement to the measured frequency. Comparing with the theoretical frequency derived from the SDOF system which shows

Table 2. Experimental and corrected SDOF formula result data of the aluminum vibrator length test.

Vibrator length L [mm]	Experimental frequency f_e [Hz]	Corrected formula frequency f [Hz]	Percentage difference Δ [%]
17	572.0	616.9	7.84
18	567.0	557.8	1.63
19	520.0	507.2	2.46
20	505.7	463.4	8.37
21	413.0	425.3	2.98
22	392.4	391.8	0.15
23	359.0	362.4	0.95
24	338.0	336.3	0.51
25	304.1	312.9	2.88

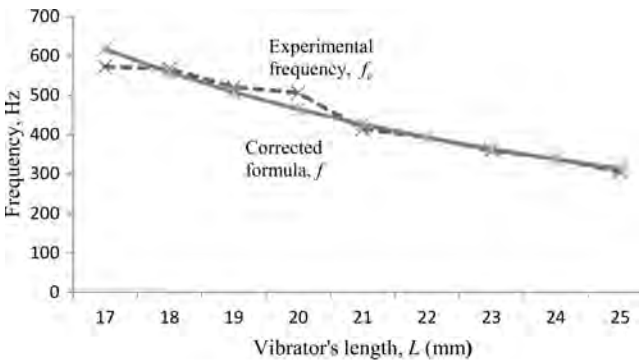

Fig. 8. Comparison graph of the experimental and corrected SDOF theoretical formula.

the maximum discrepancy of 34.59% (Table 1), the exact analysis gives a better result with the maximum discrepancy of 18.67% (Table 4). It can be clarified in Table 3 and Fig. 9 that the value from the exact analysis shows a closer match to the experimental value.

Table 3. Comparison of the fundamental frequency of the vibrator obtained using the SDOF system, exact analysis, and measurement.

Vibrator length L [mm]	Experimental frequency f_e [Hz]	SDOF system frequency f_t [Hz]	Exact solution frequency v [Hz]
17	572.0	457.9	569.2
18	567.0	408.4	507.7
19	520.0	366.6	455.7
20	505.7	330.8	411.3
21	413.0	300.1	373.0
22	392.4	273.4	339.9
23	359.0	250.2	311.0
24	338.0	229.8	285.6
25	304.1	211.7	263.21

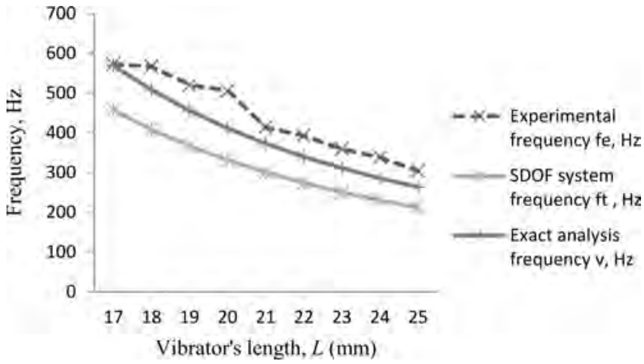

Fig. 9. Graphical comparison of the fundamental frequency of the vibrator obtained using the SDOF system, exact analysis, and measurement.

Table 4. Experimental and exact analysis values of the fundamental frequency of the sound of the aluminum vibrator.

Vibrator length L [mm]	Experimental frequency f_e [Hz]	Exact analysis frequency v [Hz]	Percentage difference Δ [%]
17	572.0	569.2	0.49
18	567.0	507.7	10.46
19	520.0	455.7	12.37
20	505.7	411.3	18.67
21	413.0	373.0	9.69
22	392.4	339.9	13.38
23	359.0	311.0	13.37
24	338.0	285.6	15.50
25	304.1	263.21	13.44

Figure 10 illustrates a graphical comparison of the frequencies obtained from the exact analysis and the measurement. It can be seen that the experimental value is always higher than the calculated frequency. A similar explanation from the SDOF analysis can be applied for the result differences as discussed before, where the production error could be the main reason for it.

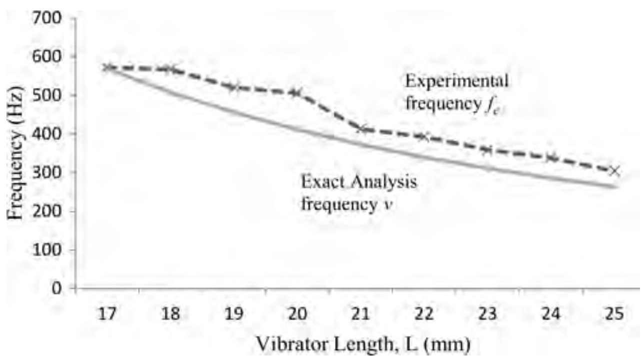

Fig. 10. Comparison of the exact analysis and experimental values of the fundamental frequency of the aluminum vibrator with a different length.

Therefore, a correction factor is also needed to account for the production errors in the exact analysis. Following a similar approach for the SDOF system, Fig. 10 is rescaled into a semilog y-axis graph which is shown in Fig. 11.

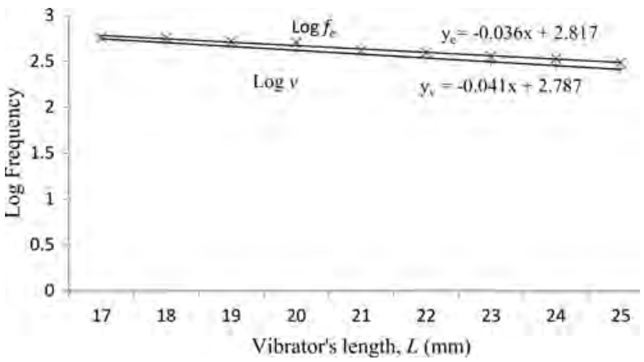

Fig. 11. Conversion of the exact solution graph into a logarithm form.

Using both linear equations from the logarithmic graph, the steps from Eq. (17) to Eq. (24) are then repeated to obtain the corrected formula for the exact analysis. The new corrected formula of the exact analysis obtained is

$$v_c = 2.34v^{0.88}. \qquad (25)$$

Table 5 compares the corrected values of the exact analysis with the experimental frequency. It shows that both sets of values are now in a better agreement, where the maximum discrepancy is reduced to 8.76%. It can further be seen in Fig. 12 that the corrected frequency is now closely matched with the measured frequency.

Table 5. Comparisons between the measured and corrected exact solutions of the fundamental frequency of the aluminum vibrator.

Vibrator length L [mm]	Experimental frequency f_e [Hz]	Corrected formula frequency v_c [Hz]	Percentage difference Δ [%]
17	572.0	622.1	8.76
18	567.0	562.5	0.79
19	520.0	511.5	1.63
20	505.7	467.4	7.57
21	413.0	428.9	3.85
22	392.4	395.2	0.71
23	359.0	365.5	1.81
24	338.0	339.1	0.33
25	304.1	315.6	3.78

Table 6 summarises the work in this paper. It shows the comparison between the frequencies of the aluminium vibrator obtained from the corrected equivalent SDOF model and corrected exact solution, with

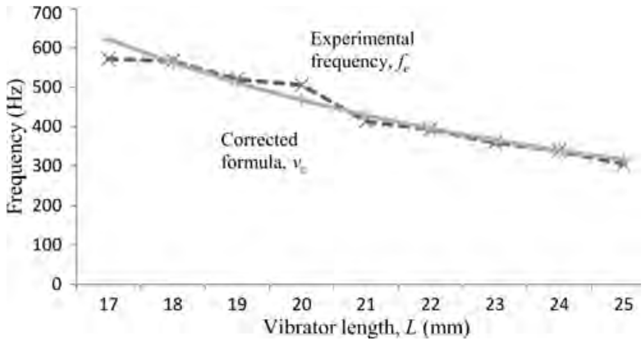

Fig. 12. Graphical comparisons between the experimental and corrected exact solutions of the fundamental frequency of the aluminum vibrator.

the actual value obtained by measurement. It can be seen that the percentage difference for both theoretical analyses with the correction factor has reduced and their values are closer to the measured fundamental frequency.

Table 6. Comparison, in percentage difference, between the frequencies obtained using corrected SDOF and corrected exact analysis, with the actual values.

Vibrator length L [mm]	Experimental frequency f_e [Hz]	SDOF frequency f [Hz]	Percentage difference Δ [%]	Exact analysis frequency v_c [Hz]	Percentage difference Δ [%]
17	572.0	616.9	7.84	622.1	8.76
18	567.0	557.8	1.63	562.5	0.79
19	520.0	507.2	2.46	511.5	1.63
20	505.7	463.4	8.37	467.4	7.57
21	413.0	425.3	2.98	428.9	3.85
22	392.4	391.8	0.15	395.2	0.71
23	359.0	362.4	0.95	365.5	1.81
24	338.0	336.3	0.51	339.1	0.33
25	304.1	312.9	2.88	315.6	3.78

4. Conclusions

This paper presented modeling of the sompoton's vibrator using a clamped bar model for the analysis of the fundamental resonance frequency. Several sompoton's vibrators made of aluminum thin plate of different length were produced using the Computer Numerical Control (CNC) machine to ensure uniformity. The equivalent single degree of freedom system (SDOF) and exact solutions were then used as a theoretical analysis method. It was found that exact formulation provides a better prediction of the vibrator's fundamental frequency as compared with the experimental measurement. However, both theoretical analysis models (the SDOF and exact analysis) show a certain percentage of deviation from the actual measurement. To solve the problem, a correction factor for the theoretical formulas was derived to account for the production error.

References

1. Carral S., Vergez C., Nederveen C.J. (2011), *Toward a Single Reed Mouthpiece of the Oboe*, Archives of Acoustics, **36**, 2, 267–282.
2. Erkut C., Karjalainen M., Huang P., Välimäki V. (2002), *Acoustical Analysis and Model-Based Sound Synthesis of the Kantele*, Journal of the Acoustical Society of America. **112**, 4, 1681–1691.
3. Fouilhe E., Goli G., Houssay A., Stoppant G. (2011), *Vibration Modes of the Cello Tailpiece*, Archives of Acoustics, **36**, 4, 741–759.
4. Gere J.M., Goodno B.J. (2009), *Mechanics of Materials*, Cengage Learning, 7th Edition, United States of America.
5. Hopkin B. (1996), *Musical Instrument Design*, See Sharp Press, 7^{th} Printing, Arizona, United States.
6. Ismail A., Samad S.A., Hussain A., Azhari C.H., Zainal M.R.M. (2006), *Analysis of the Sound of the Kompang for Computer Music Synthesis*, 4th Student Conference on Research and Development (SCOReD 2006), IEEE, pp. 95–98, Malaysia.
7. Lohri A., Carral S., Chatziioannou V. (2011), *Combination Tones in Violin*, Archives of Acoustics, **36**, 4, 727–740.
8. Marasan R. (2003), *Alat Muzik Sompoton Negeri Sabah* [in Malay], Pejabat Kebudayaan dan Kesenian Negeri Sabah, Sabah, Malaysia.
9. Merriman M. (1924), *Mechanics of Materials*, John Wiley & Sons, 10^{th} Edition, New York, London.
10. Morse P.M. (1948), *Vibration and Sound*, McGraw-Hill Book Company, Inc, 2nd Edition, United States.
11. Ong C.W., Dayou J. (2009), *Frequency Characteristic of Sound from Sompoton Musical Instrument*, Borneo Science, **25**, 71–79.
12. Rujinirum C., Phinyocheep P., Prachyabrued W., Laemsak N. (2005), *Chemical Treatment of Wood for Musical Instruments. Part I: Acoustically Important Properties of Wood for the Ranad (Thai Traditional Xylophone)*, Wood Science and Technology, **39**, 1, 77–85.
13. Skrodzka E.B., Hojan E., Proksza R. (2006), *Vibroacoustic Investigation of a Batter Head of a Snare Drum*, Archives of Acoustics, **31**, 3, 289–297.
14. Skrodzka E., Lapa A., Linde B.B.J., Rosenfeld E. (2011), *Modal parameters of two complete guitars differing in the bracing pattern of the soundboard*, Journal of Acoustical Society of America, **130**, 4, 2186–2194.
15. Someya S., Okamoto K. (2007), *Measurement of the Flow and Its Vibration In Japanese Traditional Bamboo Flute Using the Dynamic PIV*, Journal of Visualization, **10**, 4, 397–404.

PAN
ARCHIVES OF ACOUSTICS
Vol. **38**, No. 3, pp. 433–433 (2013)

DOI: 10.2478/aoa-2013-0051

Letter to the Editors

Book Review: Acoustics for Engineers – Troy Lectures in: Vol. 37, 597–600 (2012)

The author appreciate the long and thoughtful review of their book and take the opportunity to add some further information that may be useful for potential readers.

1. The book was written as a textbook for a one-semester introductory course in engineering acoustics at academic level for readers with a' mathematical background. It was not intended as a handbook which, amongst other thing, would have required a much broader coverage of the field and the relevant literature. Nevertheless, the authors feel gratified by the fact that their readers obviously use it as a source of reference in their further work in acoustics.
2. A second volume is in preparation [Blauert J. & Braasch J., "Acoustics for Communication – Troy Lectures"] and is scheduled to appear at Springer in 2014. This volume will cover many of the items that the reviewer missed in the current volume, for instance, speech and hearing, perceptual coding, sound quality, binaural technology, surround sound, auditory virtual reality, and others.
3. The way in which textbooks are distributed has changed dramatically during the last three years. Of the current book only a few hundred printed copies have been sold so far, however, it has enjoyed more than ten thousand download of the e-book version. Taking this new situation into account, the book has a website of its own, namely, http://symphony.arch.rpi.edu/∼xiangn/Springer-Book.html.

On this website confirmed errors and mistakes are listed – unless minor – and solution to the problems are provided. The collection of solutions is complete for the German language. English translations follow step by step.

All readers are invited to contribute to the website, such making the book a dynamic source of knowledge which is constantly amended and improved. In this way, the authors intend to take advantage of the social media and exploit crowd sourcing amongst their readership to the benefit of knowledge dissemination in the exciting field of acoustics. Finally, they want to thank their dear colleague, Prof. Andrzej Dobrucki for the time and effort that he has devoted to prepare the review.

Jens Blauert & Ning Xiang

PAN
ARCHIVES OF ACOUSTICS
Vol. **38**, No. 3, pp. 435–447 (2013)

DOI: 10.2478/aoa-2013-0052

Chronicle

60th Open Seminar on Acoustics
Rzeszów – Polańczyk, Poland, September 9 – 13, 2013

Abstracts

Assessment of the accuracy of the identification process of the sound source at the given level of the acoustic background

Batko Wojciech[1], batko@agh.edu.pl
Przysucha Bartosz[2]

[1] AGH University of Science and Technology
Faculty of Mechanical Engineering and Robotics
Departament of Mechanics and Vibroacoustic
al. A. Mickiewicza 30, 30-059 Kraków, Poland
[2] Lublin University of Technology
Faculty Management
Department of Quantitative Methods
of Management of Economy
Nadbystrzycka 38, 20-618 Lublin, Poland

The problem of assessments of uncertainty of the identification process of the sound source responsible for environment acoustic hazards, essential in acoustic measurements, is investigated in the paper.

Realisation of this task (determining likelihood of the result obtained in the control process) requires the determination of the density probability distribution function of the analysed source noise level Lsour. Its knowledge is the basic dependence needed for the estimation – with the required confidence level – of the interval of the possible assessment error of the noise level related to the controlled emission source. Its form can be derived from the identification equation, by the method of propagation of the measured variables distribution, it means: LM – the sound level of the controlled noise (under conditions of the analysed source emission) and Lbg the acoustic background level. The determination of the density probability distribution function of the identified noise level of the source Lsour, at the assumption that the measured values distribution is known, is discussed in the paper.

The derivation path of the density probability distribution function of variable Lsour, taking into consideration the lack of independence of variables LM and Lbg, is presented. The proposed solution was illustrated by examples of calculations the density probability distribution function of variable Lsour.

⋆ ⋆ ⋆

Comparison of uncertainty determination methods of environmental noise threat assessment

Batko Wojciech[1], batko@agh.edu.pl
Przysucha Bartosz[2]
Pawlik Paweł[1]

[1] AGH University of Science and Technology
Faculty of Mechanical Engineering and Robotics
Departament of Mechanics and Vibroacoustic
al. A. Mickiewicza 30, 30-059 Kraków, Poland
[2] Lublin University of Technology, Poland Department
of Quantitative Methods of Management of Economy
Faculty Management
Lublin

The theme of the work is the problem of assessing the uncertainty of controlled noise indicators. Analysis of uncertainty estimation obtained using two models formalisms was presented. The first is based on the law of propagation of distribution density functions of measurement variables used to determine the distribution of controlled noise indicator. The second solution is based on the formalism of Reductive Interval Arithmetic. Assessment of the results effectiveness of these solutions was realized and reference is made to the results obtained by Monte Carlo method.

⋆ ⋆ ⋆

Stability condition for active noise control using modified FX-LMS algorithm

Bismor Dariusz

Silesian University of Technology
Institute of Automatic Control
Akademicka 2a, 44-100 Gliwice, Poland

Recent discoveries allow to prove the LMS algorithm stability necessary condition for very wide group of signals. The upper bound given by the stability condition, in turn, allows to choose step sizes in the manner that gives very fast adaptation at the beginning of LMS algorithm operation, or after substantial changes are detected. However, the new condition cannot be applied for the FX-LMS algorithm, where the influence of the secondary path dynamic sand its estimate should be considered. The Modified FX-LMS algorithm and structure are a concept that allows to remove the influence of the secondary path from the error signal. Thus, the new LMS stability condition can be directly applied to the Modified FX-LMS, as long as an estimate of the secondary path is accurate enough. This paper shows the derivation of the modified FX-LMS algorithm stability condition and describes the effect of the secondary path estimation error on the step size upper bound given by the stability necessary condition. Simulations are shown for different types of signals to support the conclusion.

⋆ ⋆ ⋆

The system for marking and identification of the spots dangerous and of special importance for vision impaired persons in the big city – information given by vibrating bracelet

Bogusz Edyta[1]
Czopek Dorota[2]
Wiciak Jerzy[2]

[1] Adam Mickiewicz University
Institute of Acoustics
Umultowska 85, 61-614 Poznań, Poland
[2] AGH University of Science and Technology
Department of Mechanics and Vibroacoustics
al. A. Mickiewicza 30, 30-059 Kraków, Poland

Paper presents progress and results of psychophysical studies connected with vibration perception on the wrist of blind people. Studies were carried out under the research project entitled The development of the method for marking and identification of the spots dangerous and of special importance for vision impaired persons in the big city with use of the wave-vibration markers. Six situation which require marking were selected based on previously conducted survey. The aim of psychophysical studies was to select vibration signals which could give blind people information about zone in which they are.

It was assumed that signals should be easy, but also should enable to give six, different information. It was decided to divide test into two stages. In both stages signals were evaluated using short, 5-point, numerical and verbal ICBEN scale.

In first task, signals were presented singly to evaluate their annoyance and ease to learn and memorize After this task six signals which received the best scores was selected. In second task, signals connected into pairs were presented to evaluate their recognizability. Results of first and second task were compared and signals which were to similar were deleted from chosen six. Finally, six signals were selected and matched with following situation: staircases with differentiation of direction, rail platform, tram platform, pedestrian crossing, temporary obstacles: excavations, road works, temporary bridges and public buildings.

⋆ ⋆ ⋆

Vibrational energy transfer in a welded joint model with shell elements

Bochniak Wojciech
Cieślik Jacek

AGH University of Science and Technology
Faculty of Mechanical Engineering and Robotics
al. A. Mickiewicza 30, 30-059 Kraków, Poland

The work presents the concept of research methods in vibrational energy transfer with application to analysis of dynamics of structures that use energy of mechanical vibration as an evaluation parameter or other items related to energy. The structural surface intensity representing time-averaged flow rate of the mechanical vibration energy by unit area perpendicular to the flow direction was used in studies of the specific vibration energy flow in solids. Analysis of the spatial distribution of structural intensity allows the study of vibrational energy transfer paths and places where energy is introduced or absorbed in the mechanical structure.

The purpose of work was the research vibrational energy pathways in the flat components of welded structures including different FE models of connections. The analysis was performed for a particular model of the welded plates connected at an angle of 90° and two strips placed on the plates. Such flat welded components are widely used in the construction of buildings and vehicles.

The modeling studies were preceded by a detailed review of literature in the area of computational methods used in the analysis of welded joints in particular using the finite element method. Special attention was paid to the methods of vibration energy flow analysis using structural intensity for flat plates. Computational methods applied for the study of vibration energy pathways in the structures of complex shapes, made of flat thin items such as plates and shells so far were insufficient to solve the problem of modeling of welded joints. In the analysis of specific practical cases the problems appeared to take into account a complex boundary conditions, properties of structures and the selection of a particular type of finite element model for the analysis of vibration energy flow in the welded joints.

The major problems affecting the quality of welded joints come from the thermal energy dissipation during the merge process, which changes the structure of the welded material and causes the heterogeneity of the material structure. This results in the change of mechanical properties of the joints, stress concentration, formation of residual stresses and strains in the welds and adjacent areas. Modeling of welded joints in computational finite element analysis (FEA), particularly modeling and analysis of T-joints is a complex problem and difficult for accurate representation. Requires a special approach in selecting the model taking into account the complexity of the structure – its geometry and mechanical properties. There are commonly used simplified models of fillet welds using shell elements of increased thickness, rigid finite elements and solid elements. The best results were obtained for the calculations with use of oblique shell elements, simulating in the correct way connection of elements and bending stresses in the weld area.

There are given results done with the new approach of modeling for angled welded connections of plates. The results were compared with earlier results of modeling done by the authors. The calculation results showed a significant increase of the modeling accuracy of the vibrational energy flow in welded joints.

⋆ ⋆ ⋆

Influence of the bit rate in MP3 compression on the speech quality

Brachmański Stefan, stefan.brachmanski@pwr.wroc.pl

Wrocław University of Technology
Wybrzeże Wyspiańskiego 27, 50-370 Wrocław, Poland

Over the last years, there has been a significant development of telecommunication technologies, inter alia, in video as well as speech signal transmission. As a consequence new, more effective methods of utilization of transmission bandwidth are required. Nowadays there are multiple, different solutions in use, in which the speech signal is being transformed for more efficient transporting, storing and recognition. There are many algorithms for coding the audio signals. In this article the impact of bit rate on the quality of speech signal transmission encoded as MP3 is researched. The described measurements were done for bit rates in range between 8 kbps and 320 kbps, using two subjective methods recommended by International Telecommunication Union (ITU) – namely Absolute Category Rating and Degradation Category Rating. The assessment of the speech quality was done using the sentence lists read by a female and male lector.

⋆ ⋆ ⋆

Influence of the plaster physical structure on its acoustic properties

Brański Adam[1], abranski@prz.rzeszow.pl
Prędka Edyta[1]
Wierzbińska Małgorzata[2]
Hordij Piotr[3], greinplast@greinplast.pl

[1] Rzeszów University of Technology
Laboratory of Acoustic
Faculty of Electrical and Computer Engineering
Wincentego Pola 2, 35-959 Rzeszów, Poland
[2] Technical University of Rzeszow
Department of Materials Science
al. Powstańców Warszawy 12, 35-959 Rzeszów, Poland
[3] Greinplast
Krasne 512B, 36-007 Krasne, Poland

This work presents the main experimental results obtained from the study of plaster test pieces with different parameters of its physical structure. Mainly an aeration of plaster and amount and diameter of the pearlite in it, expressed in per cent, are considered as parameters. Other parameters are also studied, but they play a minor part, for example the different thickness of the sample. Acoustic properties, measured via the sound absorption coefficient, are researched depending on the proportions of the aeration and/or the pearlite. The results are compared to the absorption coefficients of the conventional plasters. The physical, mechanical and thermal properties are not analyzed. The results show that an improvement in the absorption coefficient is obtained. This coefficient increases with the increase of aeration and appropriate diameter and proportion of the pearlite. This is due to the increase of the open porosity.

⋆ ⋆ ⋆

Acoustic interaction of orchestra pit with the audience and the stage in the example of the opera house in Lviv

Brawata Krzysztof[1]
Kamisiński Tadeusz[1]
Kinash Roman[2]
Rubacha Jarosław[1]
Szeląg Agata[1]

[1] AGH University of Science and Technology
Faculty of Mechanical Engineering and Robotics
Department of Mechanics and Vibroacoustics
al. A. Mickiewicza 30, 30-059 Kraków, Poland
[2] AGH University of Science and Technology
Faculty of Mining and Geoengineering
Department of Geomechanics, Civil Engineering and Geotechnics
al. A. Mickiewicza 30, 30-059 Kraków, Poland

The article raises an important issue that occurs in multipurpose room equipped with orchestra pit. Placing an orchestra at a lower level relative to the stage and the audience allows to hide it from the sight of the audience, but also reduces the direct sound propagation path. It causes the need to maintain an appropriate acoustic interaction between the orchestra pit, stage and the audience. The paper presents the results of acoustic surveys and simulation calculations performed in the hall of the Opera House in Lviv which enabled the analysis of this phenomenon. The study investigated the impact of the depth of the orchestra pit, the height of the railings, the geometry of the selected reflection planes and acoustic adaptation of the orchestra pit. The goal of the study was to link the commonly known room acoustic parameters, such as G, C80 with the evaluation of the interaction of acoustic orchestra pit, stage and audience.

⋆ ⋆ ⋆

Optimization of multi-channel sound field synthesis systems in open space

Ciesielka Wojciech
Filipek Roman

AGH University of Science and Technology
al. A. Mickiewicza 30, 30-059 Kraków, Poland

The paper presents the optimization of the parameters of multi-channel sound field synthesis systems located in truncated area of open space. The work is divided into three main stages: modelling, simulation and analysis, and optimization. The first of these include the building of above-mentioned sixteen-channel sound system models using FEA implemented in ANSYS. The input parameters have been defined as sound power attenuation levels and delays for each pair of sources located symmetrically along interior area. Next the simulation and analysis of five system cases were performed. The numerical experiment has been designed with the use of hybrid experiment plan – a combination of central composite and optimal space filling design. Attenuation levels were changed in the range of 0 to 20 dB and delays from 0 to 4 ms. The final stage of the research was carried out for the optimization of different system variants using the screening method and the method based on evolutionary algorithm NSGA-II. The studies have shown that in the multi-channel sound system the modification of sound sources attenuations and delays can improve sound field parameters determined at selected points in the interior area and reduce the sound pressure level in the exterior region.

⋆ ⋆ ⋆

Modelling of wind turbine acoustic emission

Czajka Ireneusz
Suder-Dębska Katarzyna
Chlebda Krzysztof

AGH University of Science and Technology
Faculty of Mechanical Engineering and Robotics
Department of Power Systems
and Environmental Protection Facilities
al. A. Mickiewicza 30, 30-059 Kraków, Poland

In last years wind turbine noise problem is becoming much more urgent. The issue is studied in years. There are many studies of various aspects of generating, modeling and protection against this type of noise. Many of the existing models assumes that a wind turbine is a point source. One of the arguments for this approach is the small dimension of the source in relation to the measurement distance. Authors present a method of modeling the aerodynamic noise source, which is a wind turbine. This model has many weaknesses, but allows for an approximate determination of the directional pattern of such source. With the inclusion of the directional pattern, it is possible to use a point source model.

⋆ ⋆ ⋆

The influence of classical guitars' physical properties on the subjective assessment of their tonal quality

Czajkowska Marzena

Wrocław University of Technology
Wybrzeże Wyspiańskiego 27, 50-370 Wrocław, Poland

One of the main goals in musical acoustics research is to link measurable, physical properties of a musical instrument with subjective assessments of its tone quality. The aim of the research discussed in this paper was to observe the sound pressure response and structural vibrations of different class classical (nylon-stringed) guitars in relation to their tonal character and quality.

Twenty seven classical guitars of different price range have been investigated – both manufacture (18) and handmade (9) instruments. Measurement methods of determining sound pressure and body vibrational responses are presented. Structural modes of top and back plates have been measured with the aid of a scanning laser vibrometer. Additionally, sound pressure response measurements were performed in the anechoic chamber. The instruments were excited with a modal hammer or a bone vibrator. The tonal quality and characteristics of the instrument was determined based on the results of subjective assessment listening tests performed on a group of experts. The list of carefully selected subjective parameters, which represent the unique and characteristic features of classical guitars' sound quality, has been introduced. Based on correlation and descriptive statistics, the relation between established objective and subjective classical guitar parameters has been investigated and discussed.

⋆ ⋆ ⋆

The propagation of acoustic waves in an inhomogeneous medium

Czyż Henryka

Rzeszów University of Technology
Department of Physics
al. Powstańców Warszawy 12, 35-959 Rzeszów, Poland

The aim of the paper is to present the analysis of the problems the propagation of acoustic waves in an inhomogeneous medium. A suspension of dust in the air and gas bubbles in the liquid are examples of so-called grained medium. The presence of inclusions has an influence on the propagation of acoustic waves in the medium, changes since the average density and compressibility of the medium and occurs scattering of waves. In the presence of suspended solids or liquids in liquids resultant of velocity of the wave in the medium grained calculated based on considerations for the mixture. When the gas bubbles are in the liquid, changing the volume fraction of the system. Inclusions vibrate under the influence of the acoustic wave modifying it in volume.

⋆ ⋆ ⋆

Application of shape memory elements for excitation and reduction of the vibrations of the plate systems

Dąbrowski Kamil
Wiciak Jerzy

AGH University of Science and Technology
Departament of Mechanics and Vibroacoustics
al. A. Mickiewicza 30, 30-059 Kraków, Poland

From way back smart materials have had a use as technical applications in the reduction of the mechanical vibrations.The most popular materials used in this field are piezoelectric ceramics, however, they show limitations in the range of low frequencies. Materials that could fill this gap are the elements with a shape memory. Actuators made of this material generate sufficient force so as to affect the systems' movement even in very low frequencies.

This paper discusses the issue of reducing mechanical vibrations by using shape memory elements in plates with different types of fixation and means of vibration excitation. At the same time this study also presents the results of laboratory tests which are related to the analysis of the application of nitinol actuators to the reduction of the vibrations. The research was based on forcing the plate system to vibrate and providing extra energy into the system in order to control this phenomenon. The shape memory elements are meant to decrease or increase the amplitude of the vibrations in these systems.

⋆ ⋆ ⋆

Residual noise in the method of measurement of nonlinear distortion with broadband noise

Dobrucki Andrzej

Wrocław University of Technology
Wybrzeże Wyspiańskiego 27, 53-333 Wrocław, Poland

In the measurement method of nonlinear distortion with broadband noise the exciting noise is filtered with a band-stop filter, which removes a narrow frequency band of signal. This signal is given to the system under test and at the output the signal is filtered with a band-pass filter tuned for the same frequency band as removed at the input. For linear systems the output signal should be equal to zero. The measured signal is the product of nonlinear distortion. The band- pass filter at the output should have a bit narrower badwidth than the band-stop filter at the input because of finite slopes in the frequency response of both filters in their stop-bands. In the rejected frequency band the residual noise appears. Its level should be significantly lower than the expected product of nonlinearities. In the paper a method of computing of residual noise is presented. The calculation have been made for different types of filters, for different noises e.g. white or pink and different bandwidths of analysis.

⋆ ⋆ ⋆

Pyłofon – strong acoustic wave generator for surface cleaning of heat exchangers in power facilities

Felis Józef, Flach Artur
Kamisiński Tadeusz, Niewczas Bogdan

AGH University of Science and Technology
Faculty of Mechanical Engineering and Robotics
Department of Mechanics and Vibroacoustics
al. A. Mickewicza 30, 30-059 Kraków, Poland

Gradually increasing ash layers on the heating surfaces reduce the transfer of energy to the heating medium and restrict the free flow of gas in the spaces of power boilers built. Especially, it concerns the coal-fired boilers. This results in energy loss due to the increase in exhaust gas temperature. Another adverse effect of ash pollution is the need for frequent exemptions from the operation of boilers to clean heating surfaces. Therefore, it is necessary to use effective methods of cleaning the heat exchange surfaces during operation of the boilers.

The paper presents the acoustic method of removing ash layers using strong acoustic wave generated by pylofon. This method is based on the stimulation of gaseous medium oscillation, in this case the exhaust stream, with a strong acoustic wave. Exhaust reach all the boiler, which allows to propagate the acoustic wave to inaccessible areas if another method was used such as blowing ash by steam or compressed air. The device, which fully exploits the potential of this acoustic method is pylofon, which generates a strong acoustic standing wave, aimed at vulnerable to pollution boiler area. Pylofon control system allows to keep the generator in operation despite changing thermal conditions during the operation of the boiler. The typical applications of pylofons are water and steam power boilers of different capacity and desulphurisation reactors or catalysts in systems reducing emission of NOx.

⋆ ⋆ ⋆

The sensitivity analysis of multi-channel sound field synthesis systems in the open space

Filipek Roman, Ciesielka Wojciech, Gołaś Andrzej

AGH University of Science and Technology
al. A. Mickiewicza 30, 30-059 Kraków, Poland

This paper presents the results of a sensitivity analysis of multi-channel sound field synthesis systems in the open space.

The study was conducted for sixteen-channel sound control system in which local and global sensitivity of parameters inside and outside selected areas were determined. Changeable input parameters of the system were sound power attenuation levels of individual sound sources and additional delay. The output parameters were observed for the one-third octave center frequencies in the range of 62.5 to 250 Hz. The studies concerned parameter selection in such a way as to obtain at least desirable minimum SPL and the highest SPL uniformity in 15 points within the area. The second equivalent goal was the lowest possible level of the average SPL outside the listening area. To perform properly planned analysis the design of experiment method was used. It combined optimal space filling and central composite designs. The experiment was carried out on the basis of a model builded by applying FEM. Obtained output parameters have been interpolated by Kriging's algorithm and formed system meta-model. Local sensitivities were determined at points on its response surfaces. Then, by calculation of the meta-model response in 2000 pseudo-random points, Spearman's rank correlation coefficient matrix and on its basis global system sensitivities have been determined.

⋆ ⋆ ⋆

The negative aspects of automation of selected acoustic measurements performed in an anechoic chamber

Flach Artur, Kamisiński Tadeusz, Felis Józef
Pilch Adam, Zastawnik Marcin, Zborowski Andrzej

AGH University of Science and Technology
Faculty of Mechanical Engineering and Robotics
Department of Mechanics and Vibroacoustical
al. A. Mickiewicza 30, 30-059 Kraków, Poland

Institute for Sustainable Technologies
Pułaskiego 6/10, 26-600 Radom, Poland

Automation of vibroacoustic measurements is an inevitable process because of the modern requirements according to precision of a microphone positioning and the number of measurements points, that are necessary to obtain specified parameter with required accuracy. Apart from undoubted advantages of automation, every additional device in the anechoic chamber, can disturb the free field there, and should be thoroughly analyzed before and after application.

In the paper, the problem of measurements errors generated in some studies performed in the anechoic chamber using mechatronic manipulator is presented. In order to determine negative impact of positioning devices on measurements results, sound diffusion coefficient, directional characteristics of sound source and sound power level measurements were analyzed.

Basing on the results of the study, some areas of anechoic chamber were selected, where hardware of the manipulator could influence the results of measurements made there. Moreover, different constructions of the manipulators were considered and some solutions were proposed, that allow to limit the negative impact on described measurements.

⋆ ⋆ ⋆

Modal analysis of the cylindrical waveguide acoustic field, possible sources of error and its effect on consistency with the theoretical model

Gorazd Łukasz

AGH University of Science and Technology
Faculty of Mechanical Engineering and Robotics
Department of Mechanics and Vibroacoustics
al. A. Mickiewicza 30, 30-059 Kraków, Poland

The presented studies of the acoustic field inside cylindrical waveguide were aimed at qualitative and quantitative determination of its modal structure and verification of consistency of the obtained measurement results with theoretical assumptions of the hard-walled semi-infinite cylindrical waveguide model by means of solving the corresponding inverse problem. Solution of the inverse problem, i.e. determination of amplitudes of individual modes, was based on acoustic pressure distribution measurements taken on selected cross-sections of a cylindrical waveguide excited by means of a single-tone sound source located inside the system either axisymmetrically or not. Frequencies of signal applied to the source were selected in such a way that they fell between consecutive radial/circumferential mode cut-off frequencies so apart from the plane wave, also consecutive higher wave modes could be observed with the increasing excitation frequency. The analysis included acoustic field distributions inside waveguides corresponding to mathematical models of the infinite cylindrical waveguide and the semi-infinite unbaffled cylindrical waveguide, i.e. with the diffraction phenomena occurring at the open waveguide outlet taken into account in the latter case. The paper is concluded with analysis of consistency of the obtained measurement results with predictions of the theoretical model and the effect of most likely error sources of the overall error of the measurement method.

⋆ ⋆ ⋆

Application of artificial neural networks for the diagnosis of arterio-venous fistula on the basis of the acoustic signal

Grochowina Marcin[1]
Leniowska Lucyna[2]
Dulkiewicz Piotr[1]

[1] Nefron Sp. z o.o.
Wilków 82, 32-010 Kocmyrzów, Poland
[2] University of Rzeszów, Institute of Technology
Al. Rejtana 16C, 35-959 Rzeszów, Poland

In this work a new diagnostic method of arterio-venous fistula is presented. Fistula is surgically made connection between artery and vein to obtain access to subcutaneous venous vessel with high blood flow, which is essential for hemodialysis. Depending on the patient's health, the fistula is a source of various sounds. Every dysfunction may lead to thrombosis or another complication which is dangerous for life or health. Analysis of sounds generated by the blood flow through the fistula allows to detect the pathological conditions. Signal from fistula is analyzed with the use the open source library called FANN (Fast Artificial Neural Network). This solution is applied in the commercial telediagnostic system, which provides remotely tests by cellular phone.

⋆ ⋆ ⋆

Bayes networks used in application to pathological speech diagnostics

Izworski Andrzej, Wszołek Wiesław

AGH University of Science and Technology
Faculty of Mechanical Engineering and Robotics
Department of Mechanics and Vibroacoustical
al. A. Mickewicza 30, 30-059 Kraków, Poland

Bayesian Networks (BN) are one of the methods allowing formalization of process dynamics as a predictive model. They have been created about 35 years ago, and their main features are ability to show the cause-and-effect relationships, picture uncertainty as the probability distribution of variables. And also ability to compute calculations with incomplete data. Bayesian Networks were designed to induce in static situations and their direct use in evolving problems is difficult. The solution of this problem turned out to be the Dynamic Bayesian Networks, which are extended version of Bayesian Network, enhanced with stochastic representation of processes changing over time.

The Dynamic Bayesian Networks (DBN) are powerful and elastic tool that can be used to represent probabilistic models for stochastic processes. There is growing interest in application of this tool to solve practical problems, including processing and recognition of speech signal elements. Process of evaluation of pathological speech acoustic signal deformation is a matter of assignment the acoustic images, obtained from research, to certain classes. However, in opposition to other tasks, mentioned collection of classes is usually unknown earlier. It causes restricted application of classic classification methods in pathological speech analysis.

The purpose of presented paper is an attempt to use DBN to automatically find mappings, connecting collectivity of acoustic signal samples (for example, corresponding to correct and incorrect states of biological systems), with adequate indicators having practical diagnostical use.

⋆ ⋆ ⋆

Acoustic properties of biocompatible magnetic nanoparticle water suspensions

Józefczak Arkadiusz

Adam Mickiewicz University
Faculty of Physics
Institute of Acoustics
Umultowska 85, 61-614 Poznań, Poland

Magnetic nanoparticles have been most studied and have a vast potential for application in many different areas of biomedicine, from diagnostics to treatment of diseases. For medical applications nanoparticles require highly biocompatible particle surfaces. Biogenic magnetoparticles such as bacterial magnetosome particles, derived from various magnetotactic bacteria such as Magnetospirillummagnetotacticum are organelles consisting of magnetite crystals enclosed by a phospholipid membrane that offers a high degree of biocompatibility. For chemically obtained particles chemical modification of the nanoparticles surface is necessary. Many synthetic and natural polymers such as dextran or PEG are biocompatible and may be used as coatings.

Ultrasound spectroscopy is very useful in the investigation of nanoparticle suspensions (in a wide range of their concentrations and with particles of a wide range of sizes) and has advantages over many existing technologies because it is nondestructive and non-invasive, and can rapidly measure and be used to characterize systems which are optically opaque (the measurements can provide useful information up to higher concentration than optical methods). The acoustic properties of suspensions, such as velocity and attenuation of ultrasonic waves, have been measured. The method is used for determination of the hydrodynamic particle size distribution, the elastic properties, and aggregation processes under the influence of magnetic field.

⋆ ⋆ ⋆

The effects of infrasound on the levels on activation

Kasprzak Cezary, Małecki Paweł

AGH University of Science and Technology
Faculty of Mechanical Engineering and Robotics
Department of Mechanics and Vibroacoustics
al. A. Mickiewicza 30, 30-059 Kraków, Poland

The paper summarises the research data showing how low frequency sound affects the level of activation in humans. Activation levels were measured with the use of the self-assessment questionnaire, known as the Activation-Deactivation Adjective Check List (AD ACL). The research program involved three independent stages. The acoustic stimulus applied in the first stage had frequency f=13 Hz, sound pressure level SPL= 105 dB (HP). The exposure time in experiment was constant (20 min). Results indicate a statistically significant decrease of the General Activation effect following the low-frequency sound exposure.

This study is a part of the N N501 247740 research project, supported by the National Science Centre.

⋆ ⋆ ⋆

Identification of aircraft noise during acoustic monitoring by using 3D sound probe

Kłaczyński Maciej

AGH University of Science And Technology
Faculty of Mechanical Engineering and Robotics
Department of Mechanics and Vibroacoustics
al. A. Mickiewicza 30, 30-059 Kraków, Poland

Undertaking long-term acoustic measurements on sites located near an air-port is related to a problem of large quantities of recorded data, which very often represents information not related to flight operations. In such areas, usually defined as zone of limited use, often other sources of noise exist, such as roads or railway lines treated is such context as acoustic background. Manual verification of such recorded data is a costly and time-consuming process. Automatic differentiation of the tested noise source from background and precise recognition the quantitative impact of aircraft noise on the acoustic climate in a particular area is an important task. This paper presents concepts of method for identifying aircraft operations (flights, take-offs, landing), supported by experimental studies, using 3D Microflown sound intensity probe and ambisonics microphone Soundfield ST350. The proposed method is based on determining spatial sound intensity vector in tested acoustic field during the monitoring timespan. On this basis aircraft opera-tions are marked in a continuous record of noise events.

The paper has been written and the respective research undertaken within the project 2011/01/D/ST6/07178 (National Science Centre).

⋆ ⋆ ⋆

Determination of acoustic parameters of REPOWER MM92 wind turbine for changing operating conditions

Kłaczyński Maciej
Wszołek Tadeusz
Mleczko Dominik

AGH University of Science and Technology
Faculty of Mechanical Engineering and Robotics
Department of Mechanics and Vibroacoustics
al. A. Mickiewicza 30, 30-059 Kraków, Poland

In Poland, one of the most popular sources of renewable energy are wind turbines and all are onshore ones (i.e., located inland), and often are in close proximity to inhabited areas. Their operation raises issues as to environmental and health impact, in the context balancing strict standards in granting environmental permits for new wind farms and supporting renewable energy production nationwide. There has been a number of publications in Poland and worldwide concerning environmental and health impact of wind turbines operation on nearby residents and natural habitats, but these quite often came to contradictory conclusions. This article presents the results of research performed in order to determine the impact of changing operating conditions of a wind turbine caused by different weather conditions on the measured acoustic parameters (LAW – A-weighted sound power level, L_{Aeq} – A-weighted sound pressure level). Determination of acoustic impact of wind turbines has merits when it reaches its nominal operating conditions, and then its limits. That happens for wind speed for v = 10 to 25 m/s at the height of the nacelle (for example 100 m), which often translates to (depending on the stability of the atmosphere) for the wind speed at the height of the receiver (for example: 1.5 m, 4 m or 10 m) to a value $v > 5$ m/s. In this case, the standard microphone's windcscreen do not seem to cover the job. This paper presents the results of measurements taken for different wind speed.

⋆ ⋆ ⋆

Acoustic barriers in landscape

Kompała Janusz
Kozerska Katarzyna

Central Mining Institute
Plac Gwarków 1, 40-166 Katowice, Poland

In the recent years significant increase of environment noise pollution, mainly in the industrial areas, has been noticed. It is caused by the functioning of industrial objects and intensity of motor, railway and air traffic.

Currently the majority of operations yield to eliminate environment noise pollution by assembling following acoustic barriers, which due to their sizes and colouring, may be found awkward in the light of the landscape composition.

During the assembling process the sustainable development is omitted causing sharing the public space with vertical barriers resembling isolated ghettos in which ordinary inhabitants are supposed to dwell.

In the article problems associated with acoustic barriers' effectiveness, the way they are arranged in the public areas, esthetics and landscape composition were discussed.

⋆ ⋆ ⋆

The noise reduction studies of the "bionic" fan

Kopania Joanna M.[1]
Kazimierska-Grębosz Marianna[1]
Dyszlewska Krystyna[2]

[1] Lodz University of Technology
Department of Basis Technology and Industrial Ecology
[2] The Power Engineering Institute
The Aeroacoustics Laboratory of the Heat Engineering Department "ITC"

To minimize the noise emission is an important issue to be considered in the design of future of the airfoils. Solutions of the noise problems are also looking for in nature, especially in owl's. Their silent flight is possible thanks to the special structure of their feathers. Their secondary flight feathers are cut in the shape of the teeth at the leading edges and the combs of the trailing edges. The effects of noise reducing by cutting the regular teeth of the trailing edge of profiles were been studied in literature. The results depend on the size of the teeth, the width between the top of the teeth, angle of attack blade, Reynolds number, etc. In our work concern on the serrated trailing edge of the axial fan's blade. We studied the noise of fan with isosceles teeth on trailing edge of blades. The efficiency and flow rate were better for the bionic fan than the orginal. But the acoustic parameters were not good. But there were some evidences (e.g. decrease of the SPL in FFT analysis) that the teeth on the trailing edge of blade may be desirable.

⋆ ⋆ ⋆

Influence of air inlets on window sound insulation depending on mounting location

Koprowska Hanna Maria

Building Research Institute ITB
Filtrowa 1, 00-611 Warszawa, Poland

Use of air inlets, which is sometimes a necessity, significantly decreases window sound insulation. Several methods of improving the sound insulation of window systems with air inlets are proposed to maintain acoustic comfort in rooms. Results of sound insulation test of windows with air inlets, mounted in three different installation systems, have been described and discussed in this article.

⋆ ⋆ ⋆

Active noise and vibration control of circular plate with the use of MFC actuators

Kos Paweł
Leniowska Lucyna
Mazan Dominik
Sierżęga Mariusz

University of Rzeszów
Institute of Technology
Rejtana 16, 35-310 Rzeszów, Poland

An active vibration control system is proposed for suppressing small amplitude harmonic vibrations of a thin circular plate and related problem of reducing structure-borne noise. This system integrates control algorithm, intelligent materials, as well as hardware and software technologies based on LabView and NI CompactRIO platform. The PSV-400 Vibrometer was used to find the optimal sensors location and the plate resonance frequencies. The primary excitation is provided by a rectangular MFC actuator bonded to the plate, while a star shape MFC element located in the middle of the plate is used as the secondary actuator. For the considered system, the ARX method of discrete-time model identification for real-time active vibration control has been applied. On the basis of this model, the control algorithm based on pole-placement method has been developed. The simulation results show that the designed structure of a close-loop system with MFC actuators provides substantial vibration suppression.

⋆ ⋆ ⋆

Index assessment of noise hazard of work environment in opencast mines of rock material

Kosała Krzysztof

AGH University of Science and Technology
Department of Mechanics and Vibroacoustics
al. A. Mickiewicza 30, 30-059 Kraków, Poland

Central Institute for Labour Protection – National Research Institute
Czerniakowska 16, 00-701 Warszawa, Poland

Proposals for noise hazard assessment of work environment in opencast mines of rock material by means of partial and global indices were shown in the paper. The single-number global index of assessment is a function of four partial indices: the noise hazard assessment at workstation index, the impulse noise index, the continuous noise index and the sound power of machine index. Calculation procedures of indices were given in the paper.

Verification of partial indices was performed on the basis of data obtained from preliminary acoustic investigations carried out in the andesite and the limestone mines. Verification of the proposed global index demands continuation of research and analysis based on the complex acoustic measurements in opencast mine of rock material, in which the acoustic climate is assessed.

⋆ ⋆ ⋆

Acoustic waves in the sea

Kozaczka Eugeniusz, kozaczka@pg.gda.pl

Gdańsk University of Technology
Narutowicza 11/12, 80-233 Gdańsk, Poland

Polish Naval Academy
Śmidowicza 69, 81-103 Gdynia, Poland

The propagation of acoustic waves in the sea offer a number of possibilities for practical application. This paper will discuss the propogation of acoustic waves in shallow seas while naturaly taking into account factors which influence boundary conditions on the surface (air and sea water). In particular, the main factors that affect the climate of underwater acoustics will be considered, with a particular emphasis on underwater noise produced by the movement of ships. In this respect, the mechanism of the radiation of acoustic waves by a propeller is discussed as one of the most intense sources of underwater noise generated by ships and other vessels moving in the water.

Another issue that will be presented in this paper is the use of developments in underwater aquatics, and in particular non-linear acoustics, to study the structure of the seabed.

Parametric sonar, as the main practical product of nonlinear interaction of large amplitude elastic waves, is one of the most attractive tools for remote sensing studies.

The above issues will be illustrated by the results obtained from investigative research experience.

⋆ ⋆ ⋆

Active noise control using TMS320C6747 processor

Krukowicz Tomasz, Morzyński Leszek

Central Institute for Labour Protection
– National Research Institute
Czerniakowska 16, 00-701 Warszawa, Poland

In this paper an early stage of the design of active noise control system based on the TMS320C6747 is presented. Aim of the article is to introduce capabilities of the system and its limitations. Purpose of the system are in-situ situations, where the system can applied immediately without measurements and system/signal analysis using PC and special software. Results of example laboratory tests using genetic algorithm and neural network are presented.

⋆ ⋆ ⋆

Numerical study of acoustic-structure interaction of selected helicoidal resonator with flexible helicoidal profile

Łapka Wojciech

Poznan University of Technology
Institute of Applied Machanics
Piotrowo 3, 60-965 Poznań, Poland

The paper presents the results of numerical studies of acoustic-structure interaction of selected helicoidal resonator with helicoidal profile made of an elastic material. Considered a well-recognized acoustic system for one representative type of acoustic helicoidal resonator with two resonant frequencies that correspond to previous studies of the author. Due to the large range of flexible materials to study, this work focuses on the change of material density, Poisson's ratio and Young's modulus as the basic parameters describing the properties of elastic materials. The results indicate a significant interaction between the acoustic attenuation performance of helicoidal resonator and elasticity of the helicoidal profile. These interactions are most evident in the frequency range in which the helicoidal resonator is revealed to be effective acoustic damper.

⋆ ⋆ ⋆

Rotating helicoidal resonators – pilot study

Łapka Wojciech

Poznan University of Technology
Institute of Applied Machanics
Piotrowo 3, 60-965 Poznań, Poland

This paper focuses on identifying the possibility of rotation of helicoidal resonators under the influence of the air flow in duct and its acoustic and flow consequences. In order to carry out research there were made a special part of the test bench (transition), so that it was possible to rotate the helicoidal resonators placed in section of the cylindrical duct with a length of approximately 0.5 m in axis. The transition element, length of 80 cm, has a larger diameter than the inner section of the duct with the resonator (140 mm/125 mm), but the other part of the test bench is made of cylindrical ducts with a diameter of 125 mm. There were measured rotational speed of bearing-supported half a meter of cylindrical duct with helicoidal resonators inside, depending on the flow velocity. Pilot studies suggest an interesting possibilities of additional use of helicoidal resonators, as silencer and energy recuperator.

⋆ ⋆ ⋆

The study of pressure drop depending on the air flow rate in duct of selected helicoidal resonators

Łapka Wojciech[1]
Szymański Michał[2]
Górzeński Radosław[2]

[1] Poznan University of Technology
Institute of Applied Machanics
Piotrowo 3, 60-965 Poznań, Poland
[2] Poznan University of Technology
Institute of Environmental Engineering
Piotrowo 3a, 60-965 Poznań, Poland

The paper presents the measurements of pressure drop for selected three helicoidal resonators depending on the volume air flow in the cylindrical duct with a diameter of 125 mm. There were considered three helicoidal resonators with constant ratio $s/d = 1.976$, but different number of helical turns n. The first two types of resonators do not differ significantly in terms of the number of turns, $n = 0.671$ and $n = 0.695$, but this small change in spread of helicoidal profile reflects a large difference in acoustics, two resonances and one resonance, respectively. The third selected resonator has the same ratio of helical slope s to duct diameter d, s/d, but the number of turns is $n = 1.0$. It is one of the characteristics of acoustic resonance of symmetrical distribution of attenuation of sound in relation to the center frequency. The study was performed at the newly built experimental set-up for testing silencers, determining flow noise and total pressure drop.

⋆ ⋆ ⋆

Infrasound acoustics field analysis using beamforming method – a study on infrasound sensors

Małecki Paweł
Kasprzak Cezary
Olszewski Ryszard
Trojanowski Roman

AGH University of Science and Technology
Faculty of Mechanical Engineering and Robotics
Department of Mechanics and Vibroacoustics
al. A. Mickiewicza 30, 30-059 Kraków, Poland

To study infrasound acoustic field one should first develop an infrasound acquisition and measuring system. A high price of infrasound measurement reference microphones is an effective barrier from large-scale use of them. On the other hand the characteristics of the standard acoustic microphones are measured for audible range only. That doesn't mean that these microphones can't be used for infrasound studies. A small mechanical and electric circuit modification allow standard microphones to have a satisfactory effectiveness for infrasound spectrum.

After these modification an infrasound measurement reference microphone should be used to obtain the characteristics of modified standard microphones by means of comparative method. Such measurement should also help in designing a filter to compensate the possible nonlinearities in modified frequency characteristic.

This work shows a concept of an infrasound acoustic field measuring system and studies on a microphone for measuring infrasound.

⋆ ⋆ ⋆

Modeling and designing of ultrasonic welding systems

Milewski Andrzej
Kluk Piotr
Kardyś Witold
Kogut Paweł

Tele and Radio Research Institute
Ratuszowa 11, 03-450 Warszawa, Poland

This article presents the main stages and the main challenges in modeling and designing of modern ultrasonic welding and cutting systems. First, the key components of such a system, such as an ultrasonic stack (consisting of a high power ultrasonic transducer and a sonotrode) and a digitally controlled ultrasonic power supply with precise control of the output power have been considered. Next, a concept of measurement system for verification and validation of mathematical models of ultrasonic stacks and its components has been presented. Finally, a method of ultrasonic stack e-diagnosis based on ultrasonic transducer electrical impedance measurement during welding and cutting process has been described.

⋆ ⋆ ⋆

The influence of room and directivity of source on the subjective evaluation of sound

Niewiarowicz Marek

Poznań University of Medical Sciences
Department of Otolaryngology
Aleksandra Fredry 10, 61-701 Poznań, Poland

The aim of this study was to determine the influence of the type of room and directivity of source on subjective evaluation of sound. Investigations were conducted using a computer simulation technique. For three rooms, varying significantly in size and shape, impulse responses were simulated using three different sound sources – two of them corresponded to the actual loudspeaker systems and the third – an idealized source with omnidirectional characteristic. Due to the convolution operation with audio signals, which were two fragments of speech and two fragments of music, 36 test signals were obtained. Subjective study, which was attended by five normally hearing listeners, were carried out using headphones. Test signals were grouping into triads and the listeners' task was to determine a pair of the most similar sounds and a pair of the least similar sounds in every triad. The analysis of the results was performed using the method of multidimensional scaling (INDSCAL). In the second stage a parametric evaluation was performed. It consisted in determining the intensity of a given attribute of the perception space in the global acoustic sensation. Using the correlation analysis it was possible to relate a particular dimension of the multidimensional space to the attributes of the perception space.

⋆ ⋆ ⋆

An adaptive vibroacoustic control system with multiple independent feedback loops

Nowak Łukasz

Institute of Fundamental Technological Research
Polish Academy of Sciences
Pawińskiego 5B, 02-106 Warszawa, Poland

An active control system for reduction of vibroacoustic emission of plate structures with arbitrary boundary conditions is presented. The system uses small, rectangle-shaped piezoelectric transducers attached to the surfaces of the controlled structures acting as both sensors and actuators. The paper consists of three parts. The first part describes the developed and implemented algorithms for determining acoustic radiation characteristics and the optimal control parameters. The acoustic pressure distribution in the space surrounding the considered vibrating structure is computed for the free-field case using the Indirect Variational Boundary Element Method and the elaborated computational scheme. The developed optimal control algorithm is self-adjustable and has a capability of estimating modal components of the external excitation force with unknown spatial distribution basing only on the signal from piezosensors. The aim of the control is to minimize the amplitude of the acoustic pressure in a specified point of the surrounding space. In the second part the developed numerical models and the results of the simulations are described. The third part presents the physical implementation of the designed control system and the experiments performed in an anechoic chamber. Acoustic radiation characteristics of the considered structures and the control performance of the developed system are investigated and the results are compared to the results of the simulations.

⋆ ⋆ ⋆

The new series of standards for the measurement of sound insulation in buildings

Nowicka Elżbieta

Building Research Institute
Department of Acoustics
Filtrowa 1, 00-611 Warszawa, Poland

In the near future the ISO Committee will introduce new measurement standards for acoustic insulation in buildings. The ISO 16283 parts 1–3 will replace the existing series of ISO 140 Part 4, 5 and 7. ISO 16283 (all parts) describes procedures for field measurements of sound insulation in buildings. Airborne, impact and façade sound insulation are described in ISO 16283-1, ISO 16283-2 and ISO 16283-3, respectively. ISO 16283 differs from ISO 140-4, -5, and -7 in that:

- it applies to rooms in which the sound field may, or may not approximate to a diffuse field,
- it clarifies how operators can measure the sound field using a hand-held microphone or sound level meter and
- it includes additional guidance that was previously contained in ISO 140-14.

The article describes new standard and compare both methods.

⋆ ⋆ ⋆

Ultrasonic projection imaging using multielement ring probe

Opieliński Krzysztof J.
Pruchnicki Piotr
Gudra Tadeusz

Wrocław University of Technology
Wybrzeże Wyspiańskiego 27, 53-333 Wrocław, Poland

Ultrasonic projection imaging is similar to X-ray radiography. Nowadays, ultrasonic projection methods have been developed in the set-up of multielement flat arrays with miniature transducers, where one of the array acts as a transmitter and the other one is a receiver.

In the paper, a new method of the projection imaging using a 1024-element ultrasonic ring probe was presented. That ring probe allows for the choice of a projection scanning plane for any angle around an investigated object dipped in water. The fast measurement data acquisition is possible due to a parallel switching of opposite transmitting and receiving transducers in the ring of the probe and to a vertical movement of the probe. The algorithm equalizing the length of measurement rays and distances between them was elaborated for the reconstruction of projection images.

Projection research results of different media obtained by means of the elaborated measurement set-up and compared with

mammography simulations (acquired through the overlapping of X-ray tomographic images) show that ultrasonic projection method presented in this paper can be applied to the woman's breast providing diagnosis for an early detection of cancerous lesions and most of all, as an alternative or complementary method to mammography. Mammography is harmful because of ionizing radiation and invasive because of the mechanical compression of tissue.

⋆ ⋆ ⋆

Acoustic test method of single electrostatic discharges

Orzech Łukasz

Institute of Mining Technology KOMAG
Laboratory of Applied Tests
Pszczynska 37, 44-101 Gliwice, Poland

Electrostatic discharge of energy exceeding the ignition point is a potential source of explosion in the case of explosive atmosphere. To eliminate such a hazard, detailed testing of the non-metallic materials as regards collection of electrostatic charge on their surfaces and possibility of the charge flow to earthed components, is indispensable. Standard methods of electric measurements of discharge have some features that are difficult to be eliminated, when the result of high accuracy are required. The option are non-electric methods of measuring the electrostatic discharge, which do not interfere with discharging circuits and enable measuring the charge of a single brush discharge transferred from the surface of electrified material.

Use of the acoustic method to measure a single discharge, the value of which is the basis for assessing the non-metallic material safety in explosive atmospheres, is described. The measurement of acoustic effect of discharge enables to parameterize the igniting properties of the material due to accurate correlation of pressure acoustic wave parameters with the value of charge moved from a surface of electrified material. The described method can be used for an individual measurement of electrostatic discharge or can be a completion to the traditional electric measurements method in the case of both of spreading brush discharge and full discharge.

⋆ ⋆ ⋆

Using the information entropy method to assess the psychoacoustic emotions induced by sound sources

Paszkowski Waldemar

Silesian University of Technology
Faculty of Organisation and Management
Institute of Production Engineering
Roosevelta 26, 41-800 Zabrze, Poland

This article presents a multisensory approach to sound perception for the needs of assessing the emotions induced by sound sources. A connection has been identified between shaping soundscapes and the public's subjective assessment of sounds. The concept of soundscapes constitutes a new approach to managing the tasks of shaping the acoustic environment in urban areas. In this approach, task management is not limited only to shaping the acoustic climate. The essence of the new approach consists in carrying out research to identify the public's subjective impressions in order to assess the qualities of the sounds of acoustic events in the environment. An information form of representing the stimuli and emotions has been proposed to analyse sound perception.

An example has been prepared where an attempt was made to assess the impact of the stimuli on the quality of psychoacoustic emotions induced by a selected sound source using the information entropy method. The problem discussed here is a continuation of the research on the development of a qualitative assessment model to evaluate the acoustic emission of sound sources in the environment.

⋆ ⋆ ⋆

Uncertainty in sound scattering coefficient measurement

Pilch Adam
Kamisiński Tadeusz
Flach Artur
Zastawnik Marcin

AGH University of Science and Technology
Faculty of Mechanical Engineering and Robotics
Department of Mechanics and Vibroacoustics
al. A. Mickewicza 30, 30-059 Kraków, Poland

Sound diffusion structures are characterized by two main parameters, that describe the quality of the sound reflected from them. In the case of sound scattering coefficient, which is measured in reverberation chamber according to ISO 17497-1, the standard recommend the calculation of uncertainty according to the law of propagation. Only type A evaluation basing on measurement results is presented, while for example the uncertainty connected with the measurement realization of the definition of the parameter is ignored. What is more, the standard ISO 17497-1 assume, that input values (reverberation times) are independent, hence omit the estimated covariance calculation. In the paper the calculation of uncertainty in the sound scattering coefficient s is presented. The method proposed by the standard is compared with values obtained taking into account correlation between input values and the results of the Monte Carlo method. It was shown that for some frequencies, the ISO standard uncertainty is much smaller, than calculated according to the other methods.

⋆ ⋆ ⋆

Selected changes of voice properties following tonsillectomy

Potępa Łukasz
Wszołek Wiesław
Szaleniec Joanna
Steczko Andrzej
Składzień Jacek

AGH University of Science and Technology
al. A. Mickiewicza 30, 30-059 Kraków, Poland

Otolaryngological Clinic, Collegium Medicum UJ
Śniadeckich 2, 31-531 Kraków, Poland

Tonsillectomy is a kind of laryngological operation, which involves changes within articulatory structures of the vocal tract. Although these changes are not big in dimension, they can cause voice changes. As these changes can be important to some patients (e.g. actors or singers) they should be informed about such possible side effects during the medical interview with the laryngology surgeon before the decision concerning tonsillectomy will be made. Therefore the research into voice properties following tonsillectomy was necessary – and such a research was carried out by the authors of the presented paper. The recordings were made – before the surgery and around 6 weeks after the treatment. 20 patients (12 male and 8 female) were examined this way. In registered acoustic material especially vowels: /a/, /e/, /i/ and /u/ were taken into account.

During the analysis of this material following parameters was taken into account: first four formants amplitude and frequencies values and 20 successive mel-frequency cepstral coefficients for 300-mel wide filters. The results of the research show which voice parameters change after tonsillectomy and how voice quality can be worsened after this type of surgery. Detailed results of the research mentioned above will be presented.

⋆ ⋆ ⋆

Discrimination of lossy compression in musical recordings by listeners with different auditory training

Rogowska Agata[1]
Żera Jan[1,2]

[1] Warsaw University of Technology
Institute of Radioelectronics
Nowowiejska 15/19, 00-665 Warszawa, Poland
[2] The Fryderyk Chopin University of Music
Okólnik 2, 00-368 Warszawa, Poland

Audibility of lossy compression produced by four lossy codecs – Vorbis, WMA, Mp3 (Fraunhofer) and Mp3 (Lame) – in samples of classical and popular music was studied on groups of naive and experienced subjects to determine how average discrimination of compressed/decompressed sound depends on auditory training, and with participation of three subjects to determine the inter-subject differences in discrimination. At the lowest bit rates of 32 and 48 kbps compressed music was easily discriminated by all listeners. Compression became inaudible at bit rates of 80–96 kbps and higher. Trained subjects demonstrated better ability to discriminate compressed music than naive subjects by about 16 kbps on the average. There was noticeable inter-subject difference in discrimination of sound after compression by various codecs. The presence of interfering noise had limited influence on discrimination even at S/N within the range of +4 to +16 dB.

⋆ ⋆ ⋆

The influence of seats' sound absorption test method on prediction of acoustic parameters in auditoria and concert halls

Rubacha Jarosław
Kamisiński Tadeusz
Brawata Krzysztof
Szeląg Agata

AGH University of Science and Technology
Faculty of Mechanical Engineering and Robotics
Department of Mechanics and Vibroacoustics
al. A. Mickiewicza 30, 30-059 Kraków, Poland

This paper presents the own study on sound absorption by seats used in concert halls. The absorption coefficients for seats were defined using methods described by: Beranek, Kath and Kuhl, Nishihara and also on the basis of ISO 354. Afterwards, obtained results were used in the calculation model for prediction of acoustic parameters in Philharmonic Hall in Rzeszów. The comparison of room acoustic parameters derived from the simulations and measurements enabled to identify the best method for the determination of the seats' sound absorption coefficient. Since the auditorium in concert hall is the part of the highest sound absorption, it has a decisive influence on the interior acoustic parameters. The accuracy of determination of the seats' sound absorption coefficient can also improve the prediction exactness of room acoustic parameters.

⋆ ⋆ ⋆

The study of sound insulation of buildings with the use of aircraft noise and loudspeaker

Rudno-Rudziński Krzysztof,
krzysztof.rudno-rudzinski@pwr.wroc.pl

Wrocław University of Technology
Wybrzeże Wyspiańskiego 27, 53-333 Wrocław, Poland

The measurement results of airborne sound insulation of building façades have been presented. Single-family buildings were examined using the global air traffic method and the global loudspeaker method. The measured sound insulation values have been analyzed in terms of their compliance with the requirements and to determine pathways of noise from the outside to the rooms. The shortcomings of current standards in terms of their upgrades were also highlighted.

⋆ ⋆ ⋆

The effect of arrangement of sounds in a musical piece on perception of the tonal center

Smolik Damian[1]
Snakowska Anna[2]

AGH University of Science and Technology
[1] Faculty of Physics and Applied Computer Science
[2] Faculty of Mechanical Engineering and Robotics
al. A. Mickiewicza 30, 30-059 Kraków, Poland

This report constitutes a kind of résumé or synthesis of certain issues raised by the authors in their earlier conference contributions, especially those presented at the 59th Open Seminar on Acoustic (2012) and 20th Conference on Acoustic and Biomedical Engineering held in Zakopane this year. These problems are related mainly to the issue of perception of composite sounds used in music, in particular composite harmonic sound sequences. To date, no exact theory was developed that would provide a consistent description of music perception process in context of wide range of techniques and means of expression used by composers. Similarly, we lack appropriate experimental procedures creating a framework in which individual aspects of the music perception phenomenon could be measured. The research work carried out currently in this area is aimed at lying the foundations for such theory an includes studies on long-term processing of acoustic information by the human hearing system, the effect of memory processes on auditory perception, relationship between the sound material arrangement pattern in a musical piece and the ability to recognize functional interdependence in the key, rôle of symmetries and breaking them in this arrangement (especially with respect to tonal or atonal nature of perception, perception dependencies in the consonance-dissonance relationship, and many other issues.

⋆ ⋆ ⋆

A study on directivity characteristics of sound radiated from semi-infinite waveguide outlet

Snakowska Anna[1]
Gorazd Łukasz[1]
Jurkiewicz Jerzy[2]

AGH University of Science and Technology
[1] Faculty of Mechanical Engineering and Robotics
Department of Mechanics and Vibroacoustics
[2] Faculty of Electrical Engineering, Automatics, Computer Science and Biomedical Engineering
Department of Metrology
al. A. Mickiewicza 30, 30-059 Kraków, Poland

The paper presents results of measurements of directivity characteristics produced by sound wave radiated from open outlet of unflanged cylindrical waveguide and comparison of the experimental data with directivity patterns obtained theoretically on the grounds of the mathematical model of semi-infinite tube with Neumann's boundary conditions. The physical representation of the model was a finite waveguide the opposite end of which was terminated with a strongly sound-absorbing material preventing reflection of the wave (the so-called anechoic termination). The system was excited by means of a point source located either symmetrically or unsymmetrically with respect to the waveguide axis in the vicinity of the termination. Frequencies of monochromatic signal applied to the source were selected in such a way that they fell between consecutive radial/circumferential mode cut-off frequencies so apart from the plane wave, also consecutive higher wave modes could be ob-

served with the increasing excitation frequency. In order to verify consistency between the obtained measurement results and predictions of the adopted theoretical model, the measurements were carried out in spherical coordinates allowing thus to obtain 3D directivity patterns. Thanks to the use of computer-controlled turntable in the measurement system, the presented results are characterized with high angular resolution equaling to 5° for the polar angle and 15° for the azimuthal angle.

⋆ ⋆ ⋆

The identification of the sound power of sources in the presence of the incomplete information regarding their location

Suder-Dębska Katarzyna
Czajka Ireneusz
Gołaś Andrzej

AGH-University of Science and Technology
Faculty of Mechanical Engineering and Robotics
Department of Power Engineering and Environmental Protection
al. A. Mickiewicza 30, 30-059 Kraków, Poland

The side effect of the human activities, especially in areas related to the acquiring of energy sources is a varied environmental pollution. Therefore, it seems to be necessary to build a system for monitoring and managing the state of the environment. On the other hand, in order to enable the management of the environment status, it is essential to modelling the impact of the facilities on the environment.

In this paper is presented a system for monitoring and managing the state of the environment, which in its basic version focuses on the risks related to the noise. It allows to generate on demand the noise maps. For this purpose it was necessary to determine the sound power of sources. Because under real conditions the noise sources in the selected area can change its location, it seemed to be important to determine the effect of this change on sound power of the obtained values.

⋆ ⋆ ⋆

Engineering modifications of resonance absorbers to reduce the impact of surface layers

Suder-Dębska Katarzyna
Czajka Ireneusz
Śnieć Paweł

AGH University of Science and Technology
Faculty of Mechanical Engineering and Robotics
Department of Power Engineering and Environmental Protection
al. A. Mickiewicza 30, 30-059 Kraków, Poland

Resonance absorbers are readily used by architects to help mitigate the adverse acoustic phenomena occurring in various public buildings. They can be finished properly supply in any way in the framework of needs on a given object.

The current system is an acoustic pulp and cotton plaster fitted using air gap of different sizes. This system, in the basic version consists of patches of glass wool with a thickness of 20 mm, the base layer with a thickness of 3 mm and a finishing layer with a thickness of 2 mm. Finishing layer is made of the cotton fibers and the finely minced cellulose.

In this article has been analyzed the impact of the thickness of the slices constructed of glass wool, the size of the air gap and the finishing of the outer surface of the resonance absorber on the obtained sound absorption coefficients. With regard to the outer surface finishing have been tested the sample with a finishing layer applied by the manufacturer, and samples coated with additional single and double layer of paint.

⋆ ⋆ ⋆

Shaping sound reflection on the edge of reflective panels

Szeląg Agata
Kamisiński Tadeusz
Rubacha Jarosław
Brawata Krzysztof

AGH University of Science and Technology
al. A. Mickiewicza 30, 30-059 Kraków, Poland

The proposed research relates to phenomenon of sound reflection from a single reflective panel of finite dimensions and the spatial arrangement of many elements. There will be study the influence of side edge's shape on distribution of the reflected sound field. The analytical, numerical and experimental studies will take into account diffraction at the edge of panels, different distance from the source and receivers to reflective panels, different angle of incidence and reception of sound waves and also their impact on the sound reflection. The studies aim to develop a computational model that will better describe acoustic wave reflection from reflective surface than the currently used model derived only for flat and round elements. The expected result of the research will be clues to formulate guidelines for shaping panels' edges that provide even spatial and frequency distribution of acoustic field on the measurement area.

⋆ ⋆ ⋆

Modeling of subjective evaluation of sound intensity leveling between violin strings

Wrzeciono Piotr

Warsaw University of Life Sciences – SGGW
Faculty of Applied Informatics and Mathematics
Nowoursynowska 166, 02-787 Warszawa, Poland

The sound intensity leveling between the violin strings is a very important problem for violinists and violin makers. This property determines the usefulness of the instrument. If the leveling is very bad, a play on the violin is nearly impossible. Because of that, the leveling is always evaluated on violin making competitions. The evaluation of this violin's property is made by jurors of the competitions. This property can be also measured, but the relation between the objective parameters and the subjective evaluation is complicated. This work presents a modeling of subjective evaluation of the leveling. The modeling is based on a genetic algorithm and uses differences between strings expressed in dB. The AMATI multimedia database, which contains recordings and evaluations of the violins from 10th International Henryk Wieniawski Violin Making Competition, was used as a source of the violin sound and their subjective evaluations. Each violin was evaluated by four jurors. The three objective function were tested: a minimization of the mean square error, a minimization of the mean of errors and a minimization of the number of instruments, which the module of the difference between the calculated evaluation and subjective evaluation was less that one. The best result was obtained for the medians of the evaluations done by jurors, where 60% of the calculated evaluations were similar to the subjective evaluations.

⋆ ⋆ ⋆

Effect of acoustic model input parameters to the range of wind turbine noise

Wszołek Tadeusz
Mleczko Dominik
Kłaczyński Maciej

AGH University of Science and Technology
Faculty of Mechanical Engineering and Robotics
Department of Mechanics and Vibroacoustics
al. A. Mickiewicza 30, 30-059 Kraków, Poland

Since there are no dedicated methods for both measuring and calculation of noise emitted by wind turbines, reference

methods are used. Therefore modeling algorithms based on the standard ISO 9613-2. Algorithms of this standard include phisical phenomena such as absorption by the atmosphere, absorption through the ground and reflection from the surface, however, apply to sources located not far above the terrain. This requirement introduces doubt as to whether the standard algorithms are actually suitable, in particular the ground attenuation factor, wind speed and direction that change. Also, the sound power of turbine varies with the wind speed. On the other hand, in some areas, even small changes in the level of noise caused by the indicated factors may result significant changes in the noise.

Therefore, the present paper is an attempt to determine the qualitative and quantitative effects of changes in ground ratio G, temperature, wind speed and direction on the range of noise emissions from the wind turbine. The study used the wind farm located in Leki Dukielskie (Podkarpackie Province, Southeast Poland), consisting of five Repower MM92 turbines. Spectrum of sound power level (L_w) and sound level (L_{Aeq}), under varying conditions of wind turbine has been measured. The measurement results were used to verify the results of a calculation made using the universal software SoundPLAN that is dedicated for the analysis of environmental noise.

The paper has been performed within the statutory research of AGH Department of Mechanics and Vibroacoustics in 2010–2013.

⋆ ⋆ ⋆

The sound absorption coefficient as a function of the active measurement volume

Zastawnik Marcin, Kamisiński Tadeusz
Pilch Adam, Flach Artur

AGH University of Science and Technology
Faculty of Mechanical Engineering and Robotics
Department of Mechanics and Vibroacoustics
al. A. Mickiewicza 30, 30-059 Kraków, Poland

This paper concerns the discussion about correctness of determination the sound absorption coefficient for the spatial structures in reverberation chamber. The currently used procedure, described in the PN-EN ISO 354, does not take into account changes in the volume of the chamber which result from measured sample geometry. After simplified calculations one has shown that disregard of the sample volume can result in measurement error in the range of 10%. In order to verify this problem the appropriate experiment was designed. In reverberation chamber there was mounted a specially constructed floor allowing to insert the sample at a given depth. Afterwards, using this measurement setup, there was measured the sound absorption coefficient of upholstered chairs depending on the depth of their installation. Research analysis with discussion of measurement error allowed to formulate the concept of further studies on the impact of measurement area changes on the sound absorption coefficient of different spatial structures.

⋆ ⋆ ⋆

ARCHIVES OF ACOUSTICS
Vol. **38**, No. 3, pp. 449–449 (2013)

E R R A T U M

Authors: K. Szemela, W.P. Rdzanek, W.J. Rdzanek

Title: *Acoustic Power Radiated by a System of Two Vibrating Circular Membranes Located at the Boundary of Three-Wall Corner Spatial Region*

Archives of Acoustics, Vol. **37**, No. 4, pp. 463–473 (2012)

Location	It is	It should be
Eq. (1)	$\left(k_T^{(i)} - 2\nabla + 1\right) W_i\left(\cdots\right) = \cdots$	$\left(\left(k_T^{(i)}\right)^{-2} \nabla + 1\right) W_i\left(\cdots\right) = \cdots$

The correct version of the paper is available online.